UNIVERSITAT POLITÈCNICA DE VALÈNCIA
DEPARTAMENTO DE QUÍMICA
INSTITUTO UNIVERSITARIO MIXTO DE TECNOLOGÍA QUÍMICA
(UPV-CSIC)

DOCTORAL THESIS

Model Studies on the Photorepair of (6-4) Dimeric Lesions of DNA

Ana Belén Fraga Timiraos

Valencia, January 2019

Directors:
Prof. Miguel A. Miranda Alonso
Dra. Virginie Lhiaubet-Vallet

CERTIFICATION

Miguel Ángel Miranda Alonso, Full Professor of the Universitat Politècnica de València (UPV) and Virginie Lhiaubet-Vallet, Tenured Scientist of the CSIC,

CERTIFY that the Doctoral Thesis entitled "Models Studies on the Photorepair of (6-4) Dimeric Lesions of DNA" has been developed by Ana Belén Fraga Timiraos under their supervision in the Instituto Universitario Mixto de Tecnología Química (UPV-CSIC).

Prof. Miguel A. Miranda Alonso Dr. Virginie Lhiaubet-Vallet

A Marcos e meus pais

Outline

Abbreviations and Symbols

A	Acceptor
ACE	Acenaphthene
Ac_2O	Acetic anhydride
AcOH	Acetic acid
AcONa	Sodium acetate
AIP	Adiabatic ionization potential
AQ	Anthraquinone
AQS	Anthraquinone-2-sulfonate
azaU	6-azaUracil
BER	Base excision repair
BnOH	Benzyl alcohol
BP	Benzophenone
CASPT2	Complete-active-space self-consistent field second-order perturbation
CASSCF	Complete-active space self-consistent field
$CDCl_3$	Deuterated chloroform
CDI	1,1'-Carbonyldiimidazole
CHRY	Chrysene
CIDNP	Chemically induced dynamic nuclear polarization
CPD	Cyclobutane pyrimidine dimer
CRIP	Contact radical ion pair
D	Donor
DABCO	1,4-Diazabicyclo[2.2.2]octane
DCA	9,10-Dicyanoanthracene
DCN	1,4-Dicyanonaphthalene
DDQ	2,3-dichloro-5,6-dicyano-1,4-quinone
Dew	Dewar valence isomer
DFT	Density functional theory

DMA	*N,N*-dimethylaniline
DMAP	4-(Dimethylamino)pyridine
DMF	Dimethylformamide
DMSO-*d6*	Dimethylsulfoxide
DMT	4,4'-Dimethoxytrityl
DNA	Deoxyribonucleic acid
E	Energy
EA	Electron affinity
EDC	1-Ethyl-3-(3-dimethylaminopropyl)carbodiimide
EET	Excess electron transfer
ESI	Electrospray ionization
ET	Electron transfer
Et_3N	Triethylamine
EtOH	Ethanol
F	Fluorescence
FAD	Flavin adenine dinucleotide
FapyG	2,6-Diamino-4-hydroxy-5 formamidopyrimidine
ForU	5-Formyluracil
Fs-TAS	Femtosecond transient absorption spectroscopy
GGR	Global genome repair
8-HDF	8-Hydroxy-5-deazaflavin
His	Histidine
HmU	5-Hydroxymethyluracil
HOMO, HO	Highest occupied molecular orbital
HPLC	High-performance liquid chromatography
HRMS	High-resolution mass spectroscopy
IC	Internal conversion
Im	Imidazole

IP	Ionization potential
ISC	Intersystem crossing
LIIC	Linear interpolation of internal coordinates
LUMO, LU	Lowest unoccupied molecular orbital
MeCN	Acetonitrile
MeOH	Methanol
MEP	Minimum energy path
1-MN	1-Methoxynaphthalene
2-MN	2-Methoxynaphthalene
MTHF	Methenyltetrahydrofolate
NaPi	Sodium phosphate buffer
NBS	N-Bromosuccinimide
NER	Nucleotide excision repair
NHE	Normal hydrogen electrode
NMR	Nuclear magnetic resonance
OD	Optical density
OG	8-oxoGuanine
P	Phosphorescence
PBS	Phosphate-buffered saline
PET	Photoinduced electron transfer
6-4PP	(6-4) Photoproduct
PS	Photosensitizer
RNA	Ribonucleic acid
ROS	Reactive oxygen species
rt	Room temperature
S_0	Ground state
S_1	Singlet excited state
SSET	Singlet-singlet energy transfer

SSRIP	Solvent separated radical ion pair
T_1	Triplet excited state
TBAF	Tetrabutylammonium fluoride
TBDMSCl	*tert*-Butyldimethylsilyl chloride
TBTU	*N,N,N',N'*-tetramethyl-*O*-(benzotriazol-1-yl)uronium tetrafluoroborate
TCR	Transcription-coupled repair
TEAA	Triethylammonium acetate
TFA	Trifluoroacetic acid
THF	Tetrahydrofuran
TLC	Thin-layer chromatography
TMB	*N,N,N',N'*-Tetramethylbenzidine
TMPD	*N,N,N',N'*-Tetramethyl-1,4-phenyldiamine
TOF-MS	Time-of-flight mass spectrometry
TS	Transition state
TTET	Triplet-triplet energy transfer
UPLC	Ultra performance liquid chromatography
UV	Ultraviolet light
VIP	Vertical ionization potential
ZPVE	Zero-point vibrational energy
δ	Chemical shift
ε	Molar absorption coefficient
ϕ	Quantum yield
λ	Wavelength
τ	Lifetime

Chapter 1:
Introduction

1.1. Photophysics and photochemistry

Molecular photochemistry is the discipline which studies chemical reactions induced by the absorption of UV-Vis (200 - 700 nm) and infrared light (700 - 2500 nm). Organisms have evolved to take advantage and respond to light in numerous ways such as in photosynthesis, vision or the formation of Vitamin D. Understanding how these and other systems convert photons into energy or biological signals is an important issue for the chemical biology community to establish the mechanistic details of these processes.

The process starts when a chromophore which contains an organic functional group such as an alkene, aromatic ring, ketone or enone, absorbs light ($h\upsilon$) from its ground state (S_0). Upon aborption of a photon, the molecule may promote an electron from the highest occupied molecular orbital (HOMO, HO) to the lowest unoccupied molecular orbital (LUMO, LU), reaching an excited electronic state. Therefore, this excited species in the unstable singlet excited state (S_n or S_1) tends to deactivate rapidly to the stable ground state (S_0) by different pathways as shown in the Jablonski diagram[1] (Figure 1.1). This can be through non-radiative (internal conversion, IC) or radiative processes (fluorescence, F) by generation of light emission. Another pathway from S_1 involves forbidden transitions denominated intersystem crossing (ISC), in this case a change in the spin multiplicity gives rise to a triplet excited state (T_n or T_1). After that, the generated triplet excited state T_1 will deactivate to the S_0 through non-radiative (ISC) or radiative processes (phosphorescence, P).

However, deactivation of the excited states does not always lead to the original molecule in its ground state as photochemical processes might also occur to yield primary photoproducts that are chemically different from the original reactant. Photoreactions leading to new products can be efficient only if they are faster than the competing photophysical processes. In the presence of other substrates, intermolecular

processes can take place such as singlet-singlet or triplet-triplet energy transfer (SSET and TTET, respectively), electron transfer, photocycloaddition, etc.

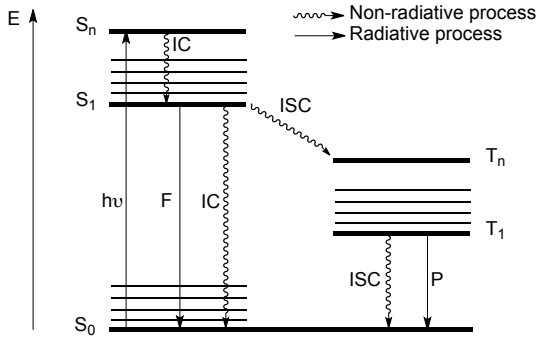

Figure 1.1. Jablonski diagram represents the electronic states of a molecule and the transitions that can occur after absorption of light.

In this context, it is important to gain knowledge in the physical properties of the different chromophores and the photoreactions they can be involved in. This doctoral thesis is centered on the photorepair mechanism of different DNA damage models induced by UV. For this reason, it is important to detail intermolecular processes such as energy transfer, electron transfer and photocycloadditions triggered by UV light.

1.1.1. Energy transfer

In this intermolecular process, the excitation energy of an excited molecule D^*, i.e. the energy donor, is transferred to a neighboring molecule A, i.e. the energy acceptor, which reaches an electronic excited state (Scheme 1.1). Thus, energy transfer permits electronic excitation of molecules A that do not absorb the incident light. The multiplicity of D^* and A^* will stipulate if it is singlet-singlet energy transfer (SSET) or triplet-triplet energy transfer (TTET).

$$D^* + A \rightarrow D + A^*$$

Scheme 1.1.

For this process to occur, the energy level of the excited state of D^* has to be higher than that of A^* (Equation 1.1) and the time scale of the energy transfer must be faster than the intrinsic lifetime of D^*.

$$\Delta G \approx \Delta H = E^{D*} - E^{A*} \quad (1.1)$$

where ΔG is the variation of the free energy of the process and E^{D*} and E^{A*} are the energies of the excited state (singlet excited state or triplet excited state) of the donor and the acceptor, respectively. These processes generally take place following two mechanisms: the *coulombic* (Förster type), or the *exchange electronic* (Dexter type).[2] The Förster type involves a dipole-dipole interaction and acts at long distances (up to 100 Å). By contrast, the Dexter type mechanism requires an effective overlap between orbitals of the donor and the acceptor and thus takes place at short distances (under 10 Å).

1.1.2. Photoinduced electron transfer

One of the most basic reactions studied in organic chemistry is photoinduced electron transfer (PET), where an electron rich donor (D) or an electron deficient acceptor (A) in its excited state transfers an electron to another acceptor or donor in its ground state. (Scheme 1.2).[3] This generates the radical anion of the acceptor and the radical cation of the donor through the formation of a contact radical ion pair (CRIP), which is also known as an exciplex. Depending on other factors, such as interaction with the solvent, the ion pair can undergo solvation to become a solvent separated radical ion pair (SSRIP) or can directly undergo back electron transfer to the ground state reactants. The SSRIP can also suffer back electron transfer to the ground state acceptor and donor, or undergo solvent cage escape to generate free radical ions in solution.

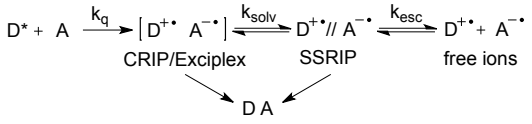

Scheme 1.2. Common PET pathways in non-viscous solvents.

The thermodynamics of these processes is controlled by the oxidation and reduction potentials of the species involved in the reaction, as well as by the energy of the excited state of the molecule that absorbs light. So, for simplicity the free energy associated with PET is given by the Rehm-Weller equation[4] (1.2).

$$\Delta G_{ct} = 23.06\left(E_{ox}^{D} - E_{red}^{A} - \frac{q^2}{\varepsilon r}\right) - E^{*} \qquad (1.2)$$

where E_{ox}^{D} and E_{red}^{A} are the oxidation and reduction potentials of the donor and acceptor, respectively, $\frac{q^2}{\varepsilon r}$ is a coulombic interaction term, and E^{*} is the excited state energy of the photosensitizer (singlet excited state or triplet excited state). Finally, the term 23.06 is the Faraday constant given in kcal/mol. This equation informs about the spontaneity of a PET reaction in solution. Therefore, it can be estimated, with a certain approximation, if the process is going to be favorable ($\Delta G < 0$, exergonic) or, for the contrary, unfavorable ($\Delta G > 0$, endergonic).

1.1.3. Photochemical [2+2] cycloadditions

The [2+2] cycloaddition reaction is the most applied reaction in organic synthesis for the formation of compounds containing a four-membered ring.[5] This way, cyclobutanes can be obtained by addition of an alkene in its ground state to a different photoexcited alkene (photocycloaddition) or by dimerization of two identical alkenes, one of them previously excited (photodimerization).[6] The photoreaction mechanism depends on the pathway to generate the photoexcited alkene (Scheme 1.3). Direct excitation can lead to the alkene lowest excited state S_1, from which [2+2] cycloaddi-

tion can occur (Scheme 1.3, pathway a). Usually, it happens when the alkenes absorb at wavelengths higher than 270 nm and their S_1 is of $\pi\pi^*$ nature such as for aryl substituted alkenes. If this is not the case, the excitation energy is readily dissipated leading to side reactions such as *cis/trans* isomerization and, thus, to low yields for the cycloaddition.

In the specific case of α,β-unsaturated carbonyl compounds, the S_1 is of $n\pi^*$ nature but a reactive T_1 is usually efficiently populated through high ISC. Thus, combination of the enone in its triplet excited state with an alkene leads to 1,4-biradical intermediate, from which the cyclobutane is formed (Scheme 1.3, pathway b).[7]

An alternative pathway is to generate the T_1 excited state of the alkene by a photosensitized reaction (Scheme 1.3, pathway c). In this case, energy transfer occurs when the triplet energy of the alkene is lower than the triplet energy of the photosensitizer (PS). Therefore, as for α,β-unsaturated carbonyl compounds, the cycloaddition takes place from the T_1 of the alkene.[8]

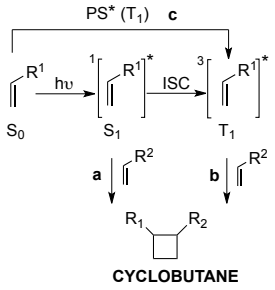

Scheme 1.3. Different pathways for the [2+2] cycloaddition reaction between alkenes: a) [2+2] cycloaddition from the S_1; b) [2+2] cycloaddition from the T_1 and c) photosensitized [2+2] cycloaddition.

Small heterocycles such as the four-membered oxetane ring can also be obtained by [2+2] photocycloaddition. In this case, a photoexcited carbonyl group and an alkene are involved in the photoreaction denominated Paternò-Büchi reaction.[6, 9-10]

The carbonyl compound is the light-absorbing chromophore, which reaches a S_1 or T_1 ($n\pi^*$) and, then, adds to the alkene (Scheme 1.4). The involvement of 1,4-biradical species derived from carbonyl triplets were studied spectroscopically and by trapping with biradical quenchers.[11] This [2+2] photoreaction competes with TTET and is favored for $n\pi^*$ triplets when the triplet energy of the alkene is comparable to or higher than that of the carbonyl group.

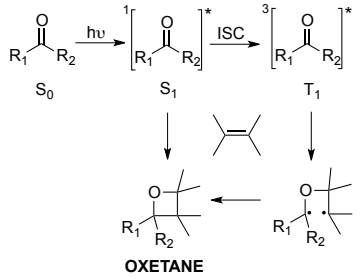

Scheme 1.4. Mechanism involved in the Paternò-Büchi reaction.

As mentioned above, four-membered ring formation is well known through [2+2] photocycloadditions of alkenes to C=C or C=O bonds, but similar cycloadditions to imines (C=N) are less common.[12] The structural requirements to lead to a four-membered azetidine ring are discussed in the Chapter 3.

1.2. DNA damage induced by light

Among the radiation emitted by the Sun that reaches the Earth's surface only 6.1% resides in the UV range, which is divided into UVC (100–290 nm), UVB (290–320 nm), and UVA (320–400 nm). Fortunately, ozone and oxygen completely block UVC radiation and absorb the majority (approximately 95%) of UVB.[13]

The incident UV radiation has important implications for human health, among them, skin cancer is one of the most harmful effects of overexposure.[14] In this context, UV is considered as a carcinogenic and mutagenic component of the solar irradiation spectrum by its ability to cause DNA damage, promotion and progression in

tumorogenesis.[15] Thus, it is important to understand the mechanisms involved in skin cancer by identifying the different DNA photoproducts and their specific contribution to mutagenesis to find relevant prevention strategies.

Regarding to harmful effects induced by UV wavelengths onto DNA, UVC would be the most effective waveband for the induction of DNA photoproducts because the DNA molecule shows the maximum absorption at 260 nm; however, as mentioned above, these wavelengths are entirely blocked by the Earth's atmosphere. Additionally, although the energy of incident UVB and UVA photons is high enough to generate DNA damage, UVA is capable of penetrating the skin more efficiently than UVB, reaching the basal layers where melanocytes and dividing stem cells are located in the dermis (Figure 1.2).[16] Moreover, UVB is considered the most mutagenic and carcinogenic since it is absorbed directly by the DNA; by contrast, UVA hardly causes directly DNA damage and only endogenous or exogenous chromophores through photosensitized reactions can cause DNA damage.

Therefore, photochemical processes leading to DNA lesions can be rationalized into two types of pathways: those involving direct absorption by DNA and those involving photosensitizers. These photoreactions lead to the formation of dimeric pyrimidine photoproducts such as cyclobutane pyrimidine dimers (CPDs), pyrimidine (6-4) pyrimidone photoproducts (6-4PPs) and oxidative lesions such as 8-oxoGuanine (OG), 2,6-diamino-4-hydroxy-5-formamidopyrimidine (FapyG), 5,6-dihydroxy-5,6-dihydrothymine (Tg), 5-hydroxymethyluracil (HmU) and 5-formyluracil (ForU) as shown in Figure 1.2.

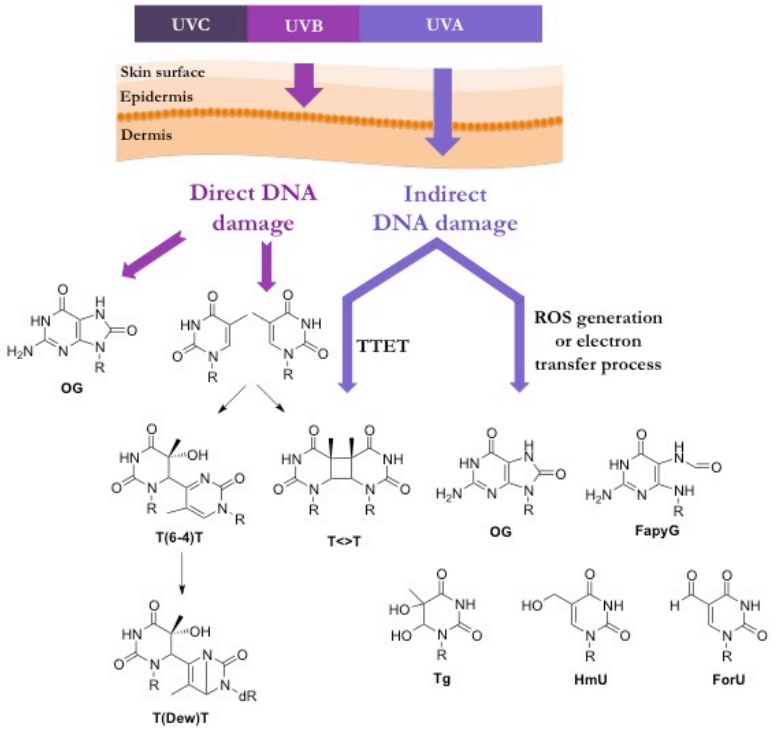

Figure 1.2. DNA lesions induced: (i) by direct absorption of UV (left) and (ii) by photosensitization (right).

1.2.1. Direct DNA damage

DNA damage induced by UVC and UVB radiation is dominated by bipyrimidine photoproducts although adenine dimers and pyrimidine photohydrates are formed as well to a much lesser extent.[17] The formation of oxidation products, more specifically OG (Figure 1.2), is also induced through photoionization in cellular DNA in a lower yield than bipyrimidine photoproducts, which agrees with the fact that guanine exhibits the lowest ionization potential among the DNA bases.[18-19]

UVB is considered the most mutagenic spectral region since it is absorbed directly by the DNA; however, UVA irradiation may also induce CPDs by direct absorption

but the yield is two or three orders of magnitude lower than for UVB and even larger than for OG in human skin.[20-21]

Therefore, *cis-syn* CPDs at TT site (T<>T in Figure 1.2) and 6-4PPs (T(6-4)T in Figure 1.2) are the main categories of bipyrimidine photoproducts resulting from UVB absorption that causes intranucleotide cross-linking by pyrimidine dimerization.[22-23] CPDs, the most frequent type of pyrimidine dimers, are formed by [2+2] cycloaddition reaction between the C5-C6 double bonds of two adjacent pyrimidine bases (i.e. TT or TC, Scheme 1.5) and they are obtained in a relatively low quantum yield (ca. 2%) in a few picoseconds, as shown by time-resolved measurement in single-stranded DNA.[24-25] Their formation involves the $\pi\pi^*$ excited state; however, the multiplicity of the excited state, S or T, is still under discussion.

The stereochemistry of the resulting bypirimidine photoproduct is governed by structural features of DNA duplex in B conformation, which is the most common in Nature. Therefore, the predominant CPD isomer is the *cis–syn* where two adjacent bases show a parallel orientation and are located on the same side with respect to the cyclobutane ring. Besides, CPD formation is influenced by the sequence context[26] as it is formed exclusively at dipyrimidines and preferentially at TT sites. The efficiency of CPD formation at different dipyrimidine sequences is estimated at a ratio of 55:33:11:1 for 5'-TT > 5'-TC > 5'-CT > 5'-CC.[27]

In addition, cytosine containing CPD lesions are particularly mutagenic since they exhibit a deamination reaction by hydrolysis to give the corresponding uracil compounds (T<>U in Scheme 1.5). The original cytosine should lead to the incorporation of guanine upon replication; but uracil would miscode for an adenine like thymine does, giving transition mutations denominated T → C at TC sites and the tandem mutation CC → TT.[28]

6-4PPs are produced by a [2+2] Paternò-Büchi cycloaddition between the C5-C6 double bond of the 5′-end pyrimidine and the C4 carbonyl group of a 3′-end thymine or the C4 imino group of a 3′-end cytosine in a tautomeric form (Scheme 1.5).[29] This reaction in DNA is proposed to occur via singlet excited state as 6-4PPs are only observed by direct irradiation and not by photosensitized triplet-triplet energy transfer (TTET).

The intermediates of the photoreaction are oxetanes or azetidines (T(ox)T or T(azt)C in Scheme 1.5), depending on whether thymine or cytosine is the 3′-end base. Both unstable intermediates are converted into their respective 6-4PPs that exhibit a 3′-end pyrimidone ring whose C4 substituent has migrated to the C5 position of the pyrimidine moiety. Furthermore, 6-4PPs can be converted to Dewar valence isomers (Dews) by a 4π electrocyclization through a singlet excited state intermediate. The formation of these photoproducts results from the presence of the pyrimidone chromophore, which absorbs photons with a maximal efficiency at around 320 nm.

6-4PPs are produced in lower yields than CPDs, being of 1:2 and 1:8 depending on the detection methods and bipyrimidine sequences.[30] Although 6-4PPs are formed in TT, TC, CT and CC sequences, they occur preferentially at TC sequences in similar yield than CPDs in TC sequences. By contrast, CT and CC sites are much less susceptible to these UVB-photoreactions.

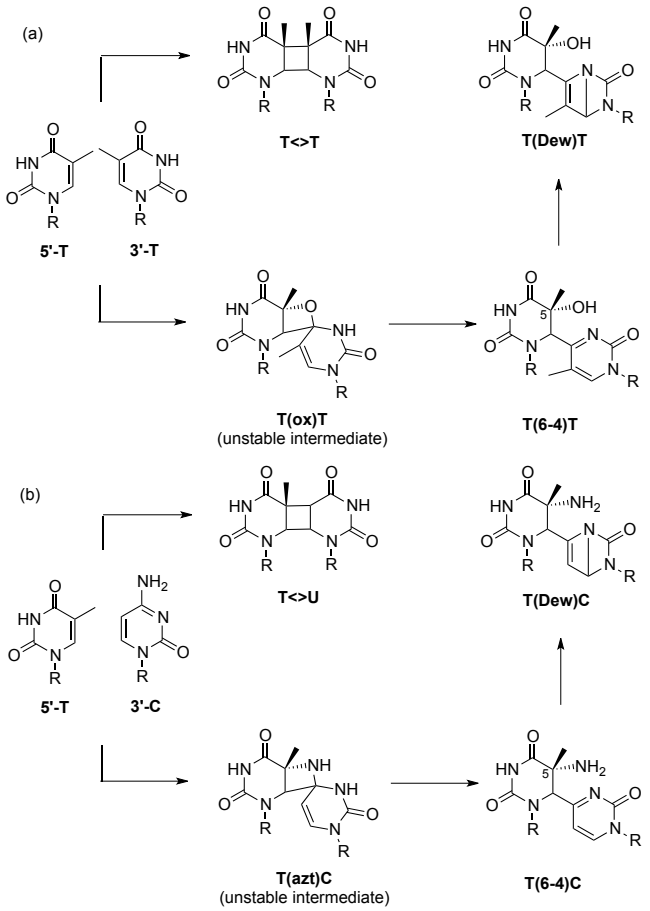

Scheme 1.5. Mechanism of CPDs and 6-4PPs formation for (a) TT and (b) TC sequences.

1.2.2. Indirect DNA damage

As mentioned before, DNA hardly absorbs in the UVA range thus most of UVA photoproducts are formed through indirect photosensitized mechanisms after light absorption by endogenous (flavin derivatives, porphyrins, specific vitamins, etc) or exogenous chromophores present in drugs, cosmetic agents, metabolites, etc. These photoreactions are generally induced by the triplet excited state of the photosensitizer ($^3PS^*$) which is longer lived than the singlet excited state. Therefore, three DNA pho-

tosensitization mechanisms can occur; two of them involve the oxidation of DNA nucleobases by electron transfer and reactive oxygen species (ROS), and the third one involves the formation of CPDs by an energy transfer process (Scheme 1.6).

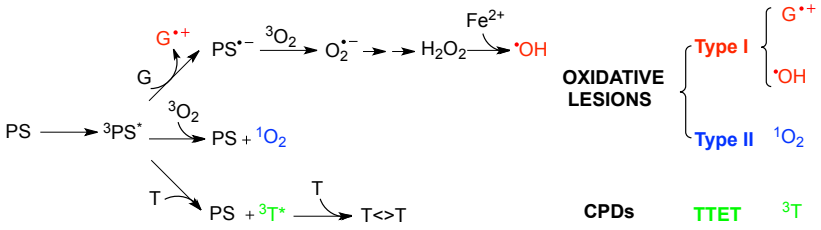

Scheme 1.6. The three different UVA photosensitization mechanisms involved in DNA: (i) one-electron oxidation from PS or addition of •OH (Type I), (ii) addition of singlet oxygen (Type II) and (iii) triplet-triplet energy transfer process (TTET).

Oxidative lesions generally arise from two types of mechanisms, called Type I and Type II processes (Scheme 1.6).[31] Type I mechanism involves one-electron oxidation by an excited chromophore, which generally leads to the formation of a radical cation of the DNA base and a radical anion of the photosensitizer (Scheme 1.6). Thus, the efficiency of this photoreaction is forced by the oxidation potential of the photosensitizer. In DNA, guanine is the main target as it exhibits the lowest ionization potential among DNA nucleobases. After an electron abstraction, guanine is converted into a radical cation ($G^{\bullet+}$) that may evolve into several products. The main pathway is hydration into the 8-hydroxy-7,8-dihydroguanyl radical (Scheme 1.7), which can be converted to OG and FapyG by a competitive one-electron oxidation or one-electron reduction, respectively.[32]

Type I photosensitization mechanism may also involve the formation of the highly reactive hydroxyl radicals ($^{\bullet}OH$), see Scheme 1.6.[29] They are obtained after release of superoxide anion $O_2^{\bullet-}$, which comes from the reaction of the photosensitizer radical anion with molecular oxygen or by release from mitochondria in response to UVA irradiation.[33] Since $O_2^{\bullet-}$ is poorly reactive with DNA, it can be converted by

spontaneous reaction or by superoxide dismutase enzyme into hydrogen peroxide (H_2O_2), followed by a redox process with Fe^{2+} or Cu^{+}, known as Fenton reaction, to give $^{\bullet}OH$. UVA has also been shown to release Fe^{2+} from ferritin that favors the Fenton reaction.[34]

By contrast to one-electron oxidation, $^{\bullet}OH$ does not show any specificity and reacts with all the components of DNA.[35] Therefore, the reaction of $^{\bullet}OH$ with purine bases leads to OG and FapyG for guanine (Figure 1.2) and 8-oxo-7,8-dihydroadenine and 4,6-diamino-5-formamidopyrimidine for adenine through formation of C8-hydroxylated radicals (Scheme 1.7). Regarding to pyrimidine bases, $^{\bullet}OH$ reacts with the C5–C6 double bond, leading to the formation of Tg and 5,6-dihydroxy-5,6-dihydrocytosine or with the methyl group of thymine leading to HmU and ForU (Figure 1.2). Besides, $^{\bullet}OH$ reacts with the 2-deoxyribose moieties by hydrogen abstraction leading to DNA strand breaks.[36]

A second oxidative pathway, denominated Type II, involves the production of singlet oxygen ($^1O_2$) that results from energy transfer from the triplet excited photosensitizer to molecular oxygen (Scheme 1.6). These reactive species show strong affinity for molecules rich in double bonds, giving rise to dioxetanes, endoperoxides or ene-oxidation products. In DNA, guanine is the only target, that is converted into a 4,8-endoperoxide through Diels Alder [4+2] photocycloaddition reaction, followed by a rearrangement and reduction to give OG (Scheme 1.7).[37]

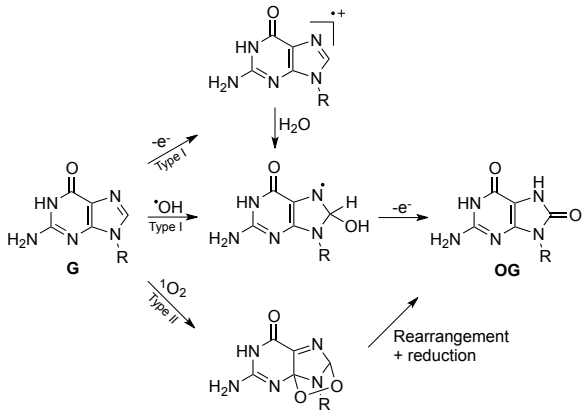

Scheme 1.7. The main mechanisms leading to the formation of OG from G. From top to bottom: (i) electron abstraction followed by hydration of the resulting radical cation, (ii) formation of a reducing radical by addition of •OH radical, and (iii) formation of an endoperoxide by addition of singlet oxygen.

In contrast to the abovementioned UVA photosensitized mechanisms leading to oxidative lesions, the third one involves the formation of CPDs through triplet-triplet energy transfer (TTET, Scheme 1.6).[8] This photoreaction requires an endogenous or exogenous chromophore that efficiently absorbs UVA, that has a high energy of triplet state and a large ISC quantum yield to convert the singlet into the triplet excited state. Under these conditions, a TTET can take place from the excited photosensitizer to a nearby DNA base, being thymine the main target because of its low-lying triplet excited state, which leads to the formation of CPDs.[38] Exogenous chromophores such as anti-inflammatory compounds or antibacterial agents of the fluoroquinolone family are potent TTET photosensitizers and have an important impact in human health.[39-40] Recently, our group reported that 6-4PPs and ForU lesions are able to act as DNA endogenous sensitizers. It was found that pyrimidone chromophore in 6-4PP lesion and ForU absorb in UVA, and that the high energy of their triplet and high ISC, allow phototriggering the [2+2] cycloaddition between two adjacent thymines.[41-42]

1.3. DNA repair

When they are not repaired correctly, the UV lesions inhibit DNA replication and transcription, leading to cell death or mutagenesis and carcinogenesis.[14-15] To maintain their genetic integrity, organisms have developed various DNA repair mechanisms, which can be divided into two general classes: (1) the dark excision pathway such as nucleotide excision repair[43] or base excision repair[44] that removes the damaged bases and replaces them with newly synthesized DNA and (2) light triggered repair that is catalyzed by photoactivated enzymes called DNA photolyases.[45]

1.3.1. Nucleotide excision repair

Nucleotide excision repair (NER) removes a wide range of structurally unrelated DNA lesions that signiticantly modify the tridimensional structure of DNA double helix such as CPDs and 6-4PPs, bulky chemical adducts, DNA-intrastrand crosslinks, and some oxidative lesions. NER operates through a "cut-and-patch" mechanism by excising and removing a short stretch of DNA (24 to 32 nucleotides long) containing the lesion, which is restored using the nondamaged strand of the DNA double helix as a template (Figure 1.3). Then, the resulting gap is filled by DNA polymerases and sealed by a DNA ligase enzyme. Two pathways (TCR[46] or GGR[47]) depending on the DNA damage signalling step are involved, being TCR much faster than GGR. However, TCR is limited to the lesions present in the transcribed strand of active genes and GGR removes lesions in the whole genome with a lower efficiency. For bypirimidine lesions, GGR removes 6-4PPs and Dews faster than CPDs because of significant perturbations induced in the duplex by the cyclobutane structure.[48-49] In cultured cells, 6-4PPs are typically removed within a few hours while CPDs can be found three days after exposure, being the repair rate even slower in skin. Moreover, the four CPDs are repaired at different rates: CT < CC < TC < TT.[50]

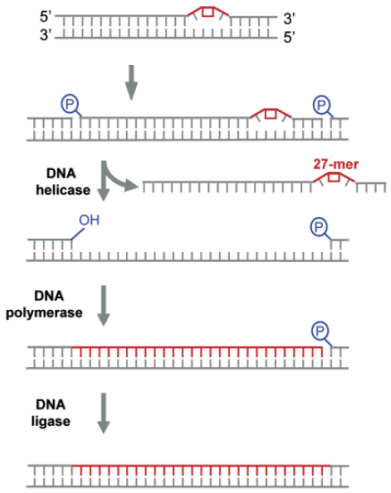

Figure 1.3. Repair mechanism of UV photoproducts by nucleotide excision repair.

1.3.2. Base excision repair

Base excision repair (BER) removes small DNA modifications such as oxidized or methylated bases through N-glycosylases action.[51] These enzymes are substrate-specific and each recognizes a limited number of modified bases such as OG for OGG1 or oxidized pyrimidines for NTHL1 and NEIL1 glycosylases. After binding to the modified bases, glycosylases cleave the N-glycosidic bond, leaving an abasic site in DNA. This is then cleaved by an endonuclease, in particular APE1, leaving a one-nucleotide gap with a 3′-end OH and a 5′-end ribosyl-phosphate. The resulting single-strand break can be repaired by a short-patch (where a single nucleotide is replaced) or long-patch BER (where 2-10 new nucleotides are synthesized) using the complementary strand as a template. By contrast with NER, BER is a fast system, which repairs single-strands breaks in less than one hour and OG in a few hours after exposure to UVA.[52]

1.3.3. Photoreactivation

By contrast to NER, photoreactivation repairs bypirimidine lesions by means of a specific class of flavoprotein and photoenzyme called photolyase that uses sunlight as energy source and only involves a protein to recognize and repair the lesion. Two types of photolyase with similar sequences and folding structure specifically repair the two bypirimidine photoproducts upon the absorption of blue light. They are classified as CPD or as (6-4) photolyases.[45, 53] CPD photolyases have been found in diverse groups such as archaea, bacteria, fungi, viruses, plants, invertebrates, and many vertebrates including aplacental mammals, whereas, (6-4) photolyases have been determined in certain organisms like *Drosophila*, silkworm, *Xenopus laevis*, and rattlesnakes. However, photolyases are absent in humans and other placental mammals although they keep homologs flavoproteins denominated cryptochromes, which are involved in various blue light-regulated functions, but typically do not repair DNA.[54-55]

Therefore, CPD or (6-4) photolyases are homologous monomeric proteins of 450-550 amino acids that contain a non-covalently bound flavin adenine dinucleotide (FAD) chromophore, which can be found in three redox states denominated fully oxidized (FAD_{ox}), semi-reduced ($FADH^{\bullet}$) and fully reduced ($FADH^{-}$, Figure 1.4) forms. Among them, the fully reduced $FADH^{-}$, which absorbs 350–500 nm light, is the repair-active form, which is essential for specifically binding to damaged DNA and for catalysis.[56] FAD_{ox} and $FADH^{\bullet}$ can be converted to $FADH^{-}$ through intraprotein electron transfer (ET) photoreaction called photoactivation that involves a chain of three tryptophan residues.[57] Moreover, photolyases present a second chromophore, 8-hydroxy-5-deazaflavin (8-HDF, Figure 1.4) or methenyltetrahydrofolate (MTHF, Figure 1.4), which acts as a light-harvesting antenna with a higher extinction coefficient than $FADH^{-}$ thereby increasing the effective absorption cross section of the enzyme by a transfer of excitation energy to the catalytic FAD cofactor.[58]

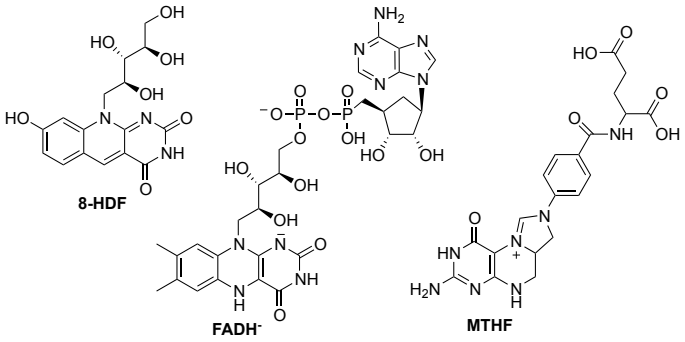

Figure 1.4. The structure of the non-covalently bound chromophores of a photolyase.

The photorepair mechanism by CPD photolyase has been fully established. The initial step consists in the absorption of a photon by the chromophore 8-HDF or MTHF, followed by energy transfer to the $FADH^-$ chromophore. Then, the photoexcited $FADH^-$ donates an electron to the CPD, inducing ring splitting of the C-C bonds to restore the two intact pyrimidines. By contrast of CPD photolyase mechanism, repair of 6-4PPs is chemically more challenging because cleavage of the C-C bond between the 5' and 3' pyrimidine nucleobases alone would yield two damaged nucleobases, thus an additional back transfer of a functional group (OH or NH_2) from the 5' to the 3' nucleobase must take place.

1.3.3.1 CPD photolyase mechanism

As mentioned before, CPD photolyase mechanism has been established and all steps have been described by means of ultrafast time-resolved spectroscopies.[59-62] The photoreaction may be summarized as follows (Scheme 1.8). Prior to repair, CPD photolyase binds to DNA and flips the CPD lesion out of the DNA duplex[63] into the active site cavity where FAD is buried to make a stable enzyme-substrate complex and ensure an efficient ET between CPD and the FAD cofactor. After photoexcitation of FAD in its fully reduced $FADH^-$ form, an electron is tranferred to the CPD in 250 ps,

leading to the semireduced radical $FADH^{\bullet}$ and to the radical anion of the CPD, which rapidly splits in 90 ps and rearranges into one intact base and the radical anion of the other base. After the dimer splitting, an electron is transferred back to $FADH^{\bullet}$ to regenerate the second base and the catalytically form $FADH^{-}$ in 700 ps.[64] Then, the CPD photolyase releases the repaired bypirimidine lesion from the binding pocket in ~50 μs[65], and can bind and repair another CPD.

The photorepair mechanism is a monophotonic process with a high quantum yield of 0.7-0.9,[45] which suggests non-negligible competition between CPD splitting (90 ps) and back electron transfer from $FADH^{\bullet}$ to $FADH^{-}$, which happens on a nanosecond timescale (2.4 ns). Although the CPD repair mechanism has been determined, the exact quantum yield and the rate of unproductive back electron transfer (2.4 ns or 350 ps) are still under discussion.[66-67]

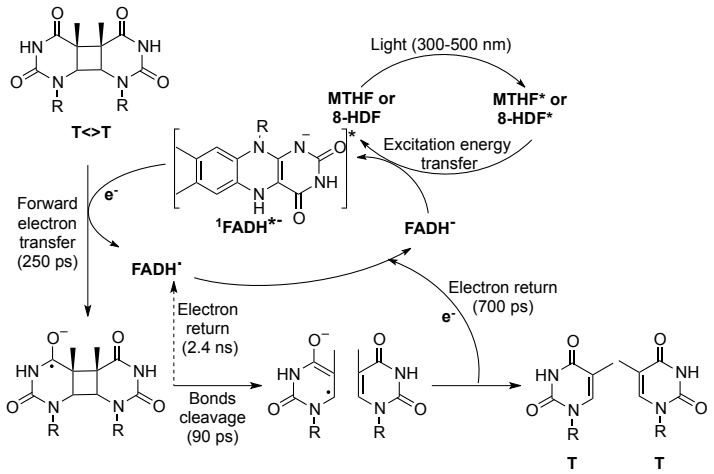

Scheme 1.8. Photorepair mechanism of CPD lesions by CPD photolyases.

1.3.3.2 (6-4) photolyase mechanism

Two main reasons attracted the interest for the repair of 6-4PPs. First, (6-4) photolyases restore (6-4) photolesions but with a lower quantum yield of repair of ca. 0.1 compared to that of CPD lesion of ca. 0.7-0.9.[45] Secondly, whereas the two-step retro-[2+2] cycloaddition reaction of the CPD lesion leads to the repaired nucleobases, the restoration of (6-4) lesions is structurally and chemically more challenging, as it requires an OH or NH_2 group transfer from 5' to the 3' nucleobase. By contrast with the CPD photolyase mechanism, researchers are still addressing the question of how (6-4) photolyases perform such return of the OH or NH_2 group, and several mechanisms have been proposed until now.

- **Thermal oxetane mechanism**

The strong structural similarity between (6-4) and CPD photolyases suggests an analogy in the photorepair mechanisms for (6-4) and CPD lesions. Therefore, it was initially proposed, that upon binding to the lesion, (6-4) photolyases first catalyze the formation of a four-membered ring intermediate (oxetane or azetidine), similar to the cyclobutane for CPDs, by a thermal reaction in the dark (Scheme 1.9).[45] Then, the splitting of this intermediate to the repaired pyrimidine bases would follow just as for CPD photolyases, by ET from the excited fully reduced $FADH^-$ to the lesion.

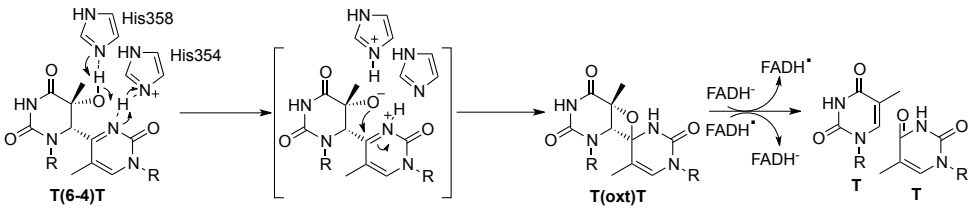

Scheme 1.9. First repair mechanism proposed for 6-4PP.

Although theoretical studies indicate that the formation of oxetane intermediate is energetically rather unfavorable for an enzyme,[68] the identification of two histidines (His) residues (His358 and His354) in the binding pocket, which are crucial for catalysis, would provide sufficient energy to close the four-membered ring intermediate by proton transfer.[69] The His residue may protonate the (6-4) photoproduct, or at least form a strong H-bond with the N3 of the 3' residue to generate a highly electrophilic iminium ion, which can be attacked by the OH or NH_2 group to form the oxetane or azetidine intermediate.

- **Non-oxetane mechanism**

In 2008, a new photorepair mechanism was postulated based on the crystal structures of *Drosophila melanogaster* (6-4) photolyase bound to a 15-mer DNA duplex containing a central T(6-4)T lesion before and after *in situ* repair.[70-71] The crystal structure before repair revealed that the lesion was flipped out of the double helix into the binding pocket of the enzyme, in a similar way to the CPD case, together with the conservation of histidines His365 and His369, which are essential for catalysis, and of a tyrosine residue (Y423). Unexpectedly, oxetane intermediate was not catalyzed in the dark by these amino acids through the abovementioned proton transfer since the lesion showed its original T(6-4)T structure. Moreover, the crystal of the enzyme-substrate after repair, using white light and dithionite as reducing agent, showed a repaired T-T in the active site with almost no change in the position of the amino residues located in the close vicinity to the lesion.[70] Therefore, the structural data of the complex enzyme-substrate before and after *in situ* repair does not support the oxetane-based mechanism assumed previously and a direct ET from $FADH^-$ to the 6-4PP was proposed, see Scheme 1.10.

Therefore, after ET from a photoexcited $FADH^-$, a radical anion of the 6-4PP is formed and a C5-OH or a C5-NH_2 is converted into a better leaving group by His365 through protonation. After that, the protonated transient NH_3 group or water mole-

cule released in C5 attacks the acylimine in C4' and it rapidly fragments to give the repaired T-T, accompanied by back electron transfer to $FADH^{\bullet}$ and loss of a proton. However, this "transient water pathway" was not supported by computational studies because of a high activation barrier, but variants of this mechanism are still under discussion.[72]

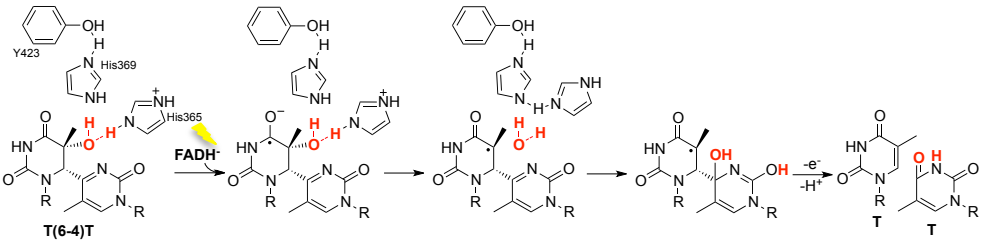

Scheme 1.10. First non-oxetane repair mechanism of 6-4PP by (6-4) photolyase. This pathway involves the formation of a transient water molecule, indicated in red.

In 2010, a modified mechanism by the (6-4) photolyases of *Arabidopsis thaliana* was postulated. This time, ultrafast fluorescence and transient absorption spectroscopy supports the formation of an oxetane or azetidine structure as short-lived species.[73] In this alternative mechanism, the main steps are the initial electron transfer from the excited reduced $FADH^{-}$ to the 6-4PP in 225 ps (similar to the photorepair reaction of CPD)[64] and the following proton transfer from protonated His364 in 425 ps. A transient zwitterion is generated where an oxygen-atom can attack the C4 position at the 3' base to form a transient oxetane structure, which rearranges to the repaired pyrimidine bases with electron return to $FADH^{\bullet}$, see Scheme 1.11. This last step takes place on a timescale of tens nanoseconds, it is much longer than for CPD case where repair is completed by electron return to $FADH^{\bullet}$ in 700 ps.

In addition, $FADH^{\bullet}$ radicals formed by the initial ET were re-reduced very quickly (in 50 ps) by back ET by contrast to CPD (in 2.4 ns). These findings revealed that the reason for the low repair quantum yield of (6–4) photolyase of ca. 0.1 is the

fast back electron transfer compared to the proton transfer step (of ca. 425 ps), which suggests that it is the critical step in the (6-4) lesion repair mechanism.

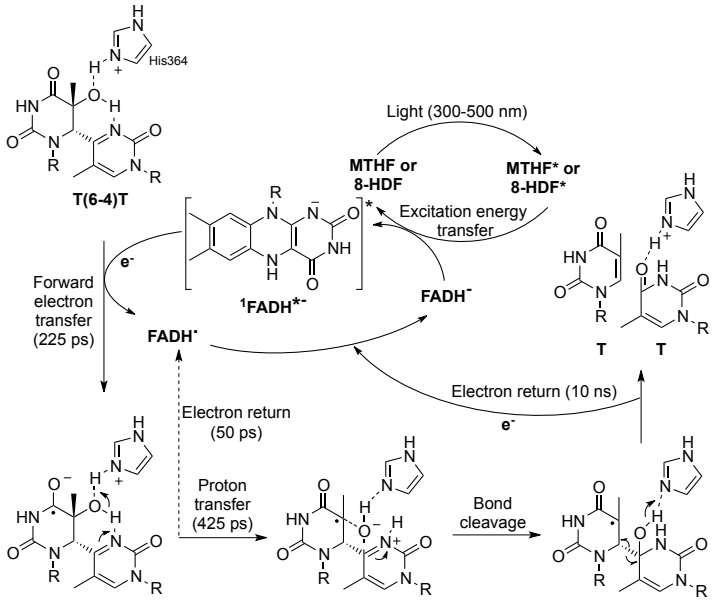

Scheme 1.11. Repair photocycle of (6-4)PP by (6-4) photolyase of *Arabidopsis thaliana*.[73]

- **Two photon mechanism**

Theoretical and experimental studies assumed that the (6-4) and CPD photolyase mechanisms are a monophotonic process where FAD cofactor absorbs only a single photon. However, the possibility of a two-photon process has been reported by a computational study in 2010.[74] They suggested that a first ET from $FADH^-$ converts T(6-4)T to the oxetane; followed by a second ET from $FADH^-$ to split the oxetane ring into the two intact thymines with the return of the electron.

In this context, in 2013 an experimental two-photon process was proposed to the repair of a T(6-4)T by *Xenopus laevis* (6-4) photolyase under single turnover flash experiments.[75] They observed that a first ET converts T(6-4)T into an intermediate X,

which absorbs at shorter wavelengths than the T(6-4)T, and with a lifetime long enough (100 s) to allow the absorption of a second photon that converts X to the final repaired product (Scheme 1.12). Interestingly, the quantum yield that they obtained for the conversion of X to intact thymines was 0.5-1, which is similar to the repair quantum yield of CPD photolyase. This analogy of cycloreversion of the four-membered ring by CPD and (6-4) photolyases made them suggest that X might be the oxetane ring intermediate. Therefore, a new mechanism that involves an oxetane ring intermediate was proposed although a positive proof of this intermediate is still lacking.

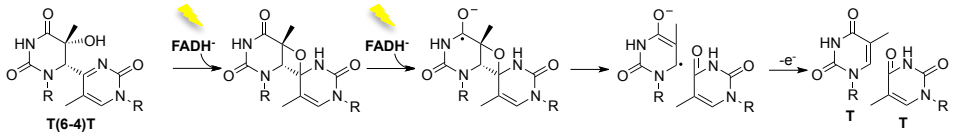

Scheme 1.12. First experimental repair mechanism of (6-4)PP by (6-4) photolyase through two photon process.

1.3.3.2.1 Investigation of the (6-4) repair mechanism with model compounds

As mentioned before, photorepair of (6-4) DNA lesions by photolyases involved a photoinduced electron transfer (PET) from FAD cofactor to the bipyrimidine lesion; however, a critical issue is whether (photo)chemical conversion of the 6-4PPs to oxetanes or azetidines is a necessary step. Besides, calculations at various levels of theory,[76] questioned the ability of the (6-4) photolyase to form the oxetane and azetidine intermediates during the repair reaction because the enormous energy necessary to run the reaction is too high for an enzyme. Unfortunately, the oxetane or azetidine intermediate involved in the proposed mechanism does not seem to be stable above -80ºC, making their characterization difficult.[77]

In this context, model systems have been developed to gain insight into the ET and ring opening of these four-member ring heterocycles. Stable oxetane adducts (ox, Figure 1.5), formed between benzophenone and thymine by Pàterno-Büchi reaction, have been reported to reverse by PET in the presence of various electron donors, which makes the theory of oxetane intermediate chemically feasible.[78] Moreover, laser flash photolysis and steady-state studies with thymine oxetane adducts provided additional support for the facile cleavage of the oxetane anionic radical.[78-80] The strongest support came from the investigation of photoinduced cycloreversion of an oxetane ring covalently linked to flavin (ox-flav, Figure 1.5).[81] In this model system, it was found that the cycloreversion is only possible through the reductive pathway with the flavin in its reduced and deprotonated state.

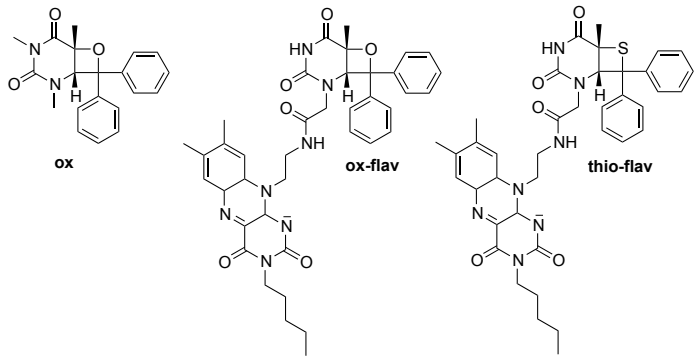

Figure 1.5. Oxetane and thiethane models studied by PET.

In contrast to the oxetane or azetidine intermediate, its sulfur analog, a thietane, formed by 360 nm irradiation of a dinucleotide 5'-*O*-thymidylyl-4-thiothymidine, was reported to be moderately stable and to interconvert with the corresponding s^5-(6-4)PP at room temperature (Scheme 1.13).[82]

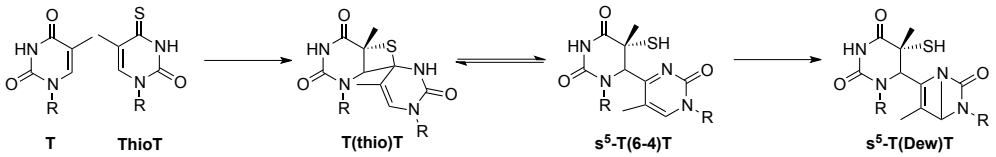

Scheme 1.13. Mechanism formation of thio analog of 6-4PP.

Longer irradiation time led to the total conversion of compound s^5-T(6-4)T into its Dewar valence isomer s^5-T(Dew)T. Indeed, T(thio)T and s^5-T(6-4)T consisted of a mixture of two slowly interconverting compounds in a 3/1 ratio. The thietane structure was evidenced by ^{1}H NMR since the chemical shift of the H6 proton of the T unit of T(thio)T is at 6.30 ppm, which is very similar to the value (6.10 ppm) of the H6 proton of a model thietane obtained by irradiation of 1,3-dimethyl-4-thiothymine in the presence of methacrylonitrile.[83]

In order to investigate if the enzymatic repair reaction with (6-4) photolyases could occur, a stable thiethane intermediate T(thio)T was inserted in an oligonucleotide d(GTATs^{4}TATG). It was shown that T(thio)T is not enzymatically repaired by *Drosophila* (6-4) photolyases, this can be attributed to inefficient binding rather than to lack of ET reactivity.[84] The lack of binding might also be due to substantial structural differences that result from differences in the lengths of C-S and either C-O or C-N bonds (1.8 versus 1.5 Å). However, the methyl s^5-T(6-4)T, which presumably cannot form the thiethane intermediate, bound the enzyme with high affinity and it was repaired sucessfully.

In this context, to support that thietanes could be cleaved by single electron donation, the cycloreversion of a stable thiethane (thio-flav, Figure 1.5), formed between thymine and thiobenzophenone and covalently linked flavin moiety, has been achieved by intramolecular PET.[85] As shown for the oxetane case, the cycloreversion required the flavin in its reduced and deprotonated state.

1.4. References

1. Jablonski, A. Z., Über den mechanismus der photolumineszenz von farbstoffphosphoren. *Phys.* **1935,** *94*, 38-46.

2. Speiser, S., Photophysics and mechanisms of intramolecular electronic energy transfer in bichromophoric molecular systems: solution and supersonic jet studies. *Chem. Rev.* **1996,** *96*, 1953-1976.

3. Kavarnos, G. J.; Turro, N. J., Photosensitization by reversible electron transfer: theories, experimental evidence and examples. *Chem. Rev.* **1986,** *86*, 401-449.

4. Weller, A., Photoinduced electron transfer in solution: exciplex and radical ion pair formation free enthalpies and their solvent dependence. *Phys. Chem. Neue Folge.* **1982,** *133*, 93-98.

5. Griesbeck, A.; Oelgemöller, M.; Ghetti, F., *CRC Handbook of Organic Photochemistry and Photobiology. 3rd Ed.* **2012**, 95-118.

6. Bach, T., Stereoselective intermolecular [2+2] photocycloaddition reactions and their application in synthesis. *Synthesis* **1998,** *5*, 683-703.

7. Schuster, D. I.; Lem, G.; Kaprinidis, N. A., New insights into an old mechanism: [2+2] photocycloaddition of enones to alkenes. *Chem. Rev.* **1993,** *93*, 3-22.

8. Cuquerella, M. C.; Lhiaubet-Vallet, V.; Bosca, F.; Miranda, M. A., Photosensitised pyrimidine dimerisation in DNA. *Chem. Sci.* **2011,** *2*, 1219-1232.

9. Buchi, G.; Inman, C. G.; Lipinsky, E. S., Light-catalyzed organic reactions. I. The reaction of carbonyl compounds with 2-methyl-2-butene in the presence of ultraviolet light. *J. Am. Chem. Soc.* **1954**, 4327-4331.

10. Paterno, E., Organic synthesis induced by light. Introductory note. *Gazz. Chim. Ital.* **1909,** *39*, 237-250.

11. Freilich, S. C.; Peters, K. S., Observation of the 1,4 biradical in the Paterno-Buchi reaction. *J. Am. Chem. Soc.* **1981,** *103*, 6255-6257.

12. Sampedro, D., Computational exploration of the photocycloaddition of imines to alkenes. *ChemPhysChem* **2006,** *7*, 2456-2459.

13. McKenzie, R. L.; Aucamp, P. J.; Bais, A. F.; Björn, L. O.; Ilyas, M.; Madronich, S., Ozone depletion and climate change: impacts on UV radiation. *Photochem. Photobiol.* **2011,** *10*, 182-198.

14. Melnikova, V. O.; Ananthaswamy, H. N., Cellular and molecular events leading to the development of skin cancer. *Mutat. Res.* **2005,** *571*, 91-106.

15. Coohill, T. P.; Peak, M. J., The effects of the ultraviolet wavelengths of radiation present in sunlight on human cells in vitro. *Photochem. Photobiol.* **1987,** *46*, 1043-1050.

16. Schuch, A. P.; Machado, C. C.; Makita, K.; Martins, C. F., DNA damage as a biological sensor for environmental sunlight. *Photochem. Photobiol.* **2013,** *12*, 1259-1272.

17. Cadet, J.; Sage, E.; Douki, T., Ultraviolet radiation-mediated damage to cellular DNA. *Mutat. Res.* **2005,** *571*, 3-17.

18. Kielbassa, C.; Roza, L.; Epe, B., Wavelength dependence of oxidative DNA damage induced by UV and visible light. *Carcinogenesis* **1997,** *18*, 811-816.

19. Gomez, M.; Banyasz, A.; Douki, T.; Markovitsi, D.; Ravanat, J., Direct oxidative damage of naked DNA generates upon absorption of UV radiation by nucleobases. *J. Phys. Chem. Lett.* **2016,** *7*, 3945-3948.

20. Mouret, S.; Baudouin, C.; Charveron, M.; Favier, A.; Cadet, J.; Douki, T., Cyclobutane pyrimidine dimers are predominant DNA lesions in whole human skin exposed to UVA radiation. *Proc. Natl. Acad. Sci.* **2006,** *103*, 13765-13770.

21. Mouret, S.; Philippe, C.; Chantegrel, J.; Banyasz, A.; Karpati, S.; Markovitsi, D.; Douki, T., UVA-induced cyclobutane pyrimidine dimers in DNA: a direct photochemical mechanism? *Org. Biomol. Chem.* **2010,** *8*, 1706-1711.

22. Pfeiter, G. P., Formation and processing of UV photoproducts: effects of DNA sequence and chromatin environment. *Photochem. Photobiol.* **1997,** *62*, 270-283.

23. Yoon, J. H.; Lee, C. S.; O'Connor, T. R.; Yasui, A.; Pfeifer, G. P., The DNA damage spectrum produced by simulated sunlight. *J. Mol. Biol.* **2000,** *299*, 681-693.

24. Garcés, F.; Dávila, C. A., Alteration in DNA irradiated with ultraviolet radiation. The formation process of cyclobutylpyrimidine dimers: cross sections, action spectra and quantum yields. *Photochem. Photobiol.* **1982,** *35*, 9-16.

25. Schereier, W. J.; Schrader, T. E.; Koller, F. O.; Gilch, P.; Crespo-Hernández, C. E.; Swaminathan, V. N.; Carell, T.; Zinth, W.; Kohler, B., Thymine dimerization in DNA is a ultrafast photoreaction. *Science* **2007,** *315*, 625-629.

26. Tornaletti, S. R. D.; Pfeifer, G. P., The distribution of UV photoproducts along the human p53 gene and its relation to mutation in skin cancer. *Oncogene* **1993,** *8*, 2051-2057.

27. Douki T, C. J., Individual determination of the yield of the main UV-induced dimeric pyrimidine photoproducts in DNA suggests a high mutagenicity of CC photolesions. *Biochemistry* **2001,** *40*, 2495-2501.

28. Peng, W.; Shaw, B. R., Accelerated deamination of cytosine residues in UV-induced cyclobutane pyrimidine dimers leads to CC to TT transitions. *Biochemistry* **1996,** *35*, 10172-10181.

29. Cadet, J.; Mouret, S.; Ravanat, J.; Douki, T., Photoinduced damage to cellular DNA: direct and photosensitized reactions. *Photochem. Photobiol.* **2012,** *88*, 1048-1065.

30. Ravanat, J. L.; Douki, T.; Cadet, J., Direct and indirect effects of UV radiation on DNA and its components. *J. Photochem. Photobiol. B: Biol.* **2001,** *63*, 88-102.

31. Foote, C. S., Definition of Type I and Type II. *Photochem. Photobiol.* **1991,** *54*, 659.

32. Cadet, J.; Douki, J.; Ravanat, J.; Mascio, P., Sensitized formation of oxidatively generated damage to cellular DNA by UVA radiation. *Photochem. Photobiol.* **2009,** *8*, 903-911.

33. Gniadecki, R. T.; Thorn, T.; Vicanova, J.; Petersen, A. B.; Wulf, H. C., Role of mitochondria in ultraviolet-induced oxidative stress. *J. Cell. Biochem.* **2000,** *80*, 216-222.

34. Pourzand, C.; Watkin, R. D.; Brown, J. E.; Tyrell, R. M., Ultraviolet A radiation induces immediate release of iron in human primary skin fibroblasts: the role of ferritin. *Proc. Natl. Acad. Sci.* **1999,** *96*, 6751-6756.

35. Cadet, J.; Delatour, T.; Douki, T.; Gasparutto, D.; Pouget, J.; Ravanat, J.; Sauvagio, S., Hydroxyl radicals and DNA base damage. *Mutation Research* **1999,** *424*, 9-21.

36. Pogozelski, W. K.; Tullius, T. D., Oxidative strand scission of nucleic acids: routes initiated by hydrogen abstraction from the sugar moiety. *Chem. Rev.* **1998,** *98*, 1089-1107.

37. Cadet, J.; Ravanat, J. L.; Martinez, G. R.; Medeiros, M. H.; Mascio, P., Singlet oxygen oxidation of isolated and cellular DNA: product formation and mechanistic insights. *Photochem. Photobiol.* **2006,** *82*, 1219-1225.

38. Bosca, F.; Lhiaubet, V.; Cuquerella, M. C.; Castell, J. V.; Miranda, M. A., The triplet energy of thymine in DNA. *J. Am. Chem. Soc.* **2006,** *128*, 6318-6319.

39. Cuquerella, M. C.; Lhiaubet-Vallet, V.; Cadet, J.; Miranda, M. A., Benzophenone photosensitized DNA damage. *Acc. Chem. Res.* **2012,** *45*, 1558-1570.

40. Lhiaubet-Vallet, V.; Cuquerella, M. C.; Castell, J. V.; Bosca, F.; Miranda, M. A., Triplet excited fluoroquinolones as mediators for thymine cyclobutane dimer formation in DNA. *J. Phys. Chem. B* **2007,** *111*, 7409-7414.

41. Vendrell-Criado, V.; Rodríguez-Muñiz, G. M.; Cuquerella, M. C.; Lhiaubet-Vallet, V.; Miranda, M. A., Photosensitization of DNA by 5-methyl-2-pyrimidone deoxyribonucleoside: (6-4) photoproduct as a possible Trojan horse. *Angew. Chem. Int. Ed.* **2013,** *52*, 1-5.

42. Aparici-Espert, I.; Garcia-Lainez, G.; Andreu, I.; Miranda, M. A.; Lhiaubet-Vallet, V., Oxidatively generated lesions as internal photosensitizer for pyrimidine dimerization in DNA. *ACS Chem. Biol.* **2018,** *13*, 542-547.

43. Le May, N. E., J. M.; Coin, F., True lies: the double life of the nucleotide excision repair factors in transcription and DNA repair. *J. Nucleic acids* **2010,** *2010*, 1-10.

44. Liu, Y. P., R.; Beard, W. A.; Kedar, P. S.; Hou, E. W.; Shock, D. D.; Wilson, S. H., Coordination of steps in single-nucleotide base excision repair mediated by apurinic/apyrimidinic endonuclease 1 and DNA polymerase beta. *J. Biol. Chem.* **2007,** *282*, 13532-13541.

45. Sancar, A., Structure and function of DNA photolyase and cryptochrome blue-light photoreceptors. *Chem. Rev.* **2003,** *103*, 2203-2207.

46. Fousteri, M.; Mullenders, L., Transcription-coupled nucleotide excision repair in mammalian cells: molecular mechanisms and biological effects. *Cell Research* **2008,** *18*, 73-85.

47. Gillet, L. C.; Schärer, O. D., Molecular mechanisms of mammalian global genome nucleotide excision repair. *Chem. Rev.* **2006,** *106*, 253-276.

48. Perdiz, D.; Grof, P.; Mezzina, M.; Nikaido, O.; Moustacchi, E.; Sage, E., Distribution and repair of bipyrimidine photoproducts in solar UV-irradiated mammalian cells. *J. Biol. Chem.* **2000,** *275*, 26732-26742.

49. Courdavault, S.; Baudouin, C.; Charveron, M.; Canguilhem, B.; Favier, A.; Cadet, J.; Douki, T., Repair of the three main types of bipyrimidine DNA photoproducts in human keratocytes exposed to UVB and UVA radiations. *DNA repair* **2005,** *4*, 836-844.

50. Mouret, S.; Charveron, M.; Favier, A.; Cadet, J.; Douki, T., Differential repair of UVB-induced cyclobutane pyrimidine dimers in cultured human skin cells and whole human skin. *DNA repair* **2008,** *7*, 704-712.

51. Hedge, M. L.; Hazra, T. K.; Mitra, S., Early steps in the DNA base excision/single-strand interruption repair pathway in mammalian cells. *Cell. Res.* **2008,** *18*, 27-47.

52. Surjana, D.; Halliday, G. M.; Damian, D. L., Nicotinamide enhances repair of ultraviolet radiation-induced DNA damage in human keratinocytes and *ex vivo* skin. *Carcinogenesis* **2013,** *34*, 1144-1149.

53. Sancar, A., Structure and function of photolyase and *in vivo* enzymology: 50th anniversary. *J. Biol. Chem.* **2008,** *283*, 32153-32157.

54. Sancar, A., No end of history for photolyases. *Science* **1996,** *272*, 48-49.

55. Chaves, I.; Pokomy, R.; Byrdin, M.; Hoang, N.; Ritz, T.; Brettel, K.; Essen, L. O.; van der Horst, G. T.; Batschauer, A.; Ahmad, M., The cryptochromes: blue light photoreceptors in plants and animals. *Annu. Rev. Plant. Biol.* **2011,** *62*, 335-364.

56. Kim, S. T. S., A.; Essenmacher, C.; Badcock, G. T., Time-resolved EPR studies with DNA photolyase: Excited-state $FADH_0$ abstracts an electron form Trp-306 to generate $FADH^-$, the catalytically active form of the cofactor. *Proc. Natl. Acad. Sci.* **1993,** *90*, 8023-8027.

57. Aubert, C.; Vos, M. H.; Mathis, P.; Eker, A. P.; Brettel, K., Intraprotein radical transfer during photoactivation of DNA photolyase. *Nature* **2000,** *405*, 586-590.

58. Kiontke, S. G., P.; Haselsberger, R.; Batschauer, A.; Essen, L. O., Structural and evolutionary aspects of antenna chromophore usage by class II photolyases. *J. Biol. Chem.* **2014,** *289*, 19659-19669.

59. Mees, A.; Klar, T.; Gnau, P.; Hennecke, A.; Eker, A. P.; Carell, T.; Essen, O., Crystal structure of a photolyase bound to a CPD-like DNA lesion after *in situ* repair. *Science* **2004,** *306*, 1789-1793.

60. MacFarlane, A. W.; Stanley, R., *Cis-syn* thymidine dimer repair by DNA photolyase in real time. *Biochemistry* **2003,** *42*, 8558-8568.

61. Kao, Y. T.; Saxena, C.; Wang, L.; Sancar, A.; Zhong, D., Direct observation of thymine dimer repair in DNA by photolyase. *Proc. Natl. Acad. Sci.* **2005,** *102*, 16128-16132.

62. Thiagarajan, V. B., M.; Eker, A. P.; Muller, P.; Brettel, K., Kinetics of cyclobutane thymine dimer splitting by DNA photolyase directly monitored in the UV. *Proc. Natl. Acad. Sci.* **2011,** *108*, 9402-9407.

63. Christine, K. S.; Macfarlane, A. W.; Yang, K.; Stanley, R. J., Cyclobutypyrimidine dimer base flipping by DNA photolyase. *J. Biol. Chem.* **2002,** *277*, 38339-38344.

64. Liu, Z.; Tan, C.; Guo, X.; Kao, Y. T.; Li, J.; Wang, L.; Sancar, A.; Zhong, D., Dynamics and mechanism of cyclobutane pyrimidine dimer repair by DNA photolyase. *Proc. Natl. Acad. Sci.* **2011,** *108*, 14831-14836.

65. Espagne, A.; Byrdin, M.; Eker, A. P. M.; Brettel, K., Very fast product release and catalytic turnover of DNA photolyase. *ChemBioChem* **2009,** *10*, 1777-1780.

66. Brettel, K. B., M., DNA photolyase: Is the nonproductive back electron transfer really much lower than forward transfer? *Proc. Natl. Acad. Sci.* **2012,** *109*, E1462.

67. Zhong, D.; Sancar, A.; Stuchebrukhov, A., Reply to Brettel and Byrdin: On the efficiency of DNA repair by photolyase. *Proc. Natl. Acad. Sci.* **2012,** *109*, E1463.

68. Heelis, P. F.; Shubin, L., Photoenzymic repair of the DNA 6-4 photoproduct - A density functional theory and semiempirical study. *J. Am. Chem. Soc.* **1997,** *119*, 2936-2937.

69. Hitomi, K. N., H.; Kim, S. T.; Mizukoshi, T.; Ishikawa, T.; Iwai, S.; Todo, T., Role of two histidines in the (6-4) photolyase reaction. *J. Biol. Chem.* **2001,** *276*, 10103-10109.

70. Maul, M. J. B., T. R.; Glas, A. F.; Cryle, M. J.; Domratcheva, T.; Schneider, S.; Schlichting, I.; Carell, T., Crystal structure and mechanism of a DNA (6-4) photolyase. *Angew. Chem. Int. Ed.* **2008,** *47*, 10076-10080.

71. Glas, A. F.; Schneider, S.; Maul, M. J.; Hennecke, U.; Carell, T., Crystal structure of the T(6-4)C lesion in complex with a (6-4) DNA photolyase and repair of UV-induced (6-4) and Dewar photolesions. *Chemistry* **2009,** *15*, 10387-10396.

72. Yamamoto, J.; Plaza, P.; Brettel, K., Repair of (6-4) lesions in DNA by (6-4) photolyase: 20 years of quest for the photoreaction mechanism. *Photochem. Photobiol.* **2017,** *93*, 51-66.

73. Li, J.; Liu, Z.; Tan, C.; Guo, X.; Wang, L.; Sancar, A.; Zhong, D., Dynamics and mechanism of repair of ultraviolet-induced (6-4) photoproduct by photolyase. *Nature* **2010,** *466*, 887-890.

74. Sadeghian, K.; Bocola, M.; Merz, T.; Schüz, M., Theoretical study on the repair mechanism of the (6-4) photolesion by the (6-4) photolyase. *J. Am. Chem. Soc.* **2010,** *132*, 16285-16295.

75. Yamamoto, J.; Martin, R.; Iwai, S.; Plaza, P.; Brettel, K., Repair of the (6-4) photoproduct by DNA photolyase requires two photons. *Angew. Chem. Int. Ed.* **2013,** *52*, 7432-7436.

76. Wang, Y.; Gaspar, P. P.; Taylor, J. E., Quantum chemical study of the electron transfer-catalyzed splitting of oxetane and azetidine intermediates proposed in the photoenzymatic repair of (6-4) photoproduct of DNA. *J. Am. Chem. Soc.* **2000,** *122*, 5510-5519.

77. Rahn, R. O.; Hosszu, J. L., Photochemical studies of thymine in ice. *Photochem. Photobiol.* **1969**, 131-137.

78. Prakash, G.; Falvey, D. E., Model studies of the (6-4) photoproduct DNA photolyase: synthesis and photosensitized splitting of a thymine-5,6-oxetane. *J. Am. Chem. Soc.* **1995,** *117*, 11375-11376.

79. Joseph, A.; Falvey, D. E., Photoinduced electron transfer cleavage of oxetane adducts of uracil and cytosine. *Photochem. Photobiol.* **2002,** *1*, 632-635.

80. Joseph, A.; Prakash, G.; Falvey, D. E., Model studies of the (6-4) photoproduct photolyase enzyme: laser flash photolysis experiments confirm radical ion intermediates in the sensitized repair of thymine oxetane adducts. *J. Am. Chem. Soc.* **2000,** *122*, 11219-11225.

81. Cichon, M. K.; Arnorld, S.; Carell, T., A (6-4) photolyase model: repair of DNA (6-4) lesions requires a reduced and deprotonated flavin. *Angew. Chem. Int. Ed.* **2002,** *41*, 767-770.

82. Clivio, P.; Fourrey, J.; Gasche, J., DNA photodamage mechanistic studies: characterization of a thietane intermediate in a model reaction relevant to "6-4" lesions. *J. Am. Chem. Soc.* **1991,** *113*, 5481-5483.

83. Fourrey, J. L.; Jouin, P.; Moron, J., Thiocarbonyl photochemistry. III. Thiethanes obtention from 4-thiouracil derivatives. *Tetrahedron Lett.* **1974,** *35*, 3005-3006.

84. Zhao, X.; Liu, J.; Hsu, D. S.; Zhao, S.; Taylor, J. S.; Sancar, A., Reaction mechanism of (6-4) photolyase. *J. Biol. Chem.* **1997,** *272*, 32580-32590.

85. Friedel, M. G.; Cichon, M. K.; Carell, T., Model compounds for (6-4) photolyases: a comparative flavin induced cleavage study of oxetanes and thietanes. *Org. Biomol. Chem.* **2005,** *3*, 1937-1941.

Chapter 2:
General Objectives

As mentioned in the introduction, this doctoral Thesis is centered on the photorepair mechanism of UV induced DNA damage. Particularly, in the cycloreversion step that is the result of a photochemically induced electron injection from the catalytic flavin-adenosine cofactor $FADH^-$ to the lesion or to the four-membered ring intermediates proposed as a key step of CPD or (6-4) photolyase mechanism, respectively. This mechanism has been resolved for the cyclobutane pyrimidine dimer, but is still under discussion for the (6-4) photoproduct. Indeed, the study of this process is not straightforward due not only to the ultrashort (some picoseconds) lifetime of the excited flavin but also to the unstable character of the oxetane or azetidine intermediates. In this context, strategies based on the development of models to mimic the four-membered ring intermediate have to be developed to investigate the electron transfer step responsible for the photocycloreversion. Therefore, the specific objectives to be addressed are:

1) To synthesize an azetidine model related to the intermediate of 6-4PP in TC sequences. To study its photoreduction triggered by photosensitizers mimicking the flavin cofactor of the photolyase through spectroscopic, electrochemical and analytical experiments as well as computational chemistry.

2) To study the photooxidation of the azetidine model with appropiate photosensitizers and compare the obtained results with those of the reductive process.

3) To design, synthesize and perform the photoreduction of oxetane and cyclobutane thymine dimer models, as four-membered ring intermediates of 6-4PP and CPD lesions, containing 8-oxoguanosine and guanosine as intrinsic photoreductants.

4) To develop the methodology to incorporate the azetidine into DNA and to investigate its photocycloreversion using 8-oxo-2'-deoxyguanosine as intrinsic photosensitizer. To extend the study using the real photorepair machinery: the CPD and (6-4) photolyase enzymes.

Chapter 3:
Photoreduction of an Azetidine Model of the (6-4) Photoproduct

3.1 Introduction

In spite of continuous exposure of the genetic material to radiation and genotoxic chemicals, DNA repair toolbox allows correcting lesions and safeguarding the integrity of the genome. The importance of this machinery has been highlighted by the Nobel Prize in Chemistry 2015 awarded jointly to Lindahl, Modrich and Sancar for their research into the mechanisms that cells use to repair DNA.[1] Among others, it has been emphasized the importance of DNA photoreactivation catalyzed by photolyases enzymes. As mentioned previously, they repair specifically bipyrimidine lesions, ie. CPDs and 6-4PPs, through a photochemically induced electron transfer from the catalytic flavin-adenosine cofactor $FADH^-$ to the lesion or to an oxetane/azetidine intermediate.[2-4] The CPD photorepair mechanism has been solved completely; however, there is still a lively discussion on the photorepair of (6-4) DNA lesions. Until now, three mechanisms have been proposed, two of them involving formation of an oxetane/azetidine intermediate triggered or not by light, followed by an electron-induced cycloreversion of this four-membered ring intermediate (Scheme 3.1, pathway (A) and (A')). The remaining mechanism lacks the oxetane/azetidine intermediate and consists on a direct photoreduction of the 6-4PP by the singlet excited state of the reduced flavin cofactor $FADH^-$ (Scheme 3.1, pathway(B)).

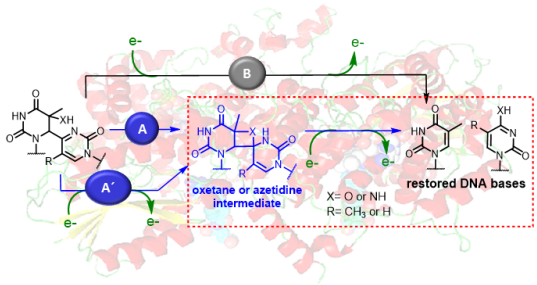

Scheme 3.1. Proposed mechanisms for the repair of the 6-4PPs by (6-4) photolyase.

Investigation of the photorepair mechanism of 6-4PPs involves an additional diffilculty compared to the CPD lesion that is the instability of the four-membered ring oxetane/azetidine intermediates. This prevents not only their isolation and characterization but also their use as substrates to investigate the electron-induced cycloreversion. Therefore, this step has been largely studied using oxetane models (see Chapter 1);[5] however, azetidine models have not been reported until now. The latter are particularly relevant to the understanding of (6-4) photolyase repair mechanism at TC sequences, the most frequent 6-4PP lesion.

A main difficulty to study azetidines resides in the synthesis of the model. As aforementioned, four-membered ring can be achieved through [2+2] photocycloadditions of alkenes to C=C, C=O or C=N.[6] In this context, oxetane models can be easily obtained from Paternò-Büchi reaction between the benzophenone carbonyl group and the double bond of the thymine[7], whereas the photochemical formation of the azetidine ring is only obtained from a "blocked" imine and an alkene. This means that the imino group must form part of a five- or six-membered ring to give rise to photochemical reactions such as photocycloaddition. The reason is ascribed to the fact that in their excited state the imino groups have a very fast deactivation due to the "twist" movement that takes place at the carbon-nitrogen double bond through which the *syn* and *anti* isomers of imines are interconverted when it is not confined in a ring system.

However, this condition alone is not sufficient for imine photoreactivity and a conjugated electron-withdrawing group like a carbonyl group or a heteroatom attached to the C-N double bond is required for cycloaddition to occur.[6, 8] Theoretical calculations with isoxazolines showed that electron-withdrawing groups destabilize the fast IC pathway from S_1, increasing the energy barrier. This way deactivation to ground state is slow enough to allow the system to spend time in S_1 where cycloaddition to alkenes is possible.[9] Therefore, it has been reported that the organic compounds suitable for the formation of azetidines by photocycloaddition are heterocy-

cles such as oxadiazoles (OXA)[10], isoindolenones (INDO)[11], isoxazolines (AZO)[8] and 6-azauracils (azaU)[12] (Figure 3.1).

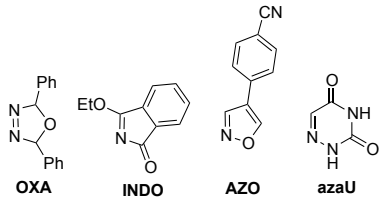

Figure 3.1. Imine compounds suitable for [2+2] photocycloadditions with alkenes.

With this background, this chapter proposes to study the photoreductive cycloreversion of an azetidine model in relation to the repair of 6-4PPs in DNA. In this context, we have chosen azaU that contains an imino group in a 6-membered ring, as a starting imine compound for the synthesis. In addition, this compound is of great interest since (i) it can be considered as a modified pyrimidine base of DNA, (ii) it has been used as a growth inhibitor in microorganisms and (iii) it shows better photochemical reactivity than canonical nucleobases, i.e. it presents an efficient ISC to T_1 ($\pi\pi^*$) being this process the dominant pathway in the relaxation of the S_1.[13]

Interestingly, the photoreductive approach has only been applied to the ring splitting of azetidin-2-ones using triethylamine or DABCO as electron donors (Scheme 3.2). However, these compounds cannot be formally considered as azetidines as the nitrogen atom belongs to a strained β-lactam.[14-15]

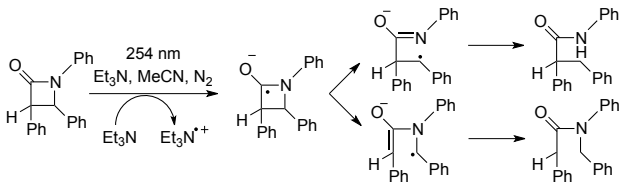

Scheme 3.2. Mechanistic pathways for ring splitting of an azetidin-2-one derivative in the presence of triethylamine.

Thus, in this chapter a photoreductive approach has been applied to the ring splitting of a stable azabipyrimidinic azetidine **T_m<>AZT_m** (Figure 3.2), where the nitrogen atom belongs to the modified base azaU, as a close model for the intermediate **T(azt)C** proposed for the repair of 6-4PPs at TC sequences. Parallel studies of photoinduced reductive cycloreversion on related cyclobutane and azetidine derivatives (**T_m<>T_m** and **DCH<>AZT_m,** Figure 3.2) have been included to ascertain how the presence of the nitrogen atom in the four-membered ring affects in the ring splitting.

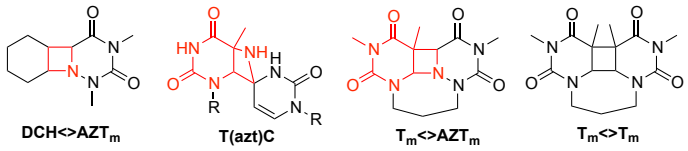

Figure 3.2. Structures of the azetidine model **T_m<>AZT_m** studied in this chapter related to the intermediate **T(azt)C** involved in the photorepair mechanism of 6-4PPs at TC sequences and the cyclobutane and azetidine derivatives **T_m<>T_m** and **DCH<>AZT_m**.

3.2 Results and discussion

3.2.1 Synthesis

We decided to synthesize the dinucleotide azetidine model **T_m<>AZT_m** in which 6-azauracil is connected with thymine through a trimethylene bridge. This previously reported compound[16-18] is a simplified model without phosphate backbone or sugar ring conformations, which eases the study of ring cycloreversion. However, **T_m<>AZT_m** was obtained by alternative synthesis from thymine as shown in the Scheme 3.3. Due to the low solubility of 6-azauracil and thymine in most common organic solvents, soluble 1,3-dimethyl derivatives were employed. The synthesis of **T_m-azaU_m** was achieved by reaction of 1-bromo-3-chloropropane with N3-methylthymine **1** and subsequent reaction of the resulting 1-(3-chloropropyl)-3-methylthymine **2** with the N3-methyl derivative of 6-azauracil. Then, **T_m<>AZT_m** was obtained as the main photoproduct by irradiation of **T_m-azaU_m** at $\lambda > 290$ nm in the presence of acetone as photosensitizer, which was used to avoid photocycloreversion of the product under direct irradiation.

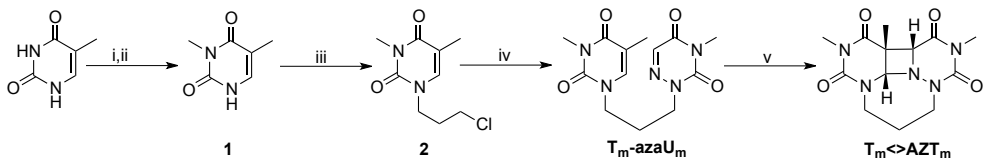

Scheme 3.3. Synthetic strategy to prepare **T_m<>AZT_m**. Reagents and conditions: (i) Ac_2O, 140 ºC, 5h; (ii) MeI, NaH, DMF, rt, 18h; (iii) 1-bromo-3-chloropropane, NaH, DMF, rt, 18h; (iv) N3-methyl-6-azauracil, NaH, MeCN, 80ºC, 18h; (v) $h\upsilon$, $\lambda > 290$ nm, acetone, 1h.

Therefore, the intramolecular [2+2] cycloaddition of $\mathbf{T_m\text{-}azaU_m}$ occurs through a photosensitized reaction (Scheme 3.4) where acetone after absorbing light, reaches its singlet excited state ($^1AC^*$) and quantitatively crosses to its triplet state ($^3AC^*$). Then, TTET occurs to populate the triplet excited state of azaU ($^3azaU^*$), which reacts with the linked thymine to form the azetidine ring. Here, acetone is a suitable sensitizer, as its triplet energy (337 kJ mol^{-1})[19] is higher than that of azaU (324 kJ mol^{-1})[20], which was estimated by phosphorescence emission measurements. In addition, high yield for the photocycloaddition was obtained since (i) the quantum yield of $^3azaU^*$ formation was estimated to be unity by acetone triplet sensitization, which is five times larger than that of uracil[13] and, (ii) the trimethylene bridge favors the rate of internal dimerization.[21-22]

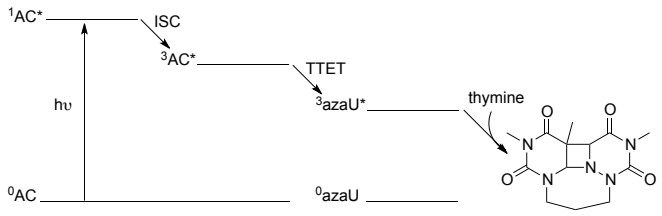

Scheme 3.4. Intramolecular [2+2] cycloaddition between aza-U and thymine through photosensitized pathway.

Once purified, the product lacks the 270 nm absorption (Figure 3.3, A) in agreement with the saturation of the C5-C6 and C5-N6 double bonds. Accordingly, photoreversion is observed when the product is irradiated at λ = 254 nm (Figure 3.3, B) through appearance of the UV absorption at 270 nm of pyrimidine analogs, supporting the formation of an aza-cyclobutane ring.

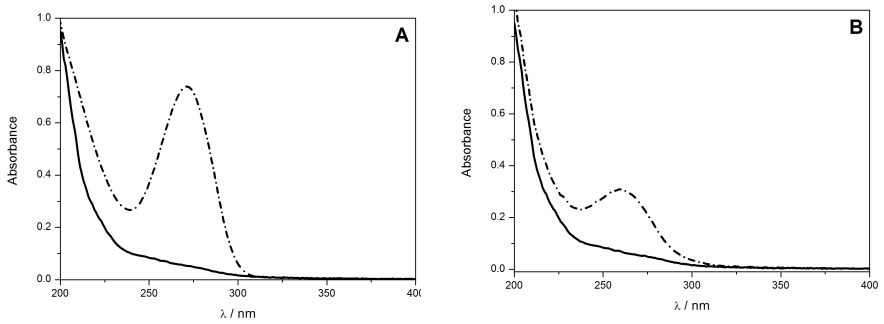

Figure 3.3. (A) UV absorption spectra of **T_m<>AZT_m** (1x10^{-5} M, solid line) and **T_m-azaU_m** (5x10^{-5} M, short dash dot line) in acetonitrile. (B) UV absorption spectra of an acetonitrile solution of **T_m<>AZT_m** before (solid line) and after (short dash dot line) irradiation for 30 min at 254 nm.

The intramolecular photodimerization of **T_m-azaU_m** leds to only one photoproduct as no traces of other photoisomers have been observed. The *cis-syn* configuration of **T_m<>AZT_m** was determined by NOE experiments (Figure 3.4) through the interaction of azetidine ring protons H_a and H_b with the C5-methyl group of the dihydrothymine moiety. The *cis-anti* and *trans-anti* isomers cannot be formed because of length of trimethylene chain. In addition, the structure of photodimer is also supported by the base-base stacking effect that should favor the formation of *cis-syn* isomer.[23] Thermal stability of **T_m<>AZT_m** in acetonitrile was also evaluated by UV/VIS measurements at 298K, and no spectral changes were detected after 48 h.

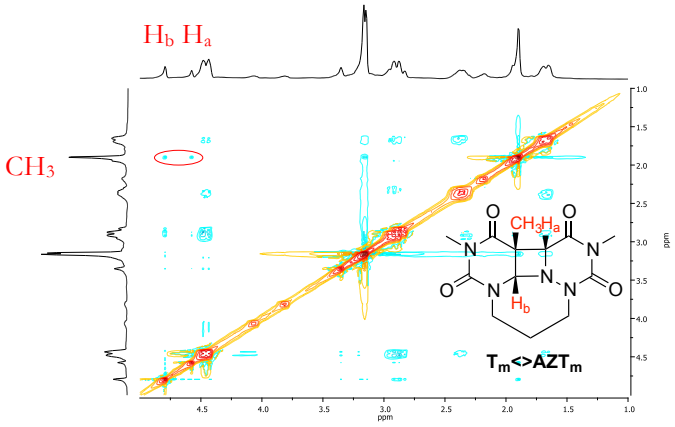

Figure 3.4 NOESY spectrum of **T_m<>AZT_m**.

The related cyclobutane derivative **T_m<>T_m** was prepared by a three-step synthesis from the commercial O,O'-bis(trimethylsilyl)-thymine, as shown in Scheme 3.5. The synthesis of **T_m-T_m** was achieved by reaction of 1,3-dibromopropane with O,O'-bis(trimethylsilyl)-thymine followed of the N3 methylation. Then, *cis-syn* **T_m<>T_m** was obtained by an intramolecular [2+2] cycloaddition of **T_m-T_m** in the presence of acetone as mentioned before.

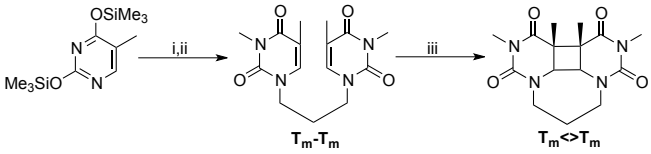

Scheme 3.5. Synthetic strategy to prepare **T_m<>T_m**. Reagents and conditions. (i) 1,3-dibromopropane, DMF, 170 ºC, 18h; (ii) MeI, NaH, DMF, rt, 18h; (iii) hυ, λ > 290 nm, acetone, 2h.

Another azetidine model (**DCH<>AZT$_m$**) was synthetized where the thymine moiety of **T$_m$<>AZT$_m$** was replaced with a cyclohexane ring. In this case, two azetidine isomers ***cis*** and ***trans*** **DCH<>AZT$_m$** were obtained from 6-aza-1,3-dimethyluracil **4** through an acetone photosensitized reaction in the presence of cyclohexene as previously reported[12] (Scheme 3.6.).

Scheme 3.6. Synthesis of ***cis*** and ***trans*** **DCH<>AZT$_m$**. Reagents and conditions: (i) hυ, λ > 290 nm, acetone, 6h

The two isomers were easily separated by flash chromatography. Their stereochemistry was determined from NMR analysis. A tentative assignment was proposed from the ^{1}H NMR spectra because, in the case of the ***cis*** isomer, the H_a, H_b and H_c protons are located on the same side of the azetidine ring. Thus, H_a should be observed as a doublet as it is coupled to H_b. By contrast, in the ***trans*** isomer, H_a does not interact with the other two protons of the ring, and thus appears as a singlet at ca. 4.0 ppm. However, this signal cannot be observed clearly as it overlaps with H_c. The NOESY 2D NMR spectrum of ***cis*** **DCH<>AZT$_m$** is in agreement with the proposed *cis* configuration as an interaction was observed between H_a and H_b protons located at 4.33 and 4.01 ppm, respectively (Figure 3.5).

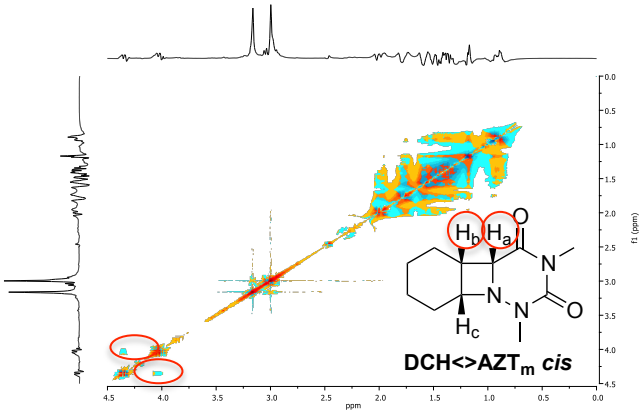

Figure 3.5. NOESY spectrum of ***cis*** **DCH<>AZT$_m$**.

3.2.3 Fluorescence experiments

The trimethylene bridge used for **T$_m$<>AZT$_m$** has been previously used in formation[21-23] and repair[24-26] studies of CPD models, and it appears to favor the interaction of the lesion with flavin singlet excited state that points to a relatively long lifetime of the dimer radical (cation or anion) involved which is presumably due to stabilization.[26-27] It is assumed that the electron transfer process occurs from the singlet excited state of the reduced flavin $FADH^-$ to the azetidine moiety. Thus, direct mechanistic information shoud, in principle, be obtained by monitoring the changes in the intensity and/or kinetics of the cofactor emission in the presence of the azetidine by steady-state and/or time-resolved fluorescence, respectively.

However, the very short lifetime of excited $FADH^-$ (in the subnanosecond timescale) does not provide a time-window compatible with diffusion-controlled intermolecular reaction.[28] To overcome this limitation, a series of photosensitizers (PS, Figure 3.6) with singlet lifetime in the nanosecond range (see **τ**, Table 3.1) and oxidation potential close to that of $^1FADH^{-*}$ (E_{ox}^{D*} of ca. -2.9 V vs. Ag/AgCl)[29] were selected (Table 3.1).[24-25, 30] They include *N,N,N′,N′*-tetramethyl-1,4-phenyldiamine (TMPD),

N,N,N´,N´-tetramethylbenzidine (TMB), *N,N*-dimethylaniline (DMA), carbazole (CAR), acenaphthene (ACE), 1-methoxynaphthalene (1-MN), 2-methoxynaphthalene (2-MN) and chrysene (CHRY).

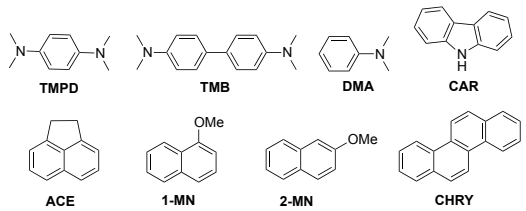

Figure 3.6. Structure of the used photosensitizers (PS).

Table 3.1. Oxidation potential (E_{ox}^{D}) and oxidation potential in the singlet excited state (E_{ox}^{D*}) of the selected PS, and bimolecular rate constant (k_q) for the quenching of the PS by $\mathbf{T_m}$**<>**$\mathbf{AZT_m}$ determined by time-resolved fluorescence.

PS	$\mathbf{E_{ox}^{D*}}$**/V vs. Ag/AgCl**	$\mathbf{E_{ox}^{D}}$**/V vs. Ag/AgCl**	**E*/kcal mol^{-1}**	$\boldsymbol{\tau}$**/ns**	$\mathbf{k_q}$[a]**/x10^9 M^{-1}s^{-1}**
TMPD	-3.3[24]	0.2	79.7	1.5	N.D.[b]
TMB	-3.2[24]	0.4	83.2	6.0	8.0 ± 0.7
DMA	-3.0[24]	0.8	89.4	2.8	7.3 ± 1.0
FADH$^-$	**-2.9**[25]				
CAR	-2.5[30]	1.2	83.1	7.4	4.0 ± 0.2
ACE	-2.5[24]	1.4	89.9	10.6	3.7 ± 0.2
1-MN	-2.5[25]	1.4	89.0	6.2	4.0 ± 0.3
2-MN	-2.3[24]	1.4	85.5	6.6	2.5 ± 0.2
CHRY	-2.1[24]	1.3	79.3	11.9	1.7 ± 0.2

[a] The experiments were performed twice and the errors correspond to average deviations. [b] Not determined because of the temporal resolution of the setup.

In this way, the PS is an excited-state electron donor, which after absorption of a photon ($^1PS^*$), donates an electron to generate the radical anion in the carbonyl group of the thymine or azaU moiety of **T_m<>AZT_m**, leading finally to the repaired bases after C-C bond cleavage as shown in Scheme 3.7. Comparison of the fluorescence experiments performed with **T_m<>AZT_m**, **T_m<>T_m** and **DCH<>AZT_m** would inform on the site for the radical anion formed and on which moiety of **T_m<>AZT_m** is involved in the electron transfer mechanism.

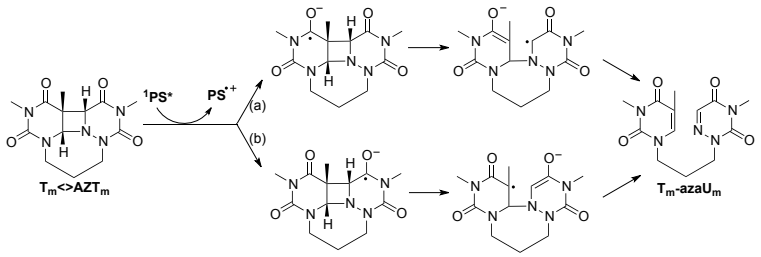

Scheme 3.7. Reductive PET mechanisms of **T_m<>AZT_m** in the presence of PS.

In a first stage, steady-state fluorescence experiments were performed to support the above mentioned PET mechanism from the singlet excited state of PS. Thus, acetonitrile solutions of the photosensitizer were prepared with an absorbance of ca. 0.15 at the excitation wavelength (λ_{exc}=310 or 375 nm) and the fluorescence intensity was measured in the absence and in the presence of **T_m<>AZT_m**. Steady-state fluorescence measurements revealed a decrease of the emission intensity for all the photosensitizers, especially for TMB and DMA (Figure 3.7b and 3.7c). In these cases, the concentrated quencher absorbs partial light when the sample is excited at 310 nm, reducing the portion of light absorbed by the photosensitizer, which thus results in a strong decrease of the emission intensity.

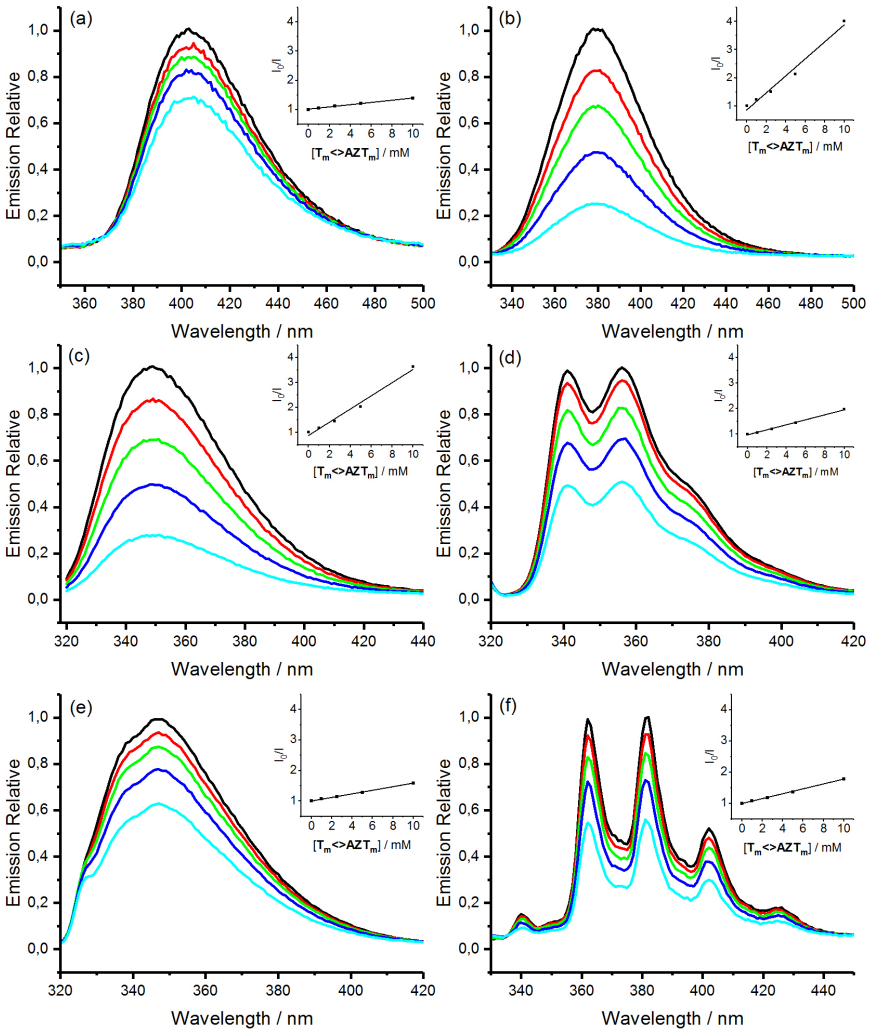

Figure 3.7. Fluorescence emission spectra for (a) TMPD (λ_{exc} =330 nm); (b) TMB (λ_{exc} =310 nm); (c) DMA (λ_{exc} =310 nm); (d) CAR (λ_{exc} =320 nm); (e) 2-MN (λ_{exc} =328 nm); (f) CHRY (λ_{exc} =320 nm); in the presence of increasing amounts of **T_m<>AZT_m** (0-10 mM). Inset: corresponding Stern-Volmer plot.

To evaluate if a dynamic quenching was taking place, i.e. that the decrease of the fluorescence intensity is not due to a filter effect or to preassociation between PS and azetidine before excitation, time-resolved fluorescence experiments were performed. The singlet excited state lifetime of all photosensitizers was shortened in the presence of $\mathbf{T_m}$**<>**$\mathbf{AZT_m}$ (Figure 3.8). The bimolecular rate constants k_q were determined from the Stern-Volmer plots representing the reciprocal of the PS lifetime as a function of $\mathbf{T_m}$**<>**$\mathbf{AZT_m}$ concentration (Figure 3.8, inset). According to the relationship given in equation 3.1 between k_q and ΔG_{ct} obtained from Rehm Weller equation 3.2, the quenching process was more efficient as E_{ox}^{D*} became increasingly negative (Table 3.1 and Figure 3.9 left), reaching the diffusion limit near -3.0 V.

By contrast, no clear correlation was obtained between k_q and the PS singlet excited state energy E^* (Figure 3.9 right) ruling out a singlet-singlet energy transfer process as responsible for the deactivation of $^1PS^*$. Altogether, these data point to an electron transfer mechanism between $^1PS^*$ and $\mathbf{T_m}$**<>**$\mathbf{AZT_m}$. It is noticeable that E_{ox}^{D*} for the $FADH^-$ photolyase cofactor is of ca. -2.9 V;[25] this value, when included in Figure 3.9 left, corresponds to a rate constant for the electron transfer process with $\mathbf{T_m}$**<>**$\mathbf{AZT_m}$ of ca. 6 x 10^9 M^{-1} s^{-1}.

$$k_q = \frac{k_{diff}}{1+0.25\left\{exp\left(\frac{\Delta G_{ct}^{\neq}}{RT}\right)+exp\left(\frac{\Delta G_{ct}}{RT}\right)\right\}} \qquad (3.1)$$

where $\Delta G_{ct} = 23.06\left(E_{ox}^{D*} - E_{red}^{A}\right)$ (3.2)

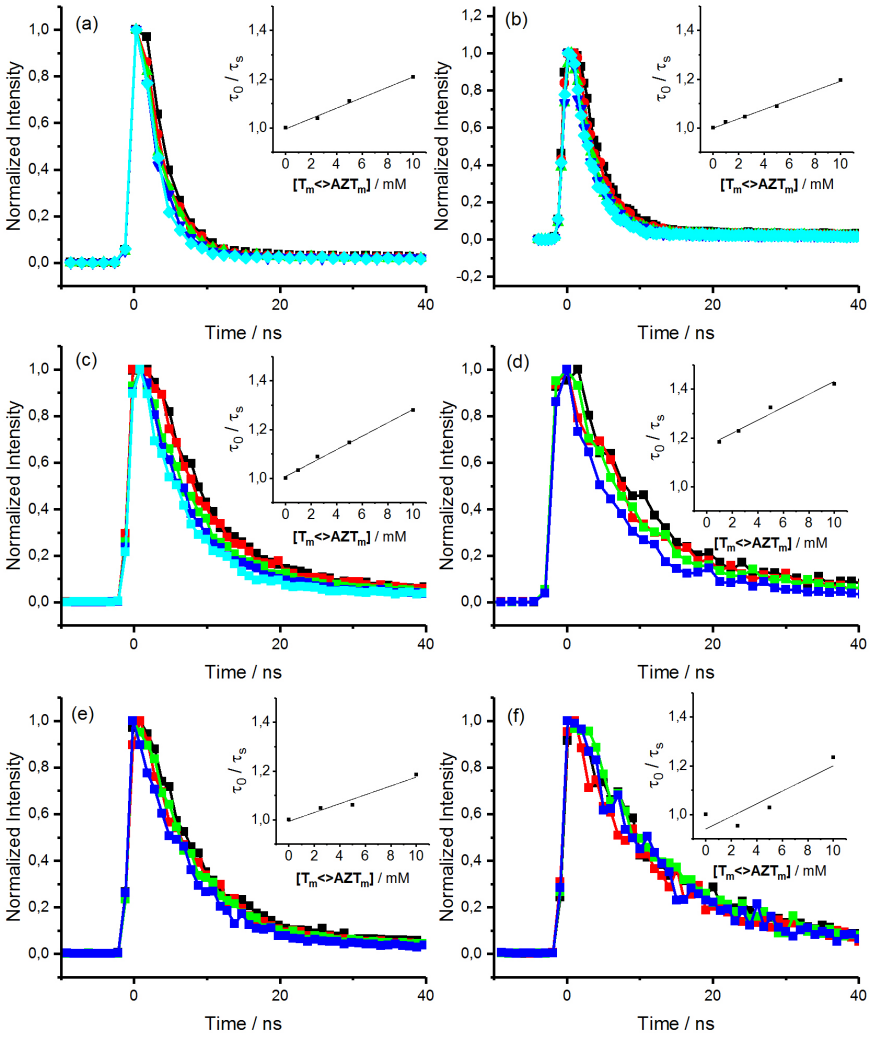

Figure 3.8. Fluorescence kinetic traces and their corresponding Stern-Volmer plot obtained for (a) TMB, (b) DMA, (c) CAR, (d) ACE, (e) 2-MN, (f) CHRY in the presence of increasing amounts of **T_m<>AZT_m** (from 0 to 10 mM), upon excitation at 310 nm.

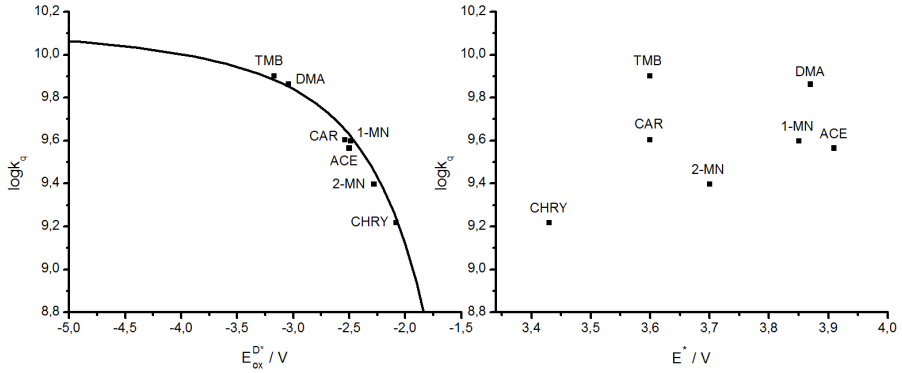

Figure 3.9. (Left) Representation of $logk_q$ obtained by time resolved fluorescence versus singlet excited state oxidation potential (E_{ox}^{D*}) and (right) singlet excited state energy of the considered photosensitizers (E^*).

To compare the influence of the aza group in the four-membered ring splitting, fluorescence experiments were performed for $\mathbf{T_m<>T_m}$ (Table 3.2, Figure 3.10). In this context, 1-MN and CHRY were selected as photosensitizers. As for $\mathbf{T_m<>AZT_m}$, steady-state and time-resolved fluorescence revealed a decrease of emission and shortening of singlet excited state lifetime of both photosensitizers. The bimolecular rate constants of the electron transfer process (k_q) were 4.0 and 1.7 x 10^9 M^{-1} s^{-1} for 1-MN and CHRY, respectively. This tendency is in agreement with the redox potential of the photosensitizer in the singlet excited state that points to 1-MN as a better reductant than CHRY. Similar values of k_q were obtained for $\mathbf{T_m<>AZT_m}$ and $\mathbf{T_m<>T_m}$, this is suggestive of a close value for the reduction potential of both substrates. In addition, these results suggest that the thymine moiety is relevant in the electron transfer process.

Table 3.2. Oxidation potential in the singlet excited state (E_{ox}^{D*}) of the selected PS, and bimolecular rate constant (k_q) for the quenching of the PS by $\mathbf{T_m<>T_m}$ determined by time-resolved fluorescence.

PS	E_{ox}^{D*}/V vs. Ag/AgCl	E_{ox}^{D}/V vs. Ag/AgCl	E*/kcal mol^{-1}	τ/ns	k_q/x10^9 M^{-1}s^{-1}
1-MN	-2.5[25]	1.4	89.0	6.2	3.9
CHRY	-2.1[24]	1.3	79.3	11.9	1.1

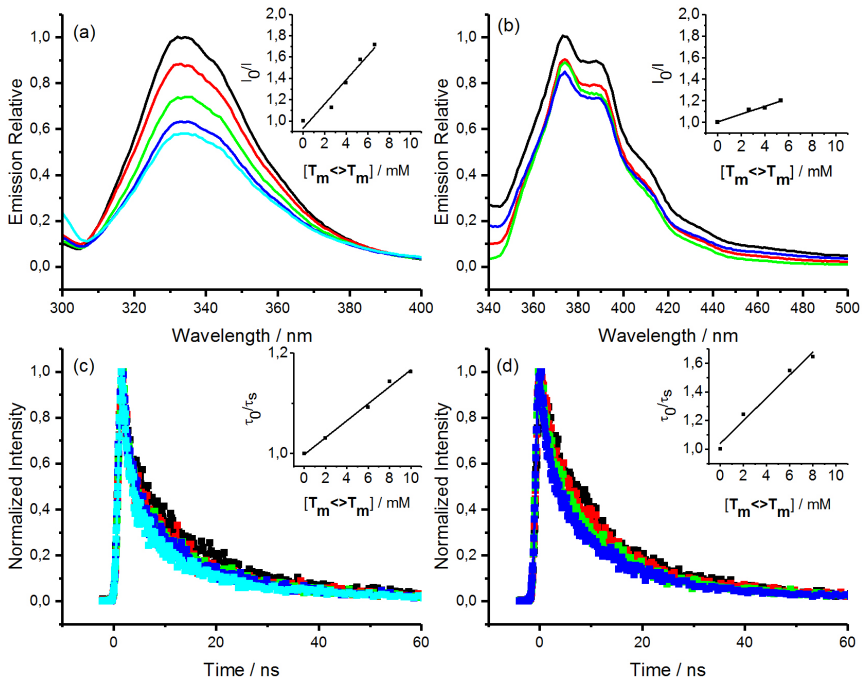

Figure 3.10. Fluorescence emission spectra (top) and kinetic traces (bottom) for (a, c) 1-MN (λ_{exc} =310 nm); (b, d) CHRY (λ_{exc} =310 nm) in the presence of increasing amounts of $\mathbf{T_m<>T_m}$ (0-7 mM). Inset: corresponding Stern-Volmer plot.

In order to support that the electron transfer involved the thymine nucleobase, fluorescence experiments were performed for **DCH<>AZT$_m$** that only has the azaU moiety. In this context, DMA and CAR were used as photoreductants for the steady-state fluorescence experiments. The emission spectra of CAR and DMA suffered only weak changes when ***trans*** **DCH<>AZT$_m$** azetidine was added, which means that electron injection is not an efficient process (Figure 3.11).

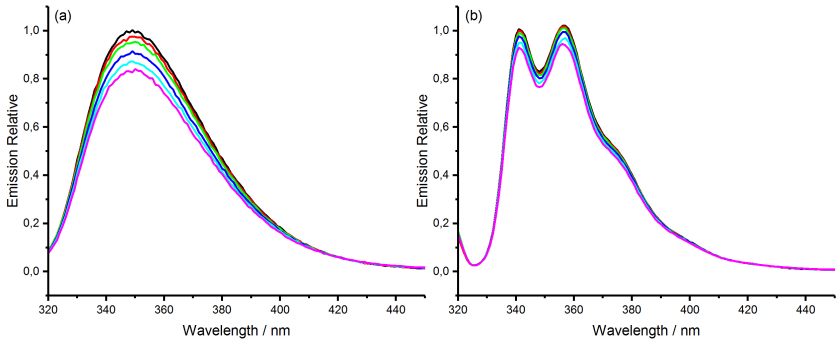

Figure 3.11. Fluorescence emission spectra for (a) DMA (λ_{exc}= 310 nm) and (b) CAR (λ_{exc}= 310 nm) in the presence of increasing amounts of ***trans*** **DCH<>AZT$_m$**.

3.2.4 Electrochemical measurements

As shown in the Rehm-Weller equation 3.3, oxidation and reduction potentials of the species involved in the photoinduced electron transfer are the essential factors that determine the feasibility of this process. In this context, the electrochemical properties of **T$_m$<>AZT$_m$** and **T$_m$<>T$_m$** were investigated by cyclic voltammetry. According to the electron injection, **T$_m$<>AZT$_m$** and **T$_m$<>T$_m$** exhibited similar behavior with an irreversible wave appearing at very negative potential of ca. -2.6 V vs. Ag/AgCl (Figure 3.12). This value is compatible with that reported for the *cis-syn* cyclobutane dimers of 1,3-dimethythymine.[31-32] Therefore, this result supports the similar values of k_q obtained for the fluorescence experiments.

Once obtained the E^{A}_{red} value, ΔG_{ct} (without taking into account the coulombic interaction) was determinated in order to know if PET is an endergonic or exergonic process. Using the E^{D}_{ox} values for TMB and CHRY photosensitizers, which are the best and worse electron donors, values of ca. -13.3 kcal/mol and 11.9 kcal/mol were obtained, respectively. This agrees with a more efficient process for TMB than for CHRY with a better k_q obtained by time-resolved fluorescence measurements.

$$\Delta G_{ct} = 23.06\left(E^{D}_{ox} - E^{A}_{red}\right) - E^{*} \qquad (3.3)$$

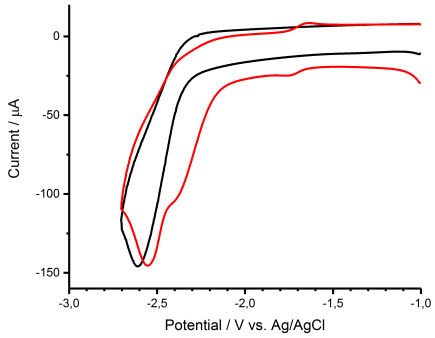

Figure 3.12. Cyclic voltammograms of **T_m<>AZT_m** (2 mM, red line) and **T_m<>T_m** (2 mM, black line) in N_2-purged DMF using 0.1 M n-Bu_4NClO_4 as electrolyte. Scan rate: 0.1 Vs^{-1}.

3.2.5 Photocycloreversion of T_m<>AZT_m

Steady-state photolysis was performed to ensure that the fluorescence quenching resulted in the expected ring splitting reaction. For this purpose, TMPD was selected as photosensitizer on the basis of the above results. Thus, an acetonitrile solution of **T_m<>AZT_m** in the presence of TMPD was irradiated monochromatically at 350 nm to make sure that the light is selectively absorbed by TMPD, avoiding this way the possibility of direct photolysis.[17-18] The sample was purged with nitrogen, irradiated for different times, and analyzed by HPLC to determine the amounts of obtained

photoproduct and remaining **T_m<>AZT_m** (Figure 3.13). Only one photoproduct was observed, which was assigned to compound **T_m-azaU_m** by comparison with an authentic sample. This demonstrates that the electron transfer process results in a clean cycloreversion of the azetidine ring.

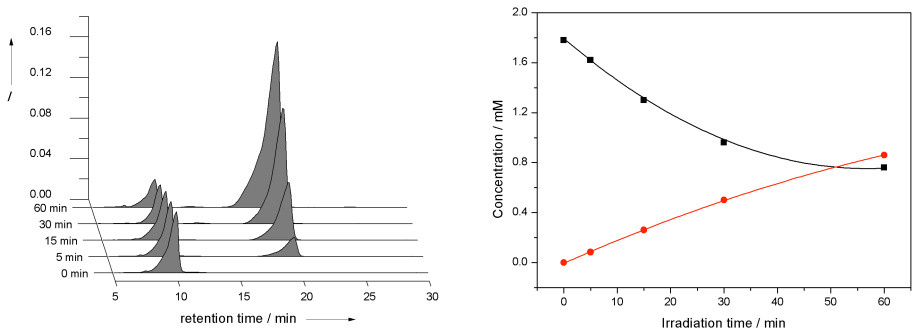

Figure 3.13. HPLC chromatogram (left) obtained after 0, 5, 15, 30, 60 min of irradiation of a mixture of **T_m<>AZT_m** (2 mM) and TMPD (4 mM) in acetonitrile with 350 nm light. Variation of the concentration of **T_m<>AZT_m** (square) and repaired **T_m-azaU_m** (circle) with the irradiation time.

In addition, experimental evidence in support of the electron transfer mechanism was obtained by UV/Vis spectrophotometry. As shown in Figure 3.14, irradiation of TMPD in the presence of **T_m<>AZT_m** resulted in the formation of a species absorbing between 500 and 650 nm, which is coincident in shape and position with the visible band of TMPD radical cation.[33] However, it is important to mention that the observed species does not correspond to the "in cage" $TMPD^{\bullet+}$ responsible for **T_m<>AZT_m** cycloreversion but to the longer-lived free radical cation escaped from the solvent cage, which is present at very low concentration (ca. 5 x 10^{-6} M).

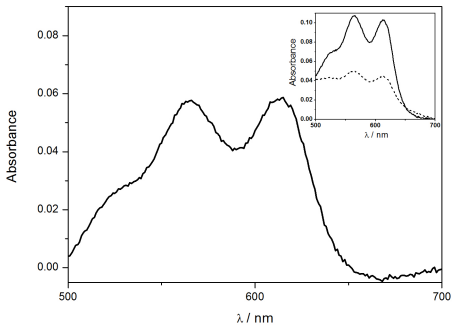

Figure 3.14. UV absorption spectra of **TMPD$^{\bullet+}$** (5 x 10^{-6} M) formed by irradiation of TMPD (4 mM) in the presence of **T_m<>AZT_m** (2 mM) for 60 min at 350 nm. For a better clarity, absorption from control experiment (TMPD irradiated alone) was subtracted. Inset: UV absorption spectra of **TMPD$^{\bullet+}$**: TMPD irradiated in presence of **T_m<>AZT_m** (line) and alone (dash line) for 60 min at 350 nm.

3.2.6 Quantum-chemistry determination of the photoreductive properties of T<>AZT

This study was performed in collaboration with the research group of Dr. Roca-Sanjúan (University of Valencia). To gain insight into the energetics involved in the injection of one electron in the azetidine and cyclobutane derivatives, the electron affinities (EAs) were computed for the *N*-demethylated compounds **T<>AZT** and **T<>T** with the density functional theory (DFT) method, the M06-2X functional and the 6-31++G(d,p) basis set. Benchmark calculations on the thymine nucleobase compared with high-level complete-active-space self-consistent field second-order perturbation theory (CASPT2) results indicate an accurate performance of the DFT/M06-2X method for the adiabatic EAs (AEAs). Table 3.3 compiles the computed gas phase and acetonitrile solution values, which also allows an estimation of the solvent effect. As expected, solvation has an important influence on the EA values because it stabi-

lizes to a higher extent the ionic states as compared to the neutral state. Moreover, Table 3.3 shows that EAs of methylated and demethylated compounds of **T<>AZT** differ slightly, thus theoretical studies with demethylated give us reliable results as for methylated compounds. According to **T<>T**, EAs are very similar to **T<>AZT**, which agrees with the comparable experimental quenching rates (k_q) for both compounds.

Table 3.3. Adiabatic electron affinities (AEAs) in eV (kcal mol^{-1} within parentheses) for **T<>AZT, T_m<>AZT_m** and **T<>T** in the gas phase and in acetonitrile computed with the DFT/M06-2X method and the 6-31++G(d,p) basis set.

	AEA
T<>AZT	
Gas phase	0.50 (11.6)
Acetonitrile	2.16 (49.9)
T_m<>AZT_m	
Gas phase	0.30 (9.0)
Acetonitrile	2.09 (48.2)
T<>T	
Gas phase	0.31 (7.1)
Acetonitrile	2.00 (46.1)

3.2.7 Decomposition mechanisms of T<>AZT radical anion

Injection of one electron into the azetidine **T<>AZT** produces the rupture of the C-C bond due to the fact that the anion of the four-membered ring is not a stable structure (Scheme 3.8). The extra electron from the photosensitizer is partially located in the σ^* orbital of the C-C bond thus weakening this bond, which breaks. For **T<>T**, previous studies[34] and the current work also indicate a more favorable open structure for the anion.

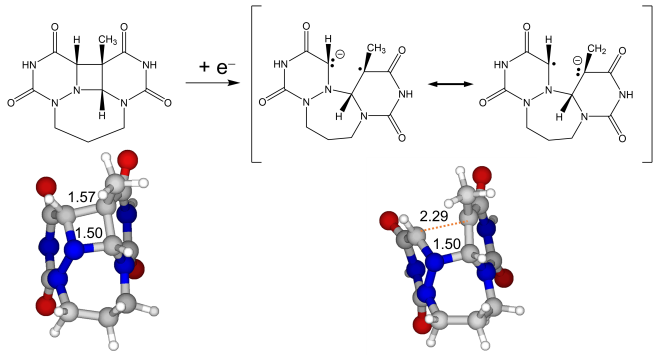

Scheme 3.8. Chemical structures (top) and geometries (bottom) of the neutral $\mathbf{T_m<>AZT_m}$ (left) and its radical anion $\mathbf{T_m<>AZT_m}^{\bullet-}$ (right). Relevant bond distances for the reaction are shown in Å.

Evolution of the system towards recovery of the thymine and 6-azauracil molecules has also been studied with appropriate reaction path computational strategies showing an electronic energy barrier height of around 13 kcal mol^{-1} (Scheme 3.9). Due to technical difficulties to accurately determine the transition state (TS) structure, an approximated procedure has been used. This approach, based on minimum energy path (MEP) and linear interpolation of internal coordinates (LIIC) calculations, gives rise to a connected path between reactant and product and provides an upper-bound value for the barrier. Therefore, the exact energy barrier height shall be expected at slightly lower energies in the range of 10-13 kcal mol^{-1}.

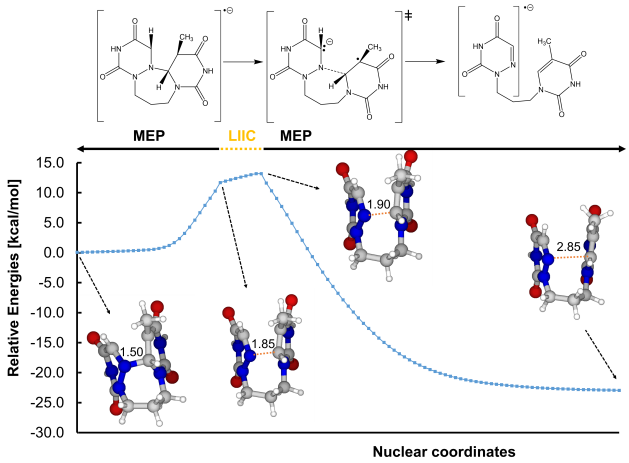

Scheme 3.9. Chemical structure of relevant points (top) and energy profile (bottom) for the C-N and C-C bond breakings of $\mathbf{T_m}$**<>**$\mathbf{AZT_m}^{\bullet-}$ obtained with MEP and LIIC computational strategies. Relevant bond distances for the reaction are shown in Å.

Regarding the electronic-structure properties, analysis of the spin density obtained with the complete-active space self-consistent field (CASSCF) method indicates a delocalization of the extra electron over the two carbon atoms which breaks at the reactant side of the cycloreversion mechanism (Figure 3.15). Once the two monomers are regenerated, the unpaired electron is localized in 6-azauracil. Therefore, these data showed that the reductive mechanism of $\mathbf{T_m}$**<>**$\mathbf{AZT_m}$ occurs via pathway b in the Scheme 3.7.

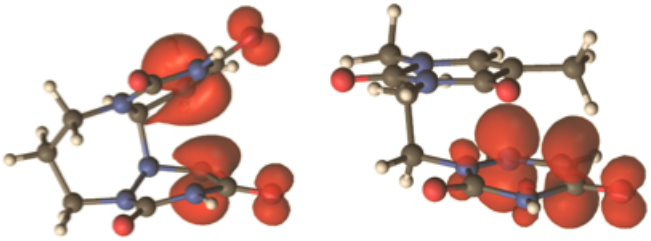

Figure 3.15. CASSCF spin-density representations for the **T<>AZT** radical anion systems at the reactant (left) and product (right) geometries, respectively. Red = excess of spin density, green = defect of spin density.

Globally, the in-vacuo mechanism described above implies energy barriers lower than 13 kcal mol^{-1} for the radical anion system. The cycloreversion process is clearly exergonic for **T<>AZT**$^{\bullet-}$. To further improve the description, we have focused on the relevant points for the present mechanism (reactants, TSs and products) and we have determined several thermochemical magnitudes using the highly accurate CASPT2 method. In particular, the activation energy ($E^{\#}$) and thermodynamics (ΔE), the zero-point vibrational energy (ZPVE) corrected values ($\Delta E_0^{\#}$ and ΔE_0) and the Gibbs free energies ($\Delta G^{\#}$ and ΔG) have been computed at both gas and solution phases. Results are compiled in Table 3.4. As it can be seen, the CASPT2 method confirms the relatively low DFT energy barrier heights and the highly exergonic character of the **T<>AZT**$^{\bullet-}$ ring opening reaction. Regarding the solvent effects, in contrast to the redox properties determined in the previous section, no significant changes are observed for the **T<>AZT**$^{\bullet-}$ cycloreversion mechanisms. This is due to the fact that along the ring opening reactions the total charge is preserved. The ZPVE correction gives rise to lower ΔEs as a consequence of the bond breakings occurring along the reactions. The same behavior is observed for ΔG, which reflects the entropy increase in the decomposition process.

Table 3.4. Computed energy differences between products and the reactants (ΔE, ΔE_0 and ΔG) and activation energies ($\Delta E^{\ddagger}$, $\Delta E_0^{\ddagger}$ and $\Delta G^{\ddagger}$) for the cycloreversion of the **T<>AZT** radical anion. Energies in kcal mol^{-1}.

Methodology	$AZT^{\bullet-}$	
	ΔE[a]	$\Delta E^{\ddagger}$
M06-2X	-29.07[b]	11.69–13.20[b]
CASPT2//M06-2X	-25.16[b]	11.88–12.85[b]
PCM-M06-2X	-29.20[c]	11.22–12.51[c]
	ΔE_0	$\Delta E_0^{\ddagger}$
M06-2X	-29.87[d]	-[e]
CASPT2//M06-2X	-25.96[d]	-[e]
	ΔG	$\Delta G^{\ddagger}$
M06-2X	-30,99[f]	-[e]
CASPT2//M06-2X	-27.08[f]	-[e]

[a] Energies related to the lowest-energy conformer of the product (see text). [b] Electronic energy (gas phase). [c] Electronic energy including solvent effects (acetonitrile). [d] Electronic energy with ZPVE corrections (gas phase). [e] No TS found. [f] Electronic energy with thermal and entropic contributions at 298.15 K and 1 atm (gas phase).

3.3 Conclusions

The present study has clearly demonstrated for the first time that the photoinduced injection of one electron into a dimeric azetidine derived from thymine leads to a clean cycloreversion and therefore to the "repair" of the nucleobases. In a first stage, the electron donation capabilities of the azetidine heterocycle have been assessed using photoreductant singlet excited state. In this context, comparison of the bimolecular rate constants obtained for $\mathbf{T_m<>AZT_m}$ and $\mathbf{T_m<>T_m}$ revealed that the presence of the nitrogen atom in the ring does not affect the reduction process; however the

thymine moiety is essential for the occurrence of the electron transfer, which agrees with the lack of fluorescence quenching in the case of **DCH<>AZT$_m$**. The electrochemical experiments support these redox properties as close reduction potentials have been registered. This fact has also been corroborated by DFT quantum chemistry, which has determined similar electron affinities. Concerning the **T$_m$<>AZT$_m$** radical anion, the injection of an electron in the heterocycle provokes the direct cleavage of the interbase C-C bond at C5, followed by splitting of the C-N at position 6, which involves a low energy barrier of ca. 13 kcal mol^{-1}, and finally leaves a radical anion centered on the 6-azauracil moiety. Altogether the obtained results are relevant to understand the process involved in of (6-4) photolyase and support the feasibility of the mechanistic pathway involving reductive splitting of an azetidine intermediate.

3.4 Experimental section

3.4.1 Synthesis

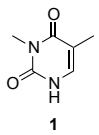

1

3,5-Dimethylpyrimidine-2,4(1*H*,3*H*)-dione (1): A solution of thymine (4.0 g, 31.7 mmol) in acetic anhydride (100 mL) was refluxed overnight. The reaction mixture was then cooled to rt and dried under vacuum. The crude product was repeatedly treated with toluene and concentrated under vacuum to give the acetyl derivative (4.8 g, 90%). The resultant acetyl derivative (4.8 g, 29.6 mmol) was added to a suspension of NaH (0.75 g, 31.4 mmol) in anhydrous acetonitrile (100 mL). After stirring for 1 hour at rt, the reaction mixture was treated with iodomethane (2.1 mL, 34.2 mmol) and stirred for 12 h at 70 ºC. The solvent was removed, and the residue was purified by flash chromatography (silica gel, 98% dichloromethane/methanol) to give **1** (2.8 g, 62%) as a white solid powder. **^{1}H NMR** (300 MHz, $CDCl_3$) δ 10.36 (br s, 1H), 7.06 (d, *J* = 4.5 Hz, 1H), 3.34 (s, 3H), 1.93 (s, 3H).**^{13}C NMR** (75 MHz, $CDCl_3$) δ 164.7 (C), 153.6 (C), 134.4 (CH), 110.4 (C), 27.4

(CH_3), 12.7 (CH_3). **HRMS (ESI)**: *m*/*z* calcd for $C_6H_9N_2O_2$ $[M+H]^+$ 141.0664, found 141.0660.

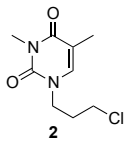

2

1-(3-Chloropropyl)-3,5-dimethylpyrimidine-2,4-(1*H*,3*H*)-dione (2): N3-methylthymine **1** (2.5 g, 17.8 mmol) was added to a suspension of NaH (0.47 g, 19.62 mmol) in dry acetonitrile (100 mL). The reaction mixture was stirred at room temperature for 1 hour followed by the addition of 1-bromo-3-chloropropane (1.9 mL, 19.62 mmol), and stirred for 12 h at 70 ºC. The solvent was removed, and the residue was purified by flash chromatography (silica gel, 98% dichloromethane/methanol) to give the product **2** (2.8 g, 60%) as a yellow oil. **^{1}H NMR** (300 MHz, $CDCl_3$) δ 7.06 (s, 1H), 3.92 (t, *J* = 6.6 Hz, 2H), 3.60 (t, *J* = 6.0 Hz, 2H), 3.37 (s, 3H), 2.25 – 2.13 (m, 2H), 1.96 (s, 3H). **^{13}C NMR** (75 MHz, $CDCl_3$) δ 163.8 (C), 151.4 (C), 138.3 (CH), 109.6 (C), 46.9 (CH_2), 41.4 (CH_2), 30.9 (CH_2), 27.8 (CH_3), 12.8 (CH_3). **HRMS (ESI)**: *m*/*z* calcd for $C_9H_{14}N_2O_2Cl$ $[M+H]^+$ 217.0744, found 217.0744.

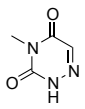

3

4-Methyl-1,2,4-triazine-3,5(2H,4H)-dione (**3**) was prepared as described for **1**. **^{1}H NMR** (300 MHz, $CDCl_3$) δ 10.39 (br s, 1H), 7.37 (s, 1H), 3.28 (s, 3H). **^{13}C NMR** (75 MHz, $CDCl_3$) δ 156.2 (C), 149.9 (C), 135.3 (CH), 26.3 (CH_3).

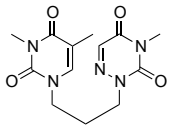

T_m-azaU_m

2-[3-(3,5-Dimethyl-2,4-dioxo-3,4-dihydropyrimidin-1(2*H*)-yl)propyl]-4-methyl-1,2,4-triazine-3,5(2*H*,4*H*)-dione (T_m-azaU_m): Potassium carbonate (2.4 g, 17.7 mmol) was added to a solution of **2** (2.8 g, 13.0 mmol) and **3** (1.5 g, 11.8 mmol) in dry acetonitrile (100 mL). The resulting solution was stirred 18 hours at 80 ºC. The solvent was removed under reduced pressure, and the crude product was washed by hot methanol to give **T_m-azaU_m** (2.5 g, 70%) as a beige solid. **^{1}H NMR** (300 MHz, $CDCl_3$) δ 7.41 (s, 1H), 7.05 (s, 1H), 4.05 (t, *J* = 6.7 Hz, 2H), 3.80 (t, *J* = 7.0 Hz, 2H), 3.34 (s, 6H), 2.27 – 2.09 (m, 2H), 1.94 (s, 3H); **^{13}C NMR** (75 MHz, $CDCl_3$) δ 163.7

(C), 155.8 (C), 151.4 (C), 148.8 (C), 137.8 (CH), 134.1 (CH), 109.8 (C), 48.6 (CH_2), 46.6 (CH_2), 27.8 (CH_3), 27.5 (CH_2), 26.8 (CH_3), 12.9 (CH_3). **HRMS (ESI)**: *m/z* calcd for $C_{13}H_{18}N_5O_4$ $[M+H]^+$ 308.1359, found 308.1350.

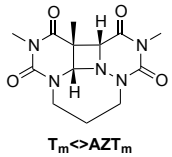

T_m<>AZT_m

Azetidine photoproduct (T_m<>AZT_m): In a Pyrex vessel ($\lambda > 290$ nm), acetone solutions of **T_m-azaU_m** ($1x10^{-2}$ M) were irradiated under nitrogen atmosphere for 1 hour using a medium pressure mercury lamp (125 W). After that time, no traces of the substrate were detected by TLC using hexane/ethyl acetate (1:3) as eluent. The irradiated solution was evaporated to dryness. The residue was washed with cold ethanol and dried *in vacuo* to give **T_m<>AZT_m** (75%) as a white solid. **^{1}H NMR** (300 MHz, $CDCl_3$) δ 4.79 (s, 1H), 4.57 (s, 1H), 4.49 - 4.41 (m, 2H), 3.14 (s, 3H), 3.12 (s, 3H), 2.97 - 2.82 (m, 2H), 2.45 – 2.26 (m, 1H), 1.88 (s, 3H), 1.75 – 1.55 (m, 1H). **^{13}C NMR** (75 MHz, $CDCl_3$) δ 165.8 (C), 164.5 (C), 150.9 (C), 149.9 (C), 80.5 (CH), 67.2 (CH), 49.1 (CH_2), 48.5 (CH_2), 45.2 (C), 28.4 (CH_3), 26.8 (CH_3), 23.3 (CH_2), 22.5 (CH_3). **HRMS (ESI)**: *m/z* calcd for $C_{13}H_{17}N_5O_4Na$ $[M+Na]^+$ 330.1178, found 330.1180.

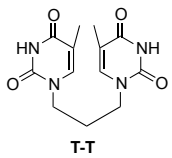

T-T

1,1'-(propane-1,3-diyl)bis(5-methylpyrimidine-2,4(1*H*,3*H*)-dione) (**T-T**): O,O'-Bis(trimethylsilyl)-thymine (1.0 g, 3.86 mmol) was added to a solution of 1,3-dibromopropane (0. 38 g, 1.68 mmol) in 6 mL of anhydrous DMF. The solution was heated to 170 ºC and stirred overnight. The reaction was cooled to 0 ºC and 2 mL of water was added to the reaction mass to precipitate the product. The precipitated was stirred for 15 min at 0 ºC. The solids were filtered off, washed with 20 mL of chloroform/methanol (1:1) and dried *in vacuo* to give compound **T-T** (0.9 g, 83%) as a white solid. **^{1}H NMR** (300 MHz, DMSO-d_6) δ 11.20 (s, 2H), 7.51 (s, 2H), 3.64 (t, J = 6.9 Hz, 4H), 2.05 – 1.79 (m, 2H). **^{13}C NMR** (75 MHz, DMSO-d_6) δ 164.2 (2C), 150.9 (2C), 141.2 (2CH), 108.5 (2C), 44.8 ($2CH_2$), 27.8 (CH_2), 11.9 ($2CH_3$).

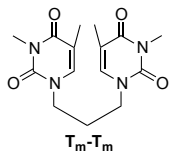

T_m-T_m

1,1'-(Propane-1,3-diyl)bis(3,5-dimethylpyrimidine-2,4(1H,3H)-dione) (T_m-T_m): T-T (0.9 g, 3.07 mmol) was added to a suspension of NaH (0.15 g, 6.14 mmol) in anhydrous DMF (10 mL). After stirring for 1 hour at room temperature, the reaction mixture was treated with iodomethane (0.4 mL, 6.14 mmol) and stirred overnight at rt. The reaction was cooled to 0 ºC and the precipitated formed was filtered off, washed with 10 mL of water and dried *in vacuo* to give compound **T_m-T_m** (0.9 g, 90%) as a white solid. **^{1}H NMR** (300 MHz, $CDCl_3$) δ 6.99 (s, 2H), 3.73 (t, *J* = 7.0 Hz, 4H), 3.29 (s, 6H), 2.06 – 2.00 (m, *J* = 5.3 Hz, 2H), 1.87 (s, 6H). **^{13}C NMR** (75 MHz, $CDCl_3$): 163.8 (2C), 151.7 (2C), 138.0 (2CH), 110.2 (2C), 46.8 ($2CH_2$), 28.6 (CH_2), 28.0 ($2CH_3$), 13.0 ($2CH_3$).

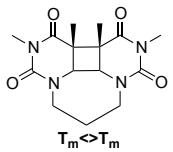

T_m<>T_m

Cyclobutane photoproduct (T_m<>T_m): An acetone solution of **T_m-T_m** ($1x10^{-2}$ M) was irradiated in a Pyrex vessel (λ > 290 nm) under nitrogen atmosphere for 2 hours using a medium pressure mercury lamp (125 W). After that time, no traces of the substrate were detected by TLC using hexane/ethyl acetate (1:3) as eluent. The irradiated solution was evaporated to dryness. The residue was washed with cold ethanol and dried *in vacuo* to give **T_m<>T_m** (0.6, 70%) as a white solid. **^{1}H NMR** (300 MHz, $CDCl_3$) δ 4.48 – 4.45 (m, 1H), 4.44 – 4.40 (m, 1H), 3.77 (s, 2H), 3.13 (s, 6H), 2.74 – 2.66 (m, 2H), 2.43 – 2.19 (m, 1H), 1.65 – 1.63 (m, 1H), 1.58 (s, 6H). **^{13}C NMR** (75 MHz, $CDCl_3$) δ 168.9 (2C), 151.3 (2C), 59.9 (2CH), 48.9 ($2CH_2$), 45.8 (2C), 28.1 ($2CH_3$), 23.8 (CH_2), 21.2 ($2CH_3$).

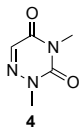

4

1,3-Dimethyl-6-azauracil (**4**)*:* 6-azauracil (1.0 g, 8.84 mmol) was added to a suspension of NaH (0.5 g, 19.45 mmol) in anhydrous DMF (22 mL) at 0 ºC. After stirring for 1 hour at rt, the reaction mixture was treated with iodomethane (1.2 mL, 19.45 mmol) and stirred for 16 hours. The solvent was removed, and the residue was purified by flash chromatography (silica gel, 100% dichloromethane) to give **4** (0.8 g, 70%) as a white solid powder. **^{1}H NMR** (300 MHz, $CDCl_3$) *δ* 7.36 (s,

1H), 3.63 (s, 3H), 3.33 ppm (s, 3H). **^{13}C NMR** (75 MHz, $CDCl_3$) δ 156.4 (C), 149.1 (C), 133.9 (CH), 39.8 (CH_3), 27.0 ppm (CH_3).

Cyclohexene-1,3-dimethyl-6-azauracil (**DCH<>AZT$_m$**). A solution of **4** (0.5 g, 3.54 mmol), 10 mL of acetone and 2.5 mL of cyclohexene in 30 mL of acetonitrile was placed in a Pyrex vessel (λ > 290 nm), purged with nitrogen and irradiated for 6 hours using a medium pressure mercury lamp (125 W). The solvent was removed, and the residue was purified by flash chromatography (silica gel, 93% dichloromethane/ethyl acetate) to give two products as white solids.

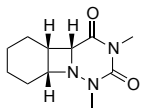

cis **DCH<>AZT$_m$**

***cis* DCH<>AZT$_m$** (0.32 g, 41%): **^{1}H NMR** (300 MHz, $CDCl_3$) δ 4.33 (d, J = 9.0 Hz, 1H), 4.01 (apparent q, J = 8.5 Hz, 1H), 3.15 (s, 3H), 2.98 (s, 3H), 2.93 (m, 1H), 2.04 – 1.93 (m, 1H), 1.84 – 1.69 (m, 1H), 1.65 – 1.30 (m, 4H), 0.99 – 0.87 ppm (m, 2H). **^{13}C NMR** (75 MHz, $CDCl_3$) δ 170.0 (C), 152.5 (C), 66.0 (CH), 63.9 (CH), 36.2 (CH), 30.4 (CH_3), 26.8 (CH_3), 23.3 (CH_2), 22.0 (CH_2), 21.4 (CH_2), 19.9 ppm (CH_2). **HRMS (ESI)**: m/z calcd for $C_{11}H_{18}N_3O_2$ $[M+H]^+$ 224.1399, found 224.1407.

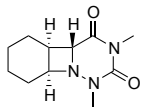

trans **DCH<>AZT$_m$**

***trans* DCH<>AZT$_m$** (0.28 g, 36%): **^{1}H NMR** (300 MHz, $CDCl_3$) δ 4.03 – 3.91 (m, 2H), 3.24 (s, 3H), 3.19 (s, 3H), 2.42 (q, J = 8.8 Hz, 1H), 2.20 – 1.58 (m, 5H), 1.49 – 1.31 (m, 1H), 1.16 – 0.96 ppm (m, 1H). **^{13}C NMR** (75 MHz, $CDCl_3$) δ 171.4 (C), 151.9 (C), 67.1 (CH), 66.9 (CH), 38.4 (CH), 33.0 (CH_3), 28.1 (CH_2), 27.4 (CH_2), 27.1 (CH_3), 22.2 (CH_2), 20.2 (CH_2). **HRMS (ESI)**: m/z calcd for $C_{11}H_{18}N_3O_2$ $[M+H]^+$ 224.1399, found 224.1392.

3.4.2 NMR Spectra (^{1}H, DEPT, ^{13}C)

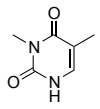

1

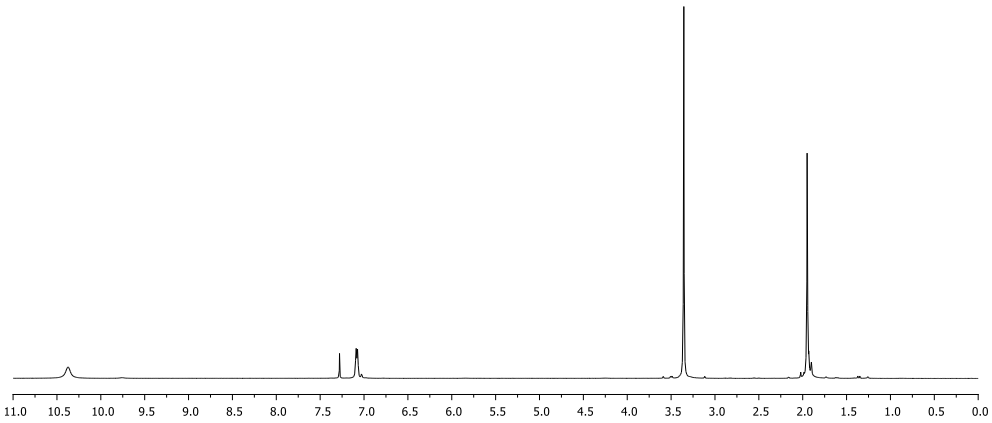
11.0
10.5
10.0
9.5
9.0
8.5
8.0
7.5
7.0
6.5
6.0
5.5
5.0
4.5
4.0
3.5
3.0
2.5
2.0
1.5
1.0
0.5
0.0

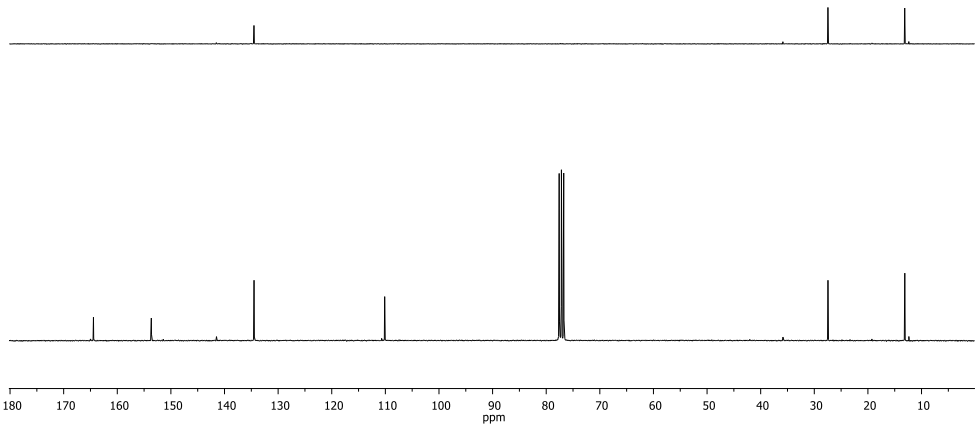
180
170
160
150
140
130
120
110
100
90
80
70
60
50
40
30
20
10
ppm

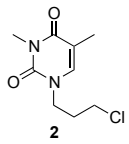
O
N
O
N
Cl

2

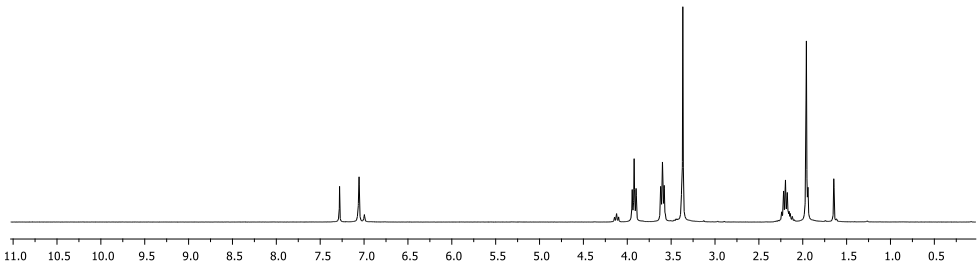
11.0 10.5 10.0 9.5 9.0 8.5 8.0 7.5 7.0 6.5 6.0 5.5 5.0 4.5 4.0 3.5 3.0 2.5 2.0 1.5 1.0 0.5

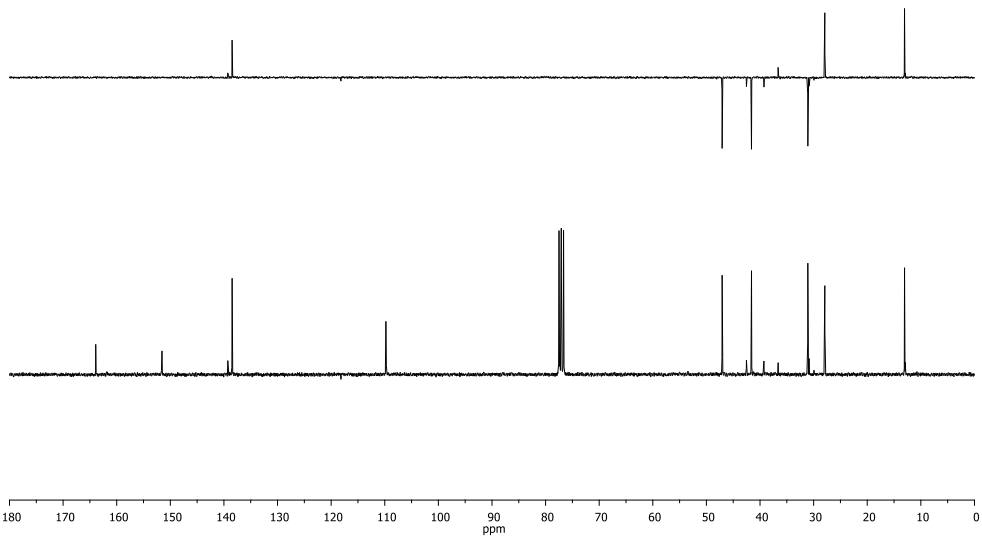
180 170 160 150 140 130 120 110 100 90 80 70 60 50 40 30 20 10 0
ppm

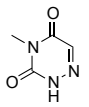

3

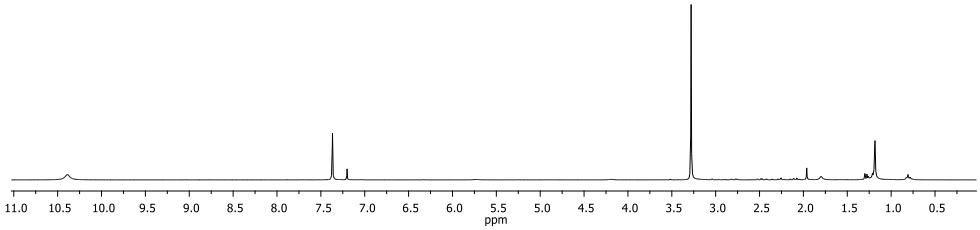
11.0 10.5 10.0 9.5 9.0 8.5 8.0 7.5 7.0 6.5 6.0 5.5 5.0 4.5 4.0 3.5 3.0 2.5 2.0 1.5 1.0 0.5
ppm

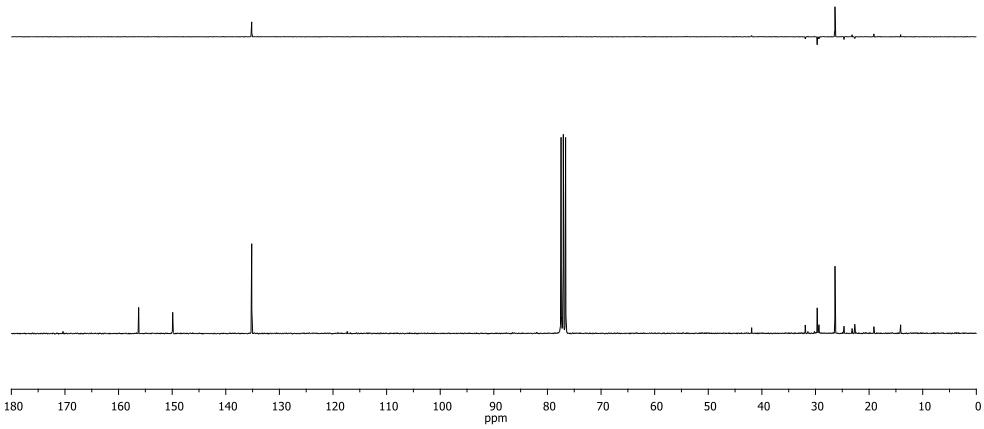
180 170 160 150 140 130 120 110 100 90 80 70 60 50 40 30 20 10 0
ppm

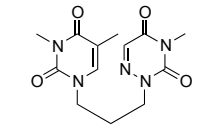

T_m-azaU_m

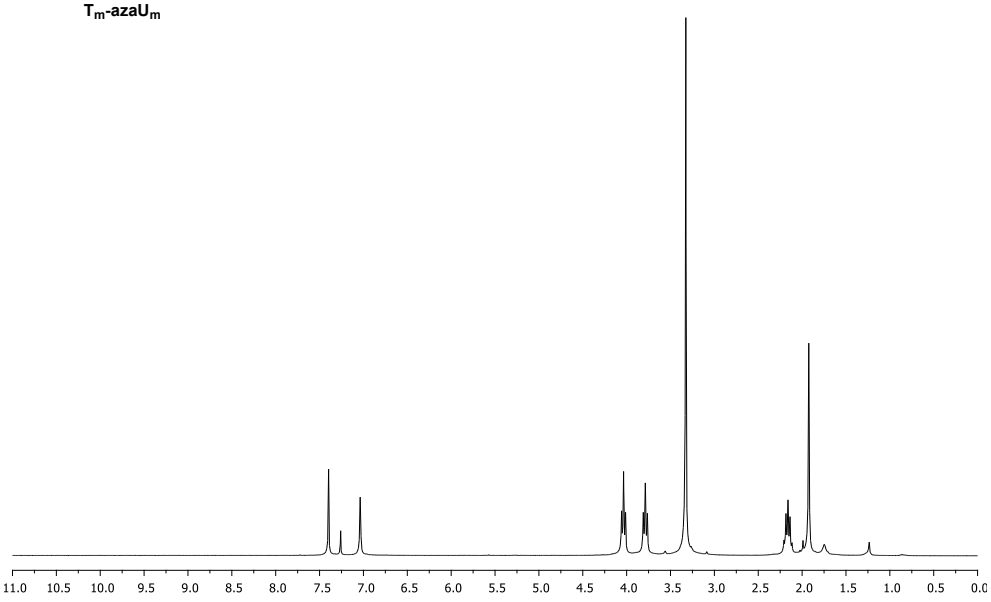
11.0 10.5 10.0 9.5 9.0 8.5 8.0 7.5 7.0 6.5 6.0 5.5 5.0 4.5 4.0 3.5 3.0 2.5 2.0 1.5 1.0 0.5 0.0

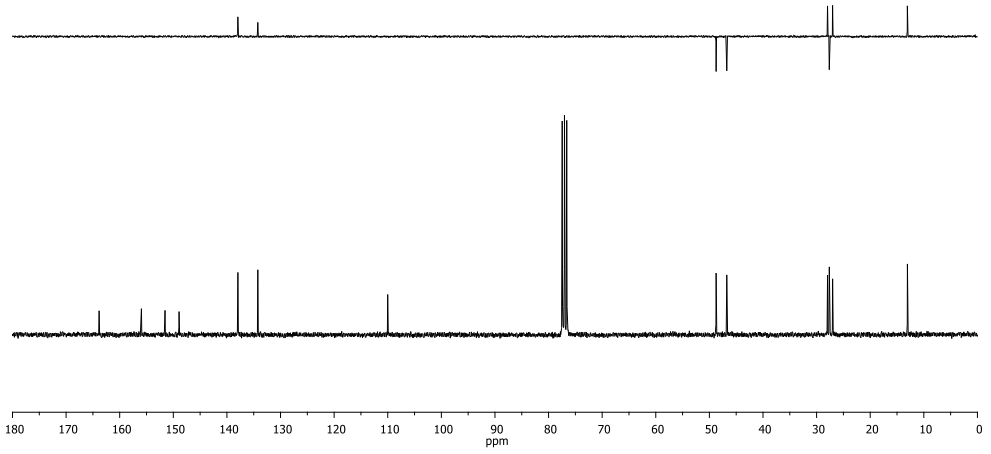
180 170 160 150 140 130 120 110 100 90 80 70 60 50 40 30 20 10 0
ppm

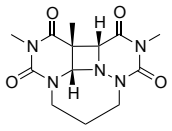

T_m<>AZT_m

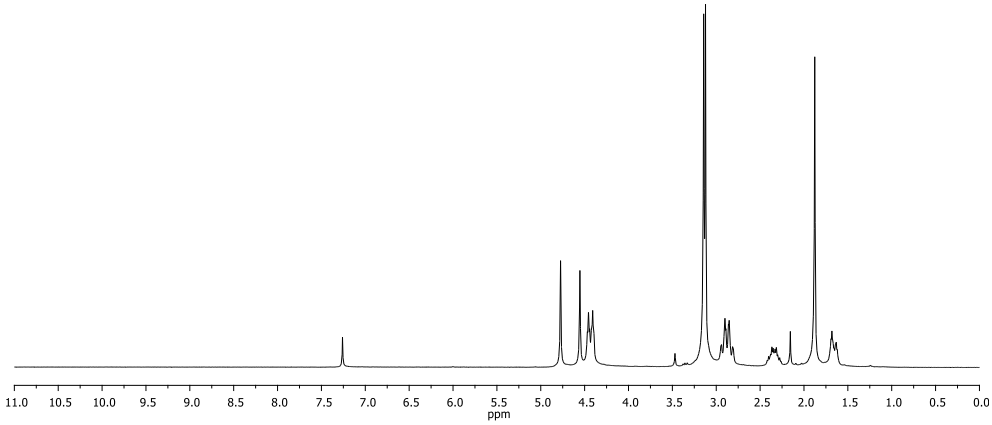
11.0 10.5 10.0 9.5 9.0 8.5 8.0 7.5 7.0 6.5 6.0 5.5 5.0 4.5 4.0 3.5 3.0 2.5 2.0 1.5 1.0 0.5 0.0
ppm

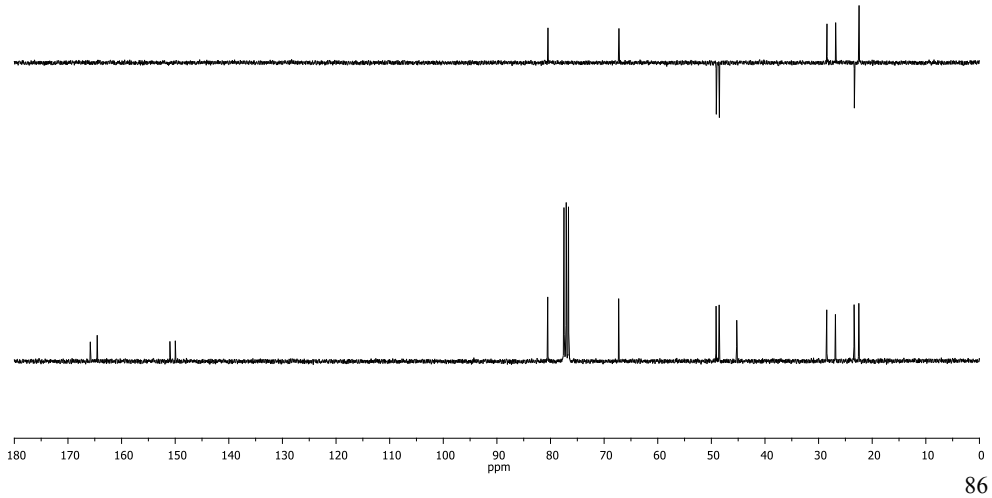
180 170 160 150 140 130 120 110 100 90 80 70 60 50 40 30 20 10 0
ppm

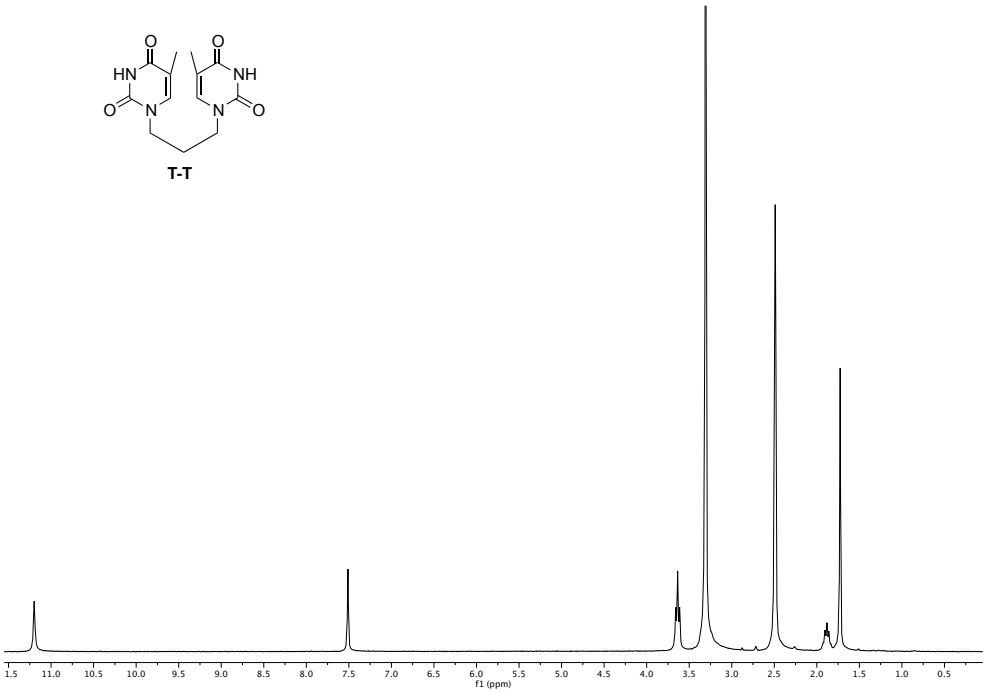
O
O
HN
NH
O
N
N
O
T-T
1.5 11.0 10.5 10.0 9.5 9.0 8.5 8.0 7.5 7.0 6.5 6.0 5.5 5.0 4.5 4.0 3.5 3.0 2.5 2.0 1.5 1.0 0.5
f1 (ppm)

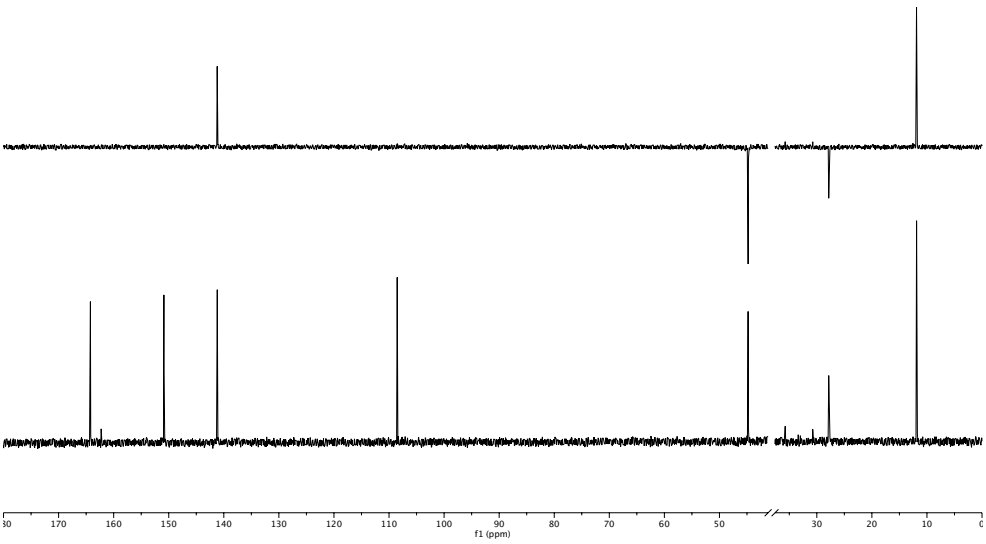
90 170 160 150 140 130 120 110 100 90 80 70 60 50 30 20 10 0
f1 (ppm)

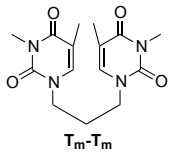

T_m-T_m

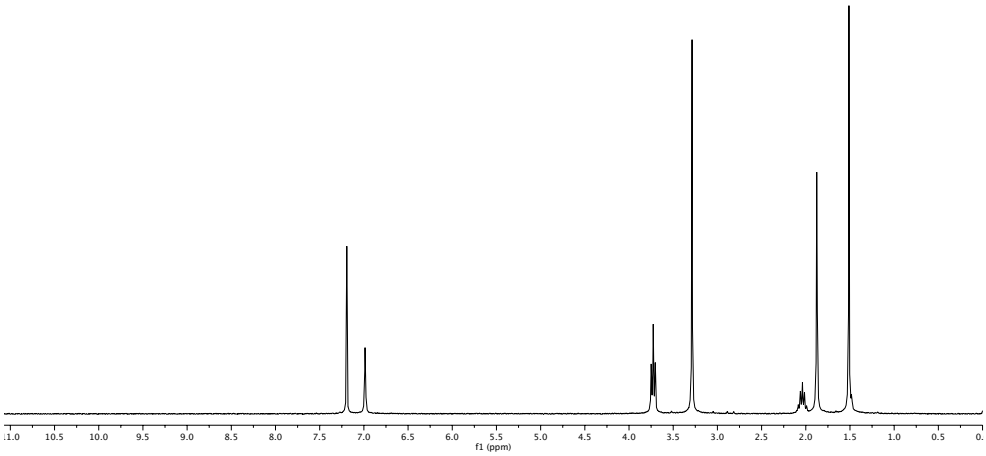

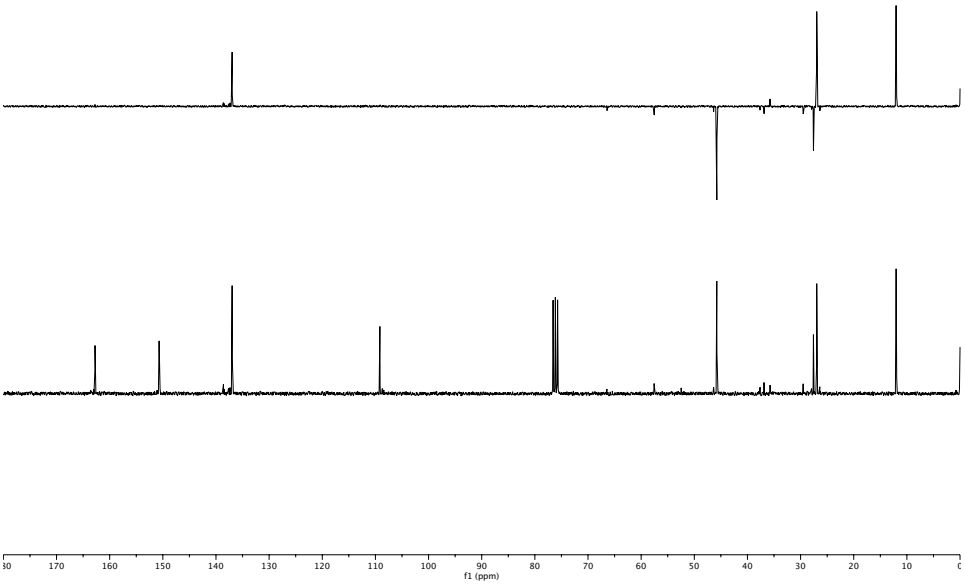

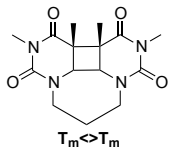

$T_m<>T_m$

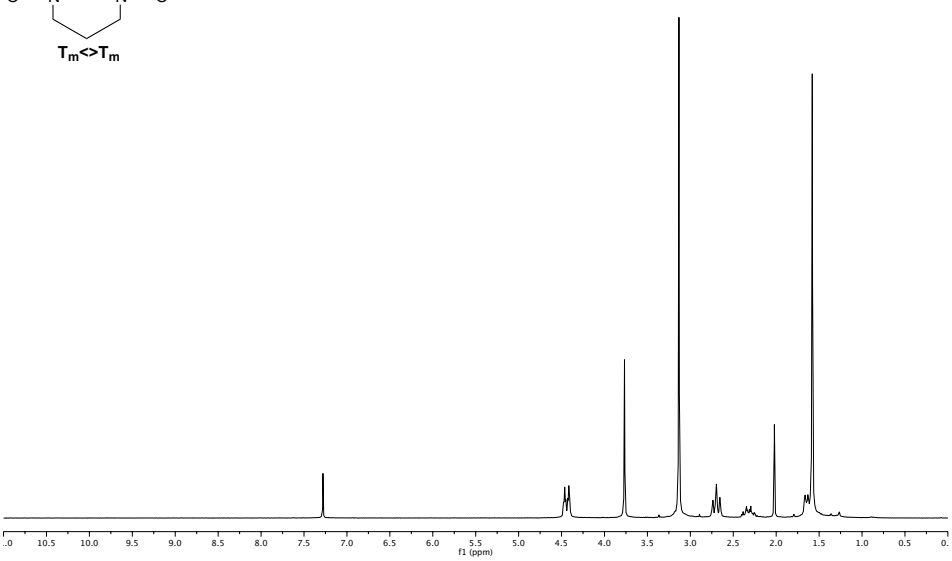

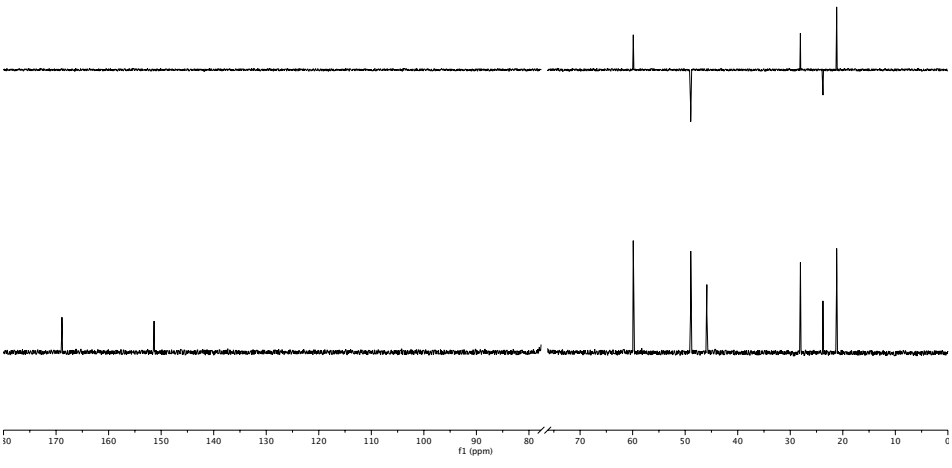

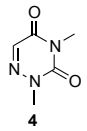
O
N
N
N
O

4

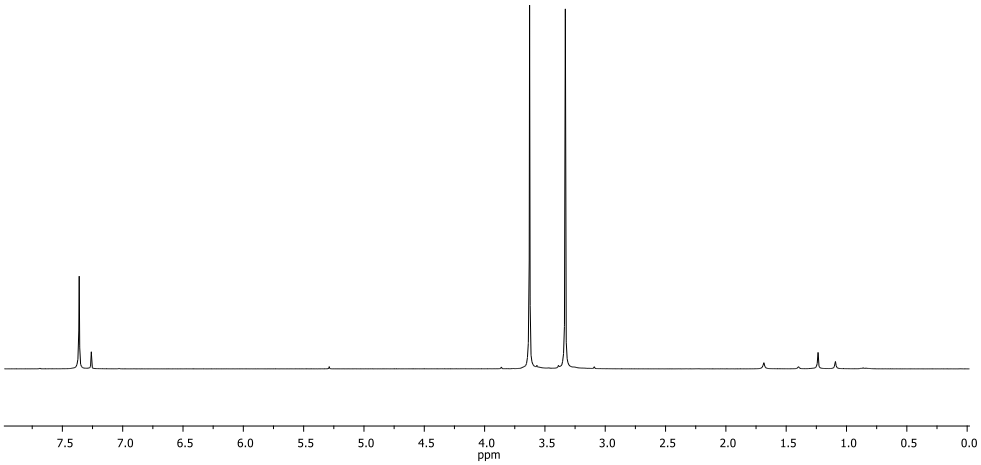
7.5
7.0
6.5
6.0
5.5
5.0
4.5
4.0
3.5
3.0
2.5
2.0
1.5
1.0
0.5
0.0
ppm

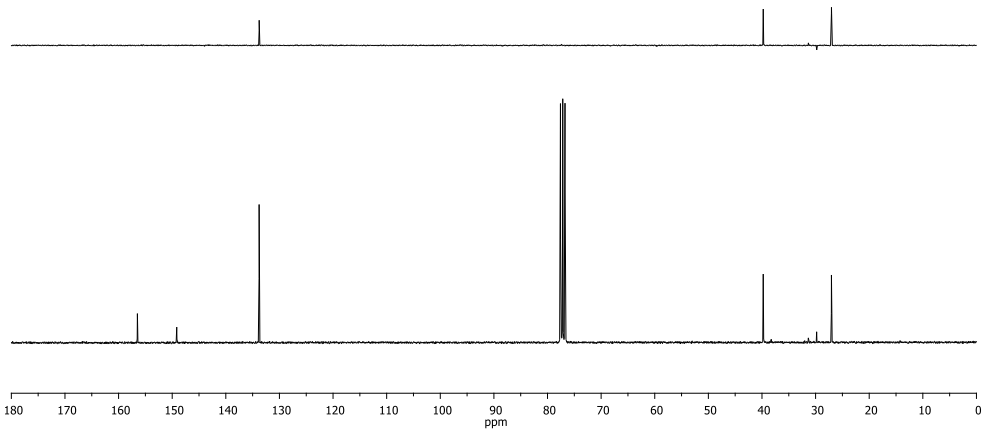
180
170
160
150
140
130
120
110
100
90
80
70
60
50
40
30
20
10
0
ppm

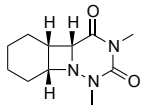
H
H
O
N
N
N
O
H

***cis* DCH<>AZT$_m$**

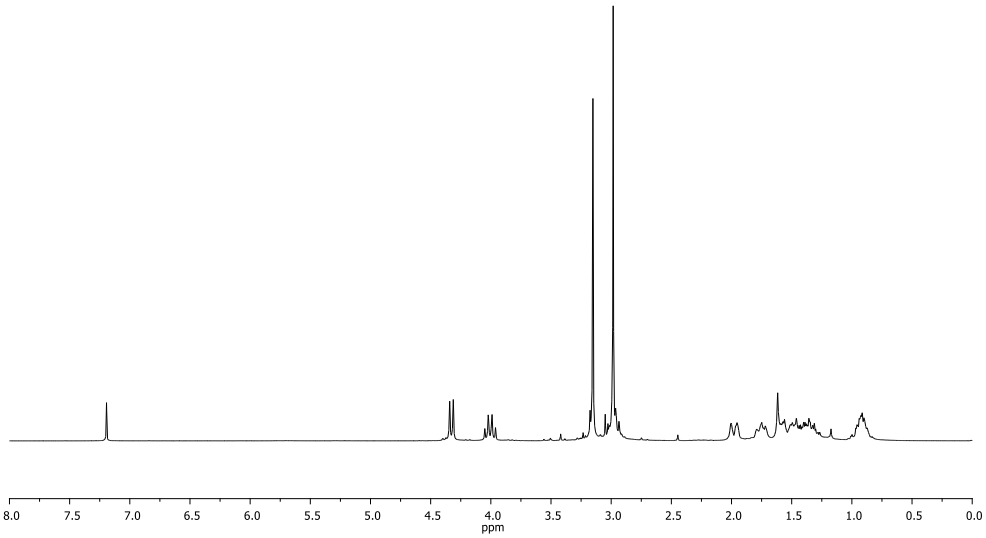
8.0
7.5
7.0
6.5
6.0
5.5
5.0
4.5
4.0
3.5
3.0
2.5
2.0
1.5
1.0
0.5
0.0
ppm

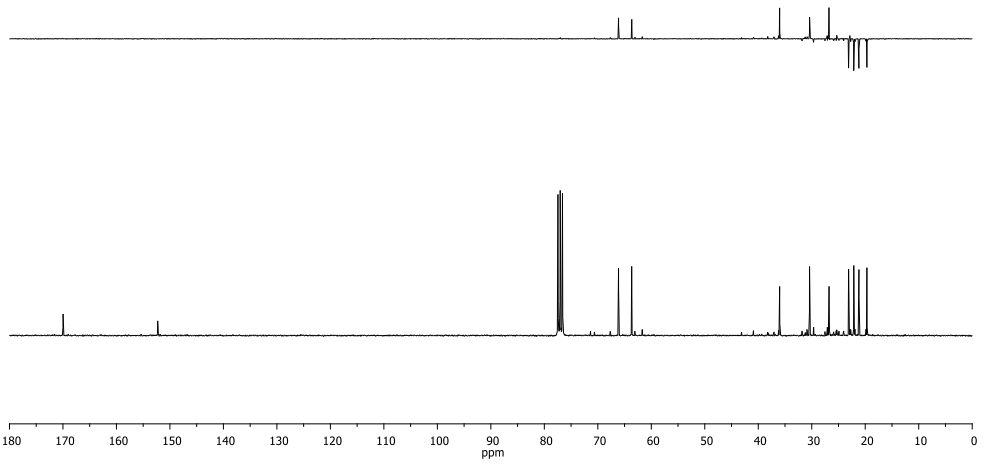
180
170
160
150
140
130
120
110
100
90
80
70
60
50
40
30
20
10
0
ppm

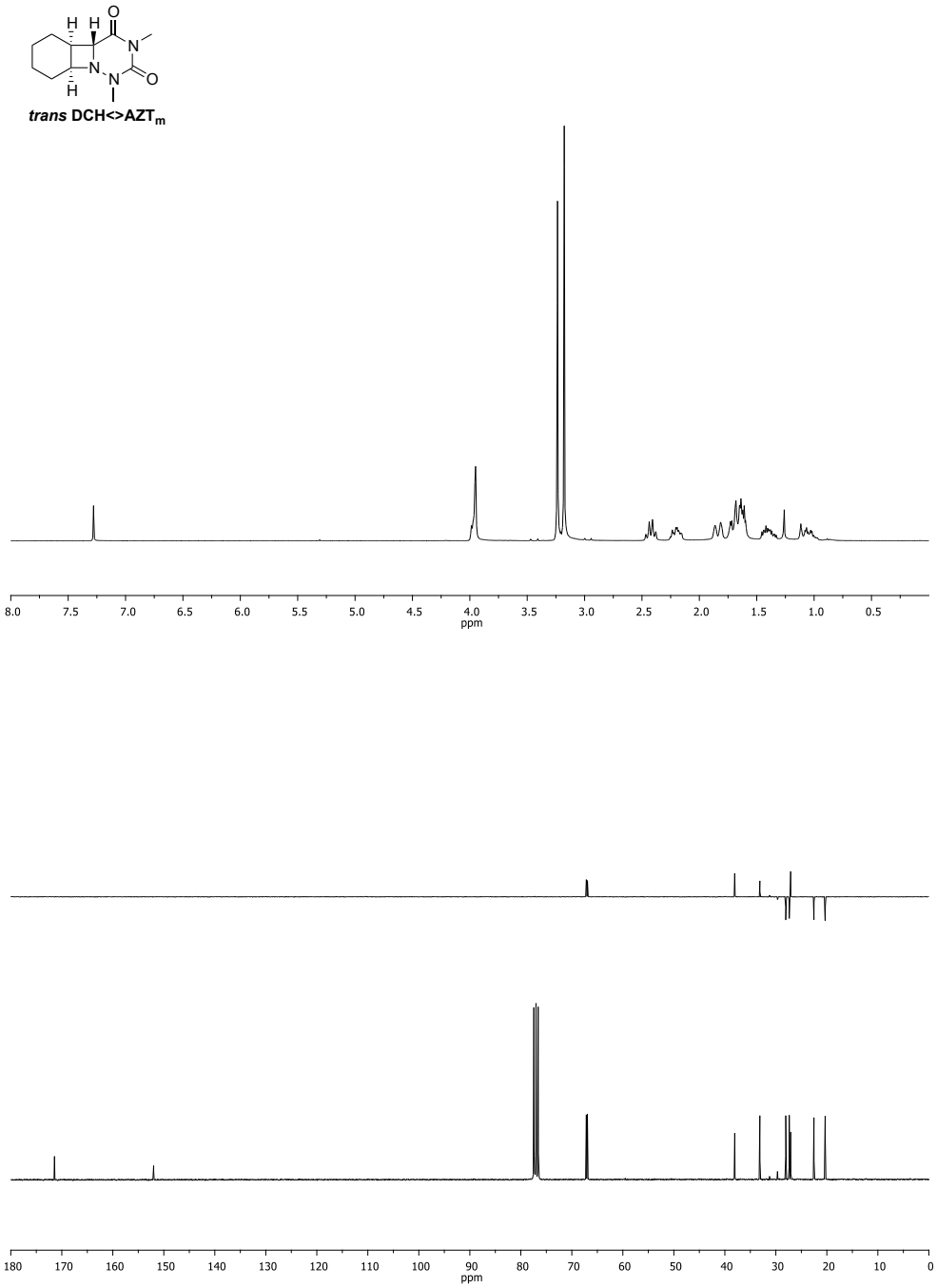
trans DCH<>AZT$_m$
8.0 7.5 7.0 6.5 6.0 5.5 5.0 4.5 4.0 3.5 3.0 2.5 2.0 1.5 1.0 0.5
ppm
180 170 160 150 140 130 120 110 100 90 80 70 60 50 40 30 20 10 0
ppm

3.4.3 Annex

Figure S1. NOESY spectrum of compounds ***cis*** and ***trans*** **DCH<>AZT$_m$**.

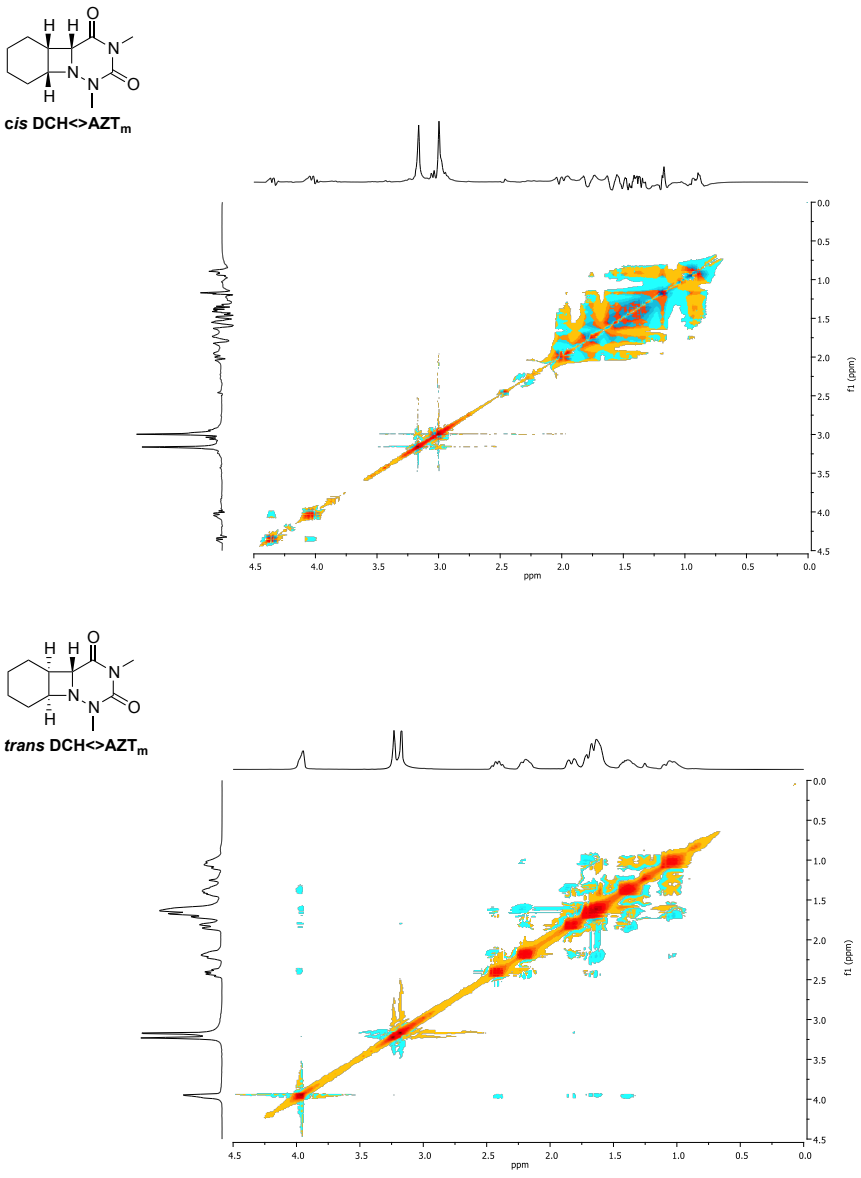

3.5 References

1. Gustafsson, C. M., http://www.nobelprize.org/nobel_prizes/chemistry/laureates/2015/advanced.html.

2. Yamamoto, J.; Plaza, P.; Brettel, K., Repair of (6-4) lesions in DNA by (6-4) photolyase: 20 years of quest for the photoreaction mechanism. *Photochem. Photobiol.* **2017,** *93*, 51-66.

3. Liu, Z.; Tan, C.; Guo, X.; Kao, Y. T.; Li, J.; Wang, L.; Sancar, A.; Zhong, D., Dynamics and mechanism of cyclobutane pyrimidine dimer repair by DNA photolyase. *Proc. Natl. Acad. Sci.* **2011,** *108*, 14831-14836.

4. Li, J.; Liu, Z.; Tan, C.; Guo, X.; Wang, L.; Sancar, A.; Zhong, D., Dynamics and mechanism of repair of ultraviolet-induced (6-4) photoproduct by photolyase. *Nature* **2010,** *466*, 887-890.

5. Perez-Ruiz, R.; Jimenez, M. C.; Miranda, M. A., Hetero-cycloreversions mediated by photoinduced electron transfer. *Acc. Chem. Res.* **2014,** *47*, 1359-1368.

6. Padwa, P., Photochemistry of the carbon-nitrogen double bond. *Chem. Rev.* **1977,** *77*, 37-68.

7. Cuquerella, M. C.; Lhiaubet-Vallet, V.; Bosca, F.; Miranda, M. A., Photosensitised pyrimidine dimerisation in DNA. *Chem. Sci.* **2011,** *2*, 1219-1232.

8. Kawamura, Y.; Kumagai, T.; Mukai, T., Photocycloaddition reaction of 3-aryl-2-isoxazolines with indene. *Chem. Lett.* **1985,** *14*, 1937-1940.

9. Sampedro, D., Computational exploration of the photocycloaddition of imines to alkenes. *ChemPhysChem* **2006,** *7*, 2456-2459.

10. Oe, K.; Tashiro, M.; Tsuge, O., Photochemistry of heterocyclic compounds. Photochemical reaction of 2,5-diaryl-1,3,4-oxadiazoles with indene. *J. Org. Chem.* **1977,** *42*, 1496-1499.

11. Anderson, D. R.; Keute, J. S.; Koch, T. H.; Moseley, R. H., Di-*tert*-butyl nitroxide quenching of the photoaddition of olefine to the carbon-nitrogen double bond of 3-ethoxyisoindolenone. *J. Am. Chem. Soc.* **1977,** *99*, 6332-6340.

12. Swenton, J. S.; Hyatt, J. A., Photosensitized cycloadditions to 1,3-dimethyl-6-azauracil and 1,3-dimethyl-6-azathymine. An imine linkage unusually reactive toward photocycloaddition. *J. Am. Chem. Soc.* **1974,** *96*, 4879-4885.

13. Kobayashi, T.; Harada, Y.; Suzuki, T.; Ichimura, T., Excited state characteristics of 6-azauracil in acetonitrile: drastically different relaxation mechanism from uracil. *J. Phys. Chem. A* **2008,** *112*, 13308-13315.

14. Perez-Ruiz, R.; Saez, J. A.; Domingo, L. R.; Jiménez, M. C.; Miranda, M. A., Ring splitting of azetidin-2-ones via radical anions. *Org. Biomol. Chem.* **2012,** *10*, 7928-7932.

15. Perez-Ruiz, R. S., J. A.; Jimenez, M. C.; Miranda, M. A., Cycloreversion of beta-lactams via photoinduced electron transfer. *Org. Biomol. Chem.* **2014,** *12*, 8428-8432.

16. Zasada-Parzynska, A.; Celewicz, L.; Golankiewicz, K., Synthesis and photochemical properties of pyrimidine-6-azapyrimidine analogs of dinucleotides with propanone bridge. *Synth. Commun.* **1984,** *16*, 1177-1185.

17. Jankowska, J.; Koroniak, H.; Golankiewicz, K., The influence of alkyl substituents on internal photodimerization of pyrimidine-6-azapyrimidine dinucleotide analogues. *Heterocycles* **1984,** *22*, 1363-1368.

18. Golankiewicz, K.; Jankowska, J.; Koroniak, H., Internal photodimerization of some pyrimidine-6-azapyrimidine dinucleotide analogues. *Heterocycles* **1984,** *22*, 67-72.

19. Kochevar, I. E.; Wagner, P. J., Quenching of triplet phenyl ketones by olefins. *J. Am. Chem. Soc.* **1972,** *94*, 3859-3865.

20. Tatake, V. G.; Desai, T. S.; Sane, P. V., Isothermal luminescence and thermo-luminescence of nucleic acid bases following gamma irradiation. *Photochem. Photobiol.* **1976,** *24*, 463-472.

21. Leonard, N.; Golankiewicz, K.; McCredie, R.; Johnson, S.; Paul, I., Synthetic spectroscopic models related to coenzymes and base pairs. III. A 1,1'-trimethylene-linked thymine photodimer of *cis-syn* structure. *J. Am. Chem. Soc.* **1969,** *91*, 5855-5862.

22. Leonard, N. J., Trimethylene bridges as synthetic spacers for the detection of intramolecular interactions. *Acc. Chem. Res.* **1979,** *12*, 423-429.

23. Browne, D. T. E., J.; Leonard, N. J., Synthetic spectroscopic models related to coenzymes and base pairs. II Evidence for intramolecular base-base interactions in dinucleotide analogs. *J. Am. Chem. Soc.* **1968,** *90*, 7302-7323.

24. Yeh, S. R.; Falvey, D. E., Model studies of DNA photorepair: energetic requirements for the radical anion mechanism determined by fluorescence quenching. *J. Am. Chem. Soc.* **1992,** *114*, 1971-1977.

25. Scannell, M. P.; Fenick, D. J.; Yeh, S.; Falvey, D. E., Model studies of DNA photorepair: reduction potentials of thymine and cytosine cyclobutane dimers measured by fluorescence quenching. *J. Am. Chem. Soc.* **1997,** *119*, 1971-1977.

26. Hartman, R. F.; Rose, S. D.; Pouwels, P. J. W.; Kaptein, R., Flavin-sensitized photochemically induced dynamid nuclear polarization detection of pyrimidine dimer radicals. *Photochem. Photobiol.* **1992,** *56*, 305-310.

27. Pouwels, J. W.; Kaptein, R.; Hartman, R. F.; Rose, S. D., Photo-CIDNP study of pyrimidine dimer splitting I: reactions involving pyrimidine radical cation intermediates. *Photochem. Photobiol.* **1995,** *61*, 563-574.

28. Kao, Y. T.; Saxena, C.; He, T. F.; Guo, L.; Wang, L.; Sancar, A.; Zhong, D., Ultrafast dynamics of flavins in five redox states. *J. Am. Chem. Soc.* **2008,** *130*, 13132-13139.

29. Kao, Y. T. S., Q. H.; Saxena, C.; Wang, L.; Zhong, D., Dynamics and mechanism of DNA repair in a biomimetic system: flavin-thymine dimer adduct. *J. Am. Chem. Soc.* **2012,** *134*, 1501-1503.

30. Trzcionka, J.; Lhiaubet-Vallet, V.; Paris, C.; Belmadoui, N.; Climent, M. J.; Miranda, M. A., Model studies on a carprofen derivative as dual photosensitizer for thymine dimerization and (6-4) photoproduct repair. *ChemBioChem* **2007,** *8*, 402-407.

31. Boussicault, F.; Kruger, O.; Robert, M.; Wille, U., Dissociative electron transfer to and from pyrimidine cyclobutane dimers: An electrochemical study. *Org. Biomol. Chem.* **2004,** *2*, 2742-2750.

32. Boussicault, F. R., M., Electron transfer in DNA and in DNA-related biological processes. Electrochemical insights. *Chem. Rev.* **2008,** *108*, 2622-2645.

33. Ide, H.; Otsuki, N.; Nishimoto, S.; Kagiya, T., Photoreduction of thymine glycol sensitized by aromatics amines in aqueous solution. *J. Chem. Soc. Perkin. Trans. 2* **1985**, 1387-1392.

34. Durbeej, B.; Eriksson, L. A., Thermodynamics of the photoenzymatic repair mechanism studied by density functional theory. *J. Am. Chem. Soc.* **2000,** *122*, 10126-10132.

Chapter 4:
Study of Azetidines Cycloreversion by Oxidative Electron Transfer

4.1 Introduction

As mentioned previously, the UV-induced CPDs and 6-4PPs are repaired by photolyases through a photoreductive process from the reduced flavin cofactor $FADH^-$. However, although CPD photolyase uses a reductive single electron transfer to initiate the cycloreversion, it has been shown that the cycloreversion of the CPD can also be achieved *in vitro* through an oxidative pathway.[1] In this context, an important result has been the long range repair of thymine dimers incorporated in DNA duplex by means of a reaction involving an electron transfer to a rhodium intercalator activated with visible light.[2] This result opened the door to consider the photooxidative approach as a relevant tool for DNA therapies, and thus, to develop new photoactive chemotherapeutic agents.

In model systems, numerous molecules and ions have been found to be able to split photochemically T<>T in solution through an oxidative pathway.[3-7] Most of the experimental investigations were performed using photosensitizers to oxidize T<>T, but oxidizing radicals and radical ions were also employed. Compounds such as potassium hexacyanoferrate (III) ($K_3Fe(CN)_6$[7] and uranyl(IV) sulfate (UO_2SO_4)[7] have been reported as inorganic photooxidants, or anthraquinone-2-sulfonate (AQS)[4], anthraquinone (AQ)[5], 9,10-dicyanoanthracene (DCA)[4], 2,3-dichloro-5,6-dicyano-1,4-quinone (DDQ)[5] and protonated 2', 3', 4', 5'-tetraacetylriboflavin (Ac_4rfH^+)[6, 8] for the organic counterparts (Figure 4.1).

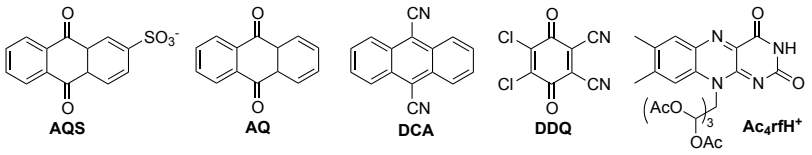

Figure 4.1. Most important photooxidants used in the studies for oxidative repair of T<>T dimers.

The assumed mechanism for oxidative splitting of T<>T is given in Scheme 4.1.[9] Electron transfer from T<>T to the oxidant leads to formation of an unstable radical cation $T^{\bullet+}$<>T of the dimer, with the charge located on the nitrogen atom, which rapidly fragments (lifetime < 1 ns)[10]. However, as the radical cation is delocalized, it is not unreasonable to propose that the C5-C5' and C6-C6' bonds are equally weakened and thus that the cleavage of two cyclobutyl bonds might be a two-step, or a concerted process. The measurement of the isotope effects on the fragmentation of C5-C5' and C6-C6' bonds of a model photodimer by an anthraquinone-sensitized cleavage supported a stepwise mechanism where the first C6-C6' bond cleavage is effectively irreversible.[11] Theoretical studies also supported the two-step mechanism via biradical structure formed after the opening C6-C6' bond.[12] Therefore, the oxidative mechanism follows two-sequential cleavage of the C6-C6' bond and the C5-C5' bond, which finally leads to a repaired base and its radical cation $T^{\bullet+}$. The latter was found to initiate a radical chain through oxidation of further dimer T<>T.[13] Photochemically induced dynamic nuclear polarization (CIDNP) experiments using AQS as PS, demonstrated the existence of both $T^{\bullet+}$<>T and its dissociation product, the monomer radical cation $T^{\bullet+}$.[14]

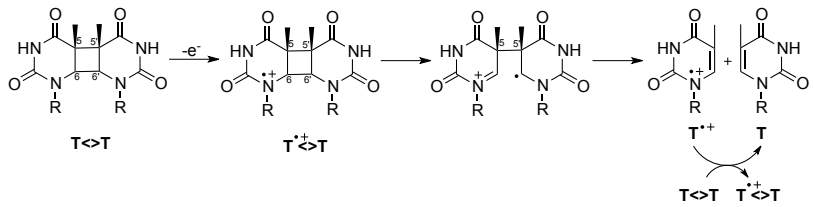

Scheme 4.1. Oxidative pathway for T<>T splitting.

In case of 6-4PPs, theoretical calculations have studied the possible involvement of both the anionic and cationic pathways in the regeneration of native pyrimidines from azetidine and oxetane lesions.[15] In this context, the oxidative cycloreversion has been widely reported for oxetane models with photooxidants such as cyanonaphtha-

lenes or tetraacetylriboflavin; and involvement of the singlet excited state of the PS was supported by fluorescence experiments.[16-17]

A nonconcerted two-step mechanism has been proposed for the splitting on the basis of the loss of products stereochemistry.[16] In addition, theoretical calculations supported this two-step mechanism for the 6-4PPs oxetane intermediate through an initial C-C bond breaking, followed by cleavage of the C-O bond.[15] Interestingly, the detection of 1,4-radical cations involved in the cycloreversion of hydroxymethyl-diphenyloxetane by intramolecular nucleophilic trapping with (thia)pyrylium salts showed that the process occurs through a nonconcerted mechanism starting with an initial cleavage of the C-O bond.[18]

Although there are a plenty of research articles with regard to oxidative cycloreversion of oxetane models, only one work dealing with azetidine models has been reported until now.[19] It addresses the cycloreversion of 1,2,3-triphenylazetidine achieved by oxidation with tris(4-bromophenyl)aminium hexachloroantimonate (also named BAHA) to lead to *cis*- and *trans*-stilbene, together with *N*-benzylideneaniline. The process was shown to ocurr through a stepwise cycloreversion of the azetidine radical through pathways a or b (Scheme 4.2).

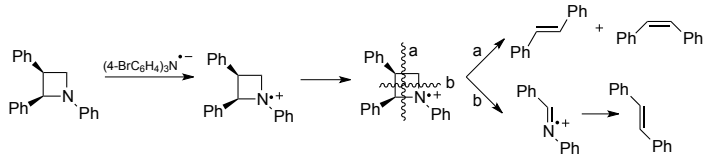

Scheme 4.2. Mechanistic pathways for the cycloreversion of azetidine radical cations.

In this context, oxidative electron transfer has only been investigated with triphenylazetidines, which are structurally unrelated to pyrimidine bases. Thus, in this chapter a photooxidative approach has been applied to the ring splitting of azabipyrimidinic azetidine **T_m<>AZT_m** previously studied in Chapter 3. Moreover,

parallel studies of photoinduced oxidative cycloreversion of **T_m<>T_m** and **DCH<>AZT_m** (Figure 4.2) have been included to investigate how the presence of the nitrogen atom in the four-membered ring affects in the ring splitting.

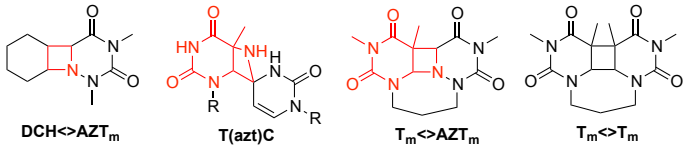

Figure 4.2. Structures of the azetidine models (**DCH<>AZT_m** and **T_m<>AZT_m**) studied in this chapter, in relation with the intermediate **T(azt)C** involved in the photorepair mechanism of 6-4PPs at TC sequences, and the cyclobutane derivative **T_m<>T_m**.

4.2 Results and discussion

4.2.1 Fluorescence experiments

Assuming that the photooxidative cycloreversion of azetidine is a nonconcerted two-step mechanism, two pathways can be proposed on the basis of the location of the formed radical cation. Thus, the photosensitizer is an electron acceptor in its excited state that, accepts an electron to generate the radical cation centered on the nitrogen atom of the thymine or azaU moiety of **T_m<>AZT_m**, followed by a two-step cleavage of C6-C6' and C5-C5' to lead to the repaired bases **T_m-azaU_m** as shown in Scheme 4.3.

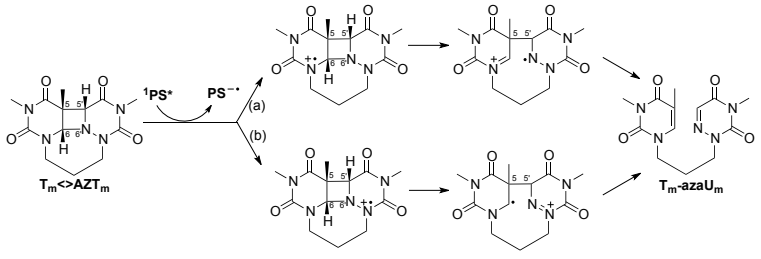

Scheme 4.3. Oxidative PET mechanisms of **T_m<>AZT_m** in the presence of PS.

In a first step, fluorescence experiments were performed with photooxidants in order to evaluate the possibility of an electron transfer process from **T_m<>AZT_m** to the singlet-excited state of the photosensitizer. In addition, the same experiments were achieved for **T_m<>T_m** and **DCH<>AZT_m** in order to know which moiety is key in the photooxidative process.

Therefore, 1,4-dicyanonaphthalene (DCN) and 9,10-dicyanoanthracene (DCA) were selected as the electron acceptors (Figure 4.3), their reduction potential in the singlet excited state (E_{red}^{D*}) being of ca. 2.4 and 1.8 V vs. Ag/AgCl, respectively.[20]

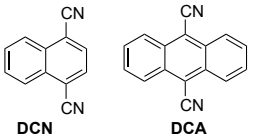

Figure 4.3. Structure of the used photosensitizers (PS).

Acetonitrile solutions of the photosensitizer were prepared with an absorbance of ca. 0.15 at the excitation wavelength (λ_{exc}=310 or 375 nm) and the fluorescence intensity was measured in the absence and in the presence of **T_m<>AZT_m**, **T_m<>T_m** or **DCH<>AZT_m**. As shown in Figure 4.4, steady-state fluorescence measurements revealed a strong decrease of the emission intensity of DCN and DCA for **T_m<>AZT_m** with k_q, obtained from Stern-Volmer plots, of 72.8 and 7.0 x 10^9 M^{-1} s^{-1}, respectively. By contrast, small quenching of the photosensitizer was obtained for **T_m<>T_m** and lower values of k_q of ca. 15.8 and 0.4 x 10^9 M^{-1} s^{-1} were determined for the DCN and DCA (Figure 4.4), respectively.

However, the rate constant for DCN/**T_m<>AZT_m** was abnormally high as it is faster than the diffusion control in acetonitrile, k_{diff} of ca. 1.9 x 10^{10} M^{-1} s^{-1}. Actually, partial light absorption by the concentrated quencher occurs when the sample is excited at 310 nm, reducing the portion of light absorbed by the photosensitizer, which results in a decrease of the emission intensity. By contrast, the longer excitation wave-

length used for DCA (λ_{exc} = 375 nm) should ensure a more selective excitation of the photooxidant.

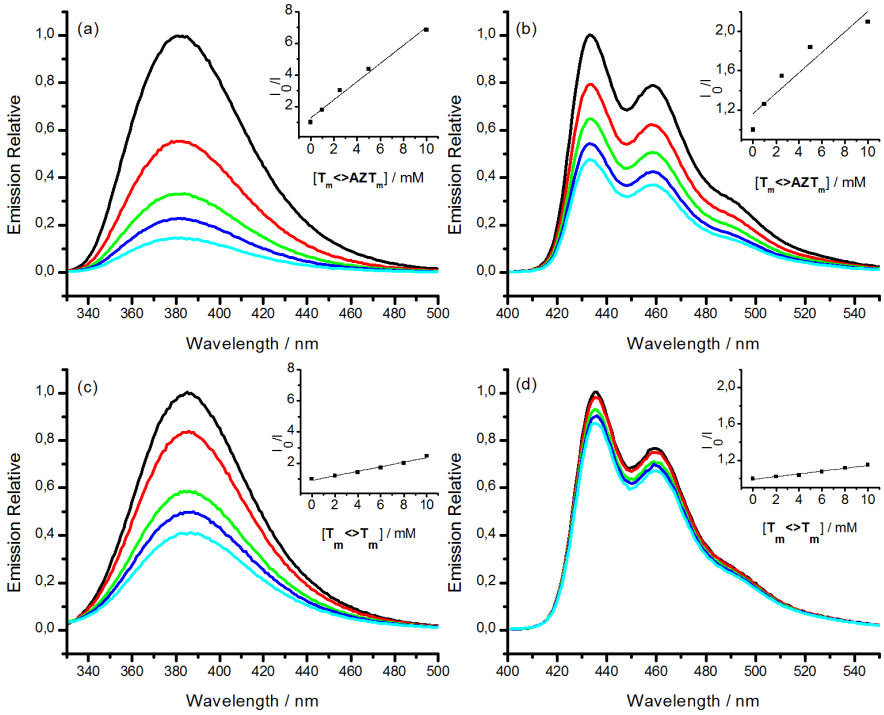

Figure 4.4. Fluorescence emission spectra for (a, c) DCN (λ_{exc}= 310 nm); (b,d) DCA (λ_{exc}= 375 nm); in the presence of increasing amounts of **T_m<>AZT_m** (top) and **T_m<>T_m** (bottom) from 0 to 10 mM.

To overcome this drawback and to evaluate whether a dynamic quenching is taking place, time-resolved fluorescence studies were performed (Figure 4.5). For the photooxidation process, a bimolecular quenching rate constant of ca. 7.8 x 10^9 M^{-1} s^{-1} was obtained for the quenching of DCN and DCA by **T_m<>AZT_m**. As expected, lower values (k_q of 3.0 and <0.5 x 10^9 M^{-1} s^{-1}) were determined with the cyclobutane derivatives as deactivating species (Table 4.1). This revealed a more difficult oxidation

of this compound by comparison with **T_m<>AZT_m**, which suggested that the azaU moiety plays a role in the photooxidative process.

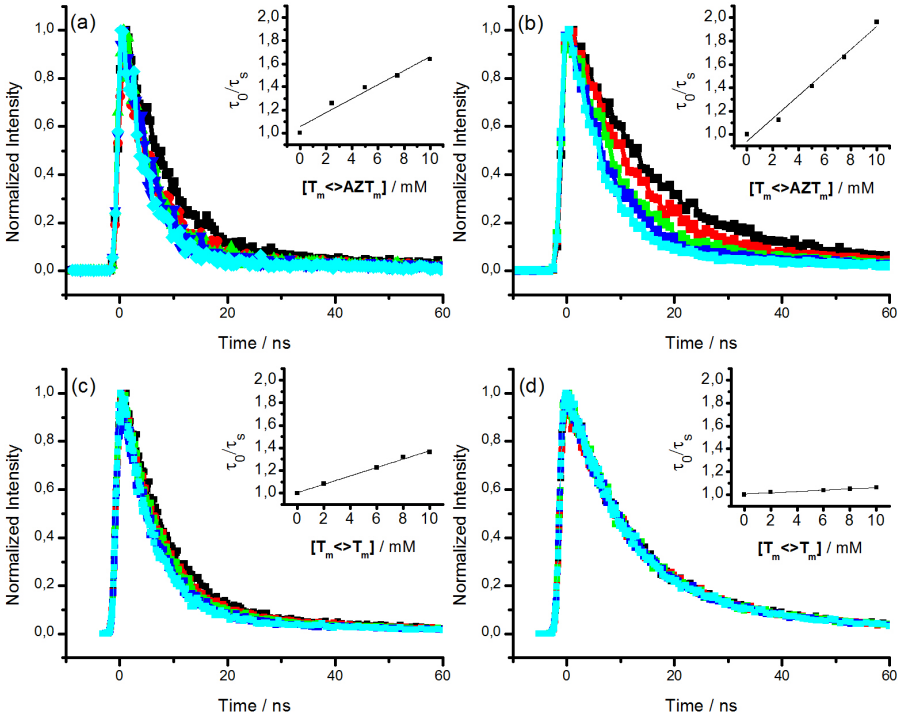

Figure 4.5. Fluorescence kinetic traces and their corresponding Stern-Volmer plot obtained for (a) DCN (λ_{exc}= 310 nm) and (b) DCA (λ_{exc}= 375 nm) in the presence of increasing amounts of **T_m<>AZT_m** (from 0 to 10 mM); (c) DCN (λ_{exc}= 310 nm) and (d) DCA (λ_{exc}= 375 nm) in the presence of increasing amounts of **T_m <>T_m** (from 0 to 10 mM).

Table 4.1. Reduction potential in the singlet excited state (E_{red}^{D*}) of the selected PS, and bimolecular rate constant (k_q) for the quenching of the PS by **T_m<>AZT_m** or **T_m<>T_m** determined by time-resolved fluorescence.

PS	τ / ns	E_{red}^{D*} / V vs. Ag/AgCl	k_q/x10^9 M^{-1}s^{-1}	
			T_m<>AZT_m	**T_m<>T_m**
DCN	7.5	2.4	7.8	3.0
DCA	12.5	1.8	7.8	<0.5

In order to support that the presence of azaU has an influence on the oxidative azetidine splitting, steady-state and time-resolved fluorescence experiments were performed with ***cis*** and ***trans*** **DCH<>AZT_m** azetidines. As anticipated, the photooxidant emissions suffered an important quenching for both azetidines although a more efficient quenching was observed for the ***cis*** isomer (Figure 4.6). Moreover, the singlet lifetime of all these photooxidants was shortened in the presence of the azetidine derivatives as shown in Figure 4.7. The bimolecular quenching rate constants (k_q, Table 4.2) were determined by Stern-Volmer plot using the data obtained by time-resolved fluorescence.[21] A remarkable difference of quenching efficiency was observed between ***cis*** and ***trans*** (see k_q, Table 4.2) as shown for steady-state fluorescence (Figure 4.6), with similar k_q values than for **T_m<>AZT_m** suggesting a close value of their oxidation potentials.

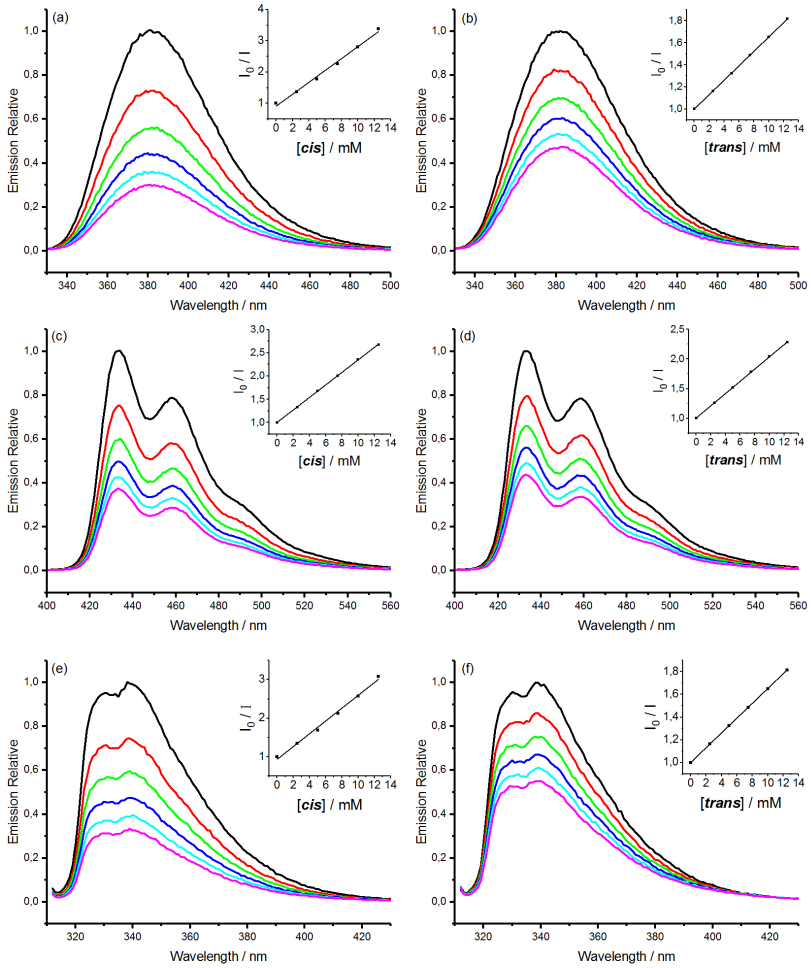

Figure 4.6. Fluorescence emission spectra for (a,b) DCN (λ_{exc}= 310 nm); (c,d) DCA (λ_{exc}= 375 nm); (e,f) CNN (λ_{exc}= 310 nm) in the presence of increasing amounts of ***cis*** (left panel) and ***trans*** (right panel) **DCH<>AZT$_m$** from 0 to 12.5 mM.

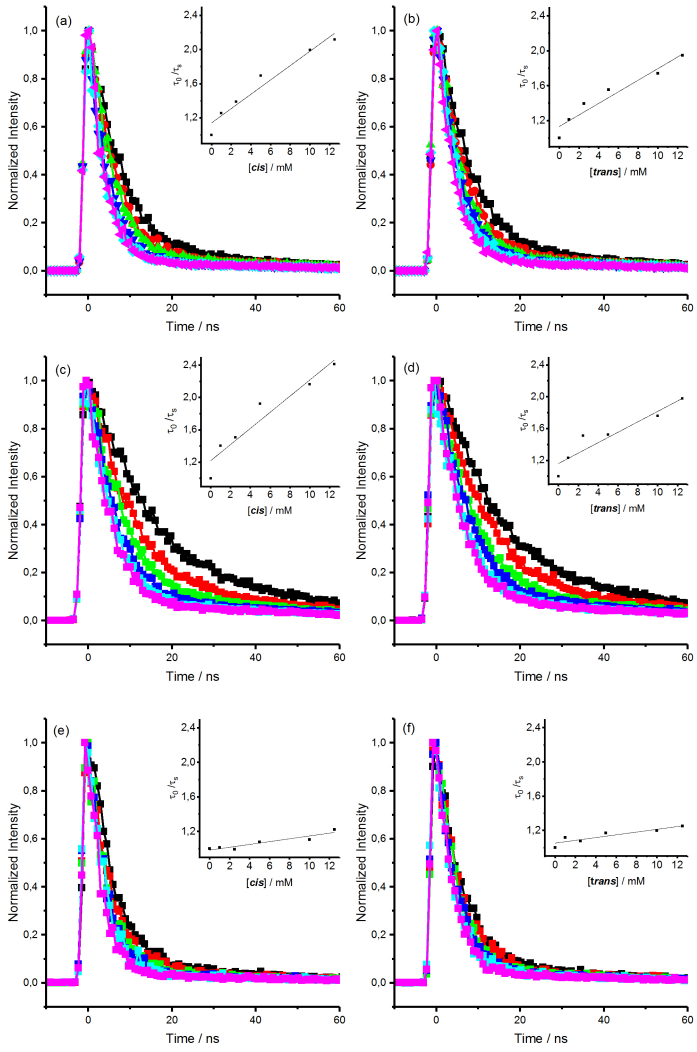

Figure 4.7. Fluorescence kinetic traces and their corresponding Stern-Volmer plot obtained for (a,b) DCN (λ_{exc}= 310 nm); (c,d) DCA (λ_{exc}= 375 nm); (e,f) CNN (λ_{exc}= 310 nm) in the presence of increasing amounts of ***cis*** (left panel) and ***trans*** (right panel) **DCH<>AZT$_m$** from 0 to 12.5 mM.

The two isomers have the same bonds and connectivity; however, they differ in the arrangement of the dihydroazauracil and cyclohexane rings. A similar stereoselectivity has previously been reported for photoreduction of the *cis-syn* and *trans-syn* diastereoisomers of cyclobutane dimethylthymine dimer.[22] The more difficult reduction of the *cis-syn* isomer was attributed to a stereoelectronic effect as the formed anion radical suffers an unfavorable charge-dipole interaction with the carbonyl in C_4 of the other pyrimidine ring. Nevertheless, this explanation cannot be extended to our ***cis*** and ***trans*** isomers as the cyclohexane ring does not provide pronounced electronic effects, and the most likely explanation relies on different constraints of the azetidine ring.

Table 4.2. Photophysical properties of the selected photosensitizers and their quenching rate constants by ***cis*** and ***trans*** **DCH<>AZT$_m$** determined by time-resolved fluorescence.

PS	**E^*/ kJ mol$^-$**	**E^{D*}_{red} / V vs. Ag/AgCl**	**k_q/x10^9 M^{-1}s^{-1}**	
			cis	***trans***
DCN	362	2.4	10	7.7
DCA	276	1.8	6.4	4.6

According to the Rehm-Weller equation, the quenching process was more efficient as E^{D*}_{red} increased, which supports an electron transfer mechanism for quenching. Indeed, singlet-singlet energy transfer can be ruled out because the absorption bands of **T$_m$<>AZT$_m$, T$_m$<>T$_m$** and **DCH<>AZT$_m$** compounds are below 300 nm. Thus, their singlet energies (E^*) can be safely estimated to be >400 kJ mol^{-1}, that is more than 25 kJ mol^{-1} higher than energy of the highest E^* of the selected photosensitizer (Table 4.2).

4.2.2 Electrochemical measurements

The different behavior observed for **T_m<>AZT_m** and **DCH<>AZT_m** in comparison with **T_m<>T_m** must be in connection with their oxidation potential. Thus, their electrochemical properties were studied by cyclic voltammetry as shown in Figure 4.8. According to the electron removal, two irreversible waves were observed for the dyad **T_m<>AZT_m**, the first one with a peak potential $E_p(1)$ at ca. 1.34 V and the second one $E_p(2)$ at ca. 1.93 V. Interestingly, ***cis*** **DCH<>AZT_m** showed a single wave at 1.30 V, which is really close to the first E_p of **T_m<>AZT_m**, and supports the similar k_q obtained by fluorescence experiments. However, a more positive value at 1.55 V was observed for ***trans*** **DCH<>AZT_m**, which means that the oxidation process is more difficult for ***trans*** than for ***cis*** as reflected by fluorescence experiments.

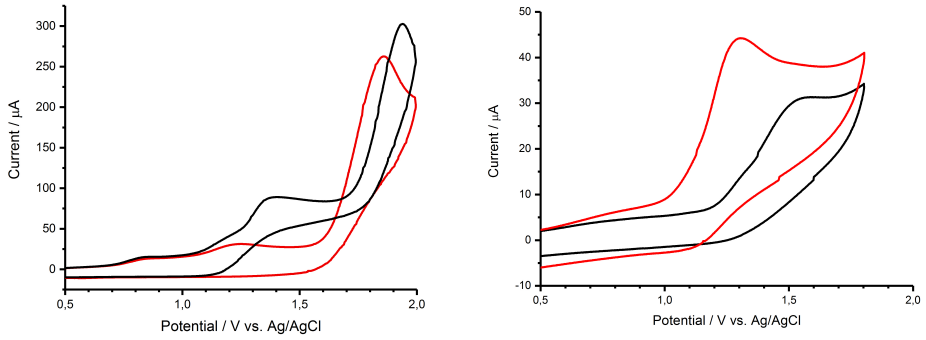

Figure 4.8. Cyclic voltammograms of: (left) **T_m<>AZT_m** (black line, 2 mM) and **T_m<>T_m** (red line, 2 mM) and (right) ***cis*** (red line, 1 mM) and ***trans*** (black line, 1 mM) **DCH<>AZT_m** in N_2-purged acetonitrile using 0.1 M n-Bu_4NClO_4 as electrolyte. Scan rate: 0.1 V.s.

The second peak of **T_m<>AZT_m** is similar to that observed for **T_m-azaU$_m$** oxidation (Figure 4.9), which indicates that the first wave leads to the cleavage of the dimer and formation of **T_m-azaU$_m$**.[23] This behavior is similar to that described for

oxetanes or thietanes, where removal of one electron leads to cleavage of the heterocyclic 4-membered ring.[24-25]

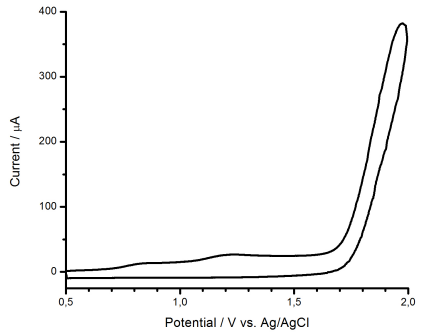

Figure 4.9. Cyclic voltammogram of **azaU-T_m** (2 mM) in N_2-purged acetonitrile using 0.1 M n-Bu_4NClO_4 as electrolyte. Scan rate: 0.1 V.s.

Concerning, **T_m<>T_m**, a single irreversible wave was observed with an E_p of 1.85 V (Figure 4.8), which is in agreement with its more difficult oxidation than that of the other compounds, and with the previously reported value of 1.83 V (vs. Ag/AgCl).[26] Altogether, these results show that there is an important stabilization of the radical cations when a nitrogen atom is part of the four-membered ring as for **T_m<>AZT_m** and **DCH<>AZT_m**, which are more easily oxidizable than **T_m<>T_m**.

4.2.3 Photocycloreversion for T_m<>AZT_m model

The photocycloreversion of cyclobutane thymine dimers in the presence of compounds acting as oxidants in their excited states has been largely reported in the literature (see for example refs [20, 27-28]). Hence, photooxidation of **T_m<>AZT_m** was attempted in the presence of DCN as the electron acceptor and analyzed by HPLC to determine the photoproducts. A deaerated acetonitrile solution of **T_m<>AZT_m** (1.5 mM) was irradiated at 330 nm in the presence of DCN (4 mM) for 100 min. As shown in Figure 4.10, under these conditions the azetidine was split giving rise to the

dyad **T$_m$-azaU$_m$**. However, a quantitative formation of **T$_m$-azaU$_m$** was not observed (Figure 4.10, inset). This can be attributed to the highly reactive pyrimidine radical cations formed, which after deprotonation, hydration and addition of O_2 lead to the formation of secondary products.[29] Indeed, a similar behavior has been described in the literature for the photocycloreversion of cyclobutane thymine (and cytosine) dimers in the presence of electron acceptors.[4] In addition, photocycloreversion of both isomers of **DCH<>AZT$_m$** with DCN did not lead to methylated azaU and cyclohexene. This can be due to (i) the formation of side products from the radical cation azaU or (ii) a different splitting pathway of the azetidine heterocycle to generate a twelve-membered ring.

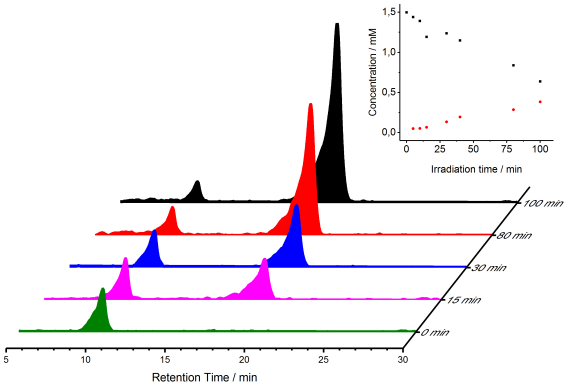

Figure 4.10. HPLC chromatograms, monitored at λ=220 nm, of the photooxidative cycloreversion of **T$_m$<>AZT$_m$** (at retention time of ca. 10 min) and **T$_m$-azaU$_m$** (at retention time of ca. 20 min) in the presence of DCN under monochromatic irradiation at 330 nm. Inset: Time course of the photoreaction (**T$_m$<>AZT$_m$**, squares and **T$_m$-azaU$_m$** circles).

4.2.4 Quantum-chemistry determination of the photooxidative properties for T_m<>AZT_m model

The study was performed in collaboration with the research group of Dr. Roca-Sanjúan (University of Valencia). To gain insight into the energetics involved in the removal of one electron in the azetidine and cyclobutane derivatives, the ionization potentials (IPs) were computed for the *N*-demethylated compounds **T<>AZT** and **T<>T** with the density functional theory (DFT) method, the M06-2X functional and the 6-31++G(d,p) basis set. Benchmark calculations on the thymine nucleobase compared with high-level complete-active-space self-consistent field second-order perturbation theory (CASPT2) results indicate an accurate performance of the DFT/M06-2X method for the vertical and adiabatic IPs (VIPs and AIPs). Table 4.3 compiles the computed gas phase and acetonitrile solution values, which also allows an estimation of the solvent effect. As expected, solvation has an important influence on the IP because it stabilizes to a higher extent the ionic states as compared to the neutral state. Moreover, Table 3.3 shows that EAs of methylated and demethylated compounds of **T<>AZT** differ slightly, thus theoretical studies with demethylated compound give us reliable results as for methylated compounds. Regarding IPs, Table 4.3 indicates significantly lower IPs values for **T<>AZT** than for **T<>T**. This allows us to interpret the fact that higher experimental quenching rates (k_q) were measured for **T<>AZT** than for **T<>T** in the case of photooxidants (DCN and DCA) (Table 4.2).

Table 4.3. Vertical (V) and adiabatic (A) ionization potentials (IPs) in eV (kcal mol^{-1} within parentheses) for **T<>AZT**, **T_m<>AZT_m** and **T<>T** in the gas phase and in acetonitrile computed with the DFT/M06-2X method and the 6-31++G** basis set.

	VIP	AIP
T<>AZT		
Gas phase	9.02 (207.9)	8.06 (185.8)
Acetonitrile	7.14 (164.7)	6.23 (143.7)
T_m<>AZT_m		
Gas phase	8.77 (202.2)	7.86 (181.3)
Acetonitrile	7.04 (162.2)	6.14 (141.7
T<>T		
Gas phase	9.30 (214.5)	8.64 (199.2)
Acetonitrile	7.57 (174.6)	6.92 (159.6)

4.2.5 Decompostition mechanism of T<>AZT radical cation

For the photooxidation, the four-membered ring is preserved in the cationic structure, in contrast to the findings obtained for the anion, which was discussed in Chapter 3. The reaction mechanism of **T<>AZT$^{\bullet+}$** implies a two-step N-C and C-C bond breaking, in which the first cleavage (N-C) requires ca. 7.5 kcal mol^{-1} and gives rise to a flat energy profile, although with no stable structure (Figure 4.11). In such region, the carbon atom of the broken bond becomes a carbocation. It can be seen in the gas-phase with the complete-active space selfconsistent field (CASSCF) spin-density representations of Figure 4.12 that the unpaired electron is localized over the nitrogen atom and to some extent also over the adjacent nitrogen atom. The second step in the mechanism corresponds to the C-C bond breaking and increases the energy barrier for the overall process up to 12.5 kcal mol^{-1}. Therefore, these data showed

that the oxidative mechanism of $\mathbf{T_m<>AZT_m}$ occurs through the pathway a in Scheme 4.3.

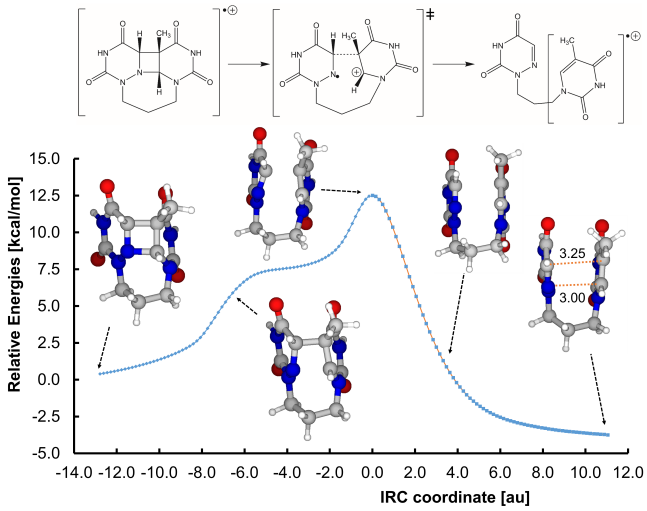

Figure 4.11. Chemical structure of relevant points (top) and energy profile (bottom) for the C-N and C-C bond breakings of $\mathbf{T<>AZT^{\bullet+}}$ obtained with MEP computational strategy.

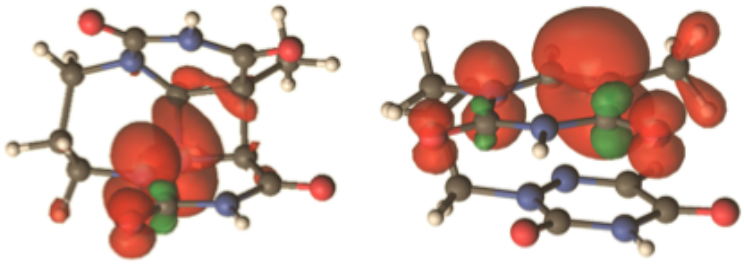

Figure 4.12. CASSCF spin-density representations for the $\mathbf{T_m<>AZT_m}$ radical cation systems at the reductant (left) and product (right) geometries. Red = excess of spin density, Green = defect of spin density.

Globally, the *in-vacuo* mechanism described above implies energy barriers lower than 13 kcal mol^{-1} for cation system. To further improve the description, we have focused on the relevant points for the present mechanism (reactants, TSs and products) and we have determined several thermochemical magnitudes using the highly accurate CASPT2 method. Results are compiled in Table 4.4. For **T$_m$<>AZT$_m^{\bullet+}$**, both methods differ in the sign of ΔE; however, the values are around zero. Regarding the solvent effects, in contrast to the redox properties determined in the previous section, no significant changes are observed for the **T$_m$<>AZT$_m^{\bullet+}$** cycloreversion mechanism. This is due to the fact that along the ring opening reactions the total charge is preserved. The ZPVE correction gives rise to lower ΔEs as a consequence of the bond breakings occurring along the reactions. The same behavior is observed for ΔG, which reflects the entropy increase in the decomposition process.

Table 4.4. Computed energy differences between products and the reactants (ΔE, ΔE_0 and ΔG) and activation energies ($\Delta E^{\ddagger}$, $\Delta E_0^{\ddagger}$ and $\Delta G^{\ddagger}$) for the cycloreversion of the **T<>AZT** radical cation. Energies in kcal mol^{-1}.

Methodology	AZT$^{\bullet+}$	
	ΔE	$\Delta E^{\ddagger}$
M06-2X	-4.89	12.52
CASPT2//M06-2X	2.21	14.77
PCM-M06-2X	-3.09	13.52
	ΔE_0	$\Delta E_0^{\ddagger}$
M06-2X	-7.36	10.73
CASPT2//M06-2X	-0.26	12.98
	ΔG	$\Delta G^{\ddagger}$
M06-2X	-8.99	11.47
CASPT2//M06-2X	-1.89	13.72

4.3 Conclusions

The photooxidative cycloreversion of azetidine models **T_m<>AZT_m** has been addressed through a multidisciplinary study including spectroscopic, electrochemical and analytical experiments complemented by computational chemistry. In a first stage, the electron accepting capabilities of this four-membered heterocycle have been established by means of photooxidant singlet excited state quenching. In this context, comparison of the bimolecular rate constants obtained for **T_m<>AZT_m** with **DCH<>AZT_m** and **T_m<>T_m** has revealed that the presence of the nitrogen atom in the ring affects its oxidation. The electrochemical experiments fully support these redox features as close oxidation peaks have been registered for **T_m<>AZT_m** and **DCH<>AZT_m**, by contrast their oxidation waves are differing in 0.5 V with **T_m<>T_m**. This variation has also been corroborated by DFT quantum chemistry, which has determined different ionization potentials of ca. 6.23 and 6.92 eV for **T_m<>AZT_m** and **T_m<>T_m**, respectively. Concerning the fate of the formed **T_m<>AZT_m** ion radicals, the cycloreversion of the ring to restore thymine and 6-azauracil bases has been evidenced by steady state photolysis followed by HPLC analysis. The photooxidative version involves a bond cleavage of C-N followed by C-C, with a similar energy barrier and a final radical cation on the thymine nucleobase. Altogether, these experimental and theoretical findings represent an important advance in the photoinduced cycloreversion of azetidines by electron transfer.

4.4 References

1. Sancar, A., Structure and function of DNA photolyase and cryptochrome blue-light photoreceptors. *Chem. Rev.* **2003,** *103*, 2203-2207.

2. Dandliker, P. J.; Holmlin, R. E.; Barton, J. L., Oxidative thymine dimer repair in the DNA helix. *Science* **1997,** *275*, 1465-1468.

3. Roth, H. D.; Lamola, A. A., Cleavage of thymine dimers sensitized by quinones. Chemically induced dynamic nuclear polarization in radical ions. *J. Am. Chem. Soc.* **1972,** *94*, 1013-1014.

4. Fenick, D. J.; Carr, H. S.; Falvey, D. E., Synthesis and photochemical cleavage of *cis-syn* pyrimidine cyclobutane dimer analogs. *J. Org. Chem.* **1995,** *60*, 624-631.

5. Sasson, S.; Elad, D., Photosensitized monomerization of 1,3-dimethyluracil photodimers. *J. Org. Chem.* **1972,** *37*, 3164-3167.

6. Hartman, R. F.; Rose, S. D.; Pouwels, P. J. W.; Kaptein, R., Flavin-sensitized photochemically induced dynamic nuclear polarization detection of pyrimidine dimer radicals. *Photochem. Photobiol.* **1992,** *56*, 305-310.

7. Rosenthal, I.; Rao, M. M., Transition metal-ion photosensitized monomerization of pyrimidine dimers. *Biochem. Biophys. Acta* **1975,** *378*, 165-168.

8. Hartman, R. F.; Rose, S. D., A possible chain reaction in photosensitized splitting of pyrimidine dimers by a protonated, oxidized flavin. *J. Org. Chem.* **1992,** *57*, 2302-2306.

9. Schmuck, C.; Wennemers, H., *Highlights in Bioorganic Chemistry: Methods and Applications*. **2005**, 352-368.

10. Pouwels, J. W.; Kaptein, R.; Hartman, R. F.; Rose, S. D., Photo-CIDNP study of pyrimidine dimer splitting I: reactions involving pyrimidine radical cation intermediates. *Photochem. Photobiol.* **1995,** *61*, 563-574.

11. Austin, R.; McMordie, S.; Begley, T. P., Mechanistic studies on DNA photolyase. Secondary deuterium isotope effects on the cleavage of the uracil photodimer radical cation and anion. *J. Am. Chem. Soc.* **1992,** *114*, 1886-1887.

12. Voityuk, A. A.; Rösch, N., A quantum chemical study of photoinduced DNA repair: on the splitting of pyrimidine model dimers initiated by electron transfer. *J. Am. Chem. Soc.* **1996,** *118*, 9750-9758.

13. Krüger, O.; Wille, U., Oxidative cleavage of a cyclobutane pyrimidine dimer by photochemically generated nitrate radicals. *Org. Lett.* **2001,** *3*, 1455-1458.

14. Young, T. N., R.; Rose, S. D., Photo-CIDNP detection of pyrimidine dimer radical cations in anthraquinone sulfonate-sensitized splitting. *Photochem. Photobiol.* **1990,** *52*, 661-668.

15. Wang, Y.; Gaspar, P. P.; Taylor, J. E., Quantum chemical study of the electron transfer-catalyzed splitting of oxetane and azetidine intermediates proposed in the photoenzymatic repair of (6-4) photoproduct of DNA. *J. Am. Chem. Soc.* **2000,** *122*, 5510-5519.

16. Nakabayashi, K.; Kojima, J.; Yasuda, T. M.; Shima, K., Organic photochemical reactions. XXVI. Photosensitized ring-cleavage reactions of 2,2-diaryloxetanes by aromatic nitriles. *Bull. Chem. Soc. Jpn.* **1989,** *62*, 96-101.

17. Prakash, G.; Falvey, D. E., Model studies of the (6-4) photoproduct DNA photolyase: synthesis and photosensitized splitting of a thymine-5,6-oxetane. *J. Am. Chem. Soc.* **1995,** *117*, 11375-11376.

18. Miranda, M. A.; Izquierdo, M. A., Stepwise cycloreversion of oxetane radical cations with initial C-O bond cleavage. *J. Am. Chem. Soc.* **2002,** *124*, 6532-6533.

19. Andreu, I.; Delgado, J.; Espinós, A.; Pérez-Ruiz, R.; Jiménez, M. C.; Miranda, M. A., Cycloreversion of azetidines via oxidative electron transfer: steady-state and time-resolved studies. *Org. Lett.* **2008,** *10*, 5207-5210.

20. Pac, C.; Ohtsuki, T.; Shiota, Y.; Yanagida, S.; Sakurai, H., Photochemical reactions of aromatic compounds. XLII. Photosensitized reactions of some selected diarylcyclobutanes by aromatic nitriles and chloranil. Implications of charge-transfer contributions on exciplex reactivities. *Bull. Chem. Soc. Jpn* **1986,** *59*, 1133-1139.

21. Stern, O.; Volmer, M., Über die abklingungszeit der fluoreszenz. *Physik. Z.* **1919,** *20*, 183-188.

22. Scannell, M. P.; Fenick, D. J.; Yeh, S.; Falvey, D. E., Model studies of DNA photorepair: reduction potentials of thymine and cytosine cyclobutane dimers measured by fluorescence quenching. *J. Am. Chem. Soc.* **1997,** *119*, 1971-1977.

23. Boussicault, F.; Kruger, O.; Robert, M.; Wille, U., Dissociative electron transfer to and from pyrimidine cyclobutane dimers: An electrochemical study. *Org. Biomol. Chem.* **2004,** *2*, 2742-2750.

24. Boussicault, F.; Robert, M., Electrochemical approach to the repair of oxetanes mimicking DNA (6−4) photoproducts. *J. Phys. Chem. B* **2006,** *110*, 21987-21993.

25. Boussicault, F.; Robert, M., Electron transfer in DNA and in DNA-related biological processes. Electrochemical insights. *Chem. Rev.* **2008,** *108*, 2622-2645.

26. Wenska, G.; Paszyc, S., Electron-acceptor-sensitized splitting of cyclobutane-type thymine dimers. *J. Photochem. Photobiol. B: Biol.* **1990,** *8*, 27-37.

27. Fenick, D. J.; Carr, H. S.; Falvey, D. E., Synthesis and photochemical cleavage of *cis-syn* pyrimidine cyclobutane dimer analogs. *J. Org. Chem.* **1996,** *60*, 624-631.

28. Pac, C.; Miyamoto, I.; Masaki, Y.; Furusho, S.; Yanagida, S.; Ohno, T.; Yoshimura, A., Chloranil-photosensitized monomerization of dimethylthymine cyclobutane dimers and effect of magnesium perchlorate. *Photochem. Photobiol.* **1990,** *52*, 973-979.

29. Cadet, J.; Vigny, P., In Bioorganic Photochemistry. *H. Morrison, Ed. Wiley: New York* **1990**, 1-272.

Chapter 5:
Photorepair of Thymine Derived Cyclobutanes and Oxetanes by 8-oxoGuanine

5.1 Introduction

Over millions of years, nature has developed catalytic RNA enzymes denominated ribozymes that play an important role in the evolution of life via the 'RNA World' hypothesis.[1] This hypothesis explains how RNA, which served as genome and as catalyst, passed its genomic role to DNA and its catalytic role to proteins. Indeed, numerous *in vitro* selection experiments have confirmed the concept that RNA can catalyze a wide range of chemical reactions such as ligation, hydrolysis, and C-C bond formation.[2] In this context, it would be interesting to investigate whether nucleic acid enzymes are capable of catalyzing photochemical reactions to repair the UV photoproducts in DNA as photolyases do. In 2004, this theory was supported by means of a deoxyribozyme formed by guanine bases in a quadruplex structure.[3] Interestingly, this deoxyribozyme acts as an antenna for excitation at 305 nm, wavelength longer than those absorbed by normal bases, and repairs efficiently cyclobutane dimers via an electron donation from an excited guanine base. Therefore, this work opened the door to investigate whether nucleic acids in their excited state are able to donate one electron to thymine dimers and repair them by analogy with CPD photolyase.

In 2007, the importance of G adjacent bases in the formation of CPDs was investigated by steady-state photolysis of series of duplexes (18 nucleotides) containing a single TT central sequence flanked by purines or pyrimidines bases.[4] Interestingly, lower levels of T<>T were found when guanosine was adjacent to the cyclobutane dimer at the 5'-side. This purine effect could be explained by considering the fact that, among the DNA bases, G has the lowest oxidation potential (E_{ox}(G) = 1.3 V vs. NHE), and thus G is the most easily oxidizable base.[5] Therefore, by analogy with CPD photolyase, electron transfer from the excited guanosine to the TT dimer was proposed to lead to the formation of the TT dimer radical anion that would cleave to

finally give rise to the initial T bases (Scheme 5.1). The overall process results in a decrease of the stationary level of CPD.

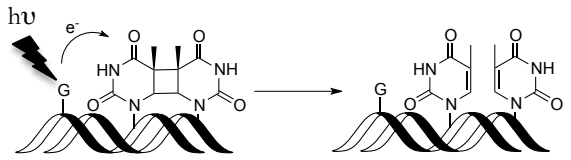

Scheme 5.1. Mechanistic pathway of CPD repair from excited guanine nucleobase by PET.

However, it was reported that the purine effect in the dimerization of TT at 302 nm was not the result of a purine-sensitized repair mechanism as previously mentioned because of the absence of purine absorption at this wavelength.[6] It was thus proposed that it is the consequence of the pyrimidine excited state quenching by electron transfer from the flanking base, which would result in the formation of an exciplex that could deactivate to the ground state via nonradiative decay rather than exciplex fluorescence or TT dimer formation. In further support of exciplex mechanism, a lower photodimer yield was observed when G is located in the 5'-position relative to the dipyrimidine site. This points to a better stacking of purine-pyrimidine sequences compared to pyrimidine-purine sequences, which would facilitate electron transfer and exciplex formation. Moreover, the determination of quantum yields for thymine photodimerization containing a single TT with flanking purines proved this purine effect, which was attributed to a combination of ground state donor-acceptor interactions between π-stacked purine and thymine bases and to an excited state exciplex formation.[7]

By contrast, femtosecond transient absorption experiments showed that electron transfer from excited G or A to T<>T does no ocurr to a significant extent in single-stranded trinucleotides.[8] However, this could be attributable to poor stacking between

the electron donor and the CPD in these short and single stranded sequences. Thus, electron transfer may be too slow to compete with fast nonradioactive deactivation of the purine $^1\pi\pi^*$ excited state, that has a lifetime of less than 1 ps.[9]

Recently, a new mechanism based on intrastrand excimer, in which the excitation is shared by two neighboring stacked bases, was proposed to repair T<>T flanked by GA nucleotides through a charge transfer state.[10] In this case, the excitation of G induces an electron migration to a nearby A giving rise to the formation of the zwitterion $G^{\bullet+}A^{\bullet-}$ that has a lifetime long enough (300 ps) to donate an electron to the adjacent T<>T lesion, which finally leads to the repaired thymine bases. By contrast, direct photoinduced repair via charge transfer from photoexcited A or G to adjacent T<>T was negligible, which agrees with the previous femtosecond transient absorption investigation.[8]

In 2011, an unusual example was reported where a DNA lesion has the capacity to repair another one, the CPDs, imitating this way the function of the flavin cofactor in CPD photolyase mechanism.[11-12] For small oligonucleotides, it has been shown that, after photoexcitation, the oxidized guanine, 8-oxoGuanine (OG), transfers an electron to an adjacent CPD lesion, which induces the splitting of the cyclobutane ring and regeneration of OG and thymine bases after a subsequent back electron transfer.

Interesting properties make OG a better candidate for DNA-damage repair than G. Although G has the lowest redox potential among the DNA bases[5] and this value can be modulated in sequences with consecutive G[13], the OG has a redox potential of ca. 0.5 V lower than that of G (E_{ox} = 0.7 V vs. NHE) and a red-shifted UV absorption with a band above 300 nm that allows selective excitation.

Since this research, the interest in the photophysical properties of OG has increased and, theoretical[14-17] and ultrafast studies[18-20] have been carried out in order to prove the ability of OG to act as an electron donor in the photoinduced electron transfer mechanism proposed for CPD repair. The lifetime of the excited state also

plays an important role. In this context, it was found that the lifetime of first excited state of OG is of ca. 0.9 ps, i.e. twice longer than that of G.[18] The ultrafast nonradiative process could avoid the occurrence of photochemical pathways and, thus, reduce CPD repair by PET despite favorable thermodynamics. However, the deactivation pathways may be different in the presence of base stacking and pairing. In this context, the UV excitation of a dinucleotide containing OG at 5' side of an adenine showed the formation of a radical ion pair with a lifetime of 60 ps that was assigned to an interbase charge transfer state, which lives much longer than the excited state of A or OG monomers.[19] Therefore, this result proved the ability of OG to transfer an electron to a stacked adenine, mimicking thus the first step of the flavin cofactor $FADH^-$ involved in the repair by photolyase. In addition, this photoreactivation may be possible despite the short lifetime of the radical ion pair in DNA because the reductive splitting step of CPD has been shown to occur in less than 100 ps.[21] Altogether, these results show that there is an ongoing discussion whether the excitation of a single purine nucleobase such as G or OG promotes or not the repair of a neighboring T<>T dimer through electron transfer.

Regarding model systems, there is a plenty of examples using CPD unit covalently linked to chromophores such as indole[22], aryl amine[23], methoxybenzene[24], flavin[25-27] or tryptophan[28]; but also using the oxetane unit[27, 29] as a model for the intermediate involved in 6-4PP repair. By contrast, no model systems of CPDs or oxetanes incorporating OG or G as electron donor have been reported. With this background, we considered to study the ability of OG and G covalently linked to an oxetane unit and to a thymine dimer to photoinduce the cycloreversion process. Firtsly, the splitting process of an oxetane model (**10**, Figure 5.1) attached to OG nucleoside was studied. Secondly, four models containing the CPD or oxetane unit were attached to OG or G nucleobases by a flexible linker (**15**, **16**, **20**, **21**, Figure 5.1) in order to study and compare the PET process between the electron donors, G and OG, and the electron acceptors CPD and oxetane.

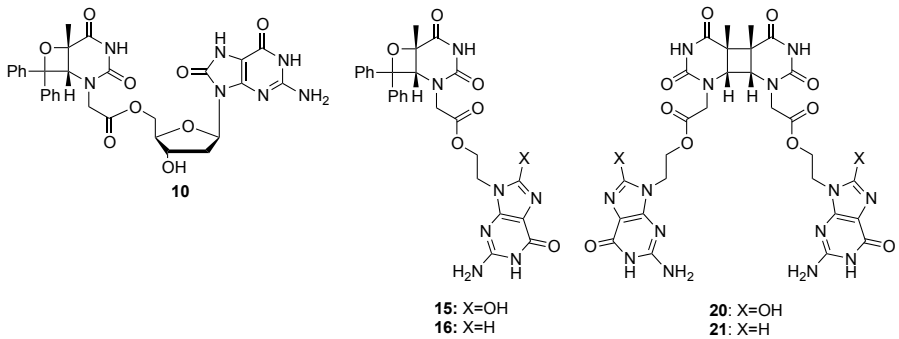

Figure 5.1. Structure of the five models with oxetane (**10**, **15**, **16**) and thymine dimer (**20**, **21**) attached to OG or G chromophores.

5.2 Results and discussion

5.2.1 Synthesis

Firstly, we decided to synthesize the model **10** (Figure 5.1) where OG nucleoside is covalently attached to an oxetane compound through the 5'-OH of the 2'-deoxyribose. Previous thymine dyads designed in our group showed a strong intramolecular interaction between the thymine and a chromophore in the excited state when this chromophore is attached in the 5' position of the 2'-deoxyribose moiety.[30] The five-step synthesis of the 3'-protected OG derivative **5**, required for the synthesis of model compound **10**, is shown in Scheme 5.2.

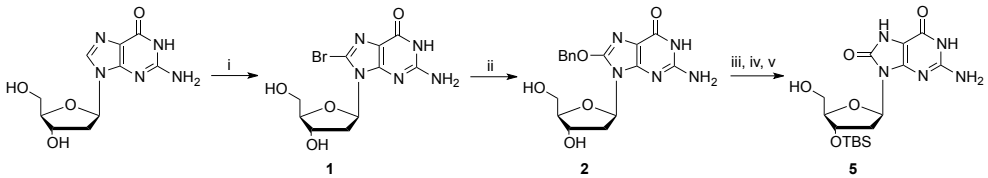

Scheme 5.2. Synthetic strategy to prepare **5**. Reagents and conditions: (i) NBS, MeCN/H_2O, rt, 45 min; (ii) Na, BnOH, DMSO, 65 ºC, 24h; (iii) 1 M HCl, MeOH, rt, 1h; (iv) TBDMSCl, Im, DMF, rt, 24h; (v) TFA/H_2O, CH_2Cl_2, 0 ºC, 4h.

To obtain the OG moiety, 2'-deoxyguanosine was brominated at the C8 position to give **1**, this step was followed by a nucleophilic substitution with sodium benzylate leading to compound **2**. The latter is highly unstable in acidic conditions and yields OG nucleoside **3** upon stirring with 1M HCl for 1 h. Then, the hydroxyl groups were protected with *tert*-butyldimethylsilyl chloride to give **4** and subsequent selective deprotection of the 5' position under mild acidic conditions led to compound **5**.

The synthesis of the oxetane model **10** started with the commercial thymine acetic acid as shown in Scheme 5.3. First, the benzyl ester **6** was prepared by esterification. Then, it was irradiated in the presence of benzophenone in a Pyrex vessel (λ > 290 nm) with a medium pressure mercury lamp (125W) to give a mixture of thymine oxetanes as the result of a Paternò-Büchi reaction.[29] Then, the stable oxetane **7** was isolated by flash chromatography. The catalytic hydrogenolysis of the benzyl ester **7** led to the oxetane acetic acid derivative **8**, and subsequent esterification with **5** gave the corresponding model **9**. Finally, deprotection of 3'-hydroxyl group under mild conditions gave the oxetane model **10**.

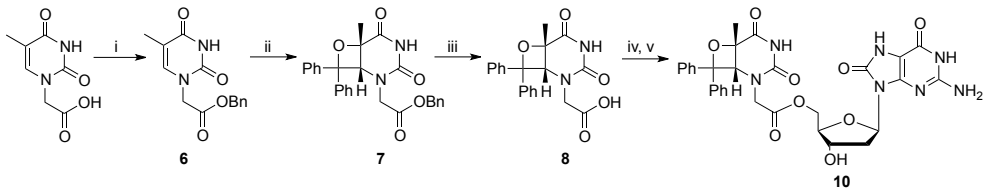

Scheme 5.3. Synthetic strategy to prepare **10**. Reagents and conditions: (i) CDI, BnOH, DMF, rt, 18h; (ii) benzophenone, hυ, λ > 290 nm, MeCN, 16h; (iii) 10% Pd/C, H_2, AcOH, rt, 4h; (iv) **5**, EDC, TBTU, DMAP, DMF, rt, 20h; (v) TBAF, THF, rt, 16h.

Secondly, we decided to synthesize four models (**15**, **16**, **20** and **21**, Figure 5.1) where OG or G nucleobases are covalently attached to a cyclobutane thymine dimer or an oxetane through a flexible and long linker. This linker was shown to favor the splitting efficiency of the four-membered ring in polar solvents through a preferred U-

shaped conformation, induced by hydrophobic interactions, which shortens the spatial distance between donor and acceptor.[31] The first step of the synthesis was to obtain the hydroxyethyl derivatives **12** and **14** as shown in Scheme 5.4. The compound **12** was easily synthetized from 2-amino-6-chloropurine in two-steps. First, the linker was introduced through alkylation with 2-bromoethoxy-*tert*-butyldimethylsilane to afford the N-9 alkylated isomer **11** with a high selectivity, this step was followed by hydrolysis to give the deprotected compound **12**. Subsequent bromination at the C8 position of **12** and hydrolysis with sodium acetate in acetic acid led to compound **14**.

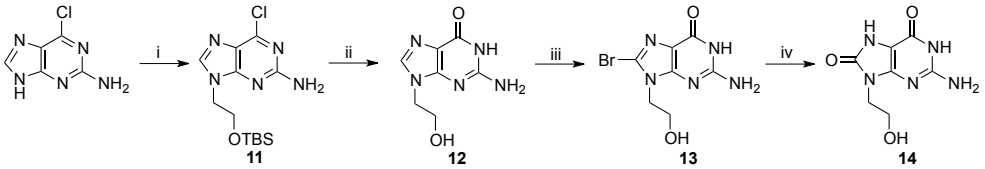

Scheme 5.4. Synthetic strategy to prepare **12** and **14**. Reagents and conditions: (i) 2-bromoethoxy-*tert*-butyldimethylsilane, NaH, DMF, rt, 24h; (ii) 2 M HCl, 100 ºC, 2h; (iii) NBS, MeCN/H_2O, rt, 30 min; (iv) AcONa, AcOH, 130 ºC, 7h.

The synthesis of the oxetane models **15** and **16** is shown in Scheme 5.5, they were obtained by esterification of the oxetane acetic acid derivative **8**, with **14** and **12**, respectively.

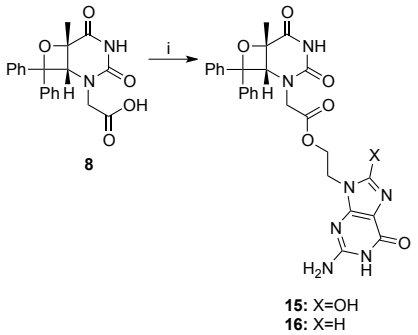

Scheme 5.5. Synthetic strategy to prepare **15** and **16**. Reagents and conditions: (i) **12** or **14**, EDC, TBTU, DMAP, DMF, rt, 24h.

For the CPD dyads, the cyclobutane pyrimidine dimer was covalently attached to two chromophores to avoid the formation of a mixture of mono- or disubstituted compounds. The preparation of the *cis-syn* thymine dimer was performed in four steps from thymine acetic acid as shown in Scheme 5.6. First, the ethyl ester **17** was prepared by Fischer esterification; then it was irradiated in a Pyrex vessel (λ > 290 nm) with a medium pressure mercury lamp (125W) using acetone as photosensitizer to give a mixture of four isomers. The *cis-syn* thymine dimer **18** was separated by flash chromatography and its structural assignment was confirmed by ^{1}H NMR, in particular the chemical shift of the proton at N3 at ca. 10.51 ppm was the same as described in the literature.[26] Hydrolysis yielded the *cis-syn* thymine dimer acetic acid derivative **19**, and subsequent esterification with **14** and **12** gave the corresponding **20** and **21** cyclobutane dimer models, respectively.

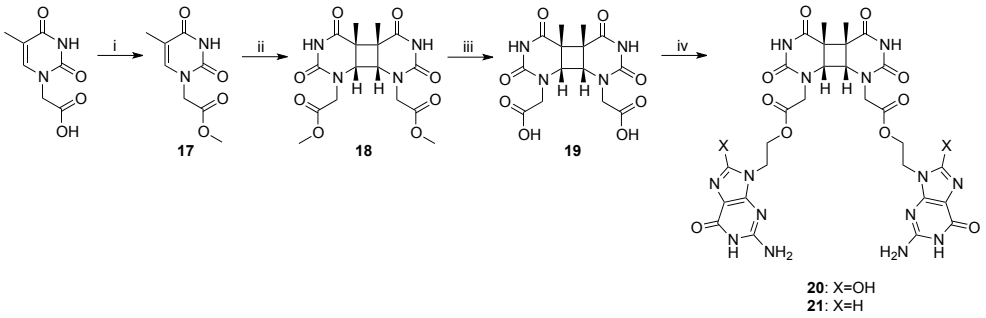

Scheme 5.6. Synthetic strategy to prepare **20** and **21**. Reagents and conditions: (i) H_2SO_4, MeOH, 100 ºC, 24h; (ii) acetone/MeCN, hυ, λ > 290 nm, 72h; (iii) 5 M HCl, 100 ºC, 30 min; (iv) **12** or **14**, EDC, TBTU, DMAP, DMF, rt, 24h.

5.2.2 Photocycloreversion

The UV absorbance spectra of **10** is shown in Figure 5.2 (left). We can observe the characteristic band of OG chromophore with a maximum at ca. 295 nm. In order to study the splitting of the four-membered ring model, steady-state photolysis

was performed using a monochromatic excitation at 308 nm where the absorption of the oxetane unit (Figure 5.2, right) is negligible, and thus the photons are mainly absorbed by the OG chromophore.

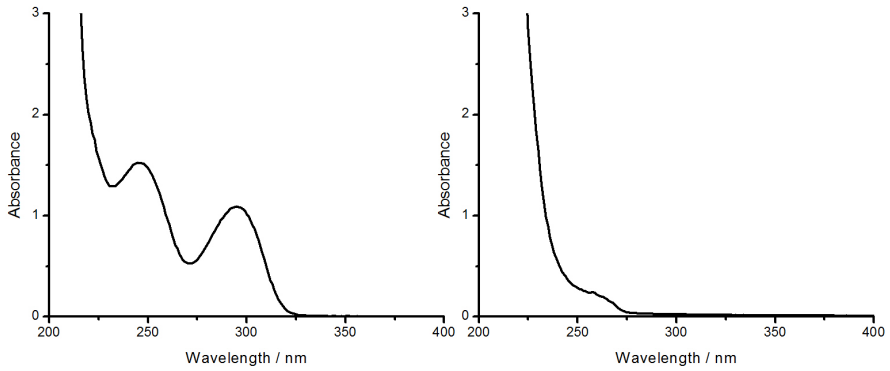

Figure 5.2. UV spectra of **10** (0.2 mM) in neutral PBS (left) and **7** (0.2 mM) in MeCN (right).

Firstly, the photosplitting of the model **10** at 308 nm was followed by UV spectrophotometry, monitoring the absorption bands at 270 nm and 250 nm that inform on the generation of the thymine and benzophenone (BP) chromophores, respectively, as shown in Scheme 5.7.

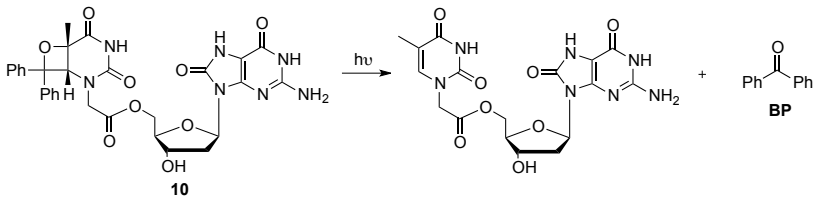

10

Scheme 5.7. Cleavage reaction of **10**.

As shown in Figure 5.3 left, an increase of the absorption at 270 nm and 250 nm was observed during the irradiation at 308 nm, which agrees with the formation of thymine chromophore attached to OG and BP. In order to ensure that the photo-

cleavage resulted in the expected photoproducts, the course of the reaction was monitored by HPLC at different irradiations times. Figure 5.3 right shows the cleavage of the oxetane model **10**, that eluted at 5.7 min, into thymine photoproduct, with retention time of 4.14 min, and BP, with retention time of 14.1 min. This assignment was confirmed by HPLC co-elution with standard compounds.

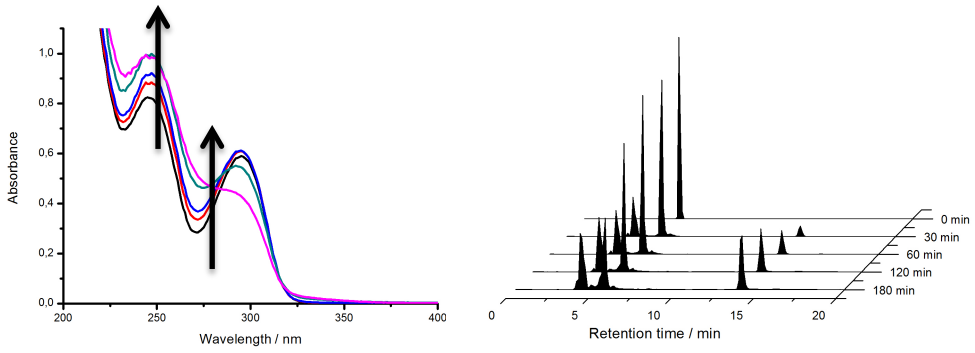

Figure 5.3. Cleavage reaction of **10** monitored by UV spectroscopy (left) and HPLC (right) at 0, 30, 60, 120 and 180 min of irradiation at 308 nm in neutral PBS.

Therefore, these data show that the photocycloreversion of oxetane model **10** involves the excited state of OG, which donates an electron to split the four-membered ring. Fluorescence experiments can support this PET mechanism from singlet excited state of PS. However, given the ultralow fluorescence quantum yields of OG (1.3 x10^{-4})[20], it was not possible to observe this intramolecular fluorescence quenching as an evidence of the electron transfer process. However, this ultrafast process can be investigated by means of femtosecond transient absorption spectroscopy, following the evolution of singlet-singlet transient absorption band (from $^1\pi\pi^*$) of OG but also intermediate species such as radical cation or anion. In this context, preliminary femtosecond transient absorption studies with **10** and OG nucleoside were performed in Carlos Crespo´s group during my first predoctoral stay. Therefore, if the electron

transfer takes place from OG, the radical cation of OG and radical anion of BP should be detected. In this way, back to back experiments (same aborption for both compounds) with 308 nm excitation were performed for OG and **10** in neutral PBS as shown in Figure 5.4. As seen for both compounds, a transient species grows in from 0.0 to 0.4 ps at 570 nm along with another band shoulder around 350 nm. In the subsequent time region from 0.4 to 4 ps, the absorption bands decrease. The spectra do not show changes after 4 ps, indicating that the excited molecules had come back to the ground state.

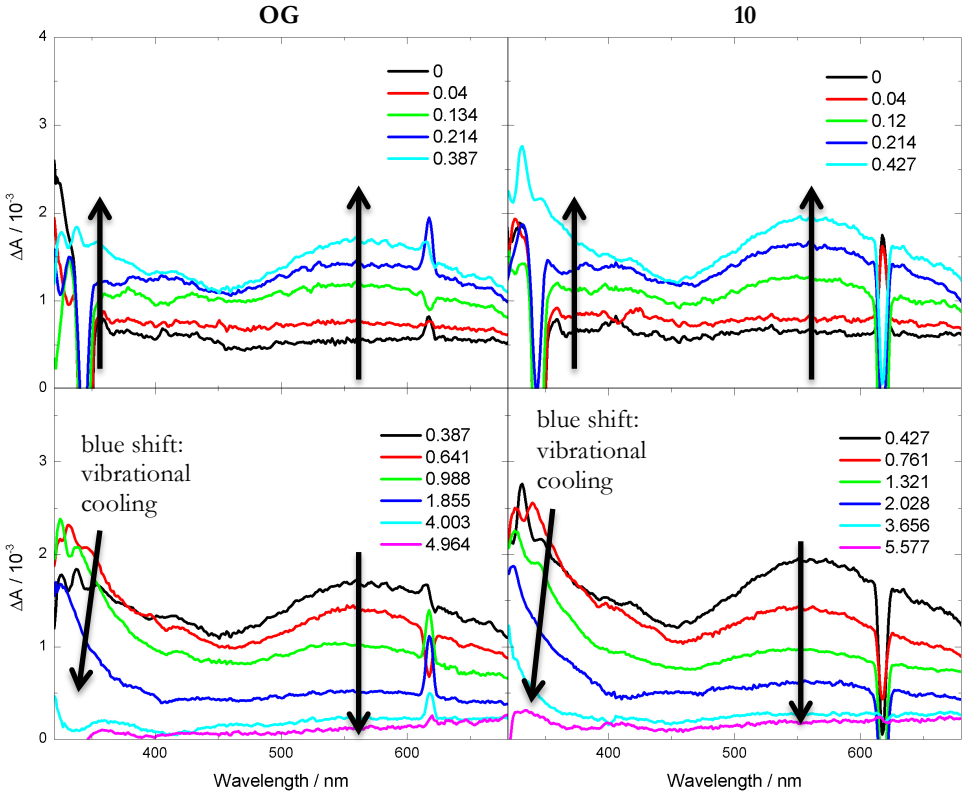

Figure 5.4. Transient absorbance changes of OG (OD 0.26) and **10** (OD 0.31) in neutral PBS. Overtone at 616 nm (2x308 nm).

In order to examine the excited state dynamics, we performed a global fitting analysis with a sequential kinetic model convoluted with an instrument response time of 200 ± 50 fs and coherence spike function. Figure 5.5 shows the best fits at 354 and 568 nm. Two lifetimes of 280 fs and 1.51 ps for OG and 240 fs and 1.29 ps for **10**, were determined. Therefore, we have assigned the 570 nm transient species to the $^1\pi\pi^*$ electronic transition of OG neutral form and the initial growth of the 350 nm signal to vibrational cooling of the hot ground-state of OG neutral form, as already described for other nucleosides.

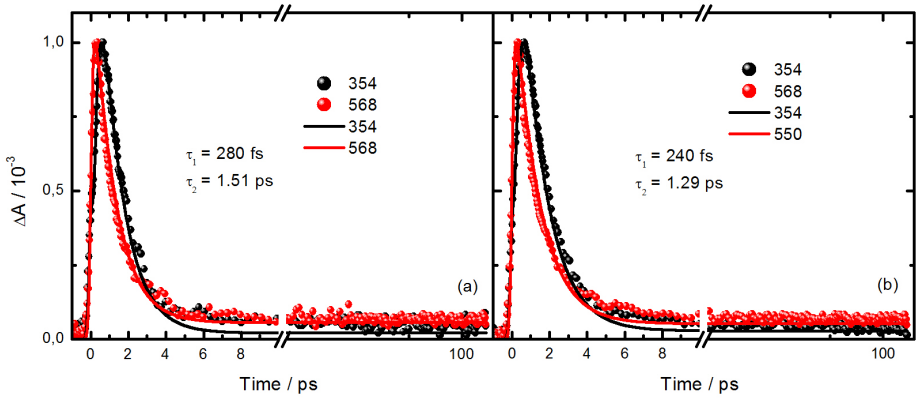

Figure 5.5. Kinetic traces and fits obtained from the global fitting analysis for: (a) OG and (b) **10** in neutral PBS.

Comparison of the spectra and kinetics of both compounds show the same excited species. It indicates that the transient species of **10** proceed only from excited state of OG. These results suggest that the molecules are unstacked and not close enough to allow efficient electron transfer. In this way, we carried out the experiments of transient absorption for OG and **10** in ethylene glycol, which is more viscous than PBS and might favor the stacked conformation. The same transient species were observed, and the only difference relies on an increase of the lifetimes. Unfortunately,

comparison of the data obtained with OG and **10** did not allow to draw clear conclusions.

In summary, since the oxetane has no significant absorption at 308 nm, OG absorbs a photon producing the excited state ^{1}OG*-OXT (Scheme 5.8). Then the excited state may relax as follows: fluorescence (k_f), internal conversion (k_{ic}), and electron transfer to the linked oxetane (k_{et}). The charge-separated species formed via electron transfer can undergo two processes, oxetane splitting (k_{spl}) or back electron transfer (k_{bet}). Therefore, there are two different competitions in these processes: (1) the photophysical process (k_f and k_{ic}) with electron transfer (k_{et}) and (2) the splitting (k_{spl}) with back electron transfer (k_{bet}).

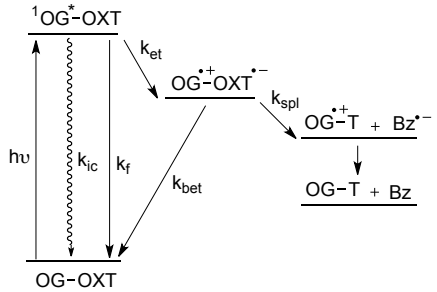

Scheme 5.8. Photophysical and photochemical processes of model **10** where OG is attached to an oxetane (OXT).

In model systems, back electron transfer (k_{bet}) was reported to lead to low splitting efficiencies.[27-28] However, internal conversion (k_{ic}) also plays an important role for PS with short lived excited states, as observed for flavin model systems.[32] Therefore, in the case of **10**, as the fluorescence process (k_f) can be neglected for OG, the main process competing with electron transfer is the nonradiative process (k_{ic}). During our measurements, the observed species for **10** proceed only from ($^1\pi\pi^*$) excited state of OG in both solvents, PBS and ethylene glycol. This might be due to the fact that **10** is almost unstacked, and radical ion pairs are not formed in a detectable quantity, the

electron transfer process being too inefficient to compete with the fast nonradioactive deactivation of OG.

In addition, the absorption bands of the formed radicals can be overlapped in the spectra with OG absorption bands at 350 and 570 nm. It was reported that the radical cation of OG has a narrow absorption band with maximum at 320 nm and a shoulder near 400 nm, which decays on millisecond time scales.[33] Concerning the radical anion of BP, formed after cleaving the radical anion of oxetane, it has a maximum band at 680 nm.[34] However, the latter species is in the limit of our detection window and, thus, it cannot be detected under our experimental conditions. Altogether, these data made us redefine the model in order to use a long and flexible linker, to bring closer the donor and acceptor moieties. The selected linker has been used in previous femtosecond spectroscopy of a thymine dimer model attached to a flavin or indole chromophore.[32, 35] Therefore, we synthetized four models where OG and G nucleobases are covalently linked to an oxetane unit (**15** and **16**, Figure 5.1) and to a cyclobutane thymine dimer (**20** and **21**, Figure 5.1) by a 5-chain flexible linker, in order to compare the ability of OG and G as electron donors.

The UV absorption spectra of **15**, **16**, **20** and **21** are shown in Figure 5.6a. In case of **15** and **20**, we can observe the characteristic band of OG chromophore with a maximum at ca. 295 nm, and that exhibits a red shifted absorption by respect to the guanine derivatives **16** and **21**. In order to study the splitting of the four-membered ring models, steady-state photolysis was performed using a monochromatic excitation at 280 nm. We selected this wavelength because it corresponds to the point where the four compounds show the same absorbance and, thus, the splitting can be achieved, for the same irradiation time, by the same number of absorbed photons for the four dyads. In addition, at this wavelength and under the conditions of concentration used (of ca. 10^{-4} M) the absorption of the CPD and oxetane unit is very small as shown in

Figure 5.6b., and thus the photons are mainly absorbed by the chromophores OG and G.

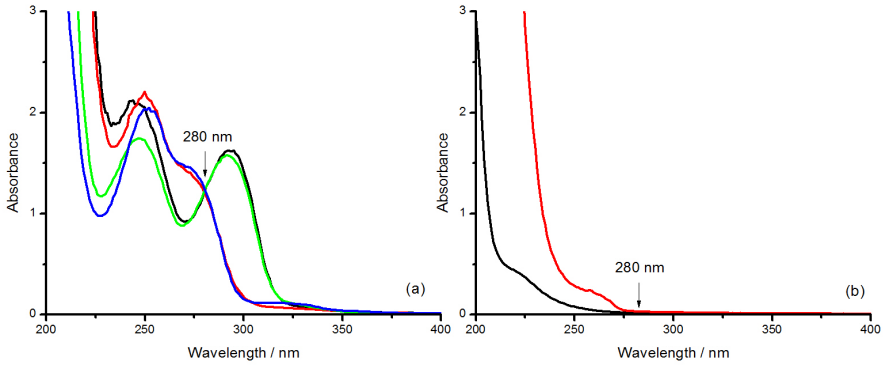

Figure 5.6. UV absorption spectra of: (a) **15** (0.2 mM, black), **16** (0.2 mM, red), **20** (0.1 mM, green) and **21** (0.1 mM, blue) in PBS at pH 7.4; (b) **18** (0.1 mM, black) and **7** (0.2 mM, red) in MeCN.

Firstly, the photosplitting of the models **15**, **16**, **20** and **21** at 280 nm was followed by UV spectrophotometry, monitoring the absorption band at 270 nm that informs on the generation of the thymine chromophore present in the purported photoproducts **22** and **23** (Scheme 5.9).

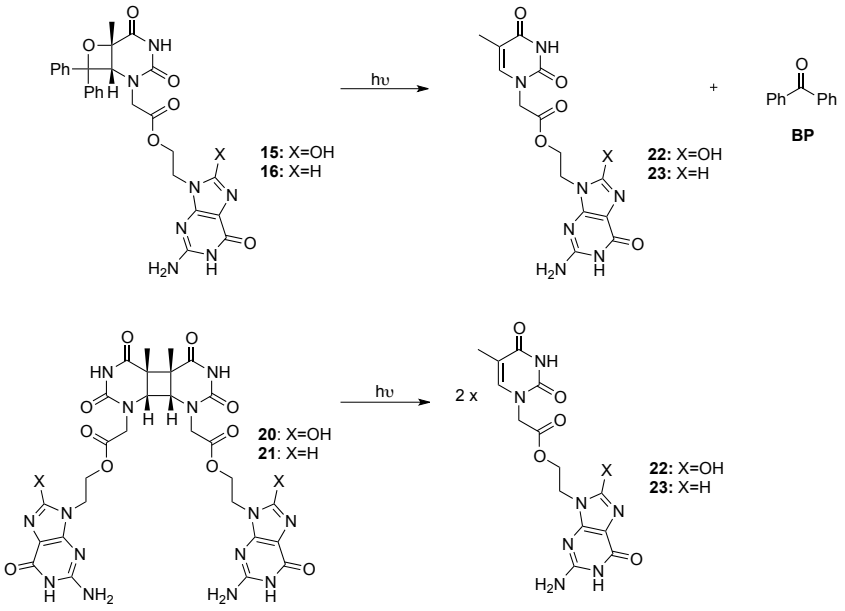

Scheme 5.9. Cleavage reaction of **15**, **16**, **20**, **21** to form **22** or **23** and BP (in the case of **15** and **16**).

As shown in Figure 5.7, an increase of the absorption at 270 nm was observed during the irradiation of all the compounds. The changes are, however, more pronounced in the case of the OG derived dyads pointing toward a higher efficiency of the process when the oxidized guanine acts as photoreductant. Moreover, another band was observed at around 250 nm for oxetane models **15** and **16**, which agrees with the formation of BP as a result of the cycloreversion.

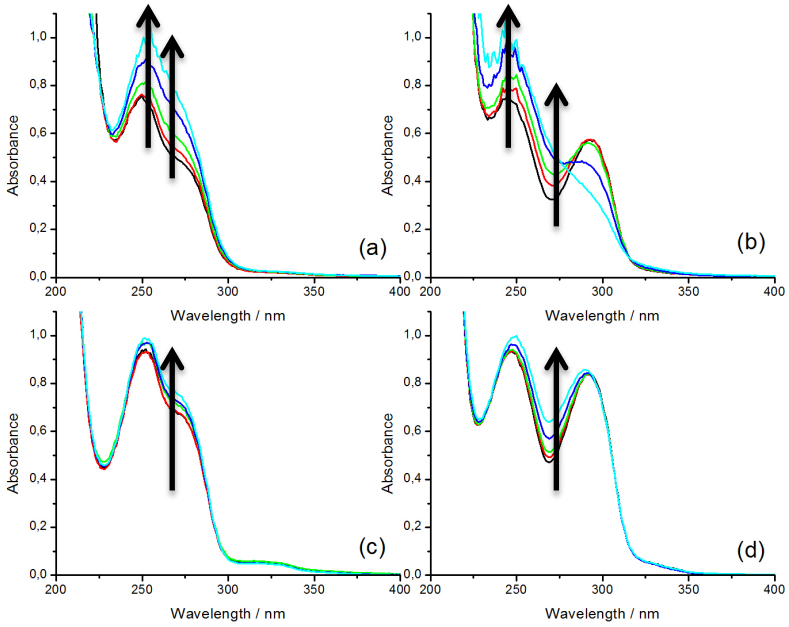

Figure 5.7. UV absorption spectra of: (a) **16** (0.2 mM), (b) **15** (0.2 mM), (c) **21** (0.1 mM), (d) **20** (0.1 mM) in PBS at pH 7.4 obtained after 0, 30, 60, 120 and 180 min of irradiation at 280 nm.

In addition, the cleavage was achieved at 295 nm to check that the observed cycloreversion is not the result of direct absorption by the oxetane and CPD unit. As shown in Figure 5.8 similar results were obtained for the two irradiation conditions, i.e. at 280 and 295 nm.

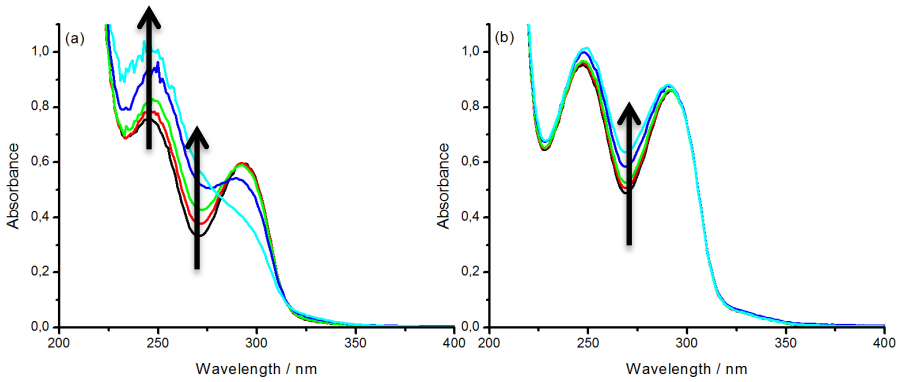

Figure 5.8. UV spectra of: (a) **15** (0.2 mM), (b) **20** (0.1 mM) in PBS at pH 7.4 obtained after 0, 30, 60, 120 and 180 min of irradiation at 295 nm.

In order to ensure that the photocleavage resulted in the expected photoproducts, the course of the reaction was monitored by HPLC at different irradiations times. Figure 5.9 shows the cleavage of the oxetane models **15** and **16**, that eluted at 30.8 min, into **22** or **23**, with retention time of 19.4 min, and BP, with retention time of 38.4 min.

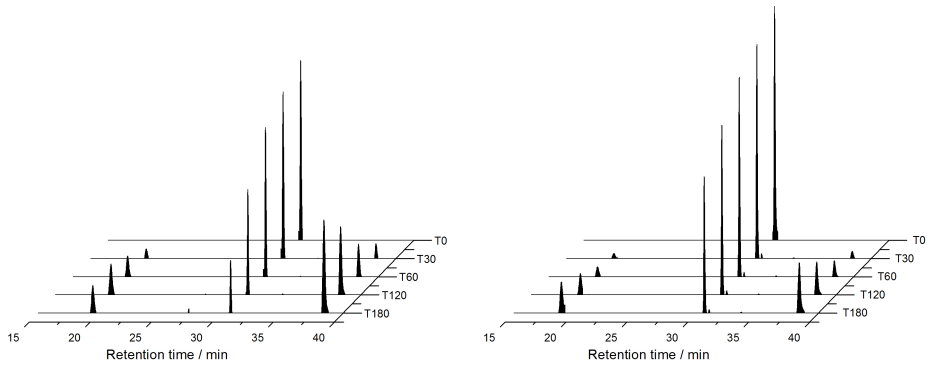

Figure 5.9. HPLC chromatograms obtained after 0, 30, 60, 120, 180 min of irradiation of **15** (0.2 mM, left) and **16** (0.2 mM, right) in PBS at pH 7.4 with 280 nm light.

For the CPD case, Figure 5.10. shows the photochemical reaction of models **20** and **21**, with retention time of 26.1 min and 23.1 min, respectively, to give the photosplitted product **22** or **23** with retention time of 18.5 min. A clean conversion was observed, as no other products were detectable in all cases.

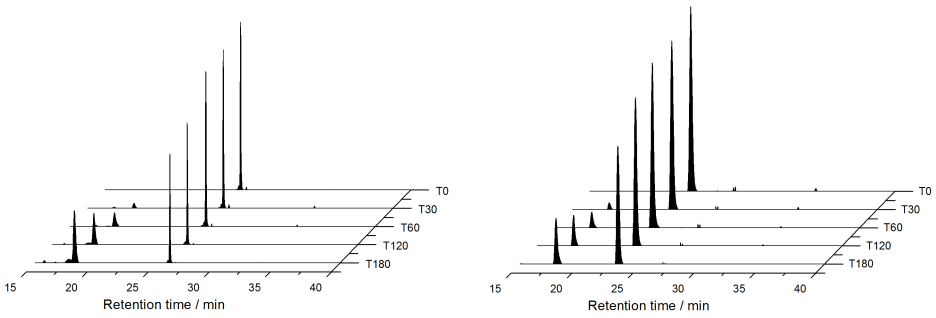

Figure 5.10. HPLC chromatograms obtained after 0, 30, 60, 120, 180 min of irradiation of **20** (0.1 mM, left) and **21** (0.1 mM, right) in PBS at pH 7.4 with 280 nm light.

To determine the efficiency of the oxetane and CPD models, we measure the splitting quantum yield, ϕ = (rate of formation of repaired model)/(rate of photon absorbed).[28] Solutions (3 mL) of **15**, **16**, **20** and **21** were irradiated at 280 nm and the increase in absorbance at 270 nm was monitored due to the regeneration of the 5,6-double bond of pyrimidine **22** or **23** and BP ($\varepsilon_{thymine}$= 7500 L $mol^{-1}cm^{-1}$ and $\varepsilon_{thymine+BP}$= 19400 L $mol^{-1}cm^{-1}$ determined by UV spectroscopy). The splitting concentration (c_{spl}) was obtained through $\Delta A_{270}/\Delta\varepsilon_{270}$ as stated by the Beer-Lambert equation. Therefore, the plot of c_{spl} against the irradiation time gives a well-fitted straight line whose slope (B), which is a splitting rate of the model compounds. Moreover, to reduce competition in absorbing the incident light at 280 nm between the models and the photoproducts, the splitting extent was controlled within 5% in all measurements.

Regarding to the number of photons absorbed by the models, the intensity of the light beam was measured by ferrioxalate actinometry, being I_0 = 2.29 x 10^{-8} einstein min^{-1}.[36] Therefore, the rate of photons absorbed by models (I_A) was obtained from the absorbance at 280 nm (irradiation wavelength) before irradiation, in terms of Beer's law (equation 5.1).

$$I_A = I_0\left(1 - 10^{A^{280}}\right) \quad (5.1)$$

These values allowed the determination of the quantum yield **Φ** through equation 5.2 where V_0 is the volume of irradiation solution.

$$\phi = \frac{rate\ of\ formation\ of\ repaired\ model}{rate\ of\ photon\ absorbed} = \frac{B}{I_A} V_o \quad (5.2)$$

The observed quantum yields for **15**, **16**, **20** and **21** were calculated and listed in Table 5.1. A more efficient splitting was observed for oxetane than for CPD models. In addition, different quantum yields were determined when OG and G are acting as the photoreductants; the photocycloreversion being almost twice as efficient in the case of the former. These values are in agreement with previous studies that have shown that the cleavage quantum yield is often much less than unity due to efficient back electron transfer when a thymine dimer or oxetane is covalently tethered to an electron-donating chromophore such as indole[28-29] or flavin[27]. Therefore, all photoinduced electron transfer-initiated chemical reactions compete with an exothermic back electron-transfer process, and quantum yields approaching the unity are reached when the rate of the chemical process is fast relative to the rate of back electron transfer.

Moreover, the obtained results are in agreement with the quantum yields reported for models where oxetane and CPD are covalently linked to flavin, with a value two fold higher for the heterocycle than for the cyclobutane ring splitting (ca. of 0.02 and 0.01, respectively).[27] Indeed, this difference can be explained by comparing the splitting rate of the oxetane radical anion (>10^7 s^{-1})[34] , which is faster than that of the

CPD radical anion (~10^6 s^{-1})[37]. Thus, the fast splitting of the oxetane radical anion competes more efficiently with BET within the zwitterionic intermediate than the radical anion of CPD does. Interestingly in photolyases, the higher efficiency of CPD photolyase (ca. of 0.7-0.9) by contrast with (6-4) photolyase (ca. of 0.1) has been attributed to factors that suppress back electron transfer.[38]

Table 5.1. Splitting efficiencies for compounds **15**, **16**, **20** and **21** in neutral PBS.

	15	**16**	**20**	**21**
ϕ	0.08	0.04	0.02	0.01

Regarding to the chromophore, the splitting is more efficient for **15** and **20** models, that is, when excited OG is the electron donor. The efficiency and ability of these photosensitizers to induce a reductive dimer splitting is related to their excited-state oxidation potentials E_{ox}^{D*}, which are listed in Table 5.2. They were determined from literature values from the oxidation potential (E_{ox}^{D})[11] and the singlet state energy, E^* (using 310 and 300 nm absorption tail as the 0-0 transition energy for OG and G, respectively), using the equation 5.3.

$$E_{ox}^{D*} = E_{ox}^{D} - \frac{E^*}{23.06} \qquad (5.3)$$

Interestingly, the OG has a more negative E_{ox}^{D*} than G or even than $FADH^-$, which agrees with its higher efficiency for cycloreversion. In order to know if the PET from G and OG to oxetane or CPD is an energetically favorable process, the free energy associated with the PET (ΔG_{ct}) was determined according to the Rehm-Weller equation 5.4 and using the previously reported E_{red}^{A} of ca. -2.2 V vs. NHE for both thymine dimer[39] and oxetane[40].

$$\Delta G_{ct} = 23.06\left(E_{ox}^{D} - E_{red}^{A}\right) - E^* \qquad (5.4)$$

As shown in Table 5.2, the process is more exergonic as E_{ox}^{D*} became increasingly negative, being most favorable for OG. These results agree with a PET mechanism from the singlet excited state of OG and G to the CPD and oxetane units.

Table 5.2. Photophysical properties of the selected PS.

PS	E_{ox}^{D} / V vs. NHE	E_{ox}^{D*} / V vs. NHE	E* / kcal mol^{-1}	ΔG / kcal mol^{-1}
OG	0.7[11]	-3.3	92.2	-25.3
G	1.2[11]	-2.9	95.3	-16.9
FADH^{-}	**0.12**[41]	**-2.8**[41]	**63.6**[41]	-10.1

As mentioned above, fluorescence experiments can support the PET mechanism from singlet excited state of PS. However, given the ultralow fluorescence quantum yields of G and OG (2.3 and 1.3 x10^{-4}, respectively)[20], it was not possible to observe the intramolecular fluorescence quenching as an evidence of the electron transfer process. In addition, up conversion fluorescence might be a useful technique to study the PET between OG and the four-membered ring in **15** and **20** models, because it could provide a cleaner decay of $^{1}OG^{*}$ without potential interference of others species such as radical anion or cation. Therefore, fluorescence experiments at the femto-second timescale are in progress in collaboration with Thomas Gustavsson's group.

5.3 Conclusions

We have synthetized model systems of thymine –derived oxetane and cyclobutane dimers connected to guanine or 8-oxoguanine, which act as photoreductants. The photocleavage of the four-membered rings was followed by UV spectrophotometry and HPLC. A more efficient cleavage was observed for OG than for G, which is related with the more negative oxidation potential of the former in its excited state.

Moreover, G is able to split the models with similar efficiency than the flavin-systems. Therefore the electron donor ability has been proven for G and for OG, with similar or even higher efficiency than $FADH^{-}$. However, the low quantum yields are the result of competition between unproductive back-electron transfer reaction and the cleavage of the dimer radical anion. In addition, up conversion fluorescence spectroscopy is being run to get more information on the PET mechanism.

5.4 Experimental section

5.4.1 Synthesis

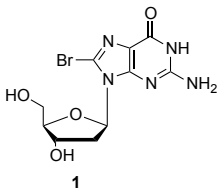

1

8-bromo-2'-dG (1). In a round bottom flask 2'-deoxyguanosine (10.0 g, 37.4 mmol) was dissolved in 400 mL MeCN and 100 mL H_2O and NBS (9.9 g, 56.1 mmol) was added in several portions. The suspension was stirred for 45 min at room temperature and subsequently evaporated to dryness. The residual solid was taken up in 350 mL acetone and stirred for 4 h at rt. Subsequently, the mixture was stored at -20°C for 48 h and filtrated. The solid was washed with cold acetone and dried to yield **1** (11.2 g, 87 %) as an orange solid. **^{1}H NMR** (300 MHz, DMSO) δ 10.79 (s, 1H), 6.49 (s, 2H), 6.15 (t, *J* = 7.3 Hz, 1H), 5.25 (d, *J* = 3.8 Hz, 1H), 4.85 (s, 1H), 4.39 (d, *J* = 2.8 Hz, 1H), 3.79 (dd, *J* = 8.4, 5.4 Hz, 1H), 3.62 (d, *J* = 10.8 Hz, 1H), 3.50 (d, *J* = 5.5 Hz, 1H), 3.26 – 3.06 (m, 1H), 2.10 (m, 1H). **^{13}C NMR** (75 MHz, DMSO) δ 155.5 (C), 153.30 (C), 151.96 (C), 120.5 (C), 117.4 (C), 87.9 (CH), 85.0 (CH), 70.8 (CH), 62.4 (CH_2), 36.5 (CH_2).

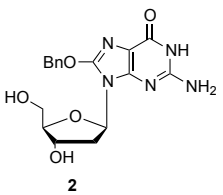

2

8-benzyloxy-2'-dG (2). Freshly cut Na metal (3.3 g, 144.9 mmol) was dissolved in benzyl alcohol (100 mL) at 60 ºC until the solution was homogeneous under nitrogen. To the resulting mixture was added **1** (10.0 g, 28.9 mmol) in DMSO (40 mL), and the mixture was heated at 65 ºC for 24 h. Then cooled to room

temperature, the reaction was poured into magnetically stirred ether (1000 mL) solvent for precipitation. The precipitated solid was filtered and precipitated with ether one more time. Then was poured in a 3 mL of water overnight to give a white precipitated **2** (3.0 g, 30%). **^{1}H NMR (300 MHz, DMSO)** δ 10.56 (s, 1H), 7.42 (dt, *J* = 14.9, 7.0 Hz, 5H), 6.31 (s, 2H), 6.08 (t, *J* = 7.1 Hz, 1H), 5.40 (s, 2H), 5.16 (d, *J* = 4.0 Hz, 1H), 4.77 (t, *J* = 5.7 Hz, 1H), 4.24 (s, 1H), 3.71 (s, 1H), 3.56 – 3.37 (m, 2H), 3.02 – 2.75 (m, 1H), 2.01 (d, *J* = 3.5 Hz, 1H). **^{13}C NMR (75 MHz, DMSO)** δ 155.7 (C), 152.8 (C), 150.9 (C), 149.9 (C), 135.7 (C), 128.4 (3CH), 110.5 (C), 87.3 (CH), 81.5 (CH), 70.9 (CH), 70.6 (CH_2), 62.1 (CH_2), 36.1 (CH_2).

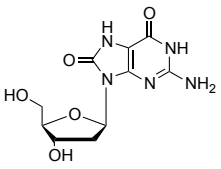

3

8-oxo-2'-dG (3). To a stirred solution of **2** (3.0 g, 8.0 mmol) in MeOH (300 mL) at rt was added 1.0 M HCl (30 mL). The reaction was stirred for 1 h. Removal of water and MeOH under reduced pressure followed by trituration of the residue from MeOH/ether afforded quantitative yield of **3**. **^{1}H NMR (300 MHz, DMSO)** δ 6.55 (s, 2H), 6.03 (dd, *J* = 8.1, 6.7 Hz, 1H), 4.32 (dd, *J* = 11.0, 8.2 Hz, 1H), 3.75 (d, *J* = 2.3 Hz, 1H), 3.57 (dd, *J* = 11.7, 4.7 Hz, 1H), 3.44 (dd, *J* = 11.7, 4.8 Hz, 1H), 2.95 (m, 1H), 1.91 (m, 1H). **^{13}C NMR (75 MHz, DMSO)** δ 153.8 (C), 152.2 (C), 151.6 (C), 147.1 (C), 98.6 (C), 87.3 (CH), 80.9 (CH), 71.4 (CH), 62.4 (CH_2), 35.5 (CH_2).

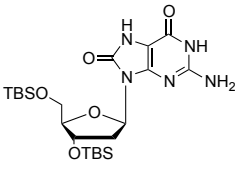

4

5',3'-*O*-(bis-*tert*-butyldimethylsilyl)-8-oxo-2'-dG (4). A mixture of **3** (2.2 g, 7.8 mmol), TBDMSCl (2.5 g, 17.1 mmol) and imidazole (1.2 g, 17.1 mmol) was stirred in 20 mL of dry DMF at room temperature for 24 h. The reaction was stopped by adding $NaHCO_3$ solution (50 mL) and extracted with ethyl acetate (50 mL). The organic layer was washed twice with brine (50 mL), dried over $MgSO_4$ and the solvent removed *in vacuo*. The crude product was purified by column chromatography (silica gel, *n*-hexane/ethyl acetate/methanol 2:2:0.4) to give **4** (2.4 g, 60%) as beige solid. **^{1}H**

NMR (300 MHz, DMSO) δ 10.72 (s, 1H), 10.59 (s, 1H), 6.37 (s, 2H), 5.98 (t, *J* = 7.2 Hz, 1H), 4.47 (t, *J* = 11.0 Hz, 1H), 3.77 (m, 1H), 3.56 (dd, *J* = 13.6, 8.8 Hz, 1H), 3.28 (m, 2H), 1.92 (m, 1H), 0.86 (s, 18H), -0.03 (s, 12H). **^{13}C NMR (75 MHz, DMSO)** δ 153.1 (C), 151.3 (C), 151.1 (C), 147.3 (C), 98.6 (C), 86.4 (CH), 80.7 (CH), 72.9 (CH), 63.0 (CH_2), 34.5 (CH_2), 25.9 (CH_3), 17.1 (C), -3.36 (CH_3).

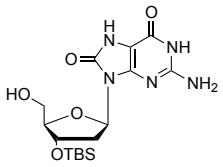

5

3'-*O*-(*tert*-butyldimethylsilyl)-8-oxo-2'-dG (5). To a solution of compound **4** (1. 5 g, 2.9 mmol) in CH_2Cl_2 (15 mL), a mixture of trifluoroacetic acid and water (0.6:1.8 mL) was added, and the reaction was stirred at 0 ºC for 4 h. The reaction was stopped by adding $NaHCO_3$ solution (10 mL) and extracted with CH_2Cl_2 (10 mL). The organic layer was washed with brine (10 mL), dried over $MgSO_4$ and the solvent removed *in vacuo*. The crude product was purified by column chromatography (silica gel, *n*-hexane/ethyl acetate/methanol 2:2:0.5) to give **5** (0.7 g, 65%) as beige solid. **^{1}H NMR (300 MHz, DMSO)** δ 10.69 (s, 1H), 10.61 (s, 1H), 6.33 (s, 2H), 5.92 (t, *J* = 7.3 Hz, 1H), 4.75 (dd, *J* = 6.8, 5.1 Hz, 1H), 4.50 (m, 1H), 3.71 (m, 1H), 3.47 (dt, *J* = 10.7, 5.3 Hz, 1H), 3.41 (m, 1H), 3.02 (m, 1H), 1.83 (m, 1H), 0.80 (s, 9H), -0.00 (s, 6H). **^{13}C NMR (75 MHz, DMSO)** δ 153.1 (C), 151.5 (C), 151.1 (C), 147.4 (C), 98.5 (C), 87.4 (CH), 81.1 (CH), 73.2 (CH), 61.9 (CH_2), 35.6 (CH_2), 25.7 (CH_3), 17.7 (C), -4.8 (CH_3).

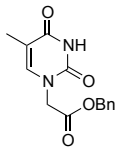

6

Thymine acetic acid benzyl ester (6). Thymine acetic acid (5.0 g, 27.1 mmol) was dissolved in DMF (50 mL), 1,1'-carbonyldiimidazole (5.0 g, 31.2 mmol) was then added. The slurry was stirred at rt for 30 min and benzyl alcohol was added (3.2 mL, 31.22 mmol). The solution was stirred at rt for 18 h. Then, H_2O (100 mL) was added at 0 ºC and the product was isolated as a white solid **6** (4.8 g, 65%) upon filtration. **^{1}H NMR (300 MHz, DMSO**) δ 11.42 (s, 1H), 7.53 (s, 1H), 7.47 (m, 5H), 5.19 (s, 2H), 4.55 (s, 2H), 1.76 (s, 3H). **^{13}C NMR (75 MHz, DMSO)** δ 168.1 (C), 164.2 (C), 150.9 (C), 141.5 (CH), 135.5 (C), 128.4 (CH), 128.2 (CH), 127.9 (CH), 108.6 (C), 66.4 (CH_2), 48.4 (CH_2), 11.8 (CH_3).

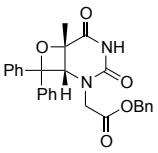

7

Thymine oxetane acetic acid benzyl ester (7). In a Pyrex vessel (λ > 290 nm), the benzyl ester **6** (4.5 g, 16.4 mmol) was dissolved in acetonitrile (444 mL) under sonication. Benzophenone (5.9 g, 32.8 mmol) was added and the solution was degassed by bubbling N_2 for 0.5 h. The solution was irradiated for 16 h with a medium pressure mercury lamp (125 W). Acetonitrile was removed *in vacuo* and the product was isolated by flash chromatography (silica gel, *n*-hexane/ethyl acetate 4:1 to 1:1). Recrystallisation from *n*-hexane/ethyl acetate (4:1) gave **7** (1.6 g, 22%) as a white solid. **^{1}H NMR (300 MHz, DMSO)** δ 10.50 (s, 1H), 7.49 – 7.16 (m, 15H), 5.29 – 5.05 (m, 2H), 4.99 (s, 1H), 4.40 (d, *J* = 17.4 Hz, 1H), 4.10 (d, *J* = 17.5 Hz, 1H), 1.51 (s, 3H). **^{13}C NMR (75 MHz, DMSO)** δ 170.0 (C), 168.4 (C), 151.2 (C), 144.3 (C), 139.5 (C), 135.6 (C), 128.4 (CH), 128.3 (CH), 128.2 (CH), 128.1 (CH), 128.0 (CH), 127.5 (CH), 125.4 (CH), 125.0 (CH), 90.9 (C), 76.1 (C), 66.3 (CH_2), 64.9 (CH), 48.1 (CH_2), 23.1 (CH_3).

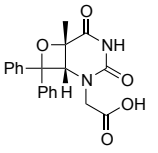

8

Thymine oxetane acetic acid (8). To a stirred solution of **7** (500 mg, 1.1 mmol) in glacial acetic acid (5 mL) was added 10% Pd/C (13 mg, 0.1 mmol). The solution was stirred under H_2 atmosphere for 4 h at atmospheric pressure. The reaction mixture was filtered through celite and the filter cake was washed with hot acetic acid (20 mL). The solvent was removed *in vacuo* to afford **8** (300 mg, 75%) as white solid. **^{1}H NMR (300 MHz, DMSO)** δ 12.97 (bs, 1H), 10.42 (s, 1H), 7.48 – 7.17 (m, 10H), 4.92 (s, 1H), 4.25 (d, *J* = 17.5 Hz, 1H), 3.85 (d, *J* = 17.5 Hz, 1H), 1.54 (s, 3H). **^{13}C NMR (75 MHz, DMSO)** δ 170.1 (C), 151.3 (C), 144.3 (C), 139.6 (C), 128.4 (CH), 128.1 (CH), 127.5 (CH), 125. 4 (CH), 124.5 (CH), 90.9 (C), 76.1 (C), 65.1 (CH), 47.9 (CH_2), 23.2 (CH_3).

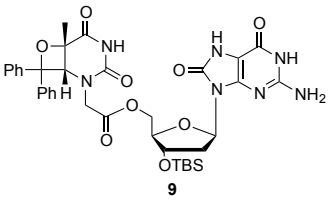

9

5'-thymine oxetane-3'-*O*-(*tert*-butyldimethylsilyl)-8-oxo-2'-dG (9). Oxetane **8** (120 mg, 0.3 mmol), EDC (65 μL, 0.4 mmol), TBTU (117 mg, 0.4 mmol), DMAP (4 mg, 0.03 mmol) were dissolved in dry DMF (6 mL)

and stirred at 0 ºC for 30 min. Then, **5** (132 mg, 0.3 mmol) was added and the solution was stirred for 20 h at rt. The reaction mixture was diluted with ethyl acetate (20 mL), washed with water (3 x 20 mL), dried over $MgSO_4$, filtered and the solvent was removed *in vacuo*. The crude product was purified by flash chromatography (silica gel, *n*-hexane/ethyl acetate/methanol 2:2:0.5) to afford **9** (136 mg, 55%) as a white solid. **^{1}H NMR (300 MHz, DMSO)** δ 10.67 (s, 1H), 10.57 (d, *J* = 3.0 Hz, 1H), 10.40 (d, *J* = 3.5 Hz, 1H), 7.37 – 7.08 (m, 10H), 6.32 (s, 2H), 5.94 (t, *J* = 7.1 Hz, 1H), 4.86 (d, *J* = 5.8 Hz, 1H), 4.52 (m, 1H), 4.34 – 4.16 (m, 2H), 4.04 (dd, *J* = 11.3, 7.4 Hz, 1H), 3.92 (dd, *J* = 17.8, 6.8 Hz, 1H), 3.81 (dd, *J* = 11.4, 7.4 Hz, 1H), 2.99 (m, 1H), 1.94 (m, 1H), 1.47 (s, 3H), 0.79 (s, 9H), -0.00 (s, 6H). **^{13}C NMR (75 MHz, DMSO)** δ 168.9 (C), 168.3 (C), 153.1 (C) 151.3 (C), 151.2 (C), 147.0 (C), 144.3 (C), 139.5 (C), 128.3 (CH), 128.1 (CH), 127.5 (CH), 125.4 (CH), 125.0 (CH), 98.5 (C), 90.9 (C), 83.5 (CH), 80.7 (CH), 76.1 (C), 72. 8 (CH), 64.9 (CH), 64,9 (CH_2), 47.7 (CH_2), 35.8 (CH_2), 25.6 (CH_3), 23.0 (CH_3), 17.6 (C), -4.84 (CH_3).

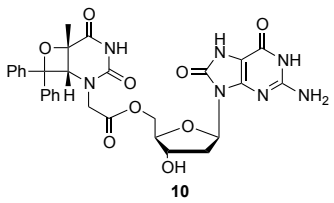

10

5'-thymine oxetane-8-oxo-2'-dG (10). To a solution of **9** (245 mg, 0.3 mmol) in THF (15 mL) was added TBAF (1.0 M in THF, 0.3 mL, 0.9 mmol). The mixture was stirred at rt for 16 h. The solvent was removed, and the residue was purified by flash chromatography (silica gel, $CHCl_3$/MeOH 5:0.5 to 5:0.1) to afford **10** (140 mg, 68%) as a white solid. **^{1}H NMR (300 MHz, DMSO**) δ 10.71 (s, 1H), 10.55 (s, 1H), 10.38 (s, 1H), 7.39 – 7.10 (m, 10H), 6.37 (s, 2H), 5.96 (t, *J* = 7.0 Hz, 1H), 5.28 – 5.11 (m, 1H), 4.87 (d, *J* = 0.8 Hz, 1H), 4.44 – 4.23 (m, 3H), 4.09 – 3.98 (m, 1H), 3.91 (dd, *J* = 17.5, 6.9 Hz, 1H), 3.79 (dt, *J* = 7.8, 4.1 Hz, 1H), 2.89 (dd, *J* = 10.8, 6.6 Hz, 1H), 2.04 – 1.92 (m, 1H), 1.48 (s, 3H). **^{13}C NMR (75 MHz, DMSO)** δ 170.1 (C), 168.4 (C), 153.1 (C), 151.4 (C), 151.2 (C), 147.1 (C), 144.3 (C), 139.5 (C), 128.3 (CH), 128.1 (CH), 127.5 (CH),

125.4 (CH), 125.0 (CH), 124.9 (CH), 98.5 (C), 90.9 (C), 83.4 (CH), 80.7 (CH), 76.1 (C), 71.0 (CH), 65.6 (CH_2), 64.9 (CH), 47.8 (CH_2), 35.5 (CH_2), 23.1 (CH_3).

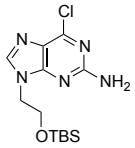

11

2-Amino-6-chloro-9-(2-ethyloxy-*tert*-butyldimethylsilane) purine (11). To an ice cold solution of 2-amino-6-chloro purine (2.8 g, 16.5 mmol) in anhydrous DMF (25 mL) was added NaH (0.4 g, 17.9 mmol). After 30 min, 2-bromoethoxy-*tert*-butyldimethylsilane (4.3 g, 18.1 mmol) was added and stirred 24 h at rt under nitrogen. Then, H_2O (25 mL) was poured and the mixture was filtrated and washed with cold water. The crude product was purified by column chromatography (silica gel, *n*-hexane/ethyl acetate 2:3) to give **11** (2.4 g, 51%) as white solid. **^{1}H NMR (300 MHz, DMSO)** δ 8.05 (s, 1H), 6.89 (s, 2H), 4.16 (t, *J* = 12 Hz, 2H), 3.89 (t, *J* = 12 Hz, 2H), 0.75 (s, 9H), -0.15 (s, 6H). **^{13}C NMR (75 MHz, DMSO)** δ 159.9 (C), 154.2 (C), 149.2 (C), 143.8 (CH), 123.4 (C), 60.3 (CH_2), 45.4 (CH_2), 25.9 (CH_3), 17.6 (C), -5.80 (CH_3). **HRMS (ESI)**: *m*/*z* calcd for $C_{13}H_{23}N_5OSiCl$ $[M+H]^+$ 328.1344, found 328.1360.

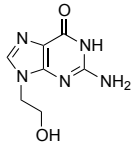

12

9-(2-ethyloxy-*tert*-butyldimethylsilane) guanine (12). A solution of **11** (2.4 g, 7.33 mmol) in 2M HCl (22 mL) was heated under reflux for 2 h. The solvent was neutralized and cooled with ice. The solid was filtered off and washed with cold H_2O to give pure **12** (1.3 g, 87%). **^{1}H NMR (300 MHz, DMSO)** δ 10.50 (s, 1H), 7.61 (s, 1H), 6.40 (s, 2H), 4.96 (t, J = 9 Hz 1H), 3.96 (t, *J* = 12 Hz, 2H), 3.69 - 3.63 (m, 2H). **^{13}C NMR (75 MHz, DMSO)** δ 156.9 (C), 153.4 (C), 151.3 (C), 137.9 (CH), 116.3 (C), 59.1 (CH_2), 45.4 (CH_2). **HRMS (ESI)**: *m*/*z* calcd for $C_7H_{10}N_5O_2$ $[M+H]^+$ 196.0825, found 196.0834.

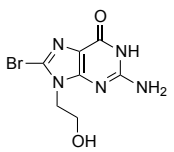

13

9-(2-ethyloxy-*tert*-butyldimethylsilane)-8-bromoguanine (13). In a round bottom flask, **12** (1.3 g, 6.1 mmol) was dissolved in 62 mL MeCN and 15 mL H_2O and NBS (1.6 g, 9.1 mmol) was added. The suspension was stirred for 30 min at rt and subsequently evaporated to dryness. The residual solid was taken up in 20 mL acetone and stirred for 30 min at

room temperature. Subsequently, the mixture was filtrated and washed with cold acetone and dried to yield **13** (0.85 g, 65%) as an beige solid. **^{1}H NMR (300 MHz, DMSO)** δ 10.64 (s, 1H), 6.55 (s, 2H), 4.98 (t, J = 10 Hz, 1H), 3.97 (t, J = 12 Hz, 2H), 3.68 – 3.62 (m, 2H). **^{13}C NMR (75 MHz, DMSO)** δ 155.7 (C), 153.9 (C), 152.5 (C), 121.4 (C), 116.6 (C), 58.8 (CH_2), 46.0 (CH_2). **HRMS (ESI)**: *m/z* calcd for $C_7H_9N_5O_2Br$ $[M+H]^+$ 273.9952, found 273.9940.

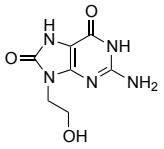

14

9-(2-hydroxyethyl)-8-oxoguanine (14). Compound **13** (0.85 g, 3.1 mmol) was dissolved in a solution of sodium acetate (2.5 g, 31.14 mmol) in glacial acetic acid (113 mL). The reaction mixture was heated at 130ºC for 7 h. Acetic acid was evaporated and a residue was codistilled with water (3 x 20 mL). The residual solid was taken up in aqueous sodium hydroxide (0.1 M, 10 mL) and heated at reflux 10 min. Then, it was acidified to pH 7 in an ice bath and the resulting precipitated filtered off, washed with water to give **14** (0.3 g, 46%) as beige solid. **^{1}H NMR (300 MHz, DMSO)** ^{1}δ 10.58 (s, 1H), 10.49 (s, 1H), 6.43 (s, 2H), 4.81 (t, J = 10 Hz, 1H), 3.68 – 3.63 (m, 2H), 3.60 – 3.57 (m, 2H). **^{13}C NMR (75 MHz, DMSO)** δ 153.7 (C), 152.5 (C), 150.7 (C), 147.9 (C), 97.7 (C), 58.5 (CH_2), 41.5 (CH_2). **HRMS (ESI)**: *m/z* calcd for $C_7H_{10}N_5O_3$ $[M+H]^+$ 212.0780, found 212.0784.

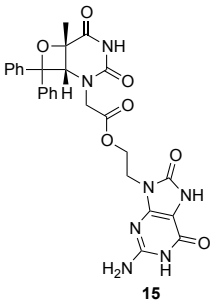

15

9-(2-(thymine oxetane) ethyl)-8-oxoguanine (15). Oxetane carboxylic acid **8** (192 mg, 0.5 mmol), EDC (102 μL, 0.6 mmol), TBTU (186 mg, 0.6 mmol), DMAP (6.4 mg, 0.05 mmol) were dissolved in dry DMF (5 mL) and stirred at 0 ºC for 30 min. Then, **14** (100 mg, 0.5 mmol) was added and the solution was stirred for 24 h at rt. The reaction mixture was diluted with H_2O (10 mL) and cooled with ice. The solid was filtered off and washed with cold water. The crude product was purified by column chromatography (silica gel, *n*-hexane/ethyl acetate/methanol 2:2:0.5) to give **15** (88 mg, 33%) as beige

solid. **^{1}H NMR (300 MHz, DMSO)** δ 10.71 (s, 1H), 10.62 (s, 1H), 10.48 (s, 1H), 7.29 (m, 10H), 6.49 (s, 2H), 4.94 (s, 1H), 4.30 – 3.88 (m, 3H), 3.88 – 1.57 (m, 3H), 1.57 (s, 3H). **^{13}C NMR (75 MHz, DMSO)** δ 170.0 (C), 168.4 (C), 153.5 (C), 152.3 (C), 151.2 (C), 147.9 (C), 144.1 (C), 139.5 (C), 128.4 (CH), 128.1 (CH), 127.5 (CH), 125.4 (CH), 125.1 (CH), 98.3 (C), 90.9 (C), 76.0 (C), 64.8 (CH), 62.3 (CH_2), 47.8 (CH_2), 38.0 (CH_2), 23.1 (CH_3). **HRMS (ESI)**: *m/z* calcd for $C_{27}H_{26}N_7O_7$ $[M+H]^+$ 560.1882, found 560.1894.

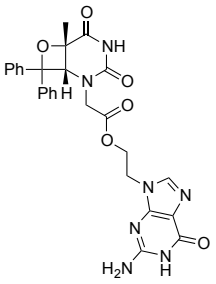
16

9-(2-(thymine oxetane) ethyl)-guanine (16). Oxetane carboxylic acid **8** (100 mg, 0.3 mmol), EDC (53 μL, 0.3 mmol), TBTU (96 mg, 0.3 mmol), DMAP (3.3 mg, 0.03 mmol) were dissolved in dry DMF (2.7 mL) and stirred at 0 ºC for 30 min. Then, **12** (53 mg, 0.3 mmol) was added and the solution was stirred for 24 h at rt. The reaction mixture was diluted with H_2O (5 mL) and cooled with ice. The solid was filtered off and washed with cold water to give **16** (71 mg, 48%) as white solid. **^{1}H NMR (300 MHz, DMSO)** δ 10.55 (s, 1H), 10.49 (s, 1H), 7.69 (s, 1H), 7.44 – 7.19 (m, 10H), 6.43 (s, 2H), 4.92 (s, 1H), 4.49 – 4.16 (m, 5H), 4.01 – 3.95 (m, 1H), 1.57 (s, 3H). **^{13}C NMR (75 MHz, DMSO)** δ 169.8 (C), 168.3 (C), 156.6 (C), 153.4 (C), 150.9 (C), 144.4 (C), 139.9 (C), 137.2 (C), 128.4 (CH), 128.1 (CH), 127.5 (CH), 125.4 (CH), 125.0 (CH), 91.1 (C), 75.9 (C), 65.1 (CH), 62.7 (CH_2), 47.8 (CH_2), 41.9 (CH_2), 22.9 (CH_3). (C8-H signat at ca. 140 ppm has not been detected due to high signal-noise) **HRMS (ESI)**: *m/z* calcd for $C_{27}H_{26}N_7O_6$ $[M+H]^+$ 544.1943, found 544.1945.

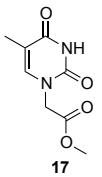
17

Methyl 2-(thymin-1-yl)acetate (17). To a stirred solution of thymine acetic acid (5 g, 27.1 mmol) in MeOH (200 mL), H_2SO_4 (1 mL) was added. The reaction was heated to reflux overnight. The solvent was evaporated under pressure, diluted with H_2O (100 mL) and cooled with ice. The solid was filtered off and washed well with cold H_2O to give pure **17** (4.2 g, 78%)

as white solid. **^{1}H NMR (300 MHz, DMSO)** δ 11.39 (s, 1H), 7.49 (s, 1H), 4.47 (s, 2H), 3.68 (s, 3H), 1.75 (s, 3H). **^{13}C NMR (75 MHz, DMSO)** δ 168.7 (C), 164.2 (C), 150.9 (C), 141.7 (CH), 108.5 (C), 52.3 (CH_3), 48.4 (CH_2), 11.8 (CH_3).

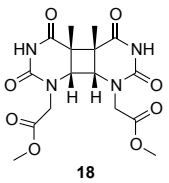
18

***Cis-syn*-thymine dimer ester (18)**. The methyl ester **17** (4 g, 20.2 mmol) was dissolved in acetone/acetonitrile (500 mL, 1:4) and the solution was degassed for 30 min. The solution was irradiated for 72 h with a medium pressure mercury lamp (125 W) in a Pyrex vessel. The reaction mixture was filtrated and evaporated to dryness *in vacuo*. The product was isolated by flash chromatography (silica gel, $CHCl_3$/MeOH 5:0.15) as white solid **18** (0.3 g, 3.8%). **^{1}H NMR (300 MHz, DMSO)** δ 10.51 (s, 2H), 4.21 (d, *J* = 17.4 Hz, 2H), 3.96 (s, 2H), 3.85 (d, *J* = 17.4 Hz, 2H), 3.65 (s, 6H), 1.35 (s, 6H). **^{13}C NMR (75 MHz, DMSO)** δ 170.4 (2C), 169.3 (2C), 152.2 (2C), 59.5 (2CH), 52.1 ($2CH_3$), 47.1 ($2CH_2$), 46.2 (2C), 18.1 ($2CH_3$).

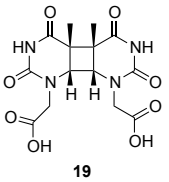
19

***Cis-syn* thymine dimer acetic acid (19)**. The diester **18** (200 mg, 0.5 mmol) was dissolved in 5 M hydrochloride (5 mL). The reaction mixture was refluxed for 30 min and then the reaction solution was concentrated *in vacuo*. The product was washed with Et_2O and dried *in vacuo* to yield a white solid **19** (0.1 g, 62%). **^{1}H NMR (300 MHz, DMSO)** δ 12.82 (s, 2H), 10.48 (s, 2H), 4.17 (d, *J* = 17.4 Hz, 2H), 3.94 (s, 2H), 3.70 (d, *J* = 17.4 Hz, 2H), 1.30 (s, 6H). **^{13}C NMR (75 MHz, DMSO)** δ 170.7 (2C), 170.1 (2C), 152.2 (2C), 59.4 (2CH), 47.2 ($2CH_2$), 46.3 (2C), 18.2 ($2CH_3$).

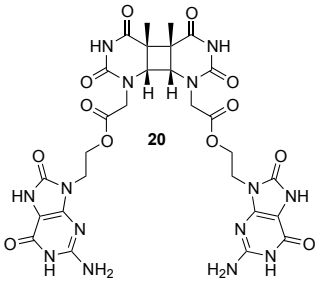

9-(2-(thymine dimer) ethyl)-8-oxoguanine (20). *Cis-syn*-thymine dimer carboxylic **19** (97 mg, 0.3 mmol), EDC (102 μL, 0.6 mmol), TBTU (186 mg, 0.6 mmol), DMAP (6.4 mg, 0.05 mmol) were dissolved in dry DMF (5 mL) and stirred at 0 ºC for 30 min. Then, **14** (100 mg, 0.5 mmol) was added and the solution was stirred for 24 h at rt. The unreacted **14** was filtered and the filtrate was diluted with H_2O (10 mL) and cooled with ice. The solid was filtered off and washed with cold water to give **20** (50 mg, 25%) as beige solid. **^{1}H NMR (300 MHz, DMSO)** δ 10.74 (s, 4H), 10.53 (s, 2H), 6.52 (s, 4H), 4.39 – 4.21 (m, 6H), 3.92 – 3.68 (m, 8H), 1.30 (s, 6H). **^{13}C NMR (75 MHz, DMSO)** δ 170.4 (2C), 168.7 (2C), 153.6 (2C), 152.4 (2C), 152.1 (2C), 151.1 (2C), 147.9 (2C), 98.6 (2C), 62.2 (2CH), 59.0 ($2CH_2$), 47.1 ($2CH_2$), 46.3 (2C), 37.9 ($2CH_2$), 18.3 ($2CH_3$). **HRMS (ESI)**: *m/z* calcd for $C_{28}H_{31}N_{14}O_{12}$ $[M+H]^+$ 755.2270, found 755.2246.

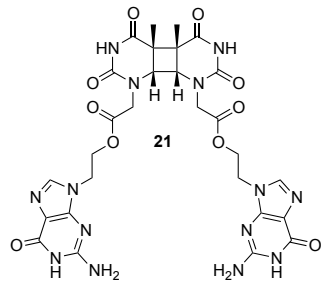

9-(2-(thymine dimer) ethyl)-guanine (21). *Cis-syn*-thymine dimer carboxylic **19** (65 mg, 0.2 mmol), EDC (34 μL, 0.4 mmol), TBTU (124 mg, 0.4 mmol), DMAP (4.3 mg, 0.03 mmol) were dissolved in dry DMF (2 mL) and stirred at 0 ºC for 30 min. Then, **12** (68 mg, 0.4 mmol) was added and the solution was stirred for 24 h at rt. The reaction mixture was diluted with H_2O (4 mL) and cooled with ice. The solid was filtered off and washed with cold water to give **21** (63 mg, 50%) as white solid. **^{1}H NMR (300 MHz, DMSO)** δ 10.58 (s, 2H), 10.54 (s, 2H), 7.68 (s, 2H), 6.46 (s, 4H), 4.42 – 4.33 (m, 4H), 4.27 – 4.18 (m, 6H), 3.88 – 3.76 (m, 4H), 1.29 (s, 6H). **^{13}C NMR (75 MHz, DMSO)** δ 170.4 (2C), 168.6 (2C), 156.6 (2C), 153.7 (2C), 152.2 (2C), 150.9 (2C), 137.6 (2CH), 116.6 (2C), 62.7 ($2CH_2$), 59.4 (2CH), 47.1 ($2CH_2$), 45.9

(2C), 41.7 ($2CH_2$), 17.9 ($2CH_3$). **HRMS (ESI)**: *m/z* calcd for $C_{28}H_{31}N_{14}O_{10}$ $[M+H]^+$ 723.2335, found 723.2348.

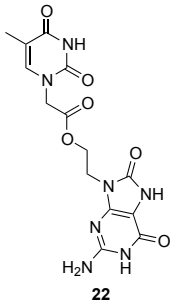

22

9-(2-(thymine) ethyl)-8-oxo-guanine (22). Thymine acetic acid (100 mg, 0.3 mmol), EDC (25.5 μL, 0.3 mmol), TBTU (93 mg, 0.3 mmol), DMAP (4.3 mg, 0.03 mmol) were dissolved in dry DMF (2 mL) and stirred at 0 ºC for 30 min. Then, **14** (51 mg, 0.3 mmol) was added and the solution was stirred for 24 h at rt. The reaction mixture was diluted with H_2O (4 mL) and cooled with ice. The solid was filtered off and washed with cold water to give **22** (45 mg, 40%) as white solid. **^{1}H NMR (300 MHz, DMSO-d_6)** δ 11.39 (s, 1H), 10.60 (s, 1H), 7.37 (s, 1H), 6.49 (s, 2H), δ 4.41 (s, 2H), 4.32 (t, *J* = 4.2 Hz, 2H), 3.86 (t, *J* = 4.9 Hz, 2H), 1.74 (s, 3H).

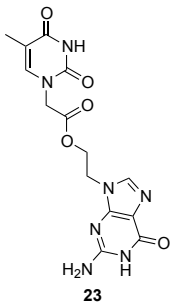

23

9-(2-(thymine) ethyl)-guanine (23). Thymine acetic acid (100 mg, 0.3 mmol), EDC (25.5 μL, 0.3 mmol), TBTU (93 mg, 0.3 mmol), DMAP (4.3 mg, 0.03 mmol) were dissolved in dry DMF (2 mL) and stirred at 0 ºC for 30 min. Then, **12** (51 mg, 0.3 mmol) was added and the solution was stirred for 24 h at rt. The reaction mixture was diluted with H_2O (4 mL) and cooled with ice. The solid was filtered off and washed with cold water to give **23** (54 mg, 50%) as white solid. **^{1}H NMR (300 MHz, DMSO-d_6)** δ 11.41 (s, 1H), 10.56 (s, 1H), 7.67 (s, 1H), 7.42 (s, 1H), 6.46 (s, 2H), 4.56 – 4.33 (m, 4H), 4.21 (t, *J* = 4.3 Hz, 2H), 1.75 (s, 3H). **^{13}C NMR (75 MHz, DMSO-d_6)** δ 168.0 (C), 164.2 (C), 156.7 (C), 153.6 (C), 151.2 (C), 150.9 (C), 141.3 (CH), 137.5 (CH), 116.5 (C), 108.7 (C), 63.3 (CH_2), 48.3 (CH_2), 41.6 (CH_2), 11.8 (CH_3).

5.4.2 NMR spectra (^{1}H, DEPT, ^{13}C)

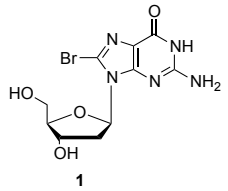
O
N
NH
Br
N
N
NH2
HO
O
OH

1

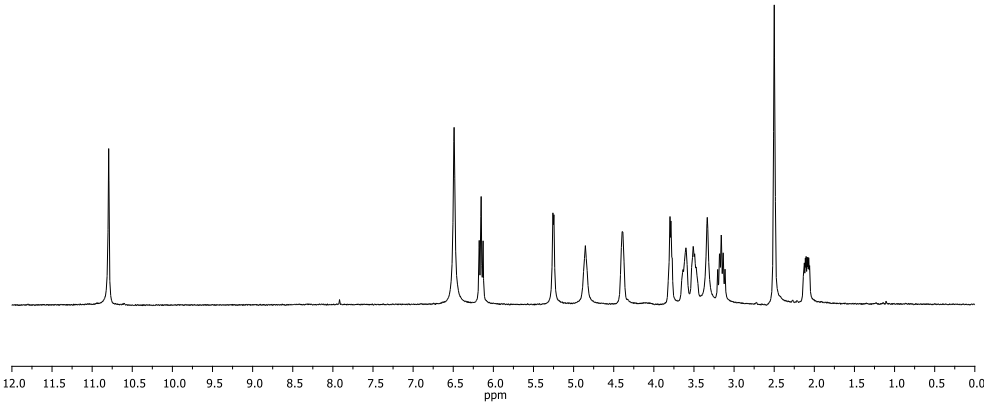
12.0 11.5 11.0 10.5 10.0 9.5 9.0 8.5 8.0 7.5 7.0 6.5 6.0 5.5 5.0 4.5 4.0 3.5 3.0 2.5 2.0 1.5 1.0 0.5 0.0
ppm

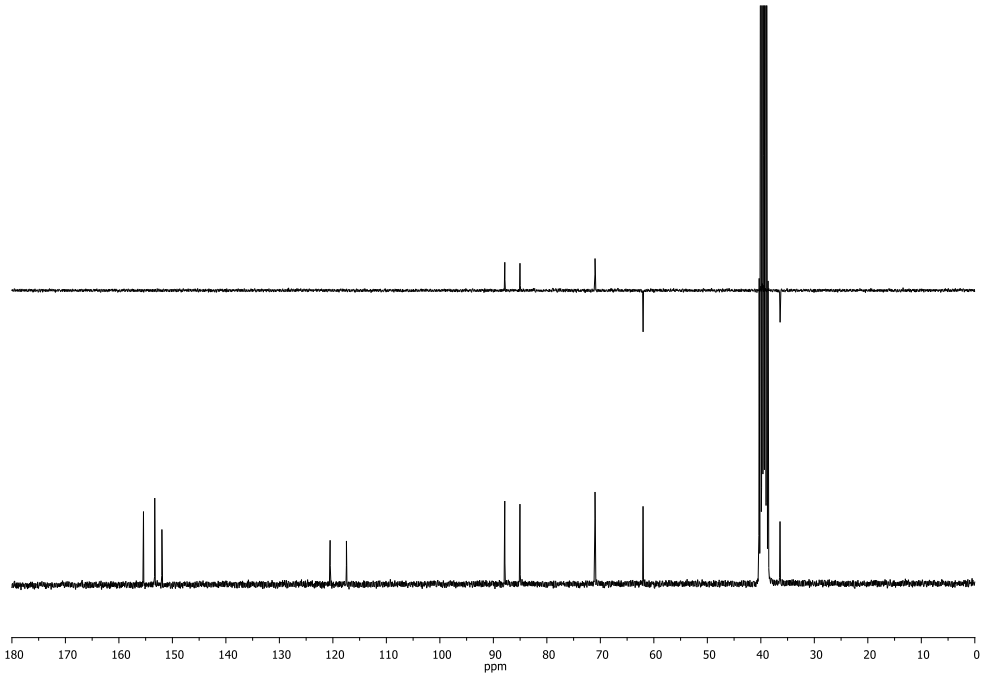
180 170 160 150 140 130 120 110 100 90 80 70 60 50 40 30 20 10 0
ppm

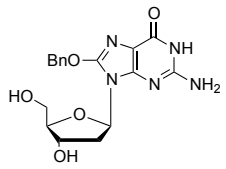
O
N
NH
BnO
N
N
NH2
HO
O
OH

2

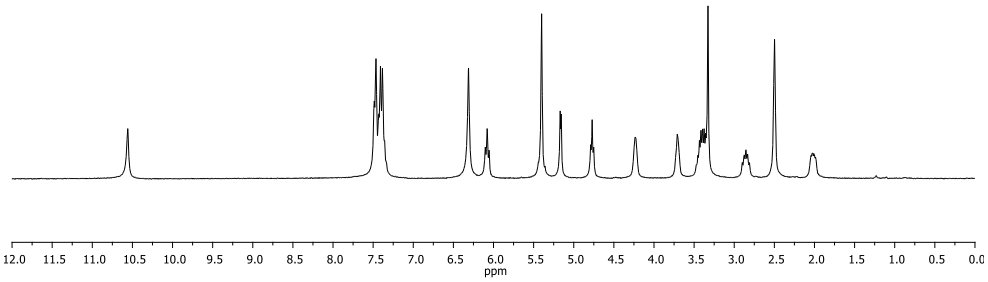
12.0 11.5 11.0 10.5 10.0 9.5 9.0 8.5 8.0 7.5 7.0 6.5 6.0 5.5 5.0 4.5 4.0 3.5 3.0 2.5 2.0 1.5 1.0 0.5 0.0
ppm

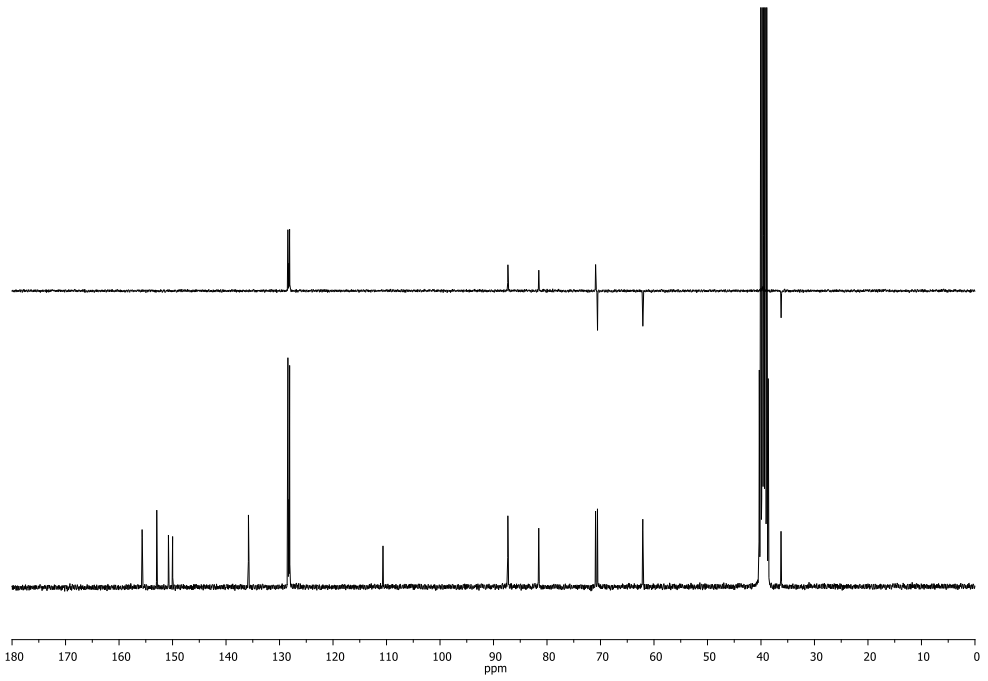
180 170 160 150 140 130 120 110 100 90 80 70 60 50 40 30 20 10 0
ppm

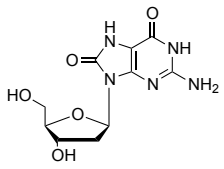
H
N
O
NH
O
N
N
NH2
HO
O
OH

3

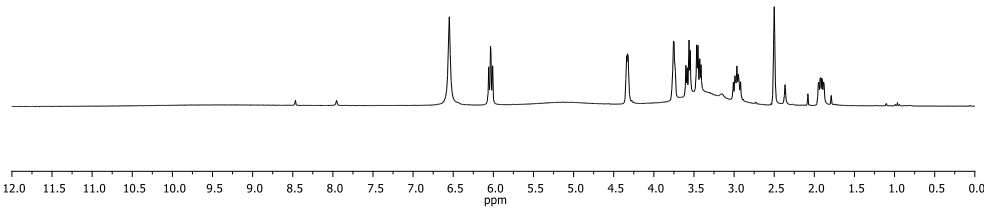
12.0 11.5 11.0 10.5 10.0 9.5 9.0 8.5 8.0 7.5 7.0 6.5 6.0 5.5 5.0 4.5 4.0 3.5 3.0 2.5 2.0 1.5 1.0 0.5 0.0
ppm

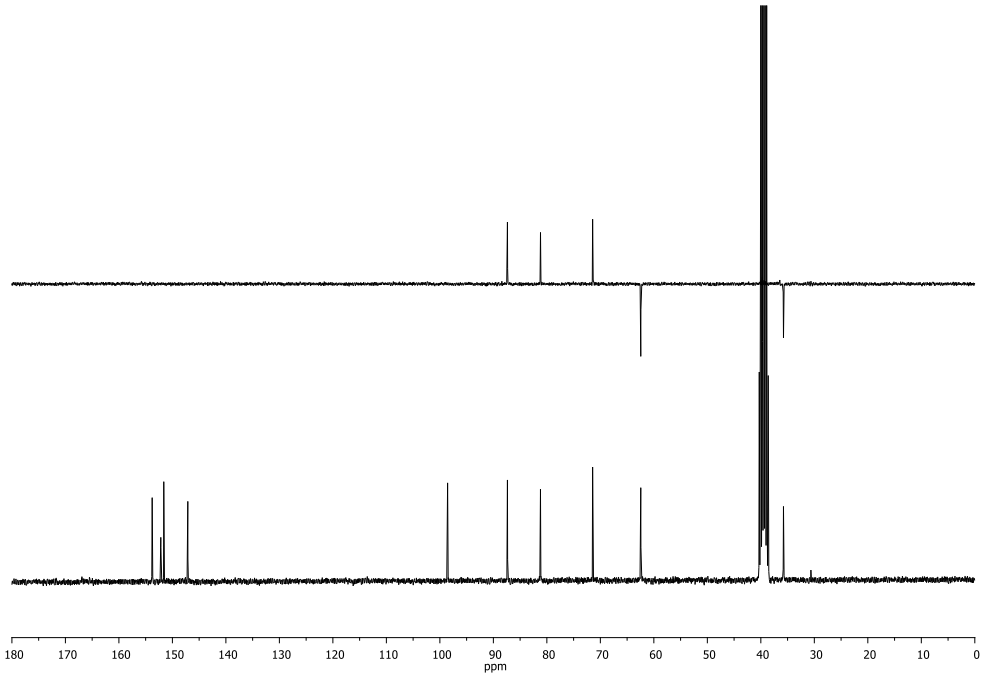
180 170 160 150 140 130 120 110 100 90 80 70 60 50 40 30 20 10 0
ppm

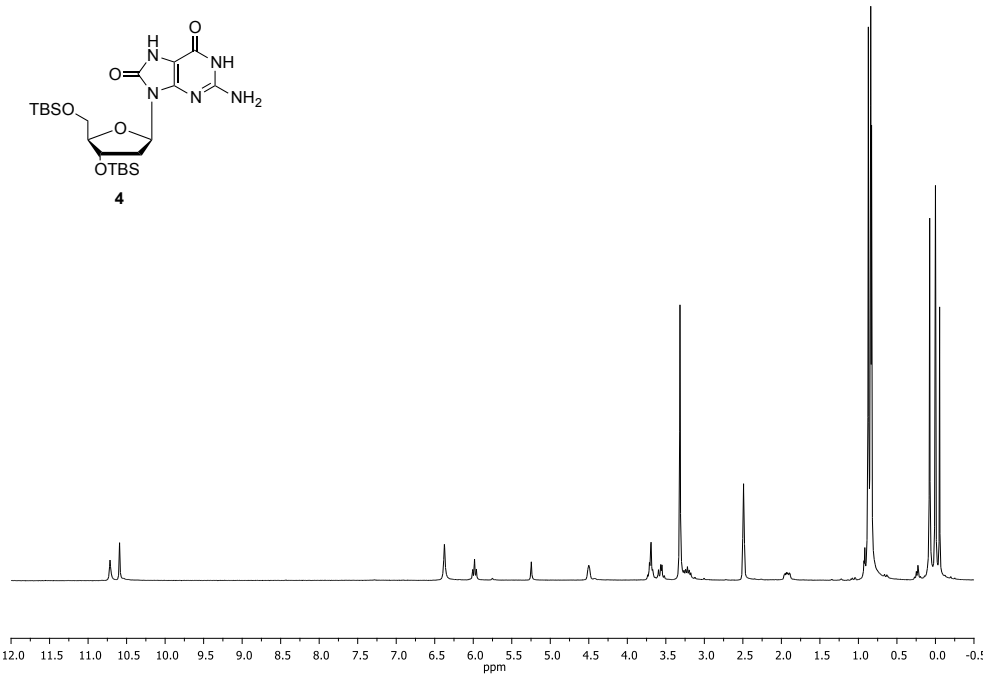
TBSO
OTBS
O
H
N
NH
NH2
12.0 11.5 11.0 10.5 10.0 9.5 9.0 8.5 8.0 7.5 7.0 6.5 6.0 5.5 5.0 4.5 4.0 3.5 3.0 2.5 2.0 1.5 1.0 0.5 0.0
ppm

4

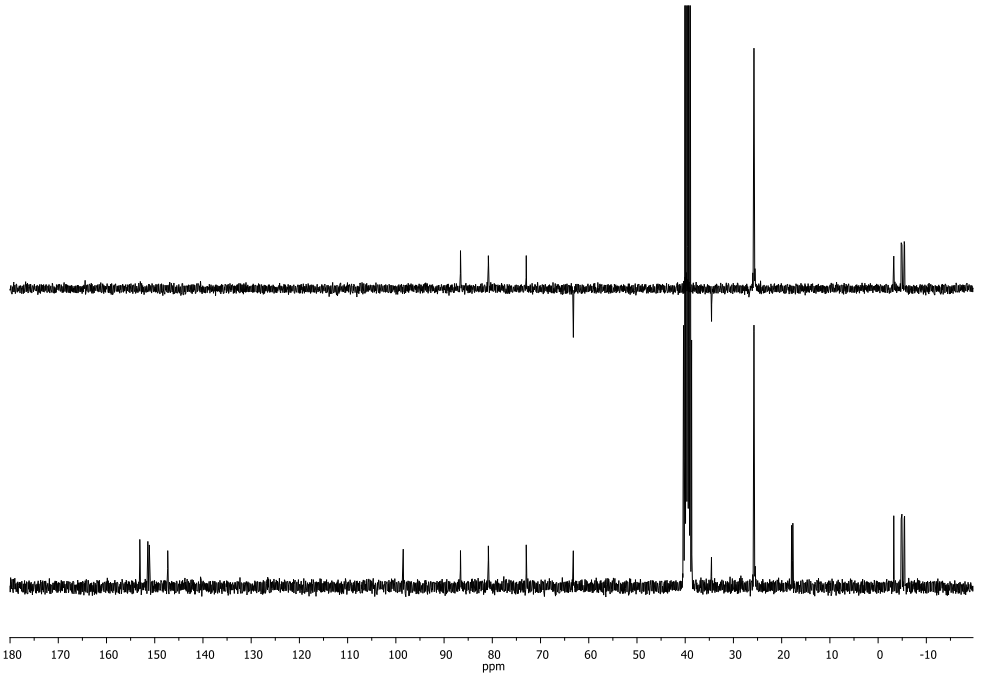
180 170 160 150 140 130 120 110 100 90 80 70 60 50 40 30 20 10 0 -10
ppm

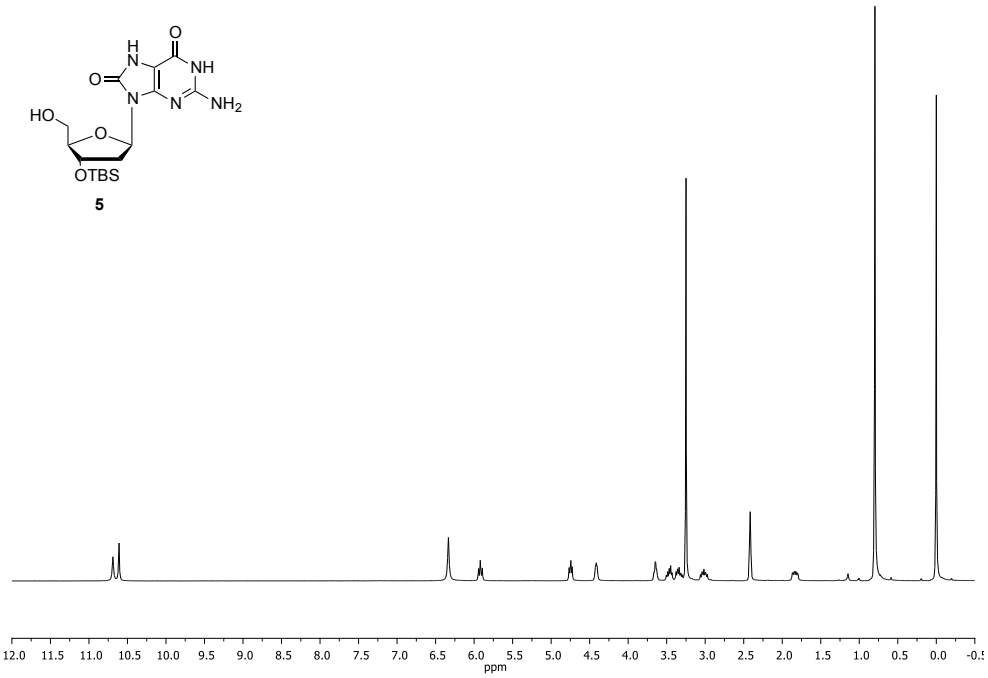
H
N
O
O
NH
N
N
NH2
HO
O
OTBS
5
12.0 11.5 11.0 10.5 10.0 9.5 9.0 8.5 8.0 7.5 7.0 6.5 6.0 5.5 5.0 4.5 4.0 3.5 3.0 2.5 2.0 1.5 1.0 0.5 0.0
ppm

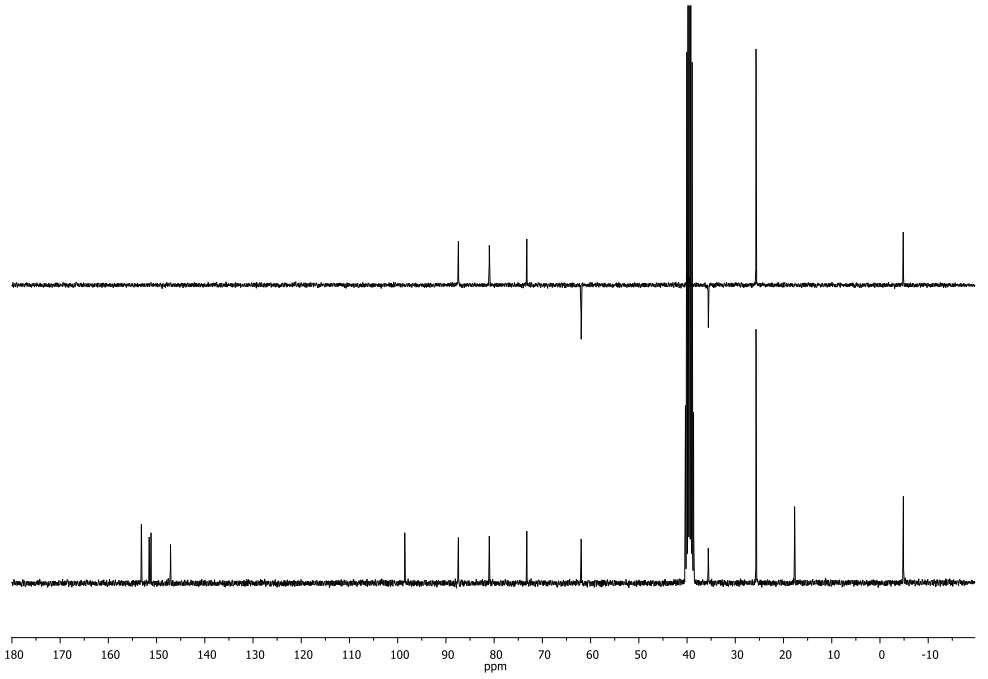
180 170 160 150 140 130 120 110 100 90 80 70 60 50 40 30 20 10 0 -10
ppm

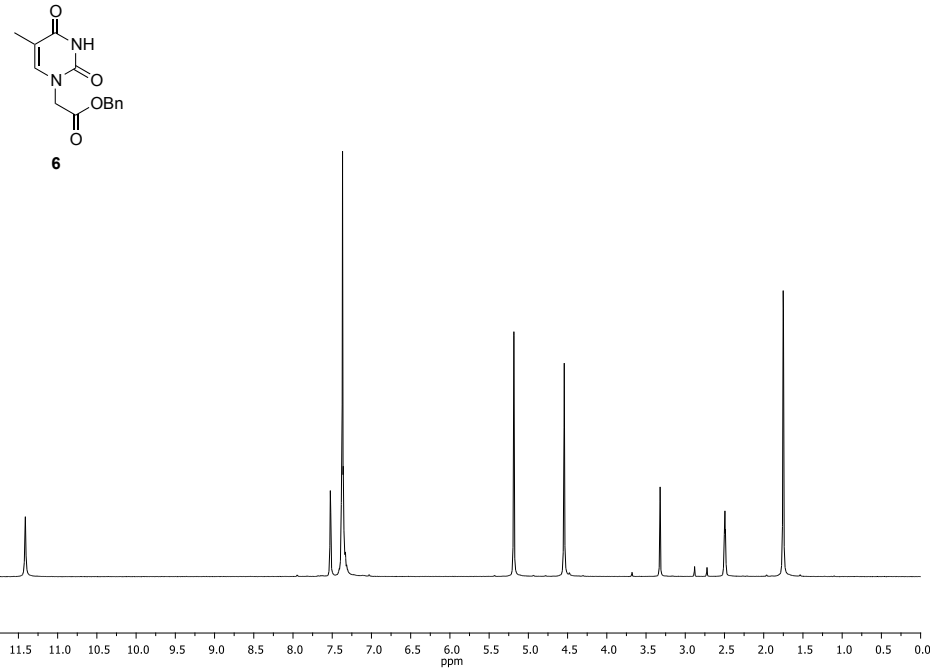
O
NH
N
O
OBn
O
6
12.0 11.5 11.0 10.5 10.0 9.5 9.0 8.5 8.0 7.5 7.0 6.5 6.0 5.5 5.0 4.5 4.0 3.5 3.0 2.5 2.0 1.5 1.0 0.5 0.0
ppm

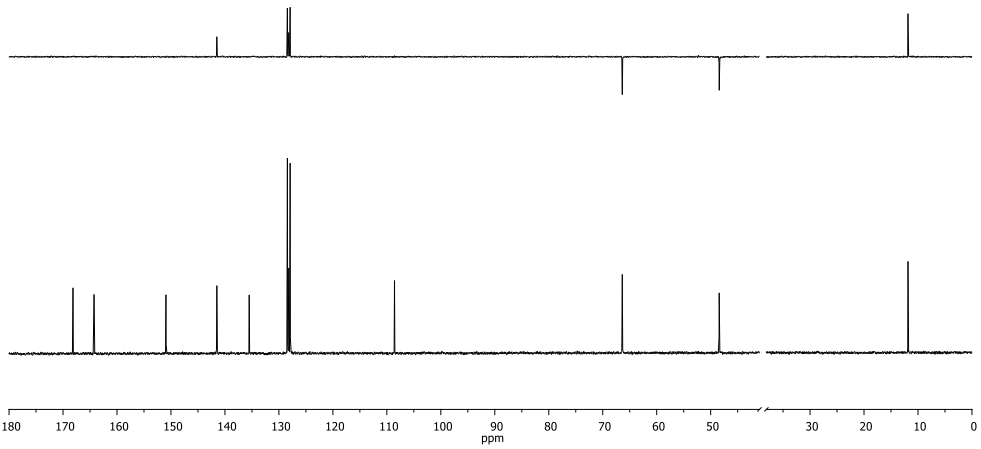
180 170 160 150 140 130 120 110 100 90 80 70 60 50 30 20 10 0
ppm

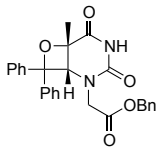
O
O
NH
Ph
N
O
Ph H
OBn
O

7

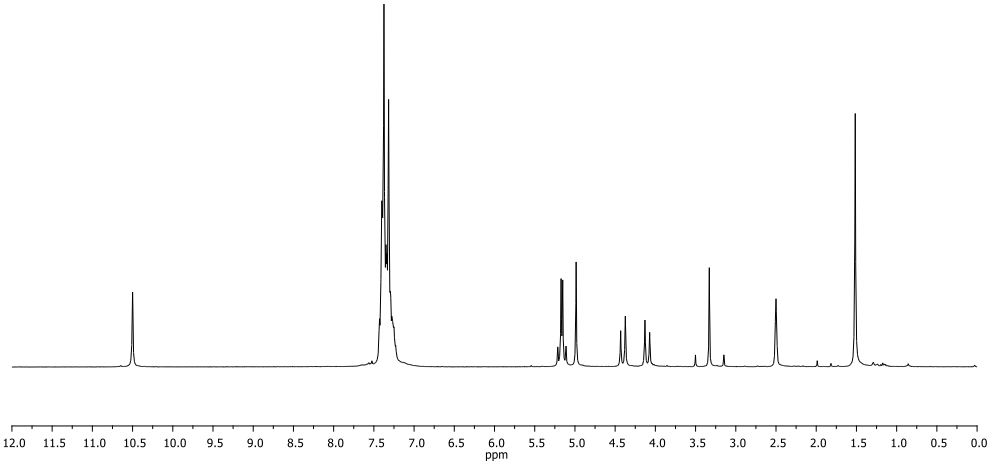
12.0 11.5 11.0 10.5 10.0 9.5 9.0 8.5 8.0 7.5 7.0 6.5 6.0 5.5 5.0 4.5 4.0 3.5 3.0 2.5 2.0 1.5 1.0 0.5 0.0
ppm

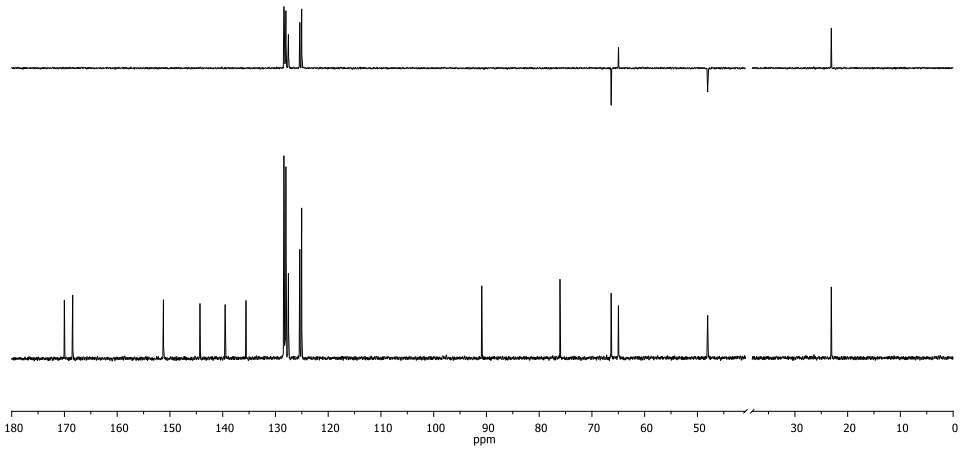
180 170 160 150 140 130 120 110 100 90 80 70 60 50 30 20 10 0
ppm

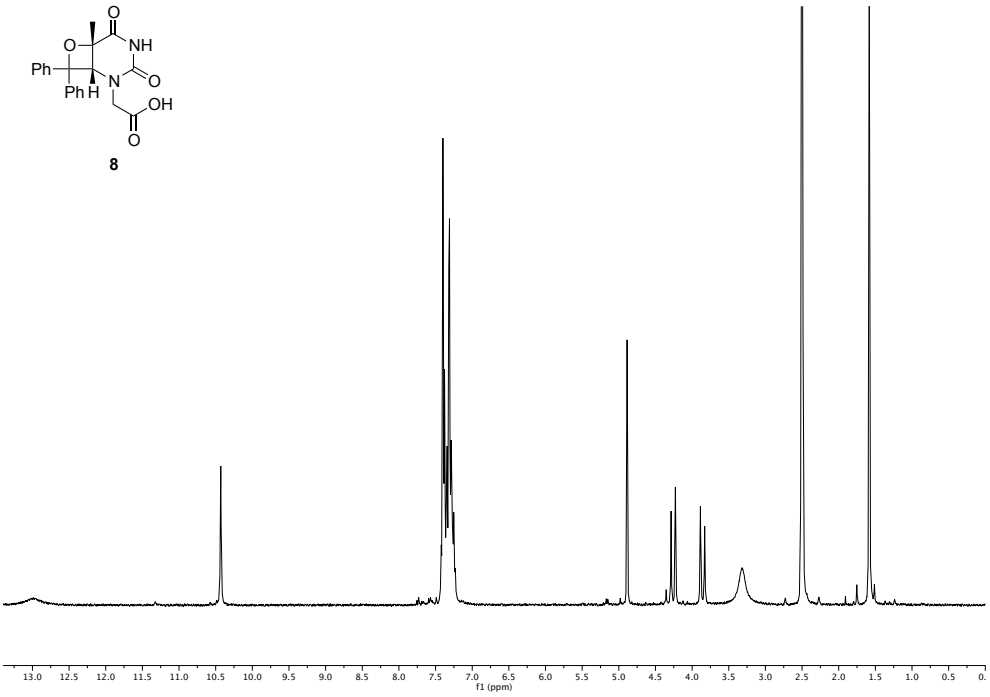
O
NH
O
Ph
N
O
Ph H
OH
O
8
13.0 12.5 12.0 11.5 11.0 10.5 10.0 9.5 9.0 8.5 8.0 7.5 7.0 6.5 6.0 5.5 5.0 4.5 4.0 3.5 3.0 2.5 2.0 1.5 1.0 0.5 0.
f1 (ppm)

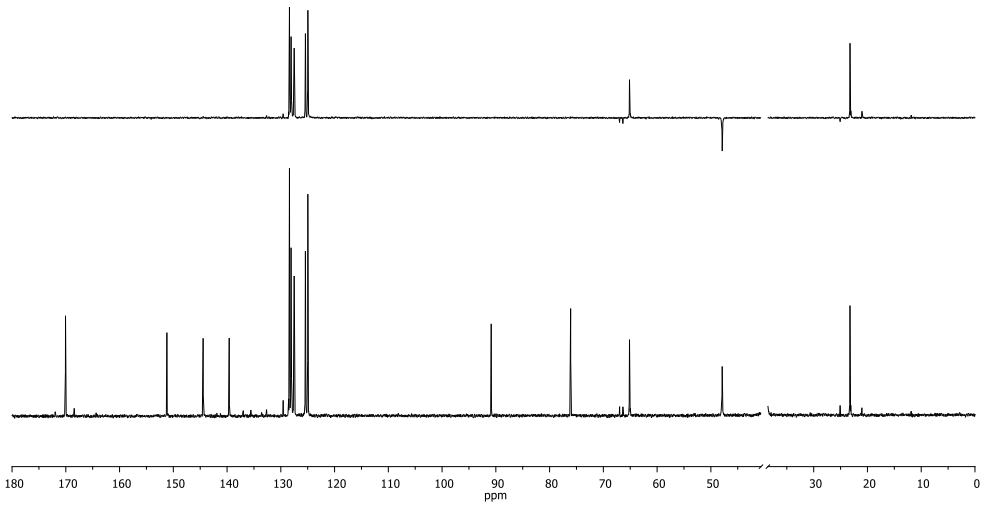
180 170 160 150 140 130 120 110 100 90 80 70 60 50 30 20 10 0
ppm

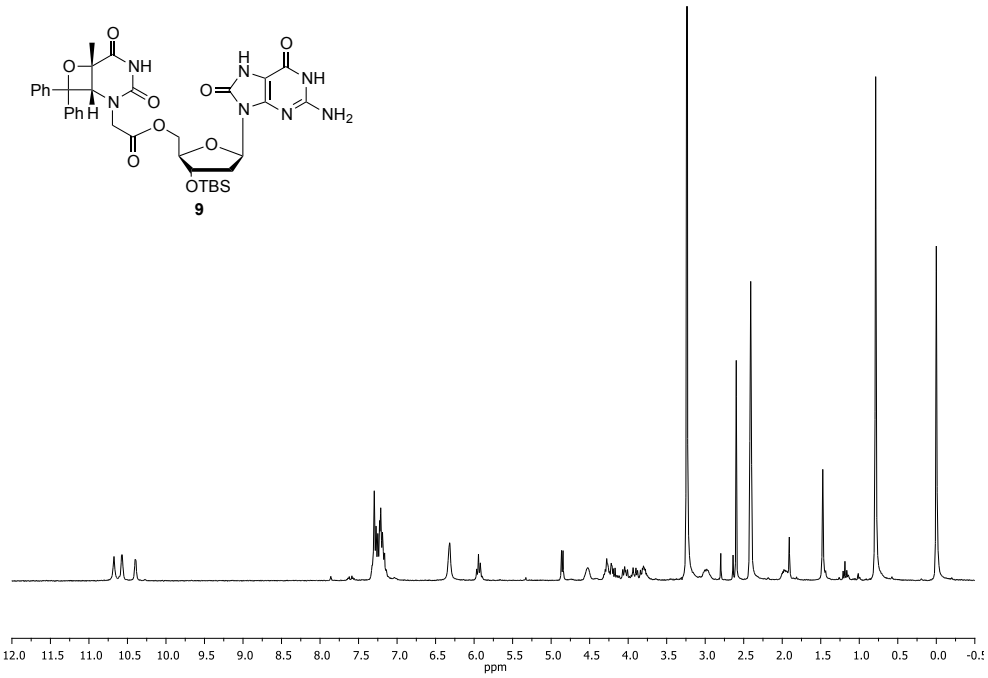
O
NH
Ph
Ph H
N
O
O
O
O
H
N
O
NH
N
N
NH2
O
OTBS
9
12.0 11.5 11.0 10.5 10.0 9.5 9.0 8.5 8.0 7.5 7.0 6.5 6.0 5.5 5.0 4.5 4.0 3.5 3.0 2.5 2.0 1.5 1.0 0.5 0.0
ppm

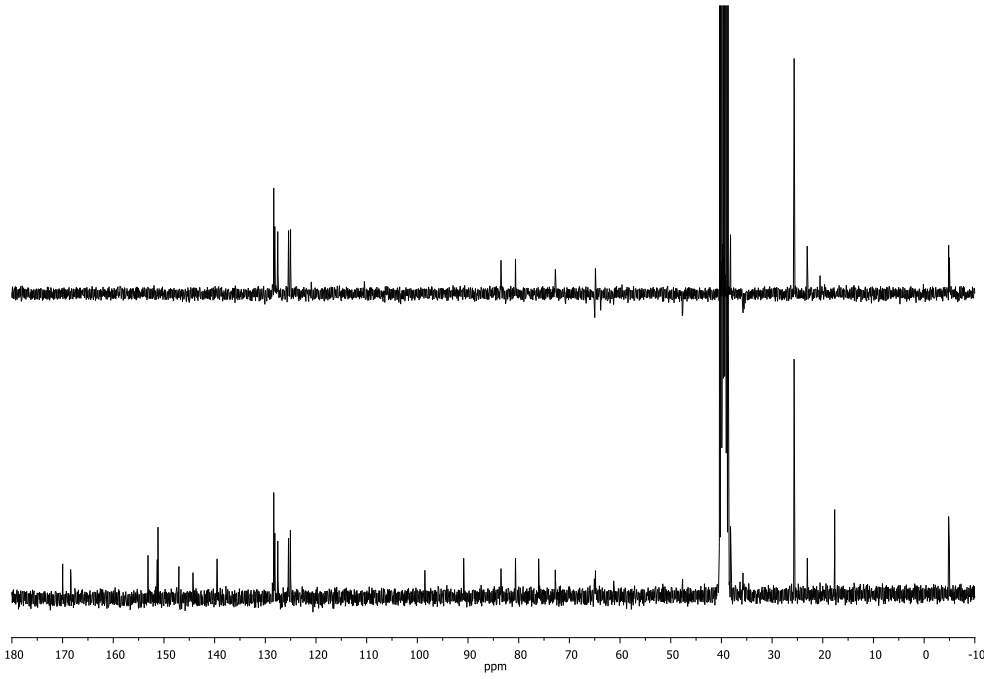
180 170 160 150 140 130 120 110 100 90 80 70 60 50 40 30 20 10 0
ppm


O
NH
Ph
N
O
Ph H
O
O
H
N
O
NH
O
N
N
NH2
O
OH

10

12.0 11.5 11.0 10.5 10.0 9.5 9.0 8.5 8.0 7.5 7.0 6.5 6.0 5.5 5.0 4.5 4.0 3.5 3.0 2.5 2.0 1.5 1.0 0.5 0.0
ppm

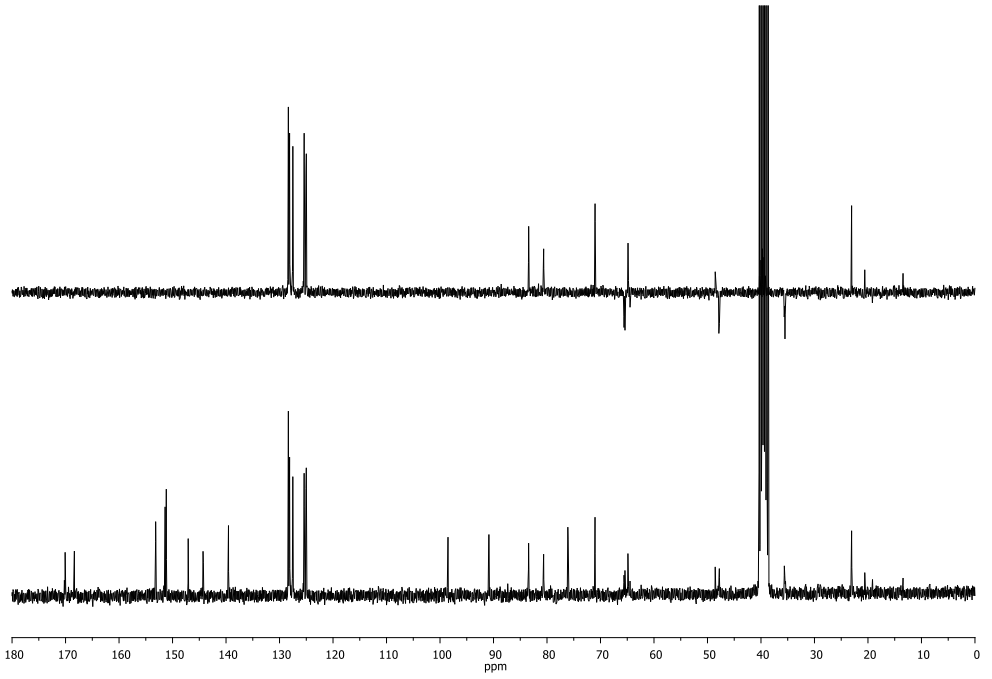
180 170 160 150 140 130 120 110 100 90 80 70 60 50 40 30 20 10 0
ppm

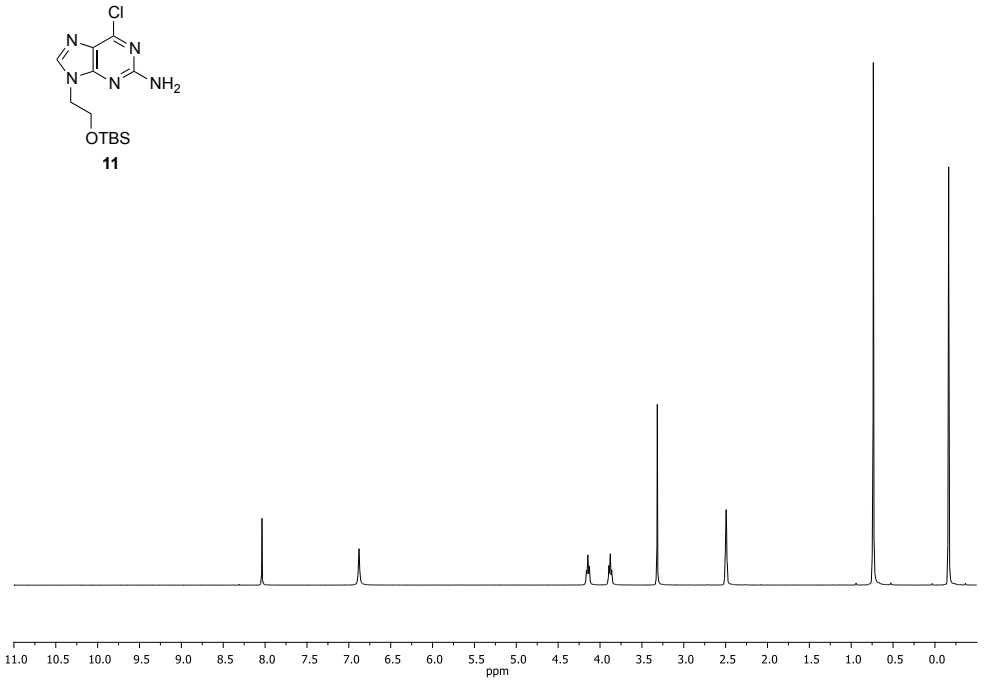
Cl
N
N
N
N
NH2
OTBS
11
11.0 10.5 10.0 9.5 9.0 8.5 8.0 7.5 7.0 6.5 6.0 5.5 5.0 4.5 4.0 3.5 3.0 2.5 2.0 1.5 1.0 0.5 0.0
ppm

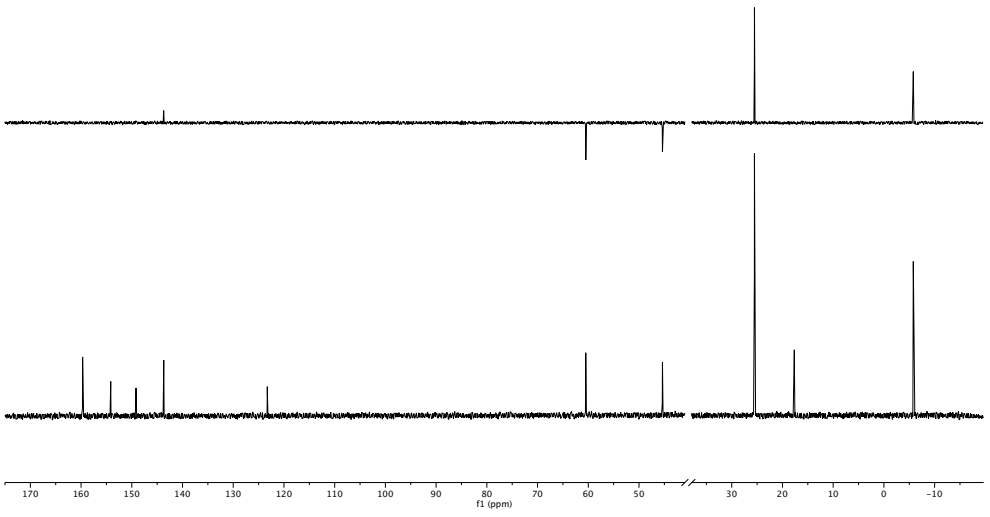
170 160 150 140 130 120 110 100 90 80 70 60 50 30 20 10 0 -10
f1 (ppm)

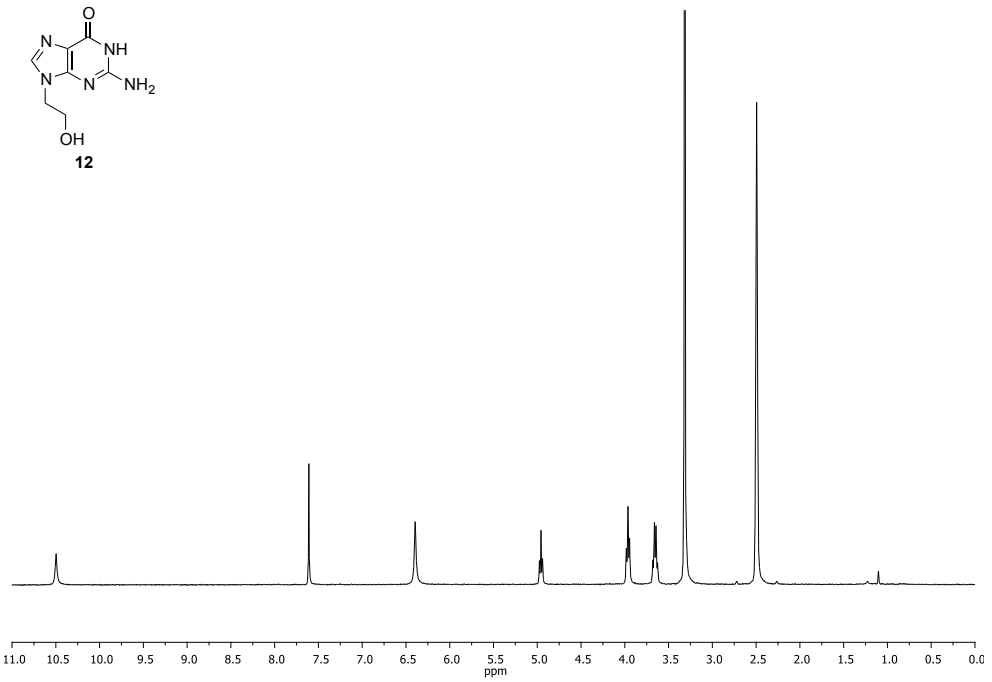
O
N
NH
N
N
NH2
OH
12
11.0 10.5 10.0 9.5 9.0 8.5 8.0 7.5 7.0 6.5 6.0 5.5 5.0 4.5 4.0 3.5 3.0 2.5 2.0 1.5 1.0 0.5 0.0
ppm

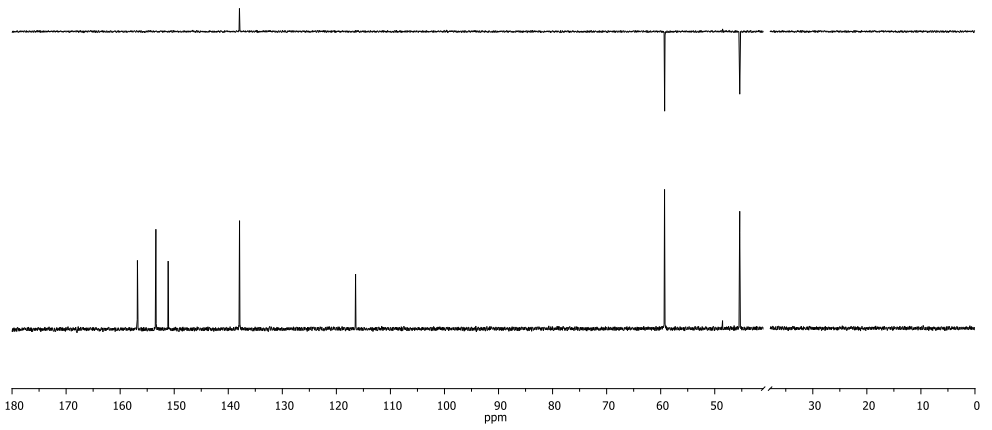
180 170 160 150 140 130 120 110 100 90 80 70 60 50 30 20 10 0
ppm

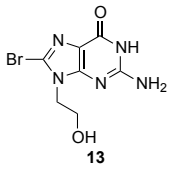
O
N
NH
Br
N
N
NH2
OH

13

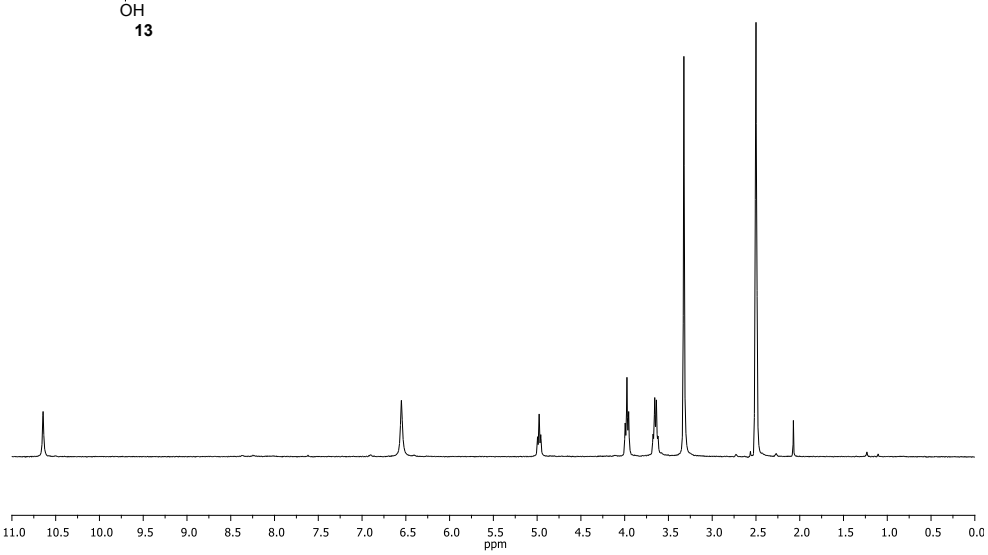
11.0 10.5 10.0 9.5 9.0 8.5 8.0 7.5 7.0 6.5 6.0 5.5 5.0 4.5 4.0 3.5 3.0 2.5 2.0 1.5 1.0 0.5 0.0
ppm

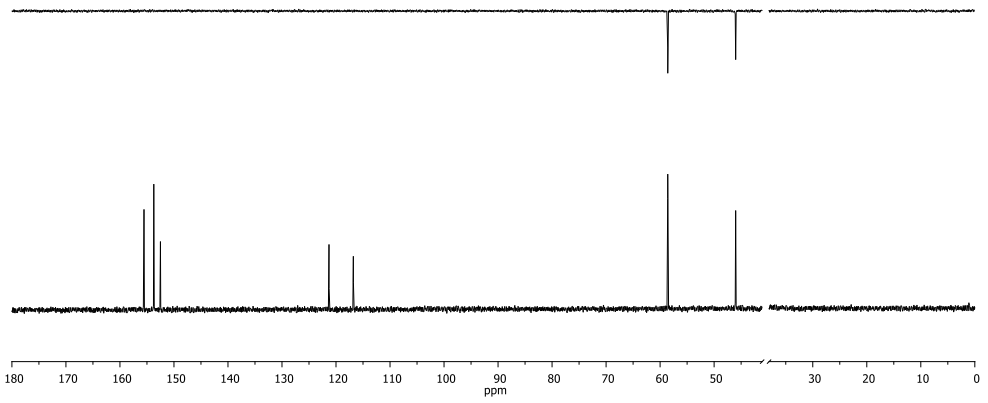
180 170 160 150 140 130 120 110 100 90 80 70 60 50 30 20 10 0
ppm

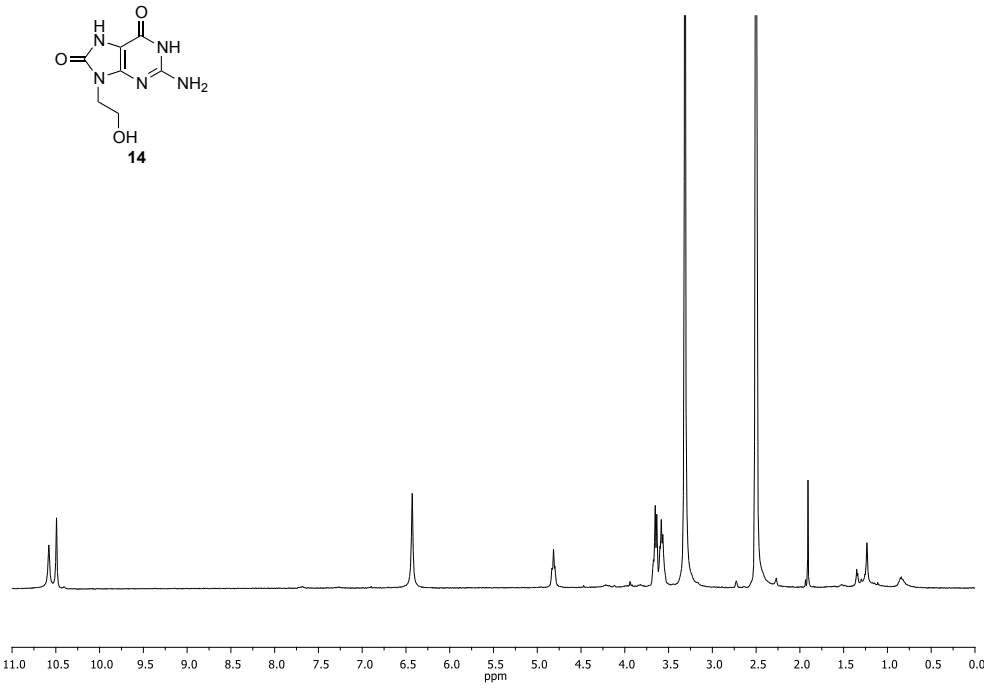
H
N
O
O
NH
N
N
NH2
OH
14
11.0 10.5 10.0 9.5 9.0 8.5 8.0 7.5 7.0 6.5 6.0 5.5 5.0 4.5 4.0 3.5 3.0 2.5 2.0 1.5 1.0 0.5 0.0
ppm

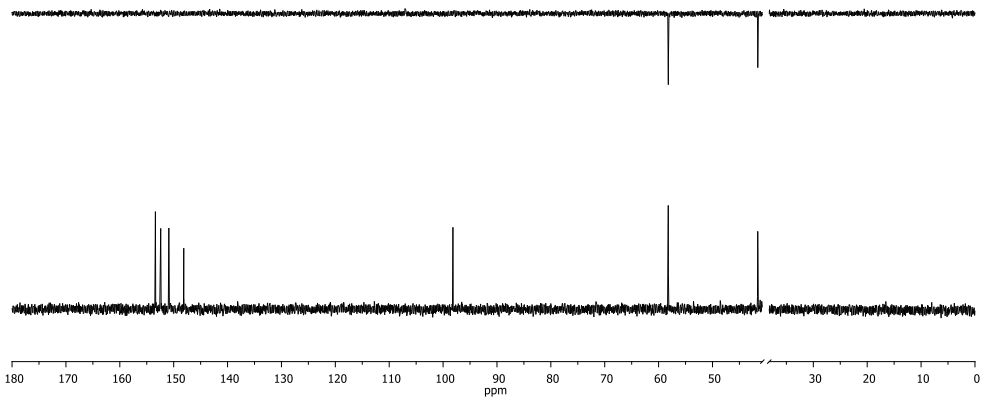
180 170 160 150 140 130 120 110 100 90 80 70 60 50 30 20 10 0
ppm

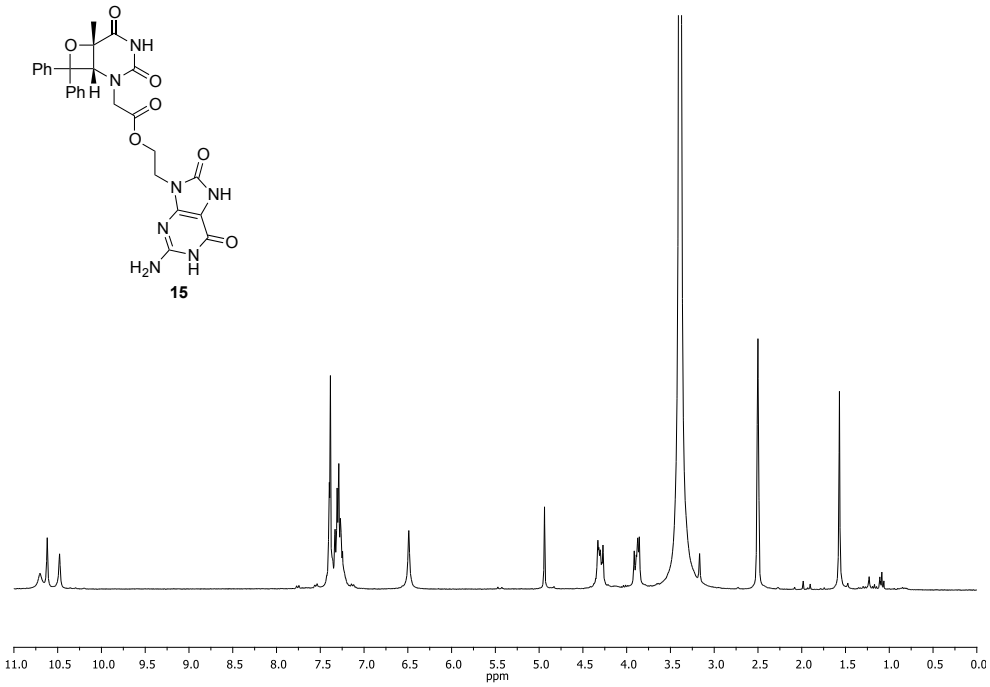
O
NH
O
Ph
N
O
Ph H
O
O
O
N
NH
N
O
H_2N
N
H

15

11.0 10.5 10.0 9.5 9.0 8.5 8.0 7.5 7.0 6.5 6.0 5.5 5.0 4.5 4.0 3.5 3.0 2.5 2.0 1.5 1.0 0.5 0.0
ppm

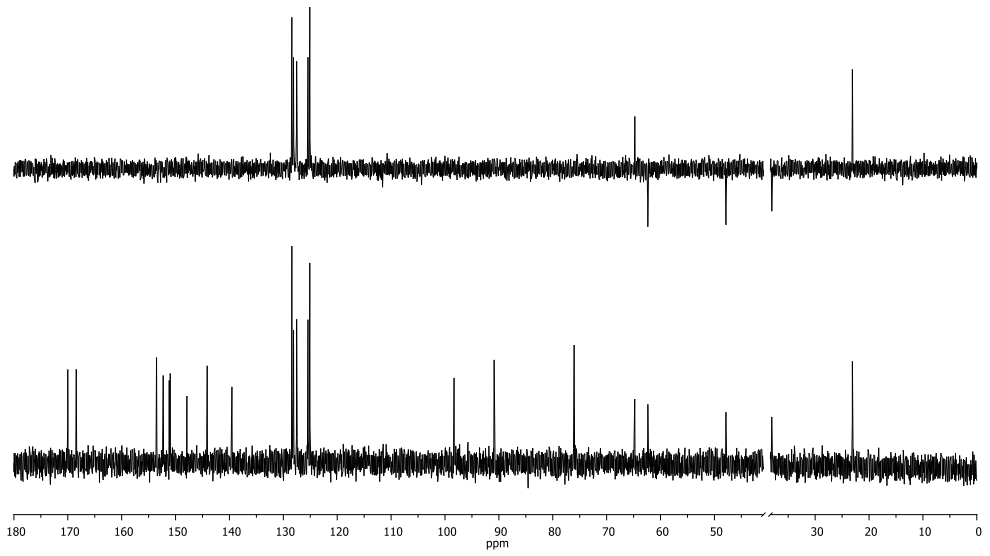
180 170 160 150 140 130 120 110 100 90 80 70 60 50 30 20 10 0
ppm

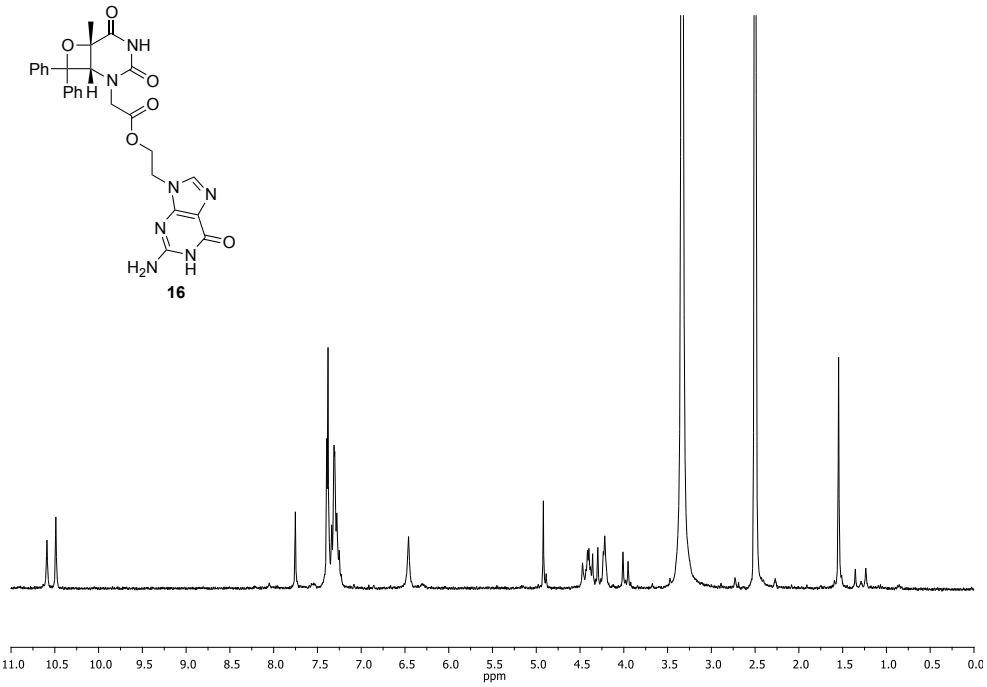
O
NH
O
Ph
N
Ph H
O
O
N
N
N
O
N
H
H_2N
11.0 10.5 10.0 9.5 9.0 8.5 8.0 7.5 7.0 6.5 6.0 5.5 5.0 4.5 4.0 3.5 3.0 2.5 2.0 1.5 1.0 0.5 0.0
ppm

16

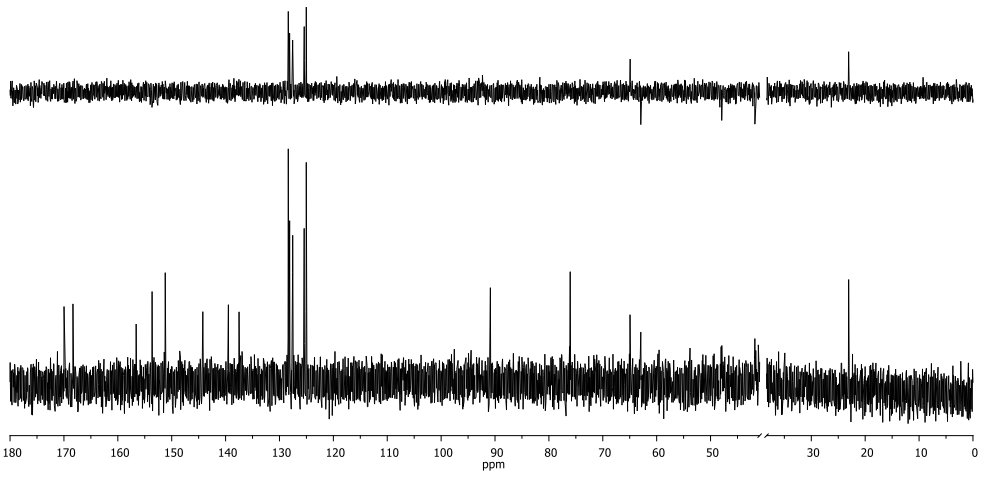
180 170 160 150 140 130 120 110 100 90 80 70 60 50 30 20 10 0
ppm

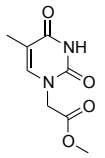
O
NH
N
O
O
O

17

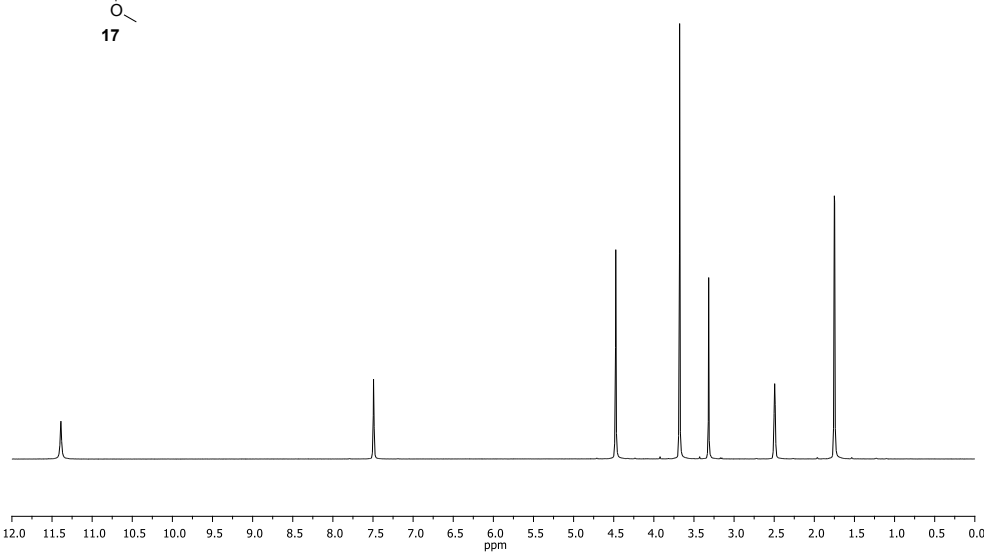
12.0 11.5 11.0 10.5 10.0 9.5 9.0 8.5 8.0 7.5 7.0 6.5 6.0 5.5 5.0 4.5 4.0 3.5 3.0 2.5 2.0 1.5 1.0 0.5 0.0
ppm

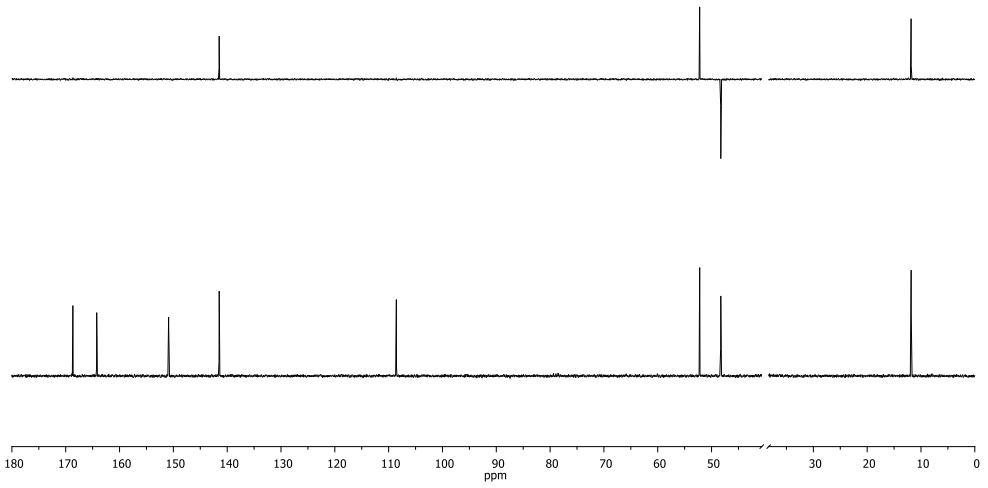
180 170 160 150 140 130 120 110 100 90 80 70 60 50 30 20 10 0
ppm

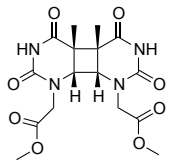
O
O
HN
NH
O
N
H
H
N
O
O
O
O
O

18

12.0 11.5 11.0 10.5 10.0 9.5 9.0 8.5 8.0 7.5 7.0 6.5 6.0 5.5 5.0 4.5 4.0 3.5 3.0 2.5 2.0 1.5 1.0 0.5 0.0
ppm

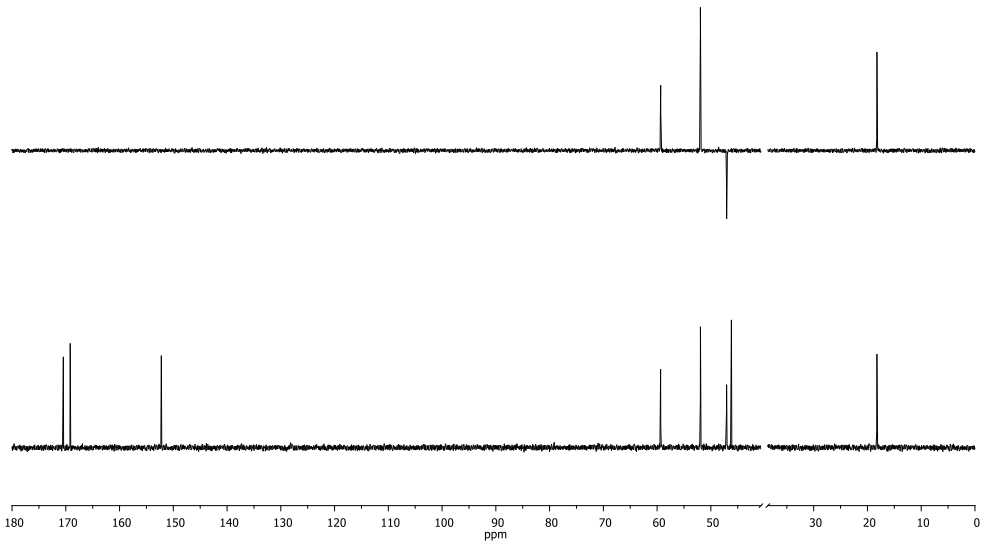
180 170 160 150 140 130 120 110 100 90 80 70 60 50 30 20 10 0
ppm

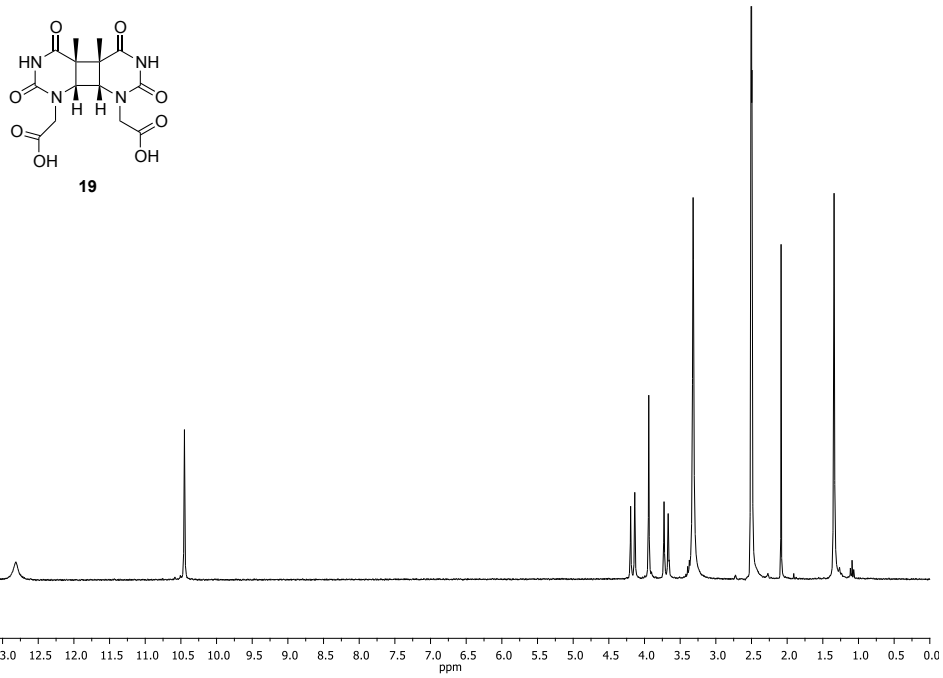
13.5 13.0 12.5 12.0 11.5 11.0 10.5 10.0 9.5 9.0 8.5 8.0 7.5 7.0 6.5 6.0 5.5 5.0 4.5 4.0 3.5 3.0 2.5 2.0 1.5 1.0 0.5 0.0
ppm

19

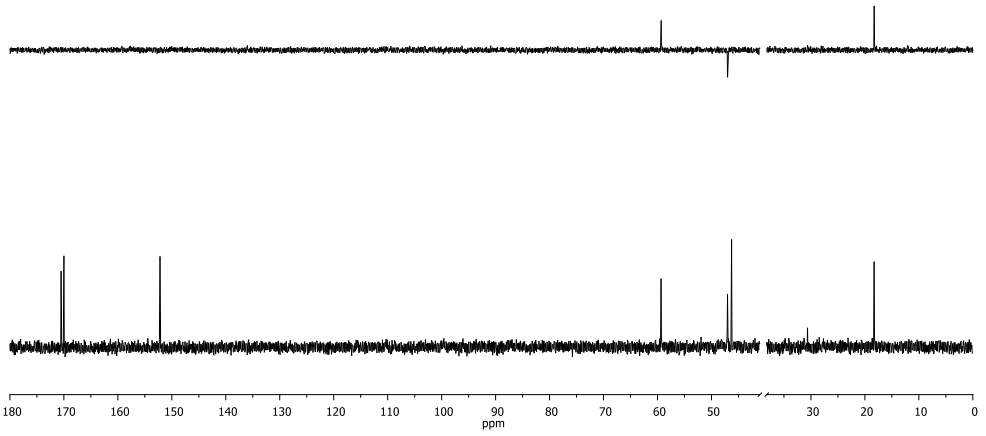
180 170 160 150 140 130 120 110 100 90 80 70 60 50 30 20 10 0
ppm

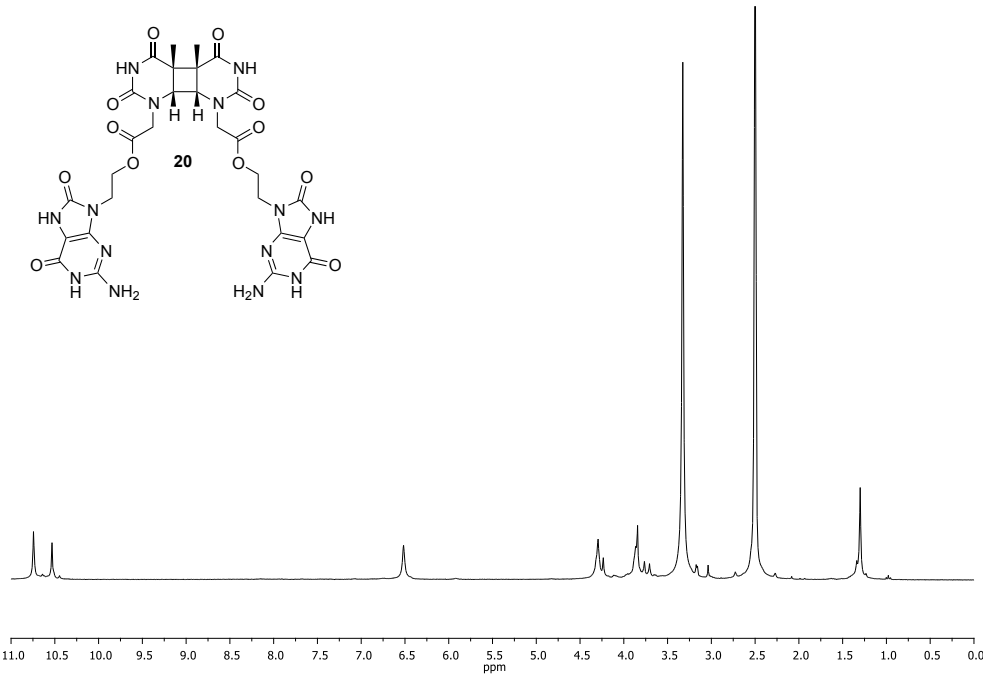
20
11.0 10.5 10.0 9.5 9.0 8.5 8.0 7.5 7.0 6.5 6.0 5.5 5.0 4.5 4.0 3.5 3.0 2.5 2.0 1.5 1.0 0.5 0.0
ppm

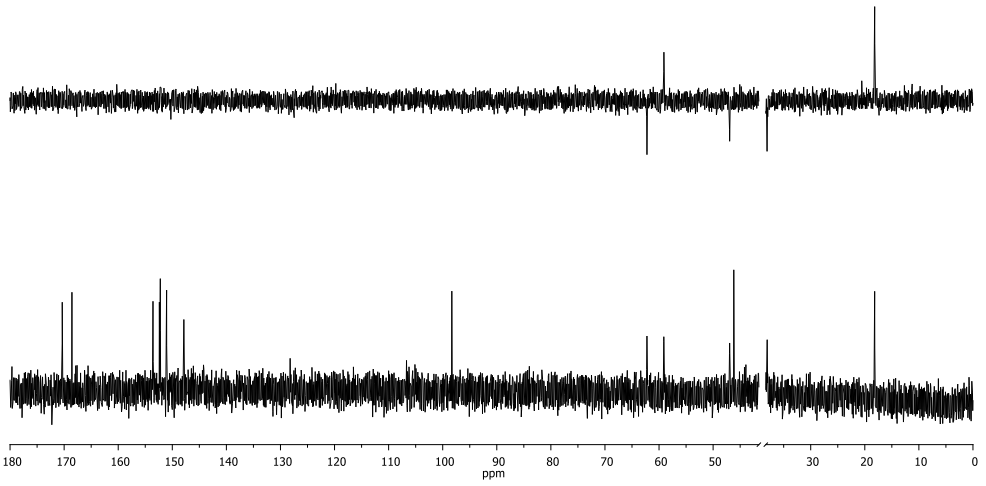
180 170 160 150 140 130 120 110 100 90 80 70 60 50 30 20 10 0
ppm

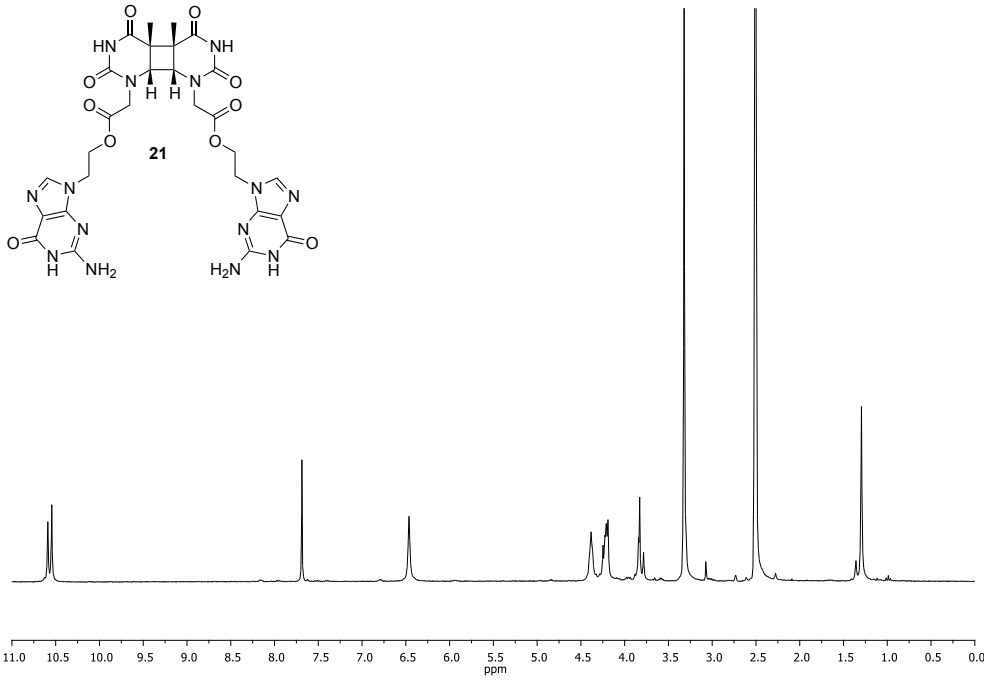
21
11.0 10.5 10.0 9.5 9.0 8.5 8.0 7.5 7.0 6.5 6.0 5.5 5.0 4.5 4.0 3.5 3.0 2.5 2.0 1.5 1.0 0.5 0.0
ppm

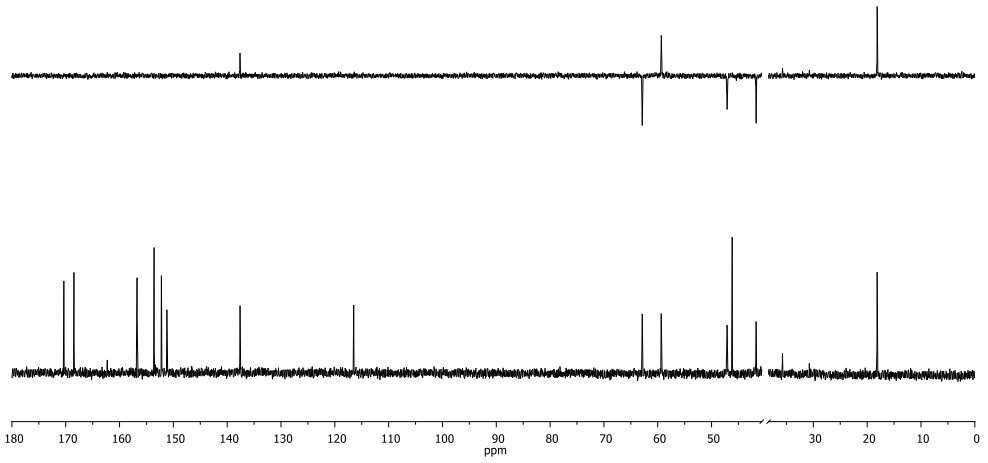
180 170 160 150 140 130 120 110 100 90 80 70 60 50 30 20 10 0
ppm

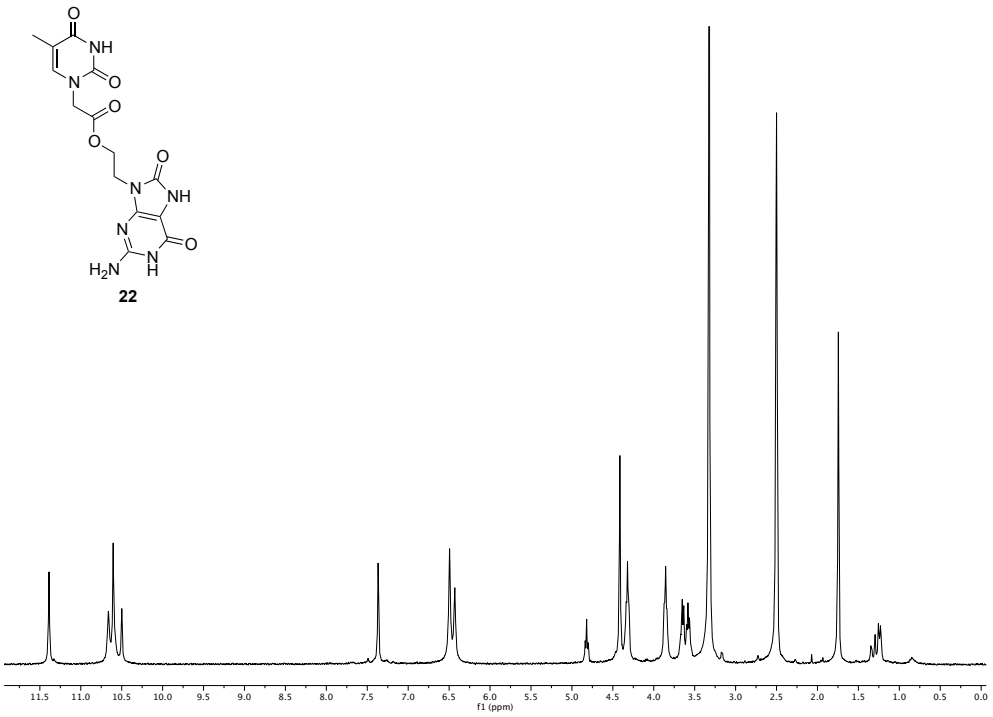
O
NH
N
O
O
O
O
N
NH
N
O
H2N
N
H
11.5
11.0
10.5
10.0
9.5
9.0
8.5
8.0
7.5
7.0
6.5
6.0
5.5
5.0
4.5
4.0
3.5
3.0
2.5
2.0
1.5
1.0
0.5
0.0
f1 (ppm)

22

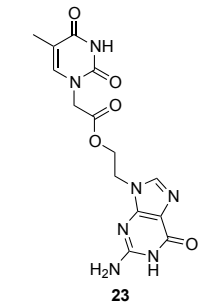

23

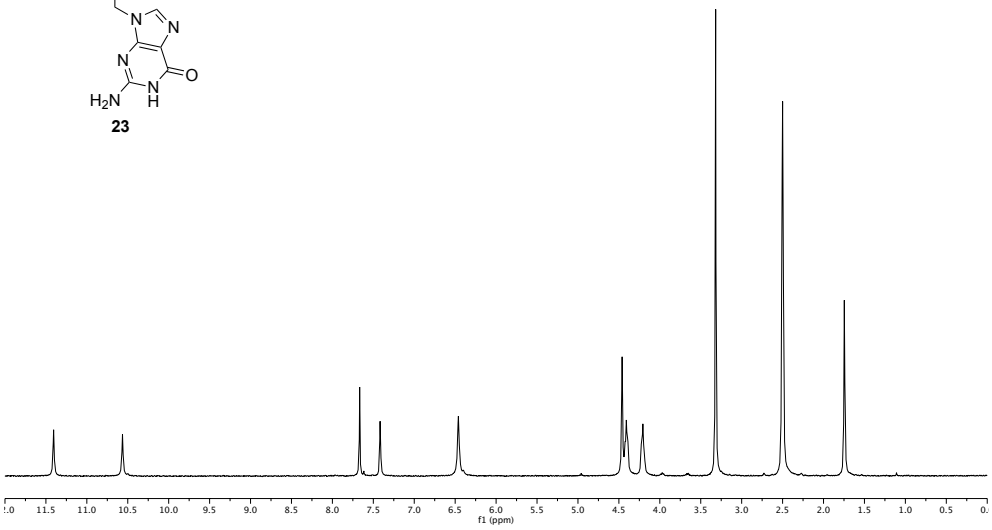

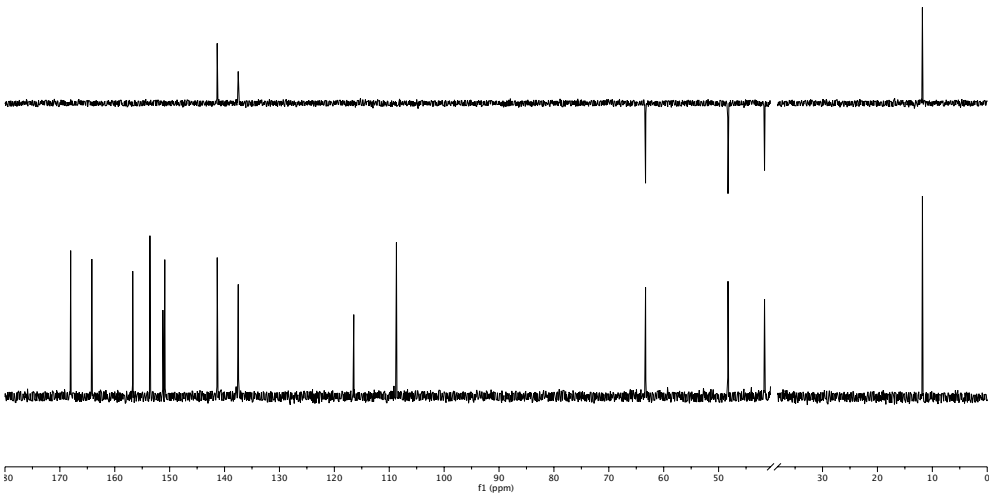

5.5 References

1. Gilbert, W., The RNA world. *Nature* **1986,** *319*, 618.

2. Chen, X.; Li, N.; Ellington, A. D., Ribozyme catalysis of metabolism in the RNA world. *Chem. Biodiversity* **2007,** *4*, 633-655.

3. Chinnapen, D. F.; Sen, D., A deoxyribozyme that harnesses light to repair thymine dimers in DNA. *Proc. Natl. Acad. Sci.* **2004,** *101*, 65-69.

4. Holman, M. R.; Ito, T.; Rokita, S. E., Self-repair of thymine dimer in duplex DNA. *J. Am. Chem. Soc.* **2007,** *129*, 6-7.

5. Steenken, S.; Jovanovic, S. V., How easily oxidizable is DNA? One-electron reduction potentials of adenosine and guanosine radicals in aqueous solution. *J. Am. Chem. Soc.* **1997,** *119*, 617-618.

6. Cannistraro, V. J.; Taylor, J. S., Acceleration of 5-methylcytosine deamination in cyclobutane dimers by G and its implications for UV-induced C-to-T mutation hotspots. *J. Mol. Biol.* **2009,** *392*, 1145-1157.

7. Pan, Z.; Hariharan, M.; Arkin, J. D.; Jalilov, A. S.; McCullagh, M.; Schatz, G. C.; Lewis, F. D., Electron donor-acceptor interactions with flanking purines influence the efficiency of thymine photodimerization. *J. Am. Chem. Soc.* **2011,** *133*, 20793-20798.

8. Pan, Z.; Chen, J.; Schreier, W. J.; Kohler, B.; Lewis, F. D., Thymine dimer photoreversal in purine-containing trinucleotides. *J. Phys. Chem. B* **2012,** *116*, 698-704.

9. Middleton, C. T.; De la Harpe, K.; Su, C.; Law, Y. K.; Crespo-Hernández, C. E.; Kohler, B., DNA excited-state dynamics: from singlet base to the double helix. *Annu. Rev. Phys. Chem.* **2009,** *60*, 217-239.

10. Bucher, B. D.; Kufner, C. L.; Schlueter, A.; Carell, T., UV-induced charge transfer states in DNA promote sequence selective self-repair. *J. Am. Chem. Soc.* **2016,** *138*, 186-190.

11. Nguyen, K. V.; Burrows, C. J., A prebiotic role for 8-oxoguanosine as a flavin mimic in pyrimidine dimer photorepair. *J. Am. Chem. Soc.* **2011,** *133*, 14586-14589.

12. Nguyen, K. V.; Burrows, C. J., Whence flavins? Redox-active ribonucleotides link metabolism and genome repair to the RNA world. *Acc. Chem. Res.* **2012,** *45*, 2151-2159.

13. Saito, I.; Nakamura, T.; Nakatani, K.; Yoshioka, Y.; Yamaguchi, K.; Sugiyama, H., Mapping of the hot spots for DNA damage by one-electron oxidation: efficacy of GG doublets and GGG triplets as a trap in long-range hole migration. *J. Am. Chem. Soc.* **1998,** *120*, 12686-12687.

14. Zhang, Y.; Dood, J.; Beckstead, A.; Li, X. B.; Nguyen, K. V.; Burrows, C. J.; Improta, R.; Kohler, B., Photoinduced electron transfer in DNA: Charge shift dynamics between 8-oxo-guanine anion and adenine. *J. Phys. Chem. B* **2015,** *119*, 7491-7502.

15. Lu, Z.; Beckstead, A.; Kohler, B.; Matsika, S., Excited state relaxation of neutral and basic 8-oxoguanine. *J. Phys. Chem. B* **2015,** *119*, 8293-8301.

16. Tuna, D.; Domcke, W., Excited-state deactivation in 8-oxo-deoxyguanosine: comparison between anionic and neutral forms. *Phys. Chem. Chem. Phys.* **2016,** *18*, 947-956.

17. Wu, X.; Karsili, T. N. V.; Domcke, W., Role of electron-driven proton-transfer processes in the ultrafast deactivation of photoexcited anionic 8-oxoguanine-adenine and 8-oxoguanine-cytosine base pairs. *Molecules* **2017,** *22*, 135-149.

18. Zhang, Y.; Dood, J.; Beckstead, A.; Chen, J.; Li, X. B.; Burrows, C. J.; Lu, Z.; Matsika, S.; Kohler, B., Ultrafast excited-state dynamics and vibrational cooling of 8-oxo-7,8-dihydro-2'-deoxyguanosine in D_2O. *J. Phys. Chem. A* **2013,** *117*, 12851-12857.

19. Zhang, Y.; Dood, J.; Beckstead, A.; Li, X. B.; Nguyen, K. V.; Burrows, C. J.; Improta, R.; Kohler, B., Efficient UV-induced charge separation and recombination in an 8-oxoguanine-containing dinucleotide. *Proc. Natl. Acad. Sci.* **2014,** *111*, 11612-11617.

20. Changenet-Barret, P.; Gustavsson, T.; Improta, R.; Markovitsi, D., Ultrafast excited-state deactivation of 8-hydroxy-2'-deoxyguanosine studied by femtosecond

fluorescence spectroscopy and quantum-chemical calculations. *J. Phys. Chem. A* **2015,** *119*, 6131-6139.

21. Liu, Z.; Tan, C.; Guo, X.; Kao, Y. T.; Li, J.; Wang, L.; Sancar, A.; Zhong, D., Dynamics and mechanism of cyclobutane pyrimidine dimer repair by DNA photolyase. *Proc. Natl. Acad. Sci.* **2011,** *108*, 14831-14836.

22. Kim, S. T.; Hartman, R. F.; Rose, S. D., Solvent dependence of pyrimidine dimer splitting in a covalently linked dimer-indole system. *Photochem. Photobiol.* **1990,** *52*, 789-794.

23. Kim, S. T.; Rose, S. D., Pyrimidine dimer splitting in covalently linked dimer-arylamine systems. *Photochem. Photobiol.* **1992,** *12*, 179-191.

24. Hartzfeld, D. G.; Rose, S. D., Efficient pyrimidine dimer radical anion splitting in low polarity solvents. *J. Am. Chem. Soc.* **1993,** *115*, 850-855.

25. Epple, R.; Wallenborn, E.; Carell, T., Investigation of flavin-containing DNA-repair model compounds. *J. Am. Chem. Soc.* **1997,** *119*, 7440-7451.

26. Butenandt, J.; Epple, R.; Wallenborn, E.; Eker, A. P.; Gramlich, V.; Carell, T., A comparative repair study of thymine- and uracil-photodimers with model compounds and a photolyase repair enzyme. *Chem. Eur. J.* **2000,** *6*, 62-72.

27. Cichon, M. K.; Arnorld, S.; Carell, T., A (6-4) photolyase model: repair of DNA (6-4) lesions requires a reduced and deprotonated flavin. *Angew. Chem. Int. Ed.* **2002,** *41*, 767-770.

28. Song, Q. H.; Tang, W. J.; Hei, X. M.; Wang, H. B.; Guo, Q. W.; Yu, S. Q., Efficient photosensitized splitting of thymine dimer by a covalently linked tryptophan in solvents of high polarity. *Eur. J. Org. Chem.* **2005**, 1097-1106.

29. Song, Q. H.; Wang, H. B.; Tang, W. J.; Guo, Q. W.; Yu, S. Q., Model studies of the (6-4) photoproduct photoreactivation: efficient photosensitized splitting of thymine oxetane units by covalently linked tryptophan in high polarity solvents. *Org. Biomol. Chem.* **2006,** *4*, 291-298.

30. Belmadoui, N.; Encinas, S.; Climent, M. J.; Gil, S.; Miranda, M. A., Intramolecular interactions in the triplet excited states of benzophenone-thymine dyads. *Chem. Eur. J.* **2006,** *12*, 553-561.

31. Tang, W. J.; Guo, Q. X.; Song, Q. H., Origin of solvent dependence of photosensitized splitting of a cyclobutane pyrimidine dimer by a covalently linked chromophore. *J. Phys. Chem. B* **2009,** *113*, 7205-7210.

32. Kao, Y. T.; Song, Q. H.; Saxena, C.; Wang, L.; Zhong, D., Dynamics and mechanism of DNA repair in a biomimetic system: flavin-thymine dimer adduct. *J. Am. Chem. Soc.* **2012,** *134*, 1501-1503.

33. Shafirovich, V.; Cadet, J.; Gasparutto, D.; Dourandin, A.; Huang, W.; Geacintov, N. E., Direct spectroscopic observation of 8-oxo-7,8-dihydro-2'-deoxyguanosine radicals in double-stranded DNA generated by one-electron oxidation at a distance by 2-aminopurine radicals. *J. Phys. Chem. B* **2001,** *105*, 586-592.

34. Joseph, A.; Prakash, G.; Falvey, D. E., Model studies of the (6-4) photoproduct photolyase enzyme: laser flash photolysis experiments confirm radical ion intermediates in the sensitized repair of thymine oxetane adducts. *J. Am. Chem. Soc.* **2000,** *122*, 11219-11225.

35. Guo, X.; Liu, Z.; Song, Q.; Wang, L.; Zhong, D., Dynamics and mechanism of UV-damaged DNA repair in indole-thymine dimer adduct: molecular origin of low repair quantum efficiency. *J. Phys. Chem. B* **2015,** *119*, 3446-3455.

36. Montalti, M.; Credi, A.; Prodi, L.; Gandolfi, T., *Handbook of Photochemistry. 3rd edition. CRC press* **2006**, 601-604.

37. Yeh, S. R.; Falvey, D. E., Model studies of DNA photorepair: radical anion cleavage of thymine dimers probed by nanosecond laser spectroscopy. *J. Am. Chem. Soc.* **1991,** *113*, 8558-8560.

38. Sancar, A., Structure and function of DNA photolyase and cryptochrome blue-light photoreceptors. *Chem. Rev.* **2003,** *103*, 2203-2207.

39. Boussicault, F.; Kruger, O.; Robert, M.; Wille, U., Dissociative electron transfer to and from pyrimidine cyclobutane dimers: An electrochemical study. *Org. Biomol. Chem.* **2004,** *2*, 2742-2750.

40. Boussicault, F.; Robert, M., Electrochemical approach to the repair of oxetanes mimicking DNA (6−4) photoproducts. *J. Phys. Chem. B* **2006,** *110*, 21987-21993.

41. Prakash, G.; Falvey, D. E., Model studies of the (6-4) photoproduct DNA photolyase: synthesis and photosensitized splitting of a thymine-5,6-oxetane. *J. Am. Chem. Soc.* **1995,** *117*, 11375-11376.

Chapter 6:
8-oxoGuanine as a Potential Intrinsic Photosensitizer for the Repair of T(6-4)C Photoproduct

6.1 Introduction

The previous chapters have focused on models to mimic the PET step involved in the photolyase repair mechanism. As a step further, it would be interesting to study how these models influence the structure of the DNA double stranded helix and how they can be repaired in short DNA strands by electron transfer.

In principle, an excited-state chromophore can inject a charge into DNA through oxidation or reduction of a proximal nucleobase to yield a radical cation or anion that may migrate in processes described as hole transfer (HT) or excess electron transfer (EET), respectively.[1] As mentioned in Chapter 1, the oxidative process is relevant in the formation of DNA damage[2]; however, EET into DNA is also an important process as it is associated with repair of UV lesions.[3] There are three mechanisms proposed for photoinduced electron transfer into DNA according to the energetic levels of donor-bridge-acceptor system: (i) the molecular wire, (ii) the superexchange mechanism and (iii) the hopping model. In all cases, a photoexcited donor with a suitable energetic level is used in order to initiate the charge transfer.[1, 4] Figure 6.1 shows that the energetic levels of the bridge in relation to those of the donor and acceptor determine the mechanism. In case of a molecular wire, the bridge states are energetically comparable to the level of the donor, and the electron can be injected into the bridge and moves incoherently to the acceptor. By contrast, in the superexchange mechanism, the brigde states are lying above those of the donor, the electron is transferred in one coherent jump and is never localized within the bridge. As a consequence, it can be expected that the electron transfer rate is distance-dependent. Finally, if the bridge state is energetically comparable to that of the photoexcited donor, an electron transport via hopping could occur as an alternative mechanism to the molecular wire. By contrast, the electron is not delocalized within the bridge during the electron hopping, which consists in a multistep process of charge, injection, charge transport and charge trapping.[1]

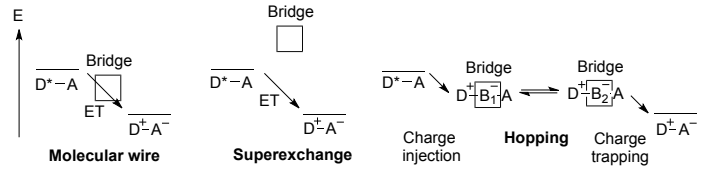

Figure 6.1. Comparison of basic mechanisms of electron transfer and transport: molecular wire, superexchange and hopping mechanism. (D: donor, A: acceptor, bridge: DNA bases, ET: electron transfer).

Excess of electron through DNA duplex has been intensively investigated.[1, 5-8] A hopping mechanism was proposed for the DNA-mediated transport over long distances involving all base pairs (T-A and C-G) and the pyrimidine radical anions $C^{\bullet-}$ and $T^{\bullet-}$ as intermediate electron carriers.[9] This theory was based on the relative reducibility of DNA bases, T (E_{red} = -2.18 V vs. NHE) > C > A > G (E_{red} = -2.76 V vs. NHE)[10], being pyrimidine bases T and C more easily reduced than the purine bases.

Therefore, for charge injection, compounds with suitable oxidation potential in the singlet excited state have been used as photoexcitable electron donors in DNA. In this context, flavin[11] (E_{ox}^{D*} = -2.8 V vs. NHE), naphthalene diamine[6] (E_{ox}^{D*} = -2.6 V vs. NHE), stilbene diether[12] (E_{ox}^{D*} = -2.3 V vs. NHE), phenothiazine[13] (E_{ox}^{D*} = -2.0 V vs. NHE), pyrene[5] (E_{ox}^{D*} = -1.8 V vs. NHE) have been covalently attached to oligonucleotides, and the electron transport has been monitored using acceptors, i.e. chemical trapping probes of electron. Pyrimidine bases have similar reduction potentials as the electron donors, thus, none can serve as an electron traps. However cyclobutane thymine dimers[14-17], thymine derived-oxetane[18-19], halouracils[6, 20], thymine glycol[21] or nitrobenzene[5] have been employed in this role to investigate electron transport along the DNA helix. All these compounds suffer an irreversible chemical change informing that they have received an extra electron. The thymine dimer and oxetane undergo cycloreversion, the halouracils release halide ions and thymine glycol looses the hydroxyl groups. This way, it is possible to measure and compare electron transfer effi-

ciencies by HPLC analysis, electrophoresis, fluorescence quenching or laser flash photolysis.

Among the donor-DNA-acceptor systems mentioned above, the flavin-DNA-cyclobutane thymine dimer or oxetane systems are of particular interest as they mimic the DNA repair process by photolyase. They have been used to elucidate the distance and sequence dependence of DNA-mediated electron transfer efficiency.[16, 19] In these systems, the dimer (or oxetane) and flavin were separated by A-T bridges and photoirradiation of the reduced and deprotonated flavin ($FADH^-$) causes the injection of the excess electron to the nearby thymine, after the hopping process through DNA using pyrimidines as stepping stones, the electron is trapped by the dimer (or oxetane). This causes cycloreversion, which was evidenced by HPLC analysis. Interestingly, in theses systems no by-products were detected, which supported the idea that DNA is more stable towards reduction than towards oxidation processes.

In this context, we propose to investigate the EET into DNA containing the azetidine model (**AZT**, Figure 6.2), described in the previous chapters, as electron trap. As mentioned in Chapter 3, spectroscopic and photochemical studies showed that injection of an electron into this heterocycle is able to induce the photocycloreversion process leading to the formation of the initial pyrimidines.[22]

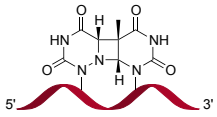

Figure 6.2. Structure of **AZT** inserted into an oligonucleotide.

Regarding to the electron donors studied throughout this Thesis, we selected 8-oxoGuanine (OG) as the best candidate since it (i) has a good oxidation potential in the singlet excited state (E_{ox}^{D*} = -3.3 V vs. NHE), (ii) has a red-shifted absorption spectrum in a spectral window that does not produce direct photoreversal of **AZT**, (iii)

OG phosphoramidite is commercially available what eases the oligonucleotide synthesis and (iv) this compound is not expected to perturb significantly the B-DNA duplex conformation, which is essential for the electron migration process.[23] Altogether, these data show that OG-AZT (electron donor-trap) system embedded in DNA might be of interest to study the repair process.

Regarding to DNA photolyases, DNA-binding and -repair studies have been achieved with modified cyclobutane thymine dimers and (6-4) lesions in order to gain deeper understanding of the lesion recognition and repair steps. In the case of the cyclobutane dimers, the phosphodiester group linking 3' and 5' sugars was replaced with isosteric formacetal to confirm that the central phosphate is not required for the recognition by CPD photolyases.[24] For 6-4PP, binding studies where the C2 carbonyl group of the 3'-pyrimidone was replaced with an iminium cation showed that, despite an efficient binding, (6-4) photolyase was not able to achieve the repair to the original bases.[25] Interestingly, a thiethane four-membered ring, formed between thymidine and 4-thiothymidine inserted in an oligonucleotide, was also used as substrate for the (6-4) photolyase reaction; however; the binding to the enzyme was not efficient, avoiding the repair to take place.[26] In spite of their potential importance during the repair of 6-4PPs at TC sequences, the repair of azetidine by photolyases has not been reported until now. With this background, it would be interesting to explore this enzymatic photoreaction using our azetidine **AZT**, which also is an aza analog of CPD, as substrate for the CPD and (6-4) photolyases.

6.2 Results and discussion

6.2.1 Synthesis of AZT

Up to now, no report exists on the incorporation of an azetidine moiety in an oligonucleotide. Thus, the first step of this study consisted in developing a method for the synthesis of our azetidine-derived oligomer (**AZT**). As previously described in

Chapter 3, this ring can be obtained through a photosensitized [2+2] photocycloaddition between 6-azauracil and thymine. However, synthesis of the desired building block and its subsequent incorporation in the oligomer by means of the typical solid-state phosphoramidite method was not straightforward because of the instability of the heterocycle during the 12-steps required in the synthesis. Therefore, we settled on generating photochemically **AZT** *in situ* using tailor-made oligonucleotides, which include a 6-azauracil, as a simple and convenient method. It was performed during my second stay in the Cynthia Burrow's group at the University of Utah.

Firstly, oligonucleotides containing 6-azauracil were synthesized on a DNA synthesizer by phosphoramidite method, linking nucleotides one by one in the 3'→5' direction, and using a repeated four-step cycle of detritylation, coupling, capping and oxidation for each A, C, T or G addition. Properly-protected nucleoside 3'-phosphoramidites were used as building blocks for chain elongation. The 6-azauracil nucleotide was incorporated at a specific site of oligonucleotide by means of its phosphoramidite building block, which is commercially available from Berry (Figure 6.3). By contrast with U or T, this phosphoramidite includes *o*-anisoyl protecting group at N3 to avoid its deprotonation at neutral pH.[27]

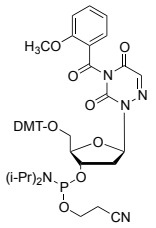

Figure 6.3. Structure of commercial 6-azauracil phosphoramidite building block.

The oligonucleotide synthesis is depicted in Scheme 6.1. At the beginning, the first protected nucleoside is pre-attached to the resin. Then, the 5'-dimethoxytrityl (DMT) protecting group is removed and the free 5'-OH attacks the phosphorus of the incoming second nucleoside, displacing its diisopropylamino group. In step 3,

unreacted 5'-OH is acetylated, preventing elongation of sequences with deletion mutations, i.e. lacking of the second nucleobase. After that, the unstable phosphite triester is converted to a stable phosphate triester; and the next cycle is run until the desired sequence is completed. Once the last nucleotide is attached, removing of the many protecting groups that are still attached, such as DMT of 5'-OH, cyanoethyl phosphate or specific protecting groups of exocyclic primary amino groups of A, C, G and 6-azauracil is achieved, and, the oligonucleotides are cleaved from the solid support and are ready for purification by reverse-phase HPLC.

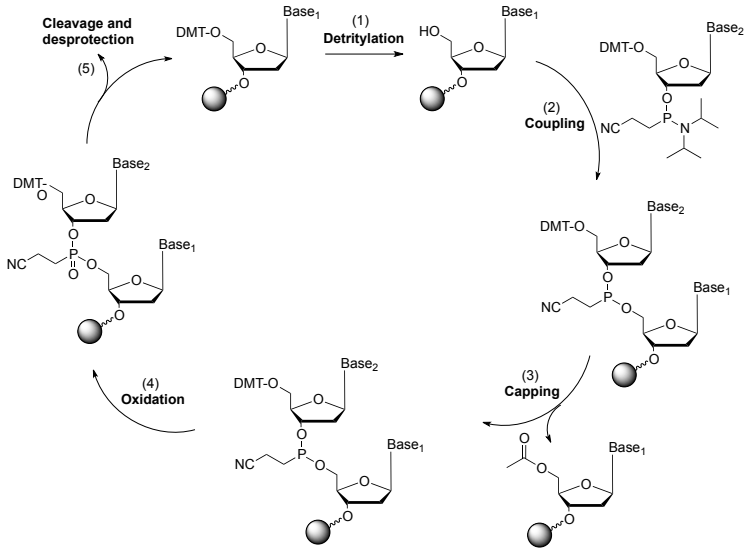

Scheme 6.1. The phosphoramidite oligonucleotide synthesis cycle: (1) trichloroacetic acid, CH_2Cl_2, 50s; (2) tetrazole, MeCN, 30s; (3) Ac_2O/pyridine/THF, N-methylimidazole, MeCN, 30s; (4) I_2, H_2O/pyridine/THF, 45s; (5) NH_4OH (cc), 55 ºC, 5h.

We planned to synthetize four oligonucleotides, two short (6-mer) and two long (18-mer), containing the 6-azauracil nucleotide at the 5'-side or 3'-side of a thymine nucleobase (Scheme 6.2). Moreover, the selected sequences only contain a dipyrimi-

dine site to ensure that, the photosensitized [2+2] cycloaddition which allows formation of **AZT**, takes place exclusively at the desired **U***-T site, and does not produce CPD at another position. Unfortunately, synthesis of 6-mer strands was not efficient enough and, thus, the purification step was too tedious to get the concentration needed for the following experiments. By contrast, 18-mers were pure enough to be used without further purification.

AF1 5'-CACAGCA**U***TACAGTACAC-3'

AF2 5'-CACAGCAT**U***ACAGTACAC-3'

AF3 5'-CA**U***TAC-3'

AF4 5'-CAT**U***AC-3'

Scheme 6.2. Sequences of synthetized oligonucleotides.

Secondly, the **AZT** was obtained through photosensitized [2+2] cycloaddition between 6-azauracil and thymine, as described in Chapter 3, using the oligonucleotides **AF1** and **AF2** (Scheme 6.3 for **AF1**).

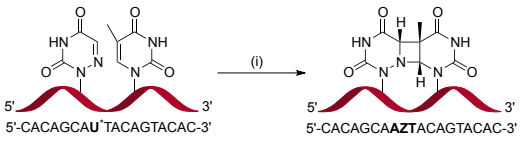

Scheme 6.3. Synthetic strategy to prepare **AF1-AZT**: (i) acetophenone, λ > 300, N_2, 0 ºC, 2h.

This approach has been successfully employed to prepare site-specific *cis-syn* T<>T in oligonucleotides.[28] However, acetone has been reported to produce side-products[29], and it has a low boiling point and can evaporate during the purging step. To circumvent these drawbacks, acetophenone was chosen as triplet photosensitizer (b.p. 202 ºC). Thus, a deaerated solution containing **AF1** (or **AF2)** and acetophenone

was irradiated at λ > 300 nm in an ice bath. The progress of the reaction was followed by reverse phase HPLC monitoring the increase of new peaks, the main peak might be the *cis-syn* isomer and the other one, the *trans-syn* counterpart as reported for cyclobutane thymine dimer (Figure 6.4, left).[28, 30] Once purified by reversed phase HPLC, formation of azetidine was confirmed by direct irradiation at 254 nm of **AZT-AF1** that, as shown in Figure 6.4 right, regenerates the initial **AF1** oligonucleotide.

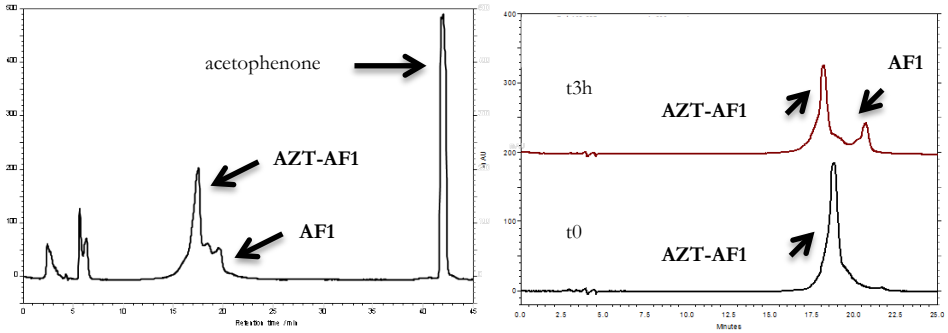

Figure 6.4. HPLC analysis of the acetophenone-photosensitized formation of **AZT-AF1** at λ > 300 nm for 2h (left) and its photocycloreversion irradiating at λ = 254 nm for 3h to regenerate **AF1** (right).

6.2.2 Photorepair of AZT by OG

As mentioned previously, OG was selected as the intrinsic reducing agent to inject, after excitation, an electron into DNA until reaching **AZT**, which will act as electron trap. The easiest way to study this process is by inserting the electron donor and acceptor in the same strand. However, the presence of OG in **AF1** or **AF2** might interfere during the *in situ* generation of **AZT**. This way, the dependence of the repair process can be investigated on base pair stability and directional effect sequence by changing the location of the base pair of OG at 5' or 3'-side to **AZT**. Thus, the oxidized guanine was introduced in the complementary strand at different sites (Scheme 6.4) ie. at 5´ (**AF5**) or 3´-side (**AF6**) or opposite (**AF7** and **AF8**) to **AZT**. These

strands were obtained by the phosphoramidite method using the commercial available phosphoramidite building block of OG. Moreover, the two strands of the designed duplexes were of different length in order to improve their separation during the HPLC analysis: **AF1/AF2** are 18-mers whereas **AF5-AF8** are 22-mers.

AZT-AF1(AF2)	5'-CACAGCA**AZT**ACAGTACAC-3'	18 mer
AF5	3'-TCTGTGTCG**O**AATGTCATGTGT-5'	22 mer
AF6	3'-TCTGTGTCGTAA**O**GTCATGTGT-5'	22 mer
AF7	3'-TCTGTGTCGTA**O**TGTCATGTGT-5'	22 mer
AF8	3'-TCTGTGTCGT**O**ATGTCATGTGT-5'	22 mer

Scheme 6.4. Sequences of the selected duplexes **AZT-AF1(AF2) / AF5-AF8**

In **AF5** and **AF6**, OG can form stable base pairs with A causing very little change in stability or structure of DNA duplex, which is essential to favor the excess electron transfer process, whereas for **AF7** and **AF8**, OG might form an unstable base pair with U* or T.[23] Regarding to the directional effect, it might be investigated the rate of repair when the base pair of OG is located immediately 5' (**AF5** and **AF8**) or 3' (**AF6** and **AF7**) to the **AZT**. Interestingly, it was reported high rate repair of T<>T by OG in the 5'→3' direction.[31] This fact was explained on the basis of better base stacking when OG is located at the 5' side of T<>T dimer, which would facilitate formation of an exciplex between the electron donor and the T<>T acceptor.[32] However, T<>T dimer cleavage by flavin does not depend on the electron transfer direction.[33]

Figure 6.5. shows the UV-absorption spectra of OG and **AZT** (obtained from the model investigated in Chapter 3). At neutral pH, the oxidatively generated nucleobase exhibits maxima at 250 and 295 nm, with a tail reaching the UVA region. By

contrast, **AZT** does not show any absorption maximum, as expected from the saturation of the C5-C6 double bond saturation of the initial pyrimidine bases.

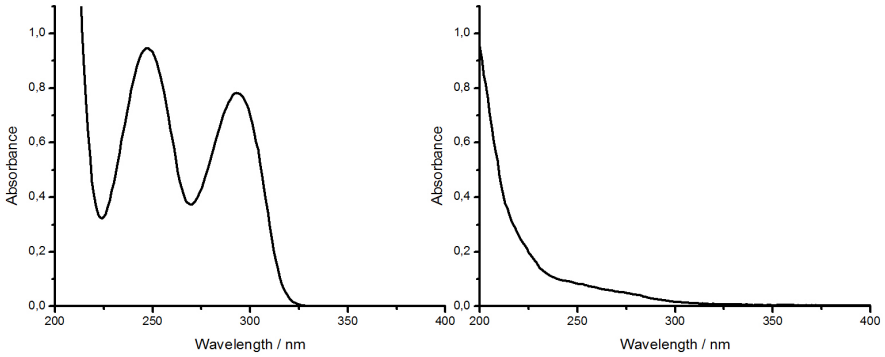

Figure 6.5. UV absorption spectra of OG in neutral phosphate buffer (left) and of **AZT** model (right) in acetonitrile.

Thus, the absorption spectra of **AF1** and **AZT-AF1** (the same for **AF2**) should correspond to the typical spectrum of single stranded oligonucleotide with a maximum at ca. 260 nm. The use of polystyrene cuvettes allows cutting off the wavelengths at $\lambda < 300$ nm, which is an important point in order to avoid direct excitation of **AZT** and its resulting photocycloreversion. In this context, a control experiment where **AZT-AF1** was irradiated using these cuvettes did not show the appearance of the repaired **AF1** oligonucleotide. This validates the experimental conditions that avoid photocycloreversion by direct irradiation of the heterocycle and, thus, OG is the only chromophore absorbing the incident light. In this way, once populated the singlet excited state, an electron transfer could take place from OG to the azetidine ring (Scheme 6.5), as described in the literature for the repair of cyclobutane thymine dimers.[31, 34]

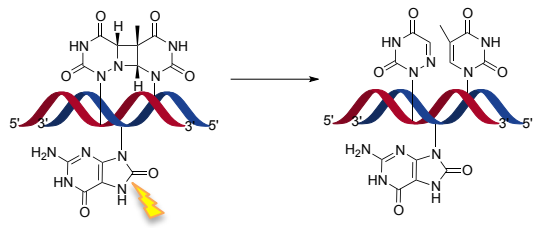

Scheme 6.5. Photorepair mechanism of **AZT-AF1** from **OG** inserted in the complementary strand by excess electron transfer at $\lambda > 300$ nm.

The first experiments were achieved with **AZT-AF1**, where 6-azauracil nucleotide is at the 5'-side of thymine nucleobase. The four combinations of **AZT-AF1** with its complementary **AF5-AF8** strand were irradiated at $\lambda > 300$ nm with UV lamps using the polystyrene cuvette and the course of the photocycloreversion process was followed by HPLC. Before irradiation, all the samples showed two peaks at 16.4 and 18.9 min that correspond to **AZT-AF1** and to the complementary strand, respectively (Figure 6.6). After irradiation, a new peak, which was assigned to **AF1** by comparison with the original sample, appeared at ca. 17.7 min and increases as a function of the irradiation time. These results show that the excitation of OG in the complementary strand triggers the photocycloreversion and leads to the repair of the lesion.

Figure 6.7 represents the comparison of repaired **AF1** peaks areas as a function of the OG location in the complementary strand. It should be mentioned that areas of the peaks were hardly obtained for **AZT-AF1** annealed with **AF7** and **AF8**, leading to a loss of accuracy in the results. However, it seems that the process is slightly more efficient for **AF5** and **AF6** where OG:A base pair is positions in 5' or 3' to the **AZT** site than for **AF7** and **AF8**. Regarding to the position of the electron donor on **AZT-AF1** repair, the same rate of repair was observed when OG was located in 5' or 3' to the **AZT** lesion. Further studies will be achieved to obtain more accurate results, and to compare the results with those obtained with **AZT-AF2** oligomer

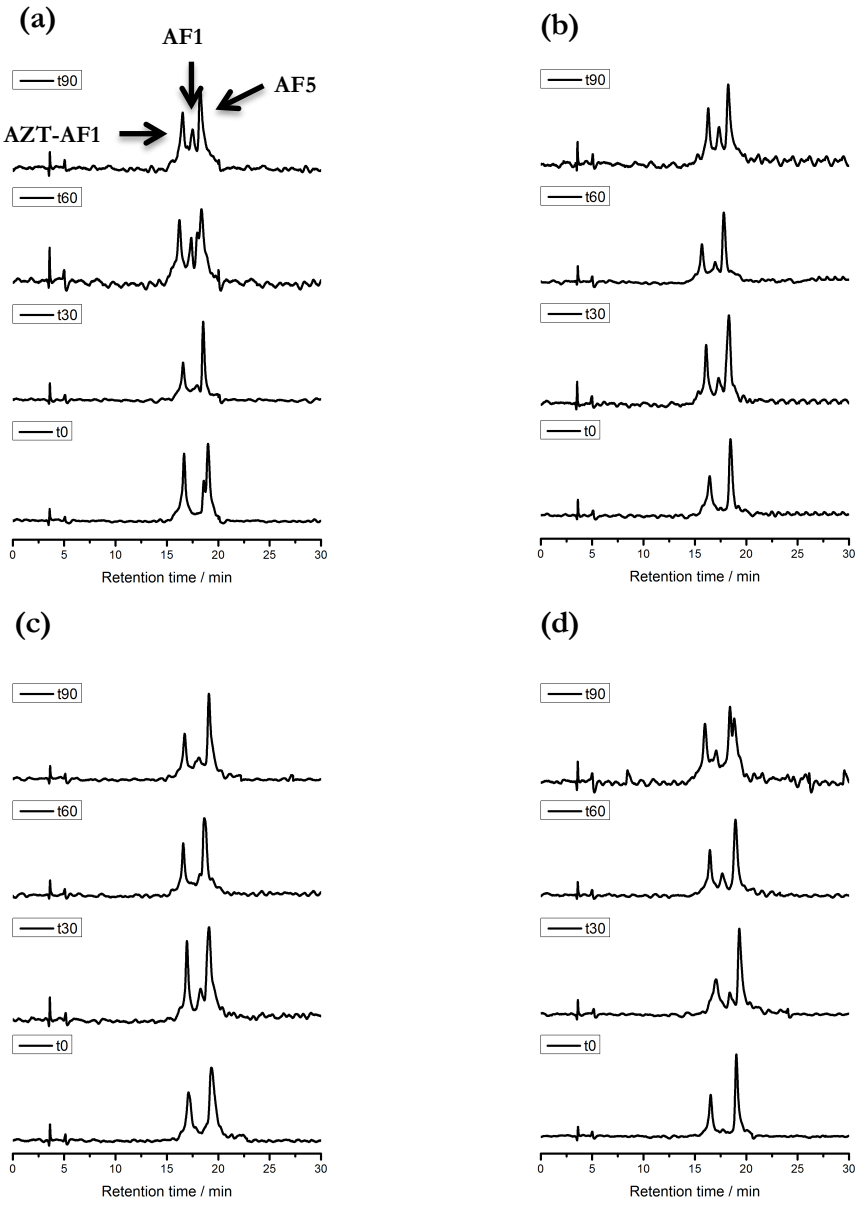

Figure 6.6. Chromatograms obtained for the irradiation of the duplexes formed between **AZT-AF1** and **AF5** (a), **AF6** (b), **AF7** (c), **AF8** (d).

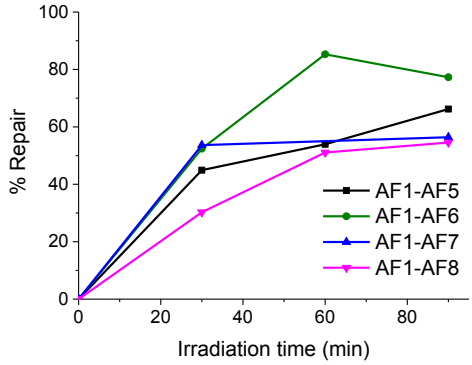

Figure 6.7. Time-dependent repair of **AZT-AF1** for the four different duplexes.

6.2.3 Photorepair of AZT by photolyases

The **AZT-AF1** oligonucleotide will also be of interest to investigate the ability of photolyases to repair this "lesion mimic". Moreover, the remarkable feature of **AZT** relies on its hybrid structure between a CPD and a 6-4PP azetidine intermediate. Therefore, photorepair experiments were performed in collaboration with Dr. Yunpei Yamamoto from Osaka University to evaluate the activity of *Thermus thermophiles* CPD photolyase (Tth) and *Xenopus laevis* (6-4) photolyase (Xl64) on **AZT-AF1**. In addition, two oligonucleotides containing the CPD and 6-4PP lesions (Scheme 6.6) were used as control experiments of Tth and Xl64 photolyases, respectively. These 14 mer oligonucleotides were synthetized on a DNA synthesizer using the phosphoramidite building blocks of *cis-syn* CPD and 6-4PP, as previously described in the literature.[35-36]

AZT-AF1 5'-CACAGC**AZT**ACAGTACAC-3' 18 mer

CPD ATCGGC**T<>T**CGCGCA 14 mer

6-4PP CAGCGG**T(6-4)T**GCCGTG 14 mer

Scheme 6.6. Sequences of the oligonucleotides studied for the photolyase assay.

As mentioned in Chapter 1, both CPD and (6-4) photolyases contain the flavin adenine dinucleotide FAD chromophore and, thereby, the analysis of their photorepair activity of **AZT-AF1** can be performed by using white light. Therefore, the 18 mer containing the **AZT** lesion, as well as CPD and 6-4PP 14 mers, were treated with Tth and Xl64 photolyases, and the reaction mixtures were analyzed by reverse phase HPLC. As shown in Figure 6.8. the CPD and 6-4PP 14 mers were converted to the undamaged 14 mer (TT 14 mer) by exposing the reaction mixture to white lighting for two hours, and the repair was confirmed by co-injection of the product with the TT 14 mer.

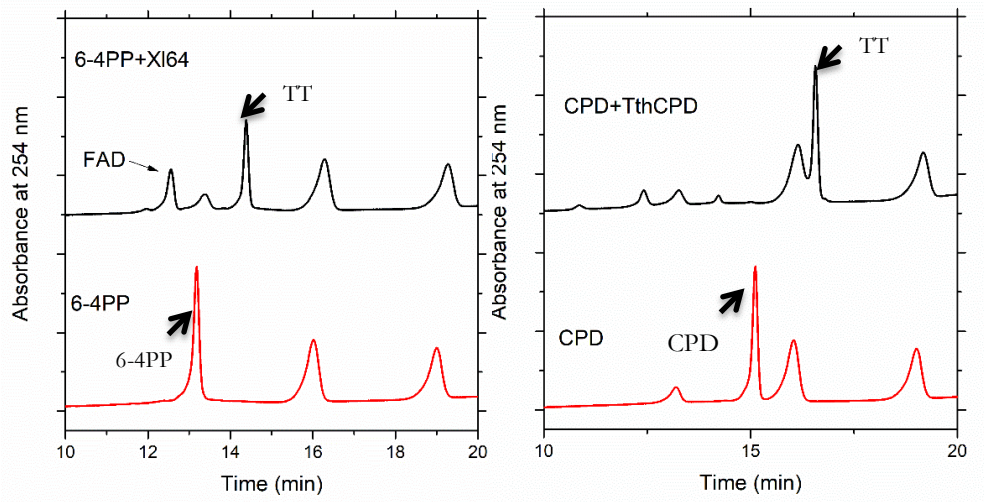

Figure 6.8. HPLC chromatograms obtained after 2h of irradiation with white light of a mixture of 6-4PP oligomer with Xl64 (left) and CPD oligomer with Tth (right). Peaks at 13, 16 and 19 min were from buffer contaminants.

Unfortunately, the peak of the **AF1** was not detected for the assay with **AZT-AF1** in the presence of both Tth and Xl64 photolyases (Figure 6.9). This fact can be explained by differents reasons. The first one is that, photolyases tend to inject electrons to the 5' side of the lesions, thus, the electron accepting potential of the 5' side

might be important. In the **AZT-AF1**, U* is in the 5' side, which may significantly perturb the electron accepting potential of the **AZT** and thus productive electron transfer might not happen. Therefore, further experiments will be achieved with **AZT-AF2** where U* is in the 3' side. As a second point, it has been reported that 6-azauracil incorporated in DNA has a significant influence on the base pair stability because of its low pK_a value of N3 (pK_a = 6.8) at neutral pH.[27] Thus, the protonation state might disturb recognition and/or repair reaction if the negatively-charged form is the major protonation state of **AZT** in neutral solution. Additional experiments at different pH values, lower than neutral, will be performed for **AZT-AF1** and **AZT-AF2** oligomers. Moreover, binding assays will be achieved in order to know the affinity of photolyases to this azetidine lesion, which is crucial for an efficient photorepair process.

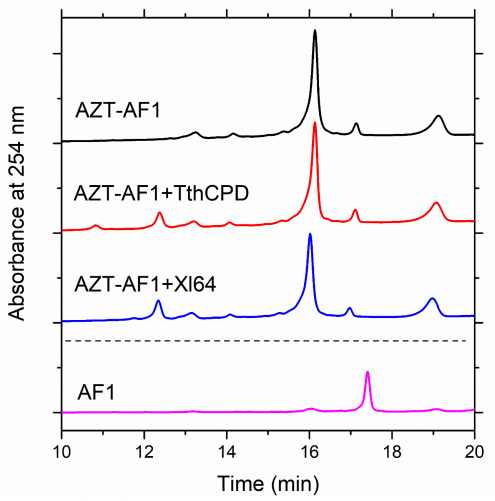

Figure 6.9. HPLC chromatograms obtained after 2h of irradiation with white light of a mixture of **AZT-AF1** with Tth (red) and Xl64 (blue).

6.3 Conclusions

An azetidine incorporated into DNA was obtained for the first time. Excess electron transfer experiments have been performed using the azetidine as electron trap. Firstly, the oxidized DNA damage OG was selected as electron donor to induce the photocycloreversion of the azetidine. Initial experiments concluded that this photoreaction is possible but that it is not sequence or direction dependent. Secondly, DNA repair by photolyase were achieved using the azetidine-derived oligomer as substrate. However, further experiments are necessary to get more information in order to know if the photorepair process can take place.

6.4 Experimental section

6.4.1 Oligonucleotide synthesis

6-azauridine phosphoramidite was purchased from Berry and G, OG, T and A phosphoramidites were purchased from Glen Research. The oligonucleotides **AF1**-**AF8** were synthesized at the DNA/Peptide Core facility at the University of Utah. Oligodeoxynucleotides were cleaved and deprotected in sealed glass vials with concentrated NH_4OH for 16 h at 55ºC in the dark. In the cases of oligonucleotides containing OG (**AF5**-**AF8**), 0.25M β-mercaptoethanol was added to the deprotection solutions to avoid the oxidation of OG. **AF5-AF8** were purified by reverse-phase HPLC on a Polaris C18 (4.6 mm i.d. x 25 cm length) column with linear gradient of 93:7 (50 mM $CH_3CO_2NH_4$: MeCN) to 83:17 over 30 min at a 1 mL min^{-1} flow. **AF1-AF2** were used whithout HPLC purification. The identity of oligomers was determined by TOF MS ES^-. Oligonucleotides CPD and 6-4PP were synthesized on an Applied Biosystems 3400 DNA synthesizer, by using the phosphoramidite building blocks of the *cis-syn* CPD and 6-4PP as described previously.[35-36]

6.4.2 Photochemical preparation of AZT oligonucleotide

The azetidines (**AZT-AF1/AZT-AF2**) were prepared through acetophenone photosensitization. Thus, a N_2 purged solution of 0.44 mL of acetophenone and 150 mL of an **AF1** or **AF2** solution (200 μM in water) was irradiated at 313 nm for 2 hours in a polystyrene cuvette lying on an ice bath. The reaction was followed by reversed phase HPLC on a Zorbax Microsorb-MV C18 column (4.6 mm i.d. x 25 cm length) with detection wavelength fixed at 260 nm and using a linear gradient of 93:7 (50 mM $CH_3CO_2NH_4$: MeCN) to 90:10 over 30 min at a 1 mL min^{-1} flow. The solution was lyophilized to eliminate part of the acetophenone and was purified by reverse-phase HPLC using the abovementioned conditions and then re-lyophilized.

6.4.3 Photorepair experiments with OG

The **AZT-AF1** 18 mer was resuspended in a buffer solution (20 mM NaPi, 100 mM NaCl, pH 7) to reach a concentration of 10 μM and was annealed with the appropriate complementary sequences (**AF5-AF8**, 10 μM) by heating 2 min at 85ºC and cooling in the dark to room temperature over 3h. The obtained double stranded oligonucleotides were irradiated with four UVB lamps (Luzchem, ranging from 280 to 400 with a maximum output at 300 nm) using polystyrene cuvettes on an ice bath. The kinetics of the reaction was followed by reverse phase HPLC with the Zorbax column at 75 ºC using a gradient of 50 mM of $CH_3CO_2NH_4$: MeCN (93:7 to 83:17 over 30 min). Under these conditions, the DNA duplex was denatured, the 22-mer complementary strand (**AF5-AF8**) being eluted at 18.9 min, while the 18-mers **AZT-AF1** and **AF1** have retention times of 16.4 and 17.7 min, respectively. The peak areas, obtained by the integration of the HPLC peaks, were normalized against extinction coefficients of each strand of **AZT-AF1** or **AF1** and used to calculate the photorepair yield.

6.4.4 Photorepair experiments with photolyases

Analysis of the CPD and (6-4) photolyase reaction was performed by HPLC, following the previous reported conditions.[25] A solution of *Thermus thermophiles* CPD photolyase or *Xenopus laevis* (6-4) photolyase (2 μM) in a buffer containing 10 mM phosphate (pH 7.0), 100 mM NaCl, 5% glycerol and 10 mM dithiothreitol, which was covered with a Pyrex lid, was illuminated on ice with 18 W fluorescent lamp at a distance of 15 cm for 30 min. A solution of CPD, 6-4PP or **AZT-AF1** oligomer (1 μM) was added to the preincubated mixture, and irradiated again for 2 h. The reaction mixture was analyzed by reverse phase HPLC with the Waters μBondasphere C18 column at 50 ºC using a gradient of 0-40% B over 20 min (A: 5% MeCN/0.1 M TEAA, B: 25% MeCN/0.1 M TEAA), with a flow rate of 1 mL min^{-1}.

6.5 References

1. Wagenknecht, H. A., Electron transfer processes in DNA: mechanisms, biological relevance and applications in DNA analytics. *Nat. Prod. Rep.* **2006,** *23*, 973-1006.

2. Cadet, J.; Douki, J.; Ravanat, J.; Mascio, P., Sensitized formation of oxidatively generated damage to cellular DNA by UVA radiation. *Photochem. Photobiol.* **2009,** *8*, 903-911.

3. Sancar, A., Structure and function of DNA photolyase and cryptochrome blue-light photoreceptors. *Chem. Rev.* **2003,** *103*, 2203-2207.

4. Wagenknecht, H. A., *From Mechanism to Application. Chapter 1. Wiley-VCH Ed.* **2005**, 1-26.

5. Maie, K.; Miyagi, K.; Takada, T.; Nakamura, M.; Yamana, K., RNA-mediated electron transfer: double exponential distance dependence. *J. Am. Chem. Soc.* **2009,** *131*, 13188-13189.

6. Ito, T.; Rokita, S. E., Reductive electron injection into duplex DNA by aromatic amines. *J. Am. Chem. Soc.* **2004,** *126*, 15552-15559.

7. Elias, B.; Genereux, J. C.; Barton, J. K., Ping-pong electron transfer through DNA. *Angew. Chem. Int. Ed.* **2008,** *47*, 9067-9070.

8. Lin, S. H.; Fujitsuka, M.; Majima, T., Sequence-dependent photocurrent generation through long-distance excess-electron transfer in DNA. *Angew. Chem. Int. Ed.* **2016,** *55*, 1-4.

9. Giese, B., Long-distance electron transfer through DNA. *Annu. Rev. Biochem.* **2002,** *71*, 51-70.

10. Seidel, C. A. M., Nucleobase-specific quenching of fluorescent dyes. Nucleobase one-electron redox potentials and their correlation with static and dynamic quenching efficiencies. *J. Phys. Chem.* **1996,** *100*, 5541-5553.

11. Behrens, C.; Cichon, M. K.; Grolle, F.; Hennecke, U.; Carell, T., Excess electron transfer in defined donor-nucleobase and donor-DNA-acceptor systems. *Top. Curr. Chem.* **2004,** *236*, 187-204.

12. Lewis, F. D.; Wasielewski, M. R., Dynamics and equilibrium for single step hole transport processes in duplex DNA. *Top. Curr. Chem.* **2004,** *236*, 45-65.

13. Wagenknecht, H. A.; Fiebig, T., *From Mechanism to Application. Chapter 9. Wiley-VCH Ed.* **2005**, 197-204.

14. Schwögler, A.; Burgdorf, L. T.; Carell, T., Self-repairing DNA based on a reductive electron transfer through the base stack. *Angew. Chem. Int. Ed.* **2000,** *39*, 3918-3920.

15. Breeger, S.; Hennecke, U.; Carell, T., Excess electron-transfer-based repair of a *cis-syn* thymine dimer in DNA is not sequence dependent. *J. Am. Chem. Soc.* **2004,** *126*, 1302-1303.

16. Behrens, C.; Burgdorf, L. T.; Schwögler, A.; Carell, T., Weak distance dependence of excess electron transfer in DNA. *Angew, Chem. Int. Ed.* **2002,** *114*, 1841-1845.

17. Giese, B.; Carl, B.; Carl, T.; Schiemann, O.; Feresin, E., Excess electron transport through DNA: a single electron repairs more than one UV-induced lesion. *Angew. Chem. Int. Ed.* **2004,** *43*, 1848-1851.

18. Stafforst, T.; Diederichsen, U., Thymine oxetanes as charge traps for chemical monitoring of nucleic acid mediated transfer of excess electrons. *Angew. Chem. Int. Ed.* **2006,** *45*, 5376-5380.

19. Breeger, S.; von Meltzer, M.; Hennecke, U.; Carell, T., Investigation of the pathways of excess electron transfer in DNA with flavin-donor and oxetane-acceptor modified DNA hairpins. *Chem. Eur. J.* **2006,** *12*, 6469-6477.

20. Ito, T.; Rokita, S. E., Excess electron transfer from an internally conjugated aromatic amine to 5-bromo-2'-deoxyuridine in DNA. *J. Am. Chem. Soc.* **2003,** *125*, 11480-11481.

21. Ito, T.; Kondo, A.; Terada, S.; Nishimoto, S., Photoinduced reductive repair of thymine glycol: implications for excess electron transfer through DNA containing modified bases. *J. Am. Chem. Soc.* **2006,** *128*, 10934-10942.

22. Fraga-Timiraos, A. B.; Lhiaubet-Vallet, V.; Miranda, M. A., Repair of a dimeric azetidine related to the thymine-cytosine (6-4) photoproduct by electron transfer photoreduction. *Angew. Chem. Int. Ed.* **2016,** *55*, 6037-6040.

23. McAuley-Hecht, K. E.; Leonard, G. A.; Gibson, N. J.; Thomson, J. B.; Watson, W. P.; Hunter, W. N.; Brown, T., Crystal structure of a DNA duplex containing 8-hydroxydeoxyguanine-adenine base pairs. *Biochemistry* **1994,** *33*, 10266-10270.

24. Butenandt, J.; Eker, A. P. M.; Carell, T., Synthesis, crystal structure, and enzymatic evaluation of a DNA-photolesion isostere. *Chem. Eur. J.* **1998,** *4*, 642-654.

25. Yamamoto, J.; Hitomi, K.; Hayashi, R.; Getzoff, E. D.; Iwai, S., Role of the carbonyl group of the (6-4) photoproduct in the (6-4) photolyase reaction. *Biochemistry* **2009,** *48*, 9306-9312.

26. Zhao, X.; Liu, J.; Hsu, D. S.; Zhao, S.; Taylor, J. S.; Sancar, A., Reaction mechanism of (6-4) photolyase. *J. Biol. Chem.* **1997,** *272*, 32580-32590.

27. Seela, F.; Chittepu, P., Oligonucleotides containing 6-aza-2'-deoxyuridine: synthesis, nucleobase protection, pH-dependent duplex stability, and metal-DNA formation. *J. Org. Chem.* **2007,** *72*, 4358-4366.

28. Jiang, N.; Taylor, J. S., *In vivo* evidence that UV-induced C=>T mutations at dipyrimidine sites could result from the replicative bypass of *cis-syn* cyclobutane dimers or their deamination products. *Biochemistry* **1993,** *32*, 472-481.

29. Mu, W.; Han, Q.; Luo, Z.; Wang, Y., Production of *cis-syn* thymine-thymine cyclobutane dimer oligonucleotide in the presence of acetone photosensitizer. *Anal. Biochem.* **2006,** *353*, 117-123.

30. Banerjee, S. K.; Borden, A.; Christensen, R. B.; LeClerc, J. E.; Lawrence, C. W., SOS-dependent replication past a single *trans-syn* T-T cyclobutane dimer gives a different mutation spectrum and increased error rate compared with replication past this lesion in uninduced cells. *J. Bacteriol.* **1990,** *172*, 2105-2112.

31. Nguyen, K. V.; Burrows, C. J., A prebiotic role for 8-oxoguanosine as a flavin mimic in pyrimidine dimer photorepair. *J. Am. Chem. Soc.* **2011,** *133*, 14586-14589.

32. Crespo-Hernández, C. E.; Cohen, B.; Kohler, B., Base stacking controls excited-state dynamics in A T DNA. *Nature* **2005,** *436*, 1141-1144.

33. Haas, C.; Kräling, K.; Cichon, M.; Rahe, N.; Carell, T., Excess electron transfer driven DNA does not depend on the transfer direction. *Angew. Chem. Int. Ed.* **2004,** *116*, 1878-1880.

34. Nguyen, K. V.; Burrows, C. J., Whence flavins? Redox-active ribonucleotides link metabolism and genome repair to the RNA world. *Acc. Chem. Res.* **2012,** *45*, 2151-2159.

35. Reyna, M. M.; Yamamoto, J.; Huang, W. C.; Tsai, M. D.; Essen, L. O.; Bessho, Y., Twist and turn: a revised structural view on the unpaired bubble of class II CPD photolyase in complex with damaged DNA. *IUCrJ* **2018,** *5*, 608-618.

36. Franz, S.; Ignatz, E.; Wenzel, S.; Zielosko, H.; Putu, E. P.; Reyna, M. M.; Tsai, M. D.; Yamamoto, J.; Mittag, M.; Essen, L. O., Structure of the bifunctional cryptochrome aCRY from *Chlamydomonas reinhardtii*. *Nucleic Acids Res.* **2018,** *46*, 8010-8022.

Chapter 7:
Instrumentation

7.1 Nuclear magnetic resonance (NMR)

The ^{1}H and ^{13}C NMR spectra were measured by a 300 MHz instrument, and $CDCl_3$ and DMSO-d_6 were used as solvent for the spectra. The solvent signal was taken as the reference using a chemical shift of δ of ca. 7.26 ppm and 2.50 ppm for ^{1}H NMR and 77.16 ppm and 39.52 ppm for ^{13}C NMR, respectively.

7.2 Absorption measurements

All UV-Vis absorption spectra were recorded on a Varian Cary 50 spectrophotometer with a quartz cell of 1 cm optical path length.

7.3 Fluorescence Measurements

Steady-state fluorescence. Steady-state fluorescence experiments were carried out on a Photon Technology International (PTI) LPS-220B spectrofluorometer equipped with a Xenon lamp of 75 W and a monochromator that covers a range from 200 to 700 nm. All experiments were performed under air in a quartz cuvette of 1 cm of optical path. The absorbance of the sensitizer was kept under 0.15 at the excitation wavelength. Stock solutions of the quenchers (0.15 M) were prepared, so it was only necessary to add microliter volumes to the sample cell to obtain appropriate concentrations of the quencher. The bimolecular rate constants $k_q(SS)$ for the reaction were obtained from the Stern-Volmer plots following the equation:

$$I_0/I = 1 + k_q(SS)\,\tau_0\,[Q] = 1 + K_{SV}\,[Q] \qquad (7.1)$$

where I_0 and I are the emission intensity in the absence of Q and after the addition of a quencher concentration [Q], respectively; K_{SV} (= $k_q(SS)\,\tau_0$) is the Stern-Volmer rate constant obtained from the slope and τ_0 is the lifetime of the photosensitizer in the absence of Q.

Time-resolved fluorescence. Measurements were performed with an EasyLife V spectrometer from OBB, equipped with a pulsed LED as excitation source; residual excitation signal was filtered in emission by using a cut-off filter. The kinetic traces were fitted by one monoexponential decay function, using a deconvolution procedure to separate them from the lamp pulse profile.

The absorbance of the sensitizer was kept at 0.15 at the excitation wavelength. Quenchers stock solutions of 0.15 M were also used for this experiment, and the rate constants k_q(TR) for the reaction were obtained from the Stern-Volmer plots following the equation:

$$1/\tau = 1/\tau_0 + k_q(TR)\,[Q] \qquad (7.2)$$

where τ_0 is the lifetime of the photosensitizer in the absence of Q and τ is the lifetime after addition of a quencher concentration [Q].

7.4 Cyclic voltammetry

Cyclic voltammetry measurements were performed with a VersaSTAT 3 potentiostat (Princeton Applied Research, Algete-Madrid, Spain) and using a three electrode standard configuration with glassy carbon as working electrode, platinum wire as counter electrode, and Ag/AgCl in 3 M NaCl as reference electrode. Measurements were carried out on N_2-purged acetonitrile or DMF solutions with 0.1 M Bu_4NClO_4 as electrolyte at a scan rate of 0.1 V s^{-1}. Ferrocene was taken as standard and measured potentials have been referenced to the $E_{1/2}$ potential of the ferrocinium/ferrocene (Fc^+/Fc) couple of 0.425 V vs. Ag/AgCl in MeCN.

7.5 Steady-state photolysis

Irradiations of the samples were run using different systems:

- A Xenon lamp (150 W or 75 W) equipped with a monochromator from Photon Technology International (PTI) for monochromatic irradiations.
- A medium pressure mercury lamp (125 W).
- A Luzchem photoreactor (model LZC-4V) with four lamps ranging from 280 nm to 400 nm with a maximum output at 300 nm.
- A FS40 UVB lamp with maximum output at 313 nm (Homophototherapy, OH, USA).

Irradiations were performed under anaerobic and aerobic conditions in a quartz cell of 1 cm optical path length, pyrex vessels or polystyrene cuvettes.

7.6 HPLC analyses

The irradiated solutions were analyzed by reverse phase HPLC using a Varian ProStar instrument equipped with a diode array detector covering a detection range from 200 to 400 nm. Two columns were used: (1) a Mediterranean Sea C18 (4.6 mm i.d. x 25 cm length, 5μ Teknokroma) with detection wavelength fixed at 270 nm. In Chapter 3 and 4, isocratic mixture of MeCN:H_2O (20:80 v/v) at a flow of 1 mL min^{-1} was used as mobile phase. In Chapter 5, isocratic mixture of MeOH:H_2O (70:30, v/v) at a flow of 1 mL min^{-1} was used for compound **10** and a linear gradient of 2:98 (MeCN:H_2O) to 65:35 over 30 min at a 1 mL min^{-1} flow was used for compounds **15**, **16**, **20** and **21**. (2) A Zorbax Microsorb-MV C18 column (4.6 mm i.d. x 25 cm length) with detection wavelength fixed at 260 nm and using a linear gradient of 93:7 (50 mM $CH_3CO_2NH_4$: MeCN) to 83:10 over 30 min at a 1 mL min^{-1} flow was used in Chapter 6.

7.7 UPLC-HRMS analyses

Exact mass values were determined by using a QTof spectrometer coupled with a liquid chromatography system with a conditioned autosampler at 10 °C. The separa-

tion was carried out on an UPLC with a BEH C18 column (50 mm Å~ 2.1 mm i.d., 1.7 μm) or HSS T3 column (150 mm Å~ 2.1 mm, 1.8 μm). The ESI source was operated in positive or negative ionization mode with the capillary voltage at 1.9 kV or 2.4 kV, respectively. The temperature of the source and desolvation was set at 80 and 400 °C, respectively. The cone and desolvation gas flows were 20 and 800 L h^{-1}, respectively. All data were collected in centroid mode. Leucine-enkephalin was used as the lock mass generating an $[M+H]^+$ ion (m/z 556.2771) or $[M-H]^-$ ion (m/z 554.2615) at a concentration of 250 pg/mL and flow rate of 50 μL min^{-1} to ensure accuracy during the MS analysis.

7.8 Femtosecond broadband transient absorption spectroscopy (fs-TAS)

A Femtosecond broadband pump-probe spectroscopy utilizing an 800 nm, 1 kHz laser source (4.0 W, 100 fs pulse, Libra-HE from Coherent Inc.) was used. The fundamental beam at 800 nm was split into the pump and probe beams using a 98/2 beam splitter, respectively. The pump beam was tuned to 308 nm using an optical parametric amplifier (TOPAS, Light Conversion). The probe beam was attenuated using an optical filter wheel and focused into a continuously translating 2 mm CaF_2 crystal used to generate a white light continuum in the spectral window from ca. 320 to 700 nm. The maximum overlap of the crosscorrelated pump and probe beams was determined from the stimulated Raman emission bands of acetonitrile and defined as time zero in the transient absorption spectra. The instrument response function was estimated to be 200 ± 50 fs from the two-photon absorption of pure methanol. A 2 mm fused silica cuvette with a magnetic stir bar was used to ensure homogeneity of the solutions. Samples were monitored for potential photodegradation using steady-state absorption spectroscopy (Cary 100 Bio Instrument, Agilent Technologies). A fresh solution was used if the absorbance of the solutions at the absorption maximum of each compound decreased by 5%. The fs-TAS kinetic data were modeled through global fit analyses using Igor Pro 6.32A. The global and target analysis method based

on a sequential kinetic model plus a constant offset, and convoluted with an instrument response function of 200 ± 50 fs, was used to extract the lifetimes and corresponding evolution associated difference spectra.

7.9 Quantum-chemistry ground-state computations

All geometry optimizations were carried out by employing the DFT method, in particular, by making use of the Minnesota DFT/M06- 2X hybrid functional and the standard 6-31++G(d,p) basis set, as implemented in the Gaussian 09 software package. This computational method provided satisfactory descriptions of the reactivity of other DNA-based open-shell and closedshell systems. Frequency calculations by using the harmonic oscillator approximation were used to obtain the ZPVEs and to verify the nature of the stationary points, by checking the absence of any imaginary frequency at the minima and the presence of only one imaginary vibrational mode (reaction coordinate) at the TS structure. For **T<>AZT**$^{\bullet+}$, IRC calculations were performed to ensure the connectivity between the TS and related minima. For **T<>AZT**$^{\bullet-}$, the TS that led to C-N bond breaking was not found because the reaction coordinate most probably depended on bond stretching and on a complex molecular reorganization of the relative orientations of the aromatic rings, as revealed by preliminary relaxed scan calculations. Therefore, MEP calculations starting from the two highest points of the relaxed scan potential energy surfaces (C-N distances of 1.85 and 1.90 Å, respectively) were conducted to connect both reactants and products, and estimate an upper bound for the energy barrier. The energy of the abovementioned molecular reorganization taking place between the two selected structures was tracked by means of the LIIC procedure, which provided a connected (and therefore, possible) path between the two geometries, thereby ensuring the absence of any energy barrier not found by the relaxed scan exploration. VIPs were computed by subtracting the energies of the neutral state from the energy of the cationic state at the equilibrium geometry of the former, whereas the AIPs were determined by subtracting the energy of the neutral state

at its corresponding equilibrium geometries from the energy of the cationic state at its equilibrium geometry. On the other hand, the AEAs were obtained by subtracting the energy of the anionic state at its optimized geometry from the energy of the neutral state at its equilibrium geometry. Thereby, positive AEAs indicated stable anionic states, whereas positive VIPs and AIPs referred to unstable cations.

The CASSCF method was used to build multiconfigurational ground-state wave functions on top of the M06-2X geometries. The active space was chosen by including the most relevant out-of-plane nitrogen lone pairs (n_N) and π and π^* molecular orbitals of the 6-azauracil and thymine moieties in the azaU-T π-stacked arrangement, that is, 12 electrons distributed into 12 molecular orbitals (12-in-12) for the neutral system. Thus, active spaces of (13-in-12) and (11-in-12) were used throughout to study the reactivity of the anionic and cationic systems, respectively. In the case of **T<>AZT**$^{\bullet-}$ at the reactant structure, one π and one π^* orbital combined to produce the corresponding σ and σ^* orbitals of the C-N bond. Similarly, at the reactant structure of the **T<>AZT**$^{\bullet+}$, two π and two π^* orbitals gave rise to the two σ/σ^* pairs of the C-N and the C-C covalent bonds.

CASPT2 was used to compute the dynamic electron correlation on top of the CASSCF wave function, and thus, provided accurate energies. An imaginary level shift of 0.2 a.u. was set to minimize the presence of weak intruder states. Regarding the IPEA parameter, the recommended value of 0.25 a.u. was used for the charged systems, as previously benchmarked for cationic and anionic DNA nucleobases, whereas the standard zeroth-order Hamiltonian (IPEA=0.0 a.u.) was employed for the neutral systems. All multiconfigurational calculations were performed with the MOLCAS8 suite of programs and the atomic natural orbital (ANO) L-type basis set with the C,N,O (4s 3p 1d)/H (2s 1p) contraction scheme (ANO-L 431/21).

Chapter 8:
General Conclusions

In this Doctoral Thesis, the photocycloreversion process of azetidines is addressed to get more insights into the proposed repair mechanism of (6-4) photoproducts by photolyases. Indeed, the processes involved in this mechanism are still under discussion, being a possible hypothesis the formation and cycloreversion of a four-membered ring heterocycle. Here, models of the highly unstable azetidine intermediate, proposed for the repair of 6-4PP at TC sequences, have been synthetized to investigate for the first time both the photoinduced reductive and oxidative process. In Chapter 3, stable azabipyrimidinic azetidines obtained from 6-azauracil and thymine or cyclohexene were synthetized in order to determine the influence of thymine moiety in the photoreduction process. Fluorescence, cyclic voltammetry, HPLC and theoretical studies showed that the injection of one electron into the azetidine derived from thymine can occur and leads to a clean cycloreversion that "repairs" the nucleobases. This points to the importance of the thymine moiety that favors a delocalization of the extra electron over the two carbon atoms. For the photooxidative process, in Chapter 4, it was evidenced that the presence of a nitrogen atom in the four-membered ring affects the redox potential being more favorable the electron transfer for the azetidine compounds than for the related cyclobutane thymine dimer.

Moreover, the study was extended to the ability of the intrinsic photoreductant OG to act as an artificial photolyase. First, in Chapter 5, the photocycloreversion of four-membered model systems bearing an oxetane or a cyclobutane thymine dimer as electron accepting moiety, covalently attached to the photoreductant, were addressed through photochemical and photophysical studies. Then, in Chapter 6, the azetidine ring was incorporated for the first time into an oligonucleotide. Photochemical studies revealed that electron migration is taking place between OG inserted in the opposite strand to the azetidine, splitting the ring and yielding the restored 6-azauracil and thymine original bases. Finally, the ability of (6-4) and CPD photolyases to recognize the azetidines derived oligonucleotide and achieve its repair is under study at this moment.

To summarize, this doctoral Thesis has provided solid bases to develop the photochemical, photophysical, photobiological study of the oxidative and reductive photocycloreversion of an azetidine. The synthesized models show interesting characteristics as "mimic" of the unstable intermediates involved in the repair of 6-4PP damage by the photolyase. This way, it has been established that these heterocycles can be "repaired" by photoreductants with a reduction potential in the excited state close to that of the reduced flavin, the active cofactor of photolyase. Therefore, photolyases must be capable to cyclorevert the azetidine proposed as a potential intermediate during the repair of (6-4) photoproduct at TC sequences. The study of our azetidine model inserted in an oligonucleotide, which is under study, should provide more details about this mechanism.

Summary-Resumen-Resum

Summary

Ultraviolet radiation is associated with the formation of certain lesions in the DNA that are at the origin of skin cancer. Among the most relevant are the damages that occur at pyrimidine bases: cyclobutane dimers (CPDs) and (6-4) photoproducts (6-4) (6-4PPs). To obtain protection from DNA photolesions, living organisms have enzymes that restore the lesions to their original form, thus maintaining genetic integrity. In some organisms, CPDs and 6-4PPs show an additional repair process, which corresponds to photoreactivation and involves enzymes called CPD and (6-4) photolyases. In particular, there is currently a lively discussion about the mechanism of repair by (6-4) photolyase. The general objective of this doctoral thesis has been to study the cycloreversion of the proposed intermediate of 6-4PP lesions as a key to support one of the mechanisms proposed so far.

In a first place, a model of the intermediate azetidine of the 6-4PP lesion for TC sequences was prepared to investigate its repair by means of electron donation by photosensitizers with suitable redox potential, mimicking the flavin cofactor of the (6-4) photolyase. Electrochemical, spectroscopic, analytical measurements as well as computational studies showed that the injection of an electron into the azetidine ring leads to a cycloreversion of the bipyrimidine azetidine to the thymine and 6-azauracil bases. It has also been shown that electron transfer only takes place if the thymine component is present in the model.

Secondly, the cycloreversion of azetidine has been investigated by means of an oxidative process in which the azetidine ring donates an electron to the photosensitizer. The comparison with a cyclobutane derivative showed that the presence of the nitrogen in the four-membered ring decreases the redox potential, facilitating thus the oxidation process.

Third, the cycloversion step has been studied with two intrinsic photosensitizers, guanine and the oxidatively generated damage 8-oxoguanine (OG), covalently bound to a CPD or to an oxetane, as a model for the intermediate of 6-4PP repair. Altogether, the spectroscopic and analytical data showed that these endogenous photosensitizers can act as electron donors mimicking, thus, the function of the flavin cofactor in photolyase.

Finally, azetidine ring has been incorporated in an oligonucleotide to study its cycloreversion by electron transfer. Based on the results of the previous chapter, OG has been chosen as a natural photoreductant. In a first step, a methodology has been developed to insert the azetidine within the oligonucleotide sequence. Then, steady-state irradiation of the duplex containing OG and the azetidine has demonstrated that the electron transfer takes place and leads to the cycloreversion of the heterocycle. In addition, preliminary experiments have been carried out to evaluate the repair of this four-membered ring, as an analog to the (6-4) photoproduct intermediate, by real CPD and (6-4) photolyases.

Resumen

La radiación ultravioleta está asociada a la formación de ciertas lesiones en el ADN que están en el origen del cáncer de piel. Entre las más relevantes se encuentran los daños que se producen en las bases pirimidínicas: los dímeros ciclobutánicos (CPDs) y fotoproductos (6-4) (6-4PPs). Como protección contra las fotolesiones del ADN, los organismos vivos disponen de enzimas que restauran las lesiones a su forma original, manteniendo así la integridad genética. Algunos organismos manifiestan un proceso de reparación adicional de los CPDs y los 6-4PPs, que corresponde a la fotorreactivación y que involucra enzimas denominadas fotoliasas CPD y (6-4). En concreto, actualmente existe una viva discusión sobre el mecanismo de reparación por la fotoliasa (6-4). El objectivo general de esta tesis doctoral ha sido estudiar la ciclorre-

versión de los intermedios clave propuestos para la lesión 6-4PP para apoyar uno de los mecanismos propuestos hasta ahora.

En primer lugar se ha preparado un modelo de la azetidina intermedia de la lesión 6-4PP en secuencias TC para investigar su reparación mediante un proceso de donación de electrones a través de fotosensibilizadores con un potencial redox adecuado, mimetizando así el cofactor flavina de la fotoliasa (6-4). Los estudios de electroquímica, espectroscopía, análisis y química computacional mostraron que la posibilidad de inyectar un electrón al anillo de la azetidina conlleva una ciclorreversión de la azetidina bipirimidínica generando las bases timina y 6-azauracilo. También se ha evidenciado que la transferencia de electrones sólo tiene lugar si el componente timina está presente en el modelo.

En segundo lugar, se ha investigado la ciclorreversión de la azetidina mediante un proceso oxidativo en cual el anillo de azetidina dona un electrón al fotosensibilizador. La comparación con un derivado ciclobutánico mostró que la presencia del nitrógeno en el anillo de cuatro miembros disminuye el potencial redox facilitando el proceso de oxidación.

En tercer lugar, el paso de ciclorreversión se ha estudiado con dos fotosensibilizadores intrínsecos, la guanina y el daño oxidativo 8-oxoguanina (OG), unidos covalentemente a un CPD o a un oxetano, como modelo del intermedio formado en la reparación del daño (6-4). En conjunto, los datos de espectroscopía y análisis cromatográfica mostraron la posibilidad de que estos fotosensibilizadores endógenos pueden actuar como dadores de electrones mimetizando, por tanto, la función del cofactor flavina en la fotoliasa.

Finalmente, el anillo de azetidina ha sido incorporado en un oligonucleótido para estudiar su ciclorreversión mediante transferencia de electrones. En base a los resultados de los capítulos previos, OG ha sido elegido como un fotorreductor natural. En un primer paso, una metodología ha sido desarrollada para insertar la azetidina dentro

de una secuencia de oligonucleótido. Luego, la irradiación en estado estacionario del dúplex que contiene OG y la azetidina ha demostrado que la transferencia de electrones tiene lugar y conlleva a la ciclorreversión del heterociclo. Además, experimentos preliminares han sido llevados a cabo para evaluar la reparación del anillo de cuatro miembros, como un análogo del intermedio generado en el caso del fotoproducto (6-4), por las fotoliasas reales CPD y (6-4).

Resum

La radiació ultravioleta està associada a la formació de certes lesions en l'ADN que podrien concluir al càncer de pell. Entre les més rellevants es troben els danys que es produïxen en les bases pirimidínicas: els dímers ciclobutánics (CPDs) i els fotoproductes (6-4) (6-4PPs) . Per a protegir-se de les fotolesions al l'ADN, els organismes vius disposen d'enzims que restauren les lesions a la seua forma original, mantenint així la integritat genètica. En alguns organismes els CPDs i els 6-4PPs manifesten un procés de reparació addicional, que correspon a la fotorreactivació on están involucrats enzims denominades fotoliases CPD i (6-4) . En concret, actualment hi ha una viva discussió sobre el mecanisme de reparació per la fotoliasa (6-4) . L'objectiv general d'esta tesi doctoral ha sigut estudiar la ciclorreversió dels intermedis clau proposats per a la lesió 6-4PP com a recolzament d' un dels mecanismes proposats fins ara.

En primer lloc s'ha preparat un model de l'azetidina intermèdia de la lesió 6-4PP en seqüències TC per a investigar la seua reparació per mitjà d'un procés de donació d'electrons per fotosensibilizadors amb un potencial redox adequat, mimetitzant així el cofactor flavina de la fotoliasa (6-4) . Els estudis d'electroquímica, espectroscòpia, anàlisi cromatogràfica i química computacional van mostrar que la possibilitat d'injectar un electró a l'anell de l'azetidina comporta una ciclorreversió de l'azetidina bipirimidínica a les bases de timina i 6-azauracil. També s'ha evidenciat que la transferència d'electrons només té lloc si la base timina està present en el model.

En segon lloc, s'ha investigat la ciclorreversión de l'azetidina mitjacant procés oxidatiu en que l'anell d'azetidina dóna un electró cap al fotosensibilizador. La comparació amb un derivat ciclobutánic va mostrar que la presència del nitrògen en el anell de quatre membres disminuïx el potencial redox facilitant el procés d'oxidació.

En tercer lloc, el pas de ciclorreversió s'ha estudiat amb dos fotosensibilizadors intrínsecs, guanina i el dany oxidatiu 8-oxoguanina (OG) , units covalentment a un CPD o a un oxetano, com a intermedi del dany (6-4) . En conjunt, les dades d'espectroscòpia i anàlisi cromatogràfica van mostrar la possibilitat que estos fotosensibilizadors endògens poden actuar com a donadors d'electrons mimetitzant, per tant, la funció del cofactor flavina en la fotoliasa.

Finalment, l'anell d'azetidina ha sigut incorporat en un oligonucleotid per a estudiar la seua ciclorreversió per mitjà de una transferència electrònica. Basant-se en els resultats dels capítols previs, OG ha sigut triat com un fotorreductor natural. En un primer pas, una metodologia ha sigut desenvolupada per a inserir l'azetidina dins d'una seqüència d'oligonucleòtid. Després, la irradiació en estat estacionari del dúplex que conté OG i l'azetidina ha demostrat que la transferència d'electrons té lloc i comporta a la ciclorreversió de l'heterocicle. A més, experiments preliminars han sigut duts a terme per a avaluar la reparació de l'anell de quatre membres, com un anàleg del intermedi en la reparació del fotoproducte (6-4) , per les fotoliases reals CPD i (6-4).

Scientific Contribution

Contributions to congresses

1. Fraga-Timiraos, A. B.; Lhiaubet-Vallet, V.; Miranda, M. A. "Synthesis and photoreduction of an azetidine model to mimic (6-4) photoproduct repair". 16th Congress of the European Society for Photobiology, Aveiro, Portugal, 31 August-4 September, **2015**. Poster.

2. Fraga-Timiraos, A. B.; Lhiaubet-Vallet, V.; Miranda, M. A. "Repair of a dimeric azetidine related to thymine-cytosine (6-4) photoproduct by electron transfer photoreduction". XXVI Biennial Meeting of Organic Chemistry, Punta Umbría, Spain, June 14-17th, **2016**. Poster and Flash communication.

3. Fraga-Timiraos, A. B.; Lhiaubet-Vallet, V.; Miranda, M. A. "Photorepair of pyrimidine dimers by 8-oxo-guanosine as a flavin mimic". XXXVI Biennial Meeting of the Royal Spanish Society of Chemistry, Sitges, Spain, June 25-29th, **2017**. Poster.

Publications

1. Fraga-Timiraos, A. B.; Francés-Monerris, A.; Rodríguez-Muñiz, G. M.; Navarrete-Miguel, M.; Miranda, M. A.; Roca-Sanjuán, D.; Lhiaubet-Vallet, V. "Experimental and theoretical study on the cycloreversion of a nucleobase-derived azetidine by photoinduced electron transfer", *Chem. Eur. J.* **2018**, *24*, 15346-15354.

2. Fraga-Timiraos, A. B.; Lhiaubet-Vallet, V.; Miranda, M. A. "Repair of a dimeric azetidine related to thymine-cytosine (6-4) photoproduct by electron transfer photoreduction", *Angew. Chem. Int. Ed.* **2016**, *55*, 6037-6040.

3. Fraga-Timiraos, A. B.; Rodríguez-Muñiz, G. M.; Peiro-Penalba, V.; Miranda, M. A.; Lhiaubet-Vallet, V. "Stereoselective fluorescence quenching in the electron transfer photooxidation of nucleobase-related azetidines by cyanoaromatics", *Molecules*, **2016**, *21*, 1683-1691.